The Critical Role of IL-23 Receptor Positive T cells in the Pathogenesis of Anterior Uveitis Associated with Spondyloarthropathy

Robert Hedley
Hertford College

Supervisors: Prof. Peter Taylor, Dr Serafim Kiriakidis, and Dr Jonathan Sherlock



Botnar Research Centre
Nuffield Department of Orthopaedics, Rheumatology and Musculoskeletal Sciences

A thesis submitted for the degree
Doctor of Philosophy
Trinity term 2021

‘I, Robert Hedley confirm that the work presented in this thesis is my own. Where information has been derived from other sources, I confirm that this has been indicated in the thesis.'



2nd July 2021

Abstract

The spondyloarthropathies (SpAs) are a group of chronic inflammatory diseases which predominantly affect the joints of the axial skeleton. However, many patients with SpA may have extra-articular manifestations within the skin and gut. Pathology of SpA in all of these tissues has been shown in recent studies to be driven by local resident populations of interleukin (IL)-23 responsive cells. The eye is also involved in these diseases, with uveitis occurring in up to 40% of patients with SpA. Therefore, it is feasible that a resident population of IL-23 responsive cells could also exist within the eye.

Recently, systemic overexpression of IL-23 in mice has shown the accumulation of a small number of γδ T cells proximal to the anterior uvea. However, although work has been done to characterize resident leukocyte populations within the anterior compartment of the eye there has been no documentation of resident lymphoid cells in these tissues and there is no evidence suggesting the presence of a sentinel cell capable of responding to IL-23.

In this study I document for the first time that a diverse population of T cells is present in the extravascular tissues of the anterior compartment of the eye in both mice and humans. I also identify the presence of a resident IL-23R+CD3+CD4-CD8- γδ T cell in the anterior compartment of the eye, providing a potential explanation for why IL-23 is capable of affecting all of these distal sterile tissues.

I then stimulate these cells to show that they have functional IL-23R activity and that IL-23 is sufficient to drive uveitis in the absence of any pro-inflammatory mediator. I achieve this *in vivo* in mice through a novel mechanism enabling the sustained localized overexpression of IL-23 in the inner eye by adeno-associated virus gene

transfer. Since I could not do this in humans, I instead stimulated human eye tissue with IL-23 *in vitro.* Here I was able to show that that IL-23 is sufficient to drive the expression of several downstream pro-inflammatory cytokines by these cells. Consistent with the concept of IL-23 being a unifying factor in SpA, I show that like the gut, skin, and joints - IL-23 can also act locally on a resident IL-23 responsive cells to drive pathology within the eye.

Acknowledgments

I thank my primary supervisor Professor Peter Taylor for mentoring me and allowing me to conduct my research in the Taylor Lab.

I would also like to thank my co-supervisor Dr Jonathan Sherlock for introducing me to the fields of spondyloarthropathy, entheseal biology, and IL-23 biology. He has provided a great amount of knowledge that has steered the direction of my thesis from the very start. The effort he put in to help establish the Oxford Ophthalmology network (now known as the Orbit Consortium) with me was key to the success of this project and will lead to many fantastic developments in the future.

I give special thanks to my co-supervisor and 'Doktorvater' Dr Serafim Kiriakidis for dedicating a lot of his time to my supervision, and never giving up on me. He has been a great mentor and an exceptional friend throughout my time working in the Taylor Lab. I could not have done this without you!

I am grateful to all senior members of the Taylor lab for their expertise and encouragement, particularly: Joanne Macdonald, Graham Wells, and Rita Pinter.

I thank Professor Andrew Dick for allowing me to conduct my research within the Inflammatory Eye Disease Group at The University of Bristol Biomedical Sciences Department, for providing me with mice, and for the financial contribution to my project.

I also want to say a massive thank you to David Copland and Colin Chu for helping me establish the novel anterior uvea IL-23 overexpression system by viral gene transfer in mice, for being fantastic mentors in the field ophthalmology, and for always making me feel very welcome whenever I travelled to Bristol.

I thank the Micron Advanced Imaging Consortium at The University of Oxford, and specifically Dr Nadia Halidi for her expertise.

I would not have been able to carry out this study without the samples provided by the Oxford Ophthalmology Network, these include those provided by Dr Srilakshmi Sharma and her team at the Oxford Eye Hospital, Professor Sarah Coupland and her team at the Liverpool University, and Dr Paul Rooney and his team at the NHS Blood and Transplant Service.

I am particularly grateful to Professor Stephanie Dakin who has been a fantastic mentor, collaborator, and friend throughout my DPhil. I will always remember our meaningful discussions over coffee breaks and our late night FACS sessions.

I could not have wished for a more fantastic DGS during my studies than Professor Afsie Sokabar. If Serafim is my doctor father, then you have definitely been my doctor mother. You have gone out of your way to mentor me and support me beyond that expected of your role. Truly you have been a pillar that has kept me standing every time that I thought I was going to fall. I cannot thank you enough!

Finally, I would like to thank my wonderful family for all of your love and support throughout the duration of my studies.

.

Table of contents

Abstract III

Acknowledgments V

Table of contents VII

Abbreviations XIII

Chapter 1 1

Introduction 1

Spondyloarthropathy (SpA) 2

Entheses – the epicentre of pathology in SpA 9

The anatomy of the eye 12

The corneoscleral coat 16

The uveal tract 16

The corneoscleral limbal region 16

Uveitis 20

Aetiology and Epidemiology of uveitis 21

Pharmaceutical management of uveitis 23

IL-23 and IL-23R – structure and function 31

IL-23 expression profile 33

Chapter 2 39

IL-23 overexpression is sufficient to drive T cell mediated uveitis. 39

Introduction 40

Interleukin (IL)-23 - a link between uveitis and spondyloarthropathy 40
Gene Transfer 43
Aims 47
Materials and methods 48
Animal strains and husbandry 48
An overview of the ShH10 IL-23 AAV production process 48
Synthesis of mouse IL-23 sequence 48
Recombinant ShH10 production 51
Purification of ShH10 vector 51
Limulus Amoebocyte Lysate assay 52
Viral titre calculation using qPCR 52
Intravitreal administration of ShH10 AAV 53
In vivo imaging techniques 54
Dissection and extraction of non-ocular mouse tissues 56
Dissection and extraction of ocular mouse tissues 56
Enzyme linked immunosorbent assay (ELISA) 56
Preparation of ocular tissues for analysis by flow cytometry 57
Statistical analysis 58
Results 60
ShH10 serotype rapidly transduces retinal cells after intravitreal delivery . 60
IL-23 is sufficient to drive inflammation of the inner eye *in vivo* in the absence of any other inflammatory signal 62

IL-23 promotes the infiltration of immune cells into the anterior and posterior compartments of the eye. 72

ShH10 IL-23 AAV driven uveoretinitis requires a Rag2-dependent cell..... 78

Discussion..... 81

Chapter 3 89

The phenotype and localisation of T cells in the anterior compartment of the eye. 89

Introduction 90

Ocular immune privilege..... 91

Sequestration of the eye from the immune system..... 91

The distribution of immune cells in the uveal tract of the normal eye 92

Aims..... 94

Materials and Methods..... 95

Animal strains and husbandry 95

Human ocular tissue..... 95

Dissection and Isolation of ocular leukocytes from human ocular tissue... 96

Flow Cytometry..... 97

Immunohistochemistry and Immunofluorescence..... 98

Lightsheet imaging 102

Statistical analysis 102

Results..... 103

Extravascular T cells are present in the anterior eye compartment in mice 103

T cells are resident within tissues surrounding and dividing the anterior and posterior chamber of the anterior cavity in the human eye 108

The relationship of resident T cells with vascular and aqueous outflow structures of the anterior compartment 122

T cells in the extravascular tissue of the ciliary body 125

T cells in the extravascular tissue of the iris 131

T cells in the extravascular tissue of the iridocorneal angle (ICA) 134

T cells in the trabecular meshwork 136

Discussion 138

Chapter 4 148

Identification of a novel resident Interleukin-23–dependent γδ T cell population in the anterior uvea in mice and humans 148

Introduction 149

The T-helper (T_H) 17 cell 149

Tγδ17 cells 153

Aims 156

Materials and Methods 157

Animal strains and husbandry 157

Dissection of mouse ocular tissue 157

Preparation of mouse ocular tissues for analysis by flow cytometry 157

GFP Immunofluorescence 160

Human ocular tissue 160

Preparation of human ocular tissues for analysis by flow cytometry 161

Modified ViewRNA assay 163

Statistical analysis 164

Results 166

The anterior compartment of healthy murine eyes contains an IL-23R+ γδ T-cell population 166

Murine anterior compartment-resident γδ T cells show a pre-activated effector phenotype 171

Production of IL-17 within the murine anterior compartment by γδ T cells 174

The anterior compartment of healthy human eyes contains an IL-23R+RORγt+ γδ T cell population 176

IL-23 promotes IL-17A expression ex-vivo in cells of the human anterior compartment 181

Phenotypic characterisation of T cells in human anterior compartment biopsy samples 185

The anterior compartment of the human eye is primed to respond to IL-17A produced by IL-23R γδ T cells 188

Discussion 190

Chapter 5 199

Final Discussion, concluding remarks, and proposed future studies 199

Appendicies..... 215

Appendix I..... 216

Supplementary Figures. 216

Appendix II..... 226

Publications..... 226

Abstracts 226

References..... 227

Abbreviations

AAV	Adeno-associated virus
APC	Antigen presenting cell
AS	Ankylosing spondylitis
BASDAI	Bath Ankylosing Spondylitis Disease Activity Index
BASFI	Bath Ankylosing Spondylitis Functional Index
CCR6	C-C motif chemokine receptor 6
CD	Cluster of differentiation
CS	Corticosteroids
DAMP	Damage-associated molecular pattern
DC	Dendritic cell
EAU	Experimental autoimmune uveitis
EIU	Endotoxin-induced uveitis
ER	Endoplasmic reticulum
ERAP1	Endoplasmic reticulum aminopeptidase 1
GC	Gene copies
GM-CSF	Granulocyte-macrophage colony-stimulating factor
GWAS	Genome-wide association study
HLA-B27	Human leukocyte antigen B27
IBD	Inflammatory bowel disease
IFN-γ	Interferon gamma
IFN-γR	Interferon gamma receptor
IL-1β	Interleukin 1 beta
IL-6	Interleukin 6
IL-17	Interleukin 17
IL-17R	Interleukin 17 receptor
IL-19	Interleukin 19
IL-22	Interleukin 22
IL-22R	Interleukin 22R
IL-23	Interleukin 23
IL-23R	Interleukin 23R
IL-24	Interleukin 24
ILC3	Type 3 Innate lymphoid cell
IRF4	Interferon regulatory factor 4
IMT	Immunosuppressant therapy
iNKT	Induced natural killer cells
IOP	Intra ocular pressure

IW	Schlemm's cannal inner wall endothelium
Jak2	Janus kinase 2
JCR	Juxtacanalicular region
JIA	Juvenile idiopathic arthritis
LPS	Lipopolysaccharide
LTi	lymphoid tissue inducer cell
MHC	Major histocompatibility complex
MMP-1	Matrix metalloproteinase-1
MMP-3	Matrix metalloproteinase-3
NK	Natural killer cell
OW	Schlemm's cannal outter wall endothelium
PASI	Psoriasis Area Severity Index
PAMP	Pathogen-associated molecular pattern
PBMC	Peripheral blood mononuclear cell
PsA	Psoriatic arthritis
PCR	Polymerase chain reaction
qPCR	Quantitative polymerase chain reaction
RA	Rheumatoid arthritis
RASF	Rheumatoid arthritis synovial fibroblasts
ReA	Reactive arthritis
ROR-γt	Retinoic acid-related orphan receptor gamma t
SFB	Segmented filamentous bacteria
SNP	Single nucleotide polymorphism
STAT3	Signal transducer and activator of transcription 3
T_H17	T helper 17 cell
TL	Tendon or ligament
TNF	Tumor necrosis factor
TNFR	Tumor necrosis factor receptor
UPR	Unfolder protein response

Chapter 1

Introduction

Spondyloarthropathy (SpA)

The spondyloarthropathies (SpAs) are a group of chronic inflammatory diseases which predominantly affect the entheseal tissue of the axial skeleton. These include psoriatic arthritis (PsA), reactive arthritis (ReA), arthritis associated with inflammatory bowel disease (IBD) including Crohn's disease and ulcerative colitis, and ankylosing spondylitis (AS) - often referred to as the prototypic member (Moll, Johnson, and Wright 1974; Rudwaleit and Baeten 2006; Taurog, Chhabra, and Colbert 2016; Bridgewood et al. 2018; Gracey et al. 2020). However, many patients with SpA may have extra-articular manifestations including involvement of the anterior uvea of the eye (Sharma and Jackson 2017), the lung apex (Farquhar et al. 1989), the aortic root (Roldan et al. 1998), and the terminal ileum (Sharif et al. 2020), with all of these tissues representing junctional sites that are also subject to repeated motion and biomechanical stressing (McGonagle et al. 2001; Watad et al. 2018).

Unlike rheumatic conditions such as RA and myasthenia gravis, diseases associated with SpA are not driven by autoreactive antibody production (Derksen, Huizinga, and van der Woude 2017; Mantegazza, Bernasconi, and Cavalcante 2018). Instead, other factors such as genetic links, mechanical strain, and variances in the constitution of the microbiome are believed to play a role in driving disease pathogenesis, often linked to increased Interleukin (IL)-23 expression and sensitivity (reviewed in Bridgewood et al. 2020).

SpA has a core genetic component dominated by the class 1 major histocompatibility complex (MHC) gene, human leukocyte antigen (HLA)-B27. The association was first identified with AS in 1973 in three separate studies (Brewerton et al. 1973; Caffrey and James 1973; Schlosstein et al. 1973) using a

lymphocytotoxicity micro-method. It is one of the strongest genetic associations with any common human disease (Li and Brown 2017). However, because of advances in high-throughput HLA sequencing, we now know that HLA-B27 is remarkably polymorphic, with 271 HLA-B27 subtypes (B27:01-B27:164) reported in 2015 (Cortes et al. 2015). The number of subtypes is still growing, but most are too rare to determine whether they are associated with AS. That being said, HLA-B*27:05 and HLA-B27:02 have been documented as the main subtypes associated with AS in Caucasians, HLA-B*27:04 and HLA-B27:07 in Asians, and HLA-B27:02 in Mediterranean populations (Taurog 2007). Two other subtypes have been shown to be neutrally associated with AS, HLA-B27:06 (a common subtype in south-east Asia) (Nasution et al. 1997), and HLA-B27:09 (a rare subtype found primarily on Sardinia) (D'Amato et al. 1995). In addition, HLA-B27 positive patients have a tendency to develop AS earlier than HLA-B27-negative patients (Feldtkeller et al. 2003; Jaakkola et al. 2006).

It has long been known that SpA carries a strong hereditary risk (de, Polman, and de 1961). The recurrence risk between first degree relatives is ~ 8.2% for AS and ~12% for SpA as a whole [6,7]. The recurrence risk between first degree relatives increases further (%) in HLAB27 positive relatives for SpA 7, and >90% in AS amongst twins (Brown et al. 1997).In this study the variants with the strongest contribution came from the MHC (20.44%), with an additional 7.38% coming from non-MHC loci. Strong clinical associations with heritability have also been observed in AS patients, including disease activity (BASDAI, 51%) (Hamersma et al. 2001), functional impairment (BASFI, 68%) (Hamersma et al. 2001), radiographic change (62%) (Brophy et al. 2004), and age that symptoms were first noticed (Brown et al. 2003).

The understanding of genetic susceptibility to SpA, particularly AS, has considerably improved due to an increase in the statistical power of genome-wide association studies (GWAS) based on single nucleotide polymorphism (SNP) arrays, such as the Illumina Immunochip (Cortes and Brown 2011).The first AS GWAS was conducted by the Wellcome Trust Case Control Consortium (WTCCC) and Australo-Anglo-American Spondylitis Consortium (TASC) in 2007, which was able to analyse 14 500 non-synonymous SNPs in 1,000 AS patients and 1500 healthy controls. This was the first study of its kind to make a definitive identification of non-MHC susceptibility loci in AS, including SNPs in IL-23 receptor (IL23R) and endoplasmic reticulum aminopeptidase 1 (ERAP1) (Burton et al. 2007). Since then a number of other studies have replicated these findings in larger cohorts (Reveille et al. 2010; Evans et al. 2011; Cortes et al. 2013; Robinson et al. 2016), with the identification of 113 AS-associated genome-wide significant variants in the largest AS case-control association consisting of 8726 AS cases, another 43536 cases in four related diseases (Crohn's disease, psoriasis, primary sclerosing cholangitis and ulcerative colitis), and 34213 healthy controls (Ellinghaus et al. 2016). Important to this study, Several SNPs in the IL-23R gene have also been found to be associated with uveitis (Jung et al. 2017), such as the homozygous GG genotype of SNP rs17375018, which is significantly associated with patients with AS and uveitis, and in Behçet's disease uveitis (Dong et al. 2013)

Nonetheless, there is a significant limitation amongst these studies in that most AS GWAS or case–control association studies have been performed in white European cohorts. Only one GWAS study has been carried out in the Han Chinese population (Kim et al. 2015). Considering the fact that a small study has already shown differences in *IL23R* SNPs associations with AS between European descent

populations and Han Chinese (Davidson et al. 2009), there are likely to be more differences noticed in larger studies. Therefore, there needs to be a large GWAS performed in the Han Chinese population in the future to elucidate more of these differences between race.

Currently, the causative link between HLA-B27, IL-23 and SpA remains unclear. Studies has shown that the majority of the AS-associated forms of HLA-B27 molecules (HLA-B27:05, HLA-B27:04 and HLA-B27:02) take longer to fold than MHC-I molecules , which are not associated with AS (Chan et al. 2005; Antoniou et al. 2004). This has also been shown to result in an accumulation of misfolded HLA-B27 molecules in the endoplasmic reticulum (ER), triggering a cellular stress response and activation of the unfolded protein response (UPR), as an attempt is made to rescue or dispose of the burden of misfolded proteins (Colbert et al. 2009; Turner et al. 2005). Interestingly, DeLay et al. (2009) also showed that macrophages undergoing a UPR in an HLA-B27 transgenic rat model of spondyloarthropathy were able to synergistically upregulate IL-23p19 (the unique subunit of the active IL-23 cytokine) in response to lipopolysaccharide (LPS). Furthermore, IL-23 was increased in the colon tissue of these rats, concurrently with the development of intestinal inflammation, IL-17 upregulation, and a fourfold expansion of IL-17-expressing CD4+ T cells. In addition, the bacterium *Chlamydia trachomatis* which is known to drive the pathogenesis of PsA has been shown to induce a stress response of the ER and elevate serum concentrations of IL-23 in this way, specifically through the induction of CHOP10, a bZIP protein involved in apoptosis and differentiation, which is able to bind to the IL-23p19 promoter to induce its expression (Goodall et al. 2010).

If a population of cells, capable of responding to IL-23, was found to be present within all the precise anatomical locations where inflammation is observed in SpA, then this mechanism of misfolded HLA-B27 induced IL-23 overexpression would provide a possible explanation for why HLA-B27 positive patients are more susceptible to SpA. However, associations between IL-23 expression and the UPR are controversial as Zeng et al. (2011) showed increased production of IL-23 by macrophages in AS patients in response to LPS occurred without induction of significant UPR, and Ciccia et al. (2014) reported that HLA-B27 misfolding in the gut of patients with AS is accompanied by activation of autophagy rather than a UPR.

The link between elevated IL-23 production and the distinct pattern of inflammation at precise anatomical locations observed in SpA, specifically those originating within the entheseal tissue of sterile/non-barrier articulating sites, has begun to be unravelled over the last decade. An entheseal resident population of IL-23R+CD3+CD4-CD8- T cells have been observed as the key producers of IL-17A and IL-22, consequent to IL-23 overexpression, within the axial skeleton and aortic root (Sherlock et al. 2012; Reinhardt et al. 2016). Type 3 innate lymphoid cells (ILC3s) have also been phenotyped as IL-17A producers at the Achilles tendon entheses in man (Cuthbert et al. 2017). However, more recently controversial evidence has been introduced suggesting the concept of IL-23 independent production of IL-17A by these resident cells (Cuthbert et al. 2019).

An interesting question arises that if the primary site of inflammation in SpA are indeed the entheses of the diseased tissue, and the driving force that unites inflammation at all these sites is IL-23 - then how and where is the IL-23 produced which reaches these sites? One hypothesis was generated in a 2011 Nature ‘Bench

to Bedside' review (Cua and Sherlock 2011), where it was speculated that the constitutively produced inflammatory cytokines, including IL-1 and IL-23, which are generated in the terminal ileum through the interaction between gut gram-positive bacteria, such as segmented filamentous bacteria (SFB), and immune-surveilling DCs, when overproduced, may spill into the systemic circulation. This would potentially promote inflammatory diseases in distal sites, such as the joints, and the eye, perhaps through action upon entheseal-resident lymphoid cell populations (**Figure 1.1**).

Supporting this hypothesis, elevated levels of IL-23 have been identified in the serum of AS patients in a number of studies (Mei et al. 2011; Chen et al. 2012; Ugur et al. 2015), and in the serum (measurement not disclosed) (Przepiera-Bedzak et al. 2016) and vitreous fluid (IL-23 >500pg/mL) (Velez et al. 2016) of patients with uveitis. The latter specifically showing an elevated level of IL-23 protein in an HLA B27 positive patients compared to healthy controls. Additionally, IL-23A gene copy number variants greater than 2 in the peripheral blood have been associated with Behçet's disease uveitis and Vogt–Koyanagi–Harada uveitis (Hou et al. 2015). Additionally, the absence of IL-23 leaves otherwise susceptible animal models, resistant to experimental autoimmune uveitis (EAU) (Luger et al. 2008; Sun et al. 2015). However, all of these studies have their individual caveats such as small sample numbers, the use of varying ELISA kits, and a wide range in the recorded measurements of IL-23, which will be discussed in greater detail in Chapter 2.

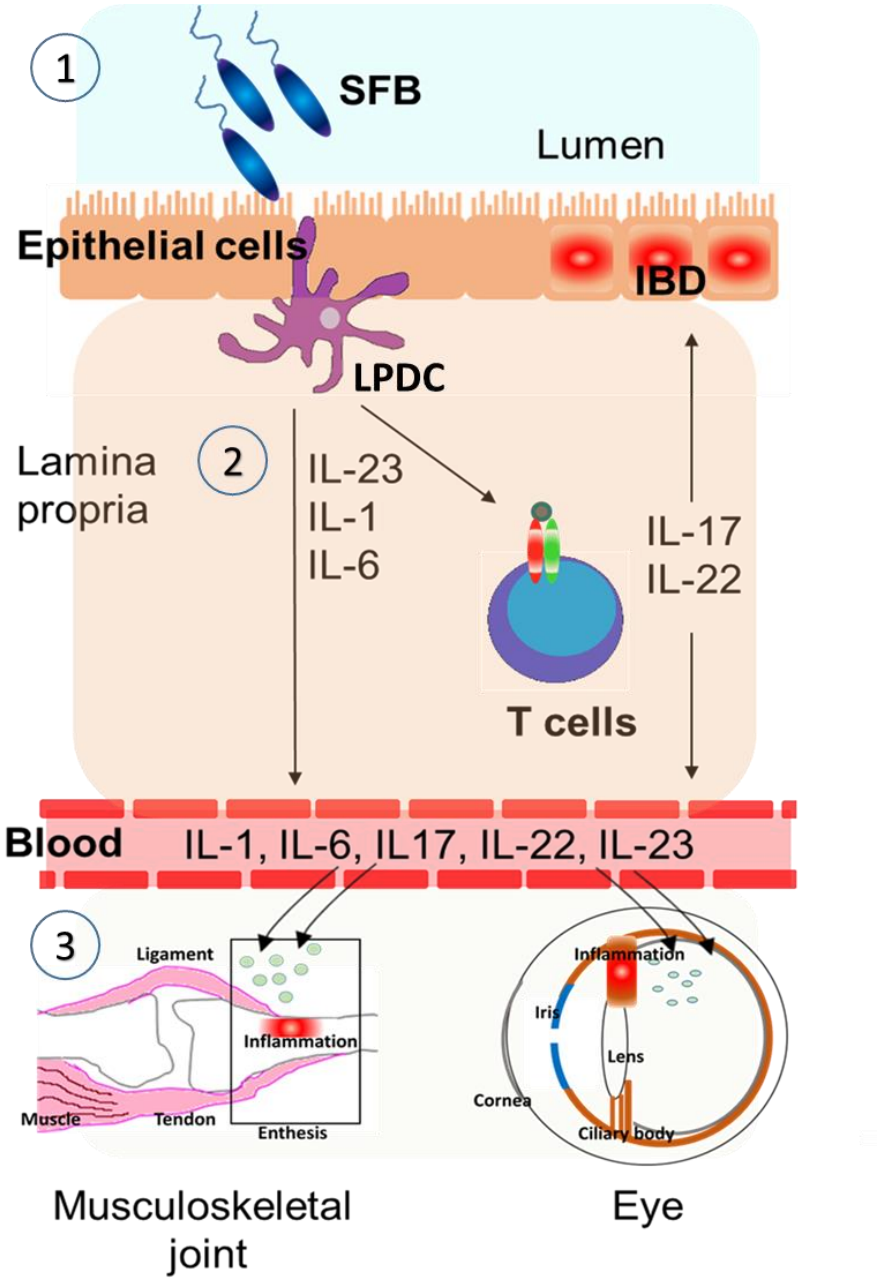


Figure1.1: Resident commensal bacteria of the mammalian gut may have a role in producing inflammatory cytokines that activate a primary immune response at sterile, peripheral, entheseal sites. (1) Gram negative bacteria, such as segmented filamentous bacteria (SFB), interact with lamina propria dendritic cells (LPDCs) of the small intestine. (2) This interaction results in the production of inflammatory cytokines by LPDCs, including IL-1, IL-6, and IL-23, and also a T cell response increasing IL-17 and IL-22. The over expression of these cytokines into the local environment may damage the epithelial barrier surface and initiate inflammatory bowel disease. (3) Inflammatory cytokines may disseminate in the vasculature to sterile, distal, entheseal sites, within musculoskeletal joints or the anterior compartment of the eye. These cytokines may then act on local immune cells at these distal sites. Altered sensitivity to IL-23 may explain why some people are predisposed to enthesitis at these distal sites.

Entheses – the epicentre of pathology in SpA

It has been hypothesised that the primary sites of inflammation in diseases associated with SpA, are the entheses. (Ball 1971; 1983; McGonagle et al. 1998a; 1998b). The entheses are insertional sites, such as where the proximal end of a tendon or ligament (TL), or joint capsule attaches to the bone. Functionally, entheses give the sturdy anchorage necessary for the significant stress burden induced by musculoskeletal structural integrity. In fact, mechanical stress is often the event that elicits the development of enthesitis (Jacques et al. 2014). In healthy individuals, repetitive trauma, experienced through work or sporting activities, may trigger enthesitis. A typical example of this is lateral epicondylitis (Rothschild 2013), which usually resolves spontaneously after avoidance of the repetitive movement. TLs are also known to flare out as they approach an attachment sites, increasing the surface area of the anchorage site (Milz et al. 2002; Milz et al. 2004; Milz, Benjamin, and Putz 2005) which may provide a clue as to why patients report pain in neighbouring structures after enthesis injury or disease.

For reasons not completely understood and potentially involving genetic factors (IL-23R polymorphisms; HLA B27) (McGonagle, Thomas, and Schett 2014), individuals with SpA have a lower threshold for the onset of enthesitis. In a study by Eder et al. (2011) it was shown that lifting heavy loads was associated with the occurrence of PsA among patients with psoriasis. A seminal study by Cambre et al. (2018) showed that mechanical stress can trigger the local expression of chemokines such as CXCL1 and CCL2, which direct the infiltration of innate immune cells to the sites of stress. Therefore, it can be hypothesised that anatomical localization of disease in patients with uveitis and other diseases associated with SpA could be partly determined by individual mechanical stress levels at entheseal sites.

Innate immune activation upon the recognition of danger signals appears to be a critical feature for understanding the rapid onset of enthesitis as well as its chronicity when such danger signals are not adequately controlled or removed (Czegley et al. 2018). In the context of uveitis and other diseases associated with SpA theses danger signals may come in the form of mechanical damage-associated molecular patterns (DAMPs), infectious pathogen-associated molecular patterns (PAMPs), or a disruption in the local cytokine mileu, and likely represent the earliest factors that lead to the activation of a cascade of inflammatory mediators that ultimately brings about clinical enthesitis.

The most compelling evidence that IL-23 is able to act directly at the enthesis to initiate and inflammatory response comes from the animal studies of Sherlock et al. 2012 and Reinhardt et al. 2016. Very low numbers of IL-23R+ cells were found organised along entheseal collagen fibres of the axial skeleton in normal B10.RIII mice through the use multiphoton and Lightsheet imaging. These cells were further phenotyped by flow cytometry, to be a mixture of αβ and γδTCR+ CD45+CD3+CD4-CD8-IL-23ReGFP+ T cells. Furthermore, after systemic IL-23 overexpression in these mice, these cells were found to produce proinflammatory cytokines including IL-17A, tumor necrosis factor (TNF)-α, and IL-22. These studies found that inflammation induced by systemic IL-23 overexpression was not limited to the musculoskeletal entheses of the axial skeleton in mice, but also developed in extra-articular structures anatomically similar to entheses such as the aortic root, valve and in the ciliary body. However, no IL-23R+ cells were reported as being present in these tissues. In addition, a more recent study also documented the presence of ILC3s within human entheseal soft tissue (Cuthbert et al. 2017). In healthy individuals, Jacques et al. (2014) have previous postulated that the normal role of

entheseal resident T cells and ILC3s at entheseal sites might be to influence bone metabolism and maintain tissue homeostasis (Jacques et al. 2014).

Mesenchymal cells constitute the majority of cells within the extracellular matrix of entheseal tissues. These include fibroblasts, chondrocytes and osteocytes. Van Hamburg et al. (2011) used passaged RA synovial fibroblasts (RASF) to show that these cells expressed functional IL-17 receptor (IL-17R) and TNF receptor (TNFR) activity. Although they did not specifically phenotype the expression of IL-17R or TNFR on RASFs, IL-17R and TNFR activity was assessed through co-culture of passaged RASFs with CCR6+ memory T cells sorted from the PBMCs of treatment-naive patients with early RA, in the presence of either IL-17 or TNF neutralising agents. T cells in the culture were stimulated with soluble anti-CD3 and anti-CD28 and cultured for 3 days. Both cytokine detection in the supernatants and intracellular flow cytometry showed that these C-C motif chemokine receptor (CCR)6+ T cells expressed and secreted IL-17A and TNF-α. Real-time quantitative polymerase chain reaction (qPCR) analysis revealed that both IL-17 and TNF-α are able to drive expression of the tissue-destructive enzymes matrix metalloproteinase (MMP)-1 and MMP-3, by RASFs. Furthermore, Gaida et al. (2012) was able to show the expression of both TNFR1 and TNFR2 on tenocytes from the human Achilles tendon.

Another study by El-Zayadi et al. (2017) revealed that IL-22 is sufficient to drive the proliferation, migration and osteogenic differentiation of mesenchymal stem cells, although they did not show specific expression of IL-22 receptor (IL-22R) on these cells. In addition, the seminal paper by Sherlock et al. 2012 identified that the axial skeleton entheseal osteoproliferative effects observed in mice after expression of systemic IL-23 are mediated by IL-22.

Certain tissues in the anterior compartment of the eye could also considered to be entheseal structures, such as: (A) the connections formed between the transverse ciliary muscles the scleral spur, and the trabecular meshwork; (B) the region of tissue connecting the iris stroma to the iris radial and longitudinal muscles; (C) the anchorage of zonule fibers to the ciliary epithelium and the lens; (D) The bridge between the longitudinal muscles and the supracoroidal lamina (fibres that bridge the choroid with the inner sclera); and (D) the attachment site of the extraocular muscles to Tenon's capsule and the limbal sclera. Recently, γ δT cells have been shown to accumulate in the region of the ciliary body proximal to the limbal sclera in the eyes of mice after systemic minicircle induced IL-23 overexpression (Reinhardt et al. 2016). However, no studies have specifically shown the presence of resident IL-17 producing cells in the anterior compartment of the eye.

The anatomy of the eye

As this study will investigate the critical role of IL-23/IL23R in uveitis, I have included the following section to first describe the anatomy of the eye. Here I carefully describe the different tissues and compartments within the eye, enabling a better understand of the following chapters.

The eye is a complex sensory organ, essentially a highly specialised extension of the brain. It is both a barrier surface and junctional site, and is composed of a range of tissue types including epithelia, connective tissue, smooth muscle, vascular tissue, and neural tissue. While some components of the eye require a high level of transparency to allow light to pass through unobstructed, other tissues are characterized by their dense pigmentation, which functions to absorb light and thus control its passage through the ocular structures. In turn these ocular structures work mechanically in conjunction to control the focussing and transmission of light

onto the retina (accommodation), while at the same time maintaining intraocular pressure homeostasis. Specialised leukocytes of the innate immune system including macrophages and DCs are present in almost all ocular tissues, from the ocular surface through to the uveal tract (McMenamin 1997, 1999). Lymphocytes, including multiple sub populations of T cells, are also found in abundance at the ocular surface (Bose et al. 2017). In contrast, early studies have shown an almost complete absence of lymphocytes within the uveal tract (McMenamin 1997; Wakefield, McCluskey, and Palladinetti 1992; Williamson, Bradley, and Streilein 1989). This observation has gone unchallenged until now as it fits with the prevailing immunological paradigm and assumptions; the eye is constantly attempting to maintain an immune privileged environment to preserve vision.

The eye is formed of three concentric layers or coats, often referred to as tunics. The outer most layer is the largely avascular, fibrous, corneoscleral coat (cornea and sclera). Inwards of this layer is the uveal tract (iris, ciliary body, and choroid). The inner most layer is known as the neural layer or retina. The coats surround and protect the contents of the eye, namely the lens and the eyes transparent media, termed the aqueous humor and vitreous body. The inner eye is divided into an anterior and posterior compartment at the point at which the lens meets the ora serrata of the anterior neural layer (**Figure 1.2**).

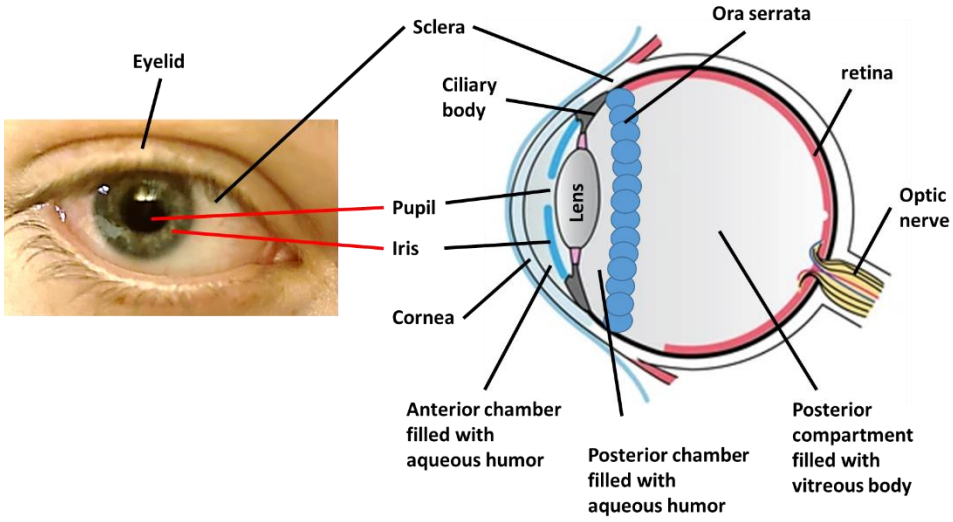


Figure 1.2: Basic anatomy of the human eye.

Furthermore, the anterior compartment can be subdivided into an anterior chamber, approximately one fifth of the eye, and a smaller posterior chamber by the iris of the uveal tract (**Figure 1.3**). The vitreous chamber, filled with vitreous fluid, is located in the posterior cavity. It has also been proposed that the cornea and external structures, including the extraocular muscles, conjunctiva, lacrimal glands, and eye lids, function as an integrated unit called the ocular surface (Cher 2014). It is important to note that there is variation in the eye structure between species. In the mouse and human eye the largest variation can be found in the posterior compartment, with the mouse eye lacking the tissue known as the macula (Fletcher et al. 2014).

Inflammation can affect all layers of the eye, the ocular surface, and both the anterior and posterior chambers. As mentioned previously, the predominant ocular disease associated with SpA is non-infectious anterior uveitis, primarily affecting the anterior uveal tract. Therefore, the focus of this study will be on the anterior section of the eye, including aspects of the anterior compartment.

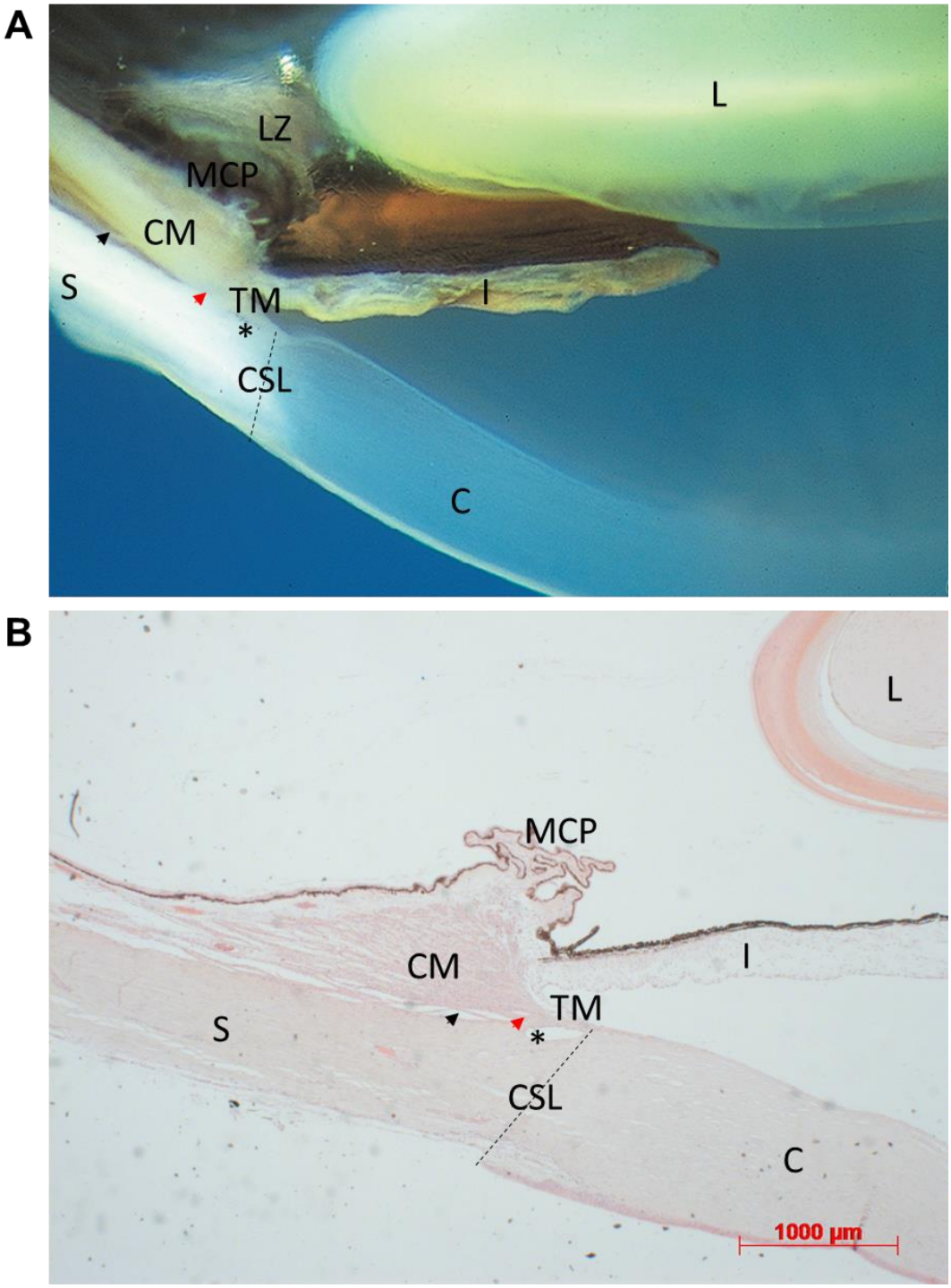


Figure 1.3: The anterior segment of the human eye. (A) Photograph of the anterior segment of the human eye adapted from Yanoff and Sassani (2015) (B) Low power light micrograph (10x objective) of a meridional section of the anterior compartment of an enucleated healthy human eye stained with haematoxylin and eosin, author's own work. The corneoscleral coat (cornea and sclera seen as a continuous structure) and uveal tract (iris, ciliary body, and choroid seen as a continuous structure) are the outer and inner layers of the eye, joined anteriorly by the scleral spur (red arrow head) and posteriorly by the supracoroidal lamina, generating the supraciliary space (black arrowhead). The canal of Schlemm (black asterisk) lies between the outer aspect of the trabecular meshwork and the corneoscleral coat. Note that the lens zonules projecting between the lens capsule and ciliary processes cannot be observed in the low power light micrograph (B). L – lens, LZ – lens zonula, C – cornea, S – sclera, CSL – corneoscleral limbus, CM – ciliary muscle, MCP – major ciliary processes, TM – trabecular meshwork, and I – iris.

The corneoscleral coat

The corneoscleral coat, is the tough fibrous outer layer of the eye. It consists of two continuous tissues: the cornea and the iris. It functions as a protective envelope for the inner ocular tissues and as an attachment site for extraocular muscles, with many other specialised functions, specific to each tissue. The anterior cornea meets the sclera at a region of extreme importance to this study, known as the corneoscleral junction or limbus. The rear of the corneoscleral coat shows the sclera terminating at the optic nerve (Yanoff and Sassani 2015).

The uveal tract

The uveal tract, coming from the Latin word for grape *uva*, is the middle layer of the eye, consisting of three continuous tissues: the iris, ciliary body, and choroid. The uveal tract has an anterior opening termed the pupil, positioned slightly inferonasal to the centre of the iris, which permits the transmission of light from the anterior chamber into the posterior chamber of the eye and onto retina. The uveal tract is sometimes known as the vascular layer as the heavily pigmented choroid, forming the posterior component of the uveal tract anastomosing at the optic nerve head, is mainly composed of blood vessels that serve to supply the inner retinal layer. The uveal tract is known to play a key role in accommodation, aqueous outflow homeostasis, and ocular immune privilege mechanics (Yanoff and Sassani 2015).

The corneoscleral limbal region

The corneoscleral limbal region is more than just an important anatomical landmark for ophthalmic surgeons, the ‘surgical limbus’ (Hamanaka 1989; Van Buskirk 1989; Gabelt and Kaufman 2005), it is the most vascular region of the anterior eye compartment, providing a route for supply of nourishment to the conjunctiva,

peripheral cornea, the sclera, and the uveal tract. It is the location of stem cell niches involved in corneal wound healing and a barrier site that permits immune surveillance of the ocular surface via the conjunctiva and tear film. It is the location of the conventional aqueous humour outflow pathway, controlling intraocular pressure (IOP) homeostasis. Moreover, the limbus is a junctional site with a wealthy collection of entheses connecting ocular tissues of the anterior compartment, many of which are highly involved in movement. Finally, it is one of the few regions of the inner eye that is not considered to be devoid of antigen presenting immune cells (Gueudry et al. 2019).

Several important architectural transitions take place at the limbus: (A) the regularly arranged collagen lamellae of the cornea give way to the more disorganized lamellae of the sclera, condensing internally into a ring to form the scleral spur (**Figure 1.4**) (Newton and Meek 1998) - a structure that houses the canal of Schlemm and aqueous collector channels; (B) the stratified squamous non-keritanized corneal epithelium gives way to the conjunctival epithelium (Yanoff and Sassani 2015); (C) anastomosis of conjunctival, episcleral (derived from the anterior ciliary artery), and lymphatic capillaries terminate at the limbus (Morrison and Van Buskirk 1983); (D) the loose conjunctival subepithelial vascularised connective tissue (substantia propria), containing immunocompetent cells such as mast cells, plasma cells, and lymphocytes, tapers off at the limbus and is absent in the cornea (Yanoff and Sassani 2015); (E) and Desçemet's membrane and the corneal endothelium terminate (Schwabes line) and transitions into the apex of the trabecular meshwork (Van Buskirk 1989) - forming the irideocorneal angle with the scleral spur, the ciliary body and iris.

The trabecular meshwork is a circumferential band of specialised sponge-like connective tissue enveloped in endothelial cells that offers resistance to approximately 90% of the total aqueous outflow of the conventional pathway (Stamer and Acott 2012; Stamer 2012). It lies adjacent to the specially adapted endothelial cell wall of Schemm's canal that provides the remaining 10% of resistance (Bill 1975). It houses the phagocytic trabecular cells that conduct surveillance and removal of erroneous matter within the aqueous humour that might result in blockage of aqueous outflow. The adult mammalian trabecular meshwork can be subdivided into three anatomical zones (**Figure 1.4**): (A) the uveal meshwork; (B) the corneoscleral meshwork; and (C) the cribriform meshwork (Yanoff and Sassani 2015).

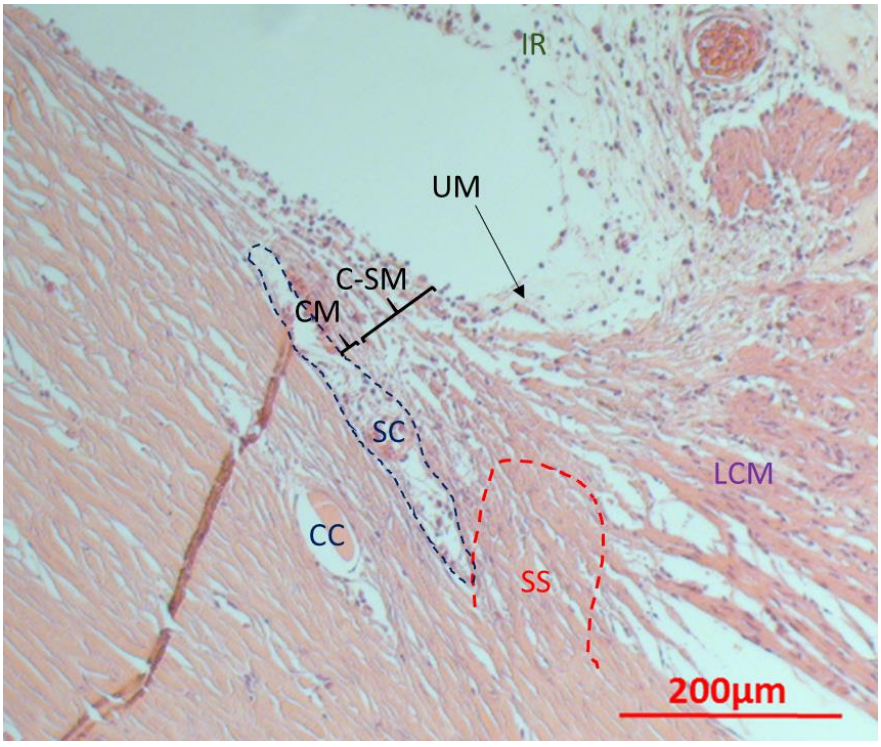


Figure 1.4: The three anatomical zones of the mammalian trabecular meshwork. Low power light micrograph (20x objective) of a transverse section of human irideocorneal angle stained with haematoxylin and eosin, authors own work. Image incorporates the trabecular meshwork, ciliary body and iris root (IR). The trabecular meshwork can be subdivided into three anatomical zones (1) the uveal meshwork (UM); (2) the corneoscleral meshwork (C-SM); (3) the cribriform meshwork (CM). It forms a barrier between the anterior chamber and Schlemm's canal (SC), and forms attachment sites with the longitudinal ciliary muscles (LCM) and scleral spur (SS). CC – collector channel.

Elastic fibers in the corneoscleral meshwork are continuous with the elastic cores of the juxtacanalicular region, which in turn are connected to the inner wall of Schlemm's canal. It is to these that the elastic tendon fibers of the anterior longitudinal ciliary muscles fuse, allowing expansion of the trabecular meshwork, and greater aqueous outflow, with contraction of these muscles (Rohen, Futa, and Lütjen-Drecoll 1981). Trabecular cells bridge the intertrabecular spaces through cytoplasmic extensions. These cells are essential to maintain a healthy meshwork for aqueous drainage. They have the capacity for extensive phagocytic activity - trapping and removing debris from aqueous fluid as it traverses the tedious labyrinth of intratrabecular and intertrabecular spaces that would otherwise result in blockage of aqueous outflow, and in fact detach themselves from the trabecular beams in a macrophage-like manner when exposed to foreign material (Rohen and van der Zypen 1968; Raviola 1982). They also contribute towards the production, replacement and modification of materials of the intertrabecular interstices that would otherwise be gradually washed out during aqueous perfusion (Polansky et al. 1984; Acott et al. 1988; Bylsma et al. 1988).

Schlemm's canal is a unique, circumferential, endothelium lined vessel, encircling the cornea. In humans, it measures between 200 and 400μm in the anteroposterior axis, and is usually no more than 50-60μm deep (Forrester et al. 2021). Because of its close apposition to the juxtacanalicular region (JCR) of the trabecular meshwork, not all endothelium of Schlemm's canal are the same. As a result, endothelium of Schlemm's canal is divided into inner (IW) and outer (OW) wall endothelium that differ in morphology, cell-specific marker expression, specialised cellular organelles, and function. However, these differences may be due to the variations in biomechanical environment between the inner and outer wall, rather than any

underlying biological or biochemical differences. Aqueous humour that has passed into the lumen of Schlemm's canal is drained through multiple external collector channels in the canals' OW, later merging with the intra- and epi-scleral veins (Ashton and Smith 1953).

Uveitis

Uveitis is defined as inflammation of the vascular uveal tract of the eye, including the iris, ciliary body, and choroid; however, adjacent structures such as the retina, optic nerve, vitreous, and sclera may also be affected. In clinical practice, a broad anatomical division has proven more relevant to patient management and an international consensus was standardised in 2005 (Jabs, Nussenblatt, and Rosenbaum 2005). The division includes anterior (involvement of the iris and ciliary body), intermediate, and posterior uveitis (both involving the retina and choroid) or panuveitis (if the whole eye is involved). Anterior uveitis is easily recognised due to the severity of symptoms which include: ciliary injection, miosis (which may pre-dispose to the formation of posterior synechiae), fibrinous exudate (typically seen in HLA-B27-associated anterior uveitis), and hypopyon (a feature of intense inflammation where cellular infiltrate settles in the inferior part of the anterior chamber) (Kanski and Bowling 2011) **(Figure 1.5)**.

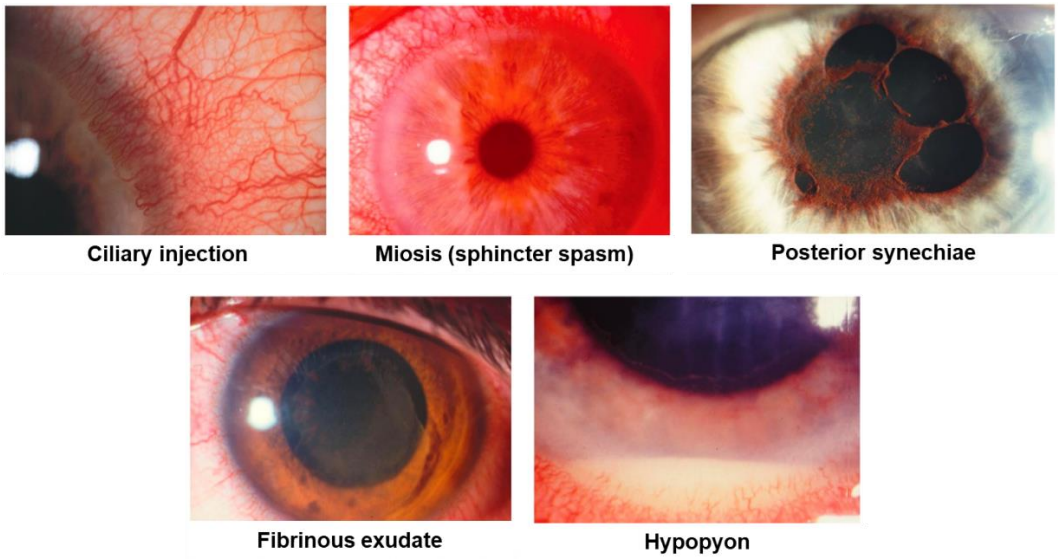


Figure 1.5: Symptoms of anterior uveitis. Photographic images adapted from Kanski and Bowling 2011**.**

Aetiology and Epidemiology of uveitis

Uveitis constitutes a significant cause of ocular morbidity, accounting for 5-10% of the population with visual loss worldwide (Miserocchi et al. 2013). It also has a disproportionately large economic burden for its prevalence, estimated at $242 million per year in the US (Suttorp-Schulten and Rothova 1996). The incidence and prevalence of various uveitis subtypes depend on age, sex, race, geographic distribution, environmental influence, genetic factors, and social habits (Chang and Wakefield 2002; Wakefield and Chang 2005). A recent epidemiological review found that in developing countries the incidence of uveitis has been estimated between 17 and 52 per 100,000 of population per year, and the prevalence as 38–714 cases per 100,000 of population (Tsirouki et al. 2018). Whereas, an older study conducted by Muñoz-Fernández and Martín-Mola (2006)(Muñoz-Fernández and Martín-Mola 2006) found that uveitis was implicated in up to 25% of cases of blindness in the developing world.

Undoubtedly, uveitis aetiology is heterogeneous. Rosendbaum (2019) has suggested this can be broken down into as few as 7 categories: Infectious (bacteria, virus, parasite), systemic immune-mediated disease, syndromes confined primarily to the eye (pars planitis, sympathetic ophthalmia, and punctate inner choroidopathy), trauma related, medication induced, masquerade uveitis, and idiopathic (where no underlying cause is identified). Common infectious causes include tuberculosis, syphilis, herpetic viruses and parasitic diseases such as toxoplasmosis (Lin 2015; Chan and Chee 2019). Commonly associated systemic autoimmune disorders include AS, IBD, psoriasis, RA, BD, sarcoidosis, or juvenile idiopathic arthritis (JIA), and autoimmune diseases that preferentially affect ocular tissues - such as Vogt-Koyanagi-Harada, white dot syndromes, sympathetic ophthalmia, and birdshot chorioretinopathy (Valenzuela et al. 2020). Masquerade and medication-induced uveitis aetiologies are relatively rare. The most common form of masquerade uveitis is often a B cell lymphoma confined to the eye or brain (Smith et al. 2003; Smith et al. 2002). Medications do not usually cause uveitis, but potential culprits include: the 3rd generation bisphosphonate, zoledronate (Patel et al. 2013), TNFα inhibitors (Lim, Fraunfelder, and Rosenbaum 2007), checkpoint inhibitors (the anti-programmed death-1 receptor agents, pembrolizumab and nivolumab; the anti-programmed death-ligand-1 agent, atezolizumab; the anti-cytotoxic lymphocyte antigen-4 agent, ipilimumab) (Conrady et al. 2018), and antibiotics, including moxifloxacin and ciprofloxacin (Eadie, Etminan, and Mikelberg 2015). Likely do to the heterogeneous nature of uveitis, most instances of anterior uveitis are labelled as idiopathic (Rosenbaum 2015).

Anterior uveitis is the most frequently observed extra-articular manifestation of SpA and can be seen in up to 40% of patients (Martin, Smith, and Rosenbaum 2002).

More specifically, the prevalence of uveitis among patients with AS, is estimated to be 33%, 25% among patients with reactive arthritis (ReA), 6-9% among patients with PsA, 13% in undifferentiated SpA, and 2-5% among patients with IBD (Greenstein, Janowitz, and Sachar 1976; Lambert and Wright 1976; Paiva et al. 2000; Bernstein et al. 2001; Yilmaz et al. 2007; Zeboulon, Dougados, and Gossec 2008; Canouï-Poitrine et al. 2012; Peluso et al. 2015). Furthermore, in patients with any type of uveitis, the prevalence of AS has been reported to be 15%, in cases when the patient presents with acute anterior uveitis, it rises to 30–50%, and if the patient presents with acute anterior uveitis and is HLA-B27-positive it rises significantly to 84–90% (Fernández-Melón et al. 2004; Muñoz-Fernández and Martín-Mola 2006). Several genes outside of the MHC have also been associated with increased risk of anterior uveitis in a GWAS study, including: ERAP1, a gene desert on chromosome 2p15, and IL23R (Robinson et al. 2015).

It should be noted that uveitis associated with PsA and IBD presents in a more diverse manner compared to AS or ReA. It has been found to be associated with an insidious onset, is bilateral and chronic in duration, and can also affect the posterior compartment of the eye (Lyons and Rosenbaum 1997; Paiva et al. 2000). Furthermore, a Danish nationwide cohort study documented that the relationship between PsA and uveitis has been shown to be more strongly associated than that with psoriasis alone (Egeberg et al. 2015). In addition, IBD in particular, is commonly associated with episcleritis and scleritis.

Pharmaceutical management of uveitis

Specific antimicrobial therapies with or without corticosteroids (CS) are used in cases of infectious uveitis. On the other hand, management of non-infectious uveitis includes the use of CS, immunosuppressive agents, and more recently biologics

such as TNFα inhibitors (reviewed in Valenzuela et al. 2020). Topical CS are the first line of therapy in patients with non-infectious uveitis, especially anterior uveitis, as these drugs are inexpensive, potent, and act fast (McGhee 1992; Cunningham and Wender 2010). The caveat of topical CS is that they are usually unable to penetrate posterior to the lens. If topical CS fail to modify disease, then local injection of CS can be administered into the vitreous humour (posterior compartment of the eye) (Poetker and Reh 2010; Knickelbein et al. 2017; Rossi, Ribi, and Guex-Crosier 2019). However, this can be uncomfortable for the patient and risks include cataract and glaucoma which can ultimately result in visual impairment and blindness (Rothova et al. 1996; Poetker and Reh 2010; Lowder et al. 2011). Immunosuppressant therapy (IMT) - such as antimetabolites (methotrexate, mycophenolate mofetil, azathioprine), calcineurinic inhibitors (cyclosporine, tacrolimus), and alkylating agents (cyclophosphamide, chlorambucil) can also be used to treat uncontrolled inflammation (Knickelbein et al. 2017; Rossi, Ribi, and Guex-Crosier 2019; Hassan et al. 2019).

If uveitis is refractory to systemic CS and IMT or patients become intolerant to such therapies, a good sight-saving measure is the use of biological agents (Mercier et al. 2018; Trivedi and Katelaris 2019). Biologic agents specifically target relevant immunological pathways involved in disease pathogenesis. Guidelines on the use of biological agents in the treatment of uveitis were published in 2018 by the FOCUS (Fundamentals of Care for Uveitis) group, consisting of 146 international experts who graded the strength of published evidence and who used consensus methodology (Dick et al. 2018).

One noteworthy class of biologic agents now used in the treatment of uveitis in both adult and paediatric patients are TNFα inhibitors, specifically infliximab and

adalimumab (Knickelbein et al. 2017; Hassan et al. 2019; Imrie and Dick 2007; Cordero-Coma, Yilmaz, and Onal 2013; Chen and Sheu 2017; Sood and Angeles-Han 2017; Cann et al. 2018). TNFα is a pro-inflammatory cytokine that participates in the pathophysiology of autoimmune and inflammatory diseases, such as RA and SpA (Sieper et al. 2015; Mitulescu et al. 2018), and TNFα blockers which have been used for the treatment of these diseases since 1999 (Maini et al. 1999). Clinical trials have demonstrated the effectiveness of anti-TNFα in treating uveitis (Kruh et al. 2014; Vallet et al. 2016), showing reduced levels of ocular inflammation, as well as an increase of the likelihood of preserving visual acuity (more than 90% in some cases), and an increases in the quality of life of uveitis patients (Fabiani et al. 2019; Leal et al. 2019; Sharma et al. 2019). Despite this, current therapies for uveitis are not optimal, and around 35% of patients remain visually disabled with a demonstrably poor quality of life (Rothova et al. 2004; Tugal-Tutkun et al. 2004; Murphy et al. 2007; Babu and Mahendradas 2013). Furthermore, TNFα inhibitors are effective in patients refractive to CS and antimetabolites but in some cases, they stop working after a time and also increase the risk of infection (Sharma, Dick, and Ramanan 2009).

Targeting the IL-23/IL-17 axis is could be an attractive alternative to TNFα inhibitors when treating anterior uveitis. Previous *in vivo* animal studies have shown that IL-23, in the absence of any other inflammatory signal, can drive inflammation in many of the tissues associated with SpA (Reinhardt et al. 2016; Sherlock et al. 2012; Chen et al. 2018; Chen et al. 2020). These include the axial skeleton, skin, and gut. Mice with systemic IL-23 overexpression achieved through DNA mini-circle injection, using the same IL-23 hyperkine sequence as in this study, also developed mild psoriatic skin lesions with epidermal thickening, aortic valve inflammation, an

accumulation of γ/δ T cells at the entheseal tissue in spine and ankle joints, aortic valve and root, and most interesting to this study within the anterior compartment of the eye (Reindhardt et al. 2016). In addition elevated levels of IL-23 were identified in: (A) serum (Mei et al. 2011; Ugur et al. 2015) and in intestinal biopsy samples (Ciccia et al. 2009) from AS patients; (B) in human psoriatic skin (Lee et al. 2004); and (C) serum (Przepiera-Będzak, Fischer, and Brzosko 2016) and vitreous fluid (Velez et al. 2016) of patients with specific uvitides. Furthermore, IL-23A gene copy number variants greater than 2 in the peripheral blood have been associated with Behçet's disease uveitis and Vogt–Koyonagi–Harad uveitis (Hou et al. 2015). However, all of these studies have caveats which will be discussed in greater detail and compared to the data of this study towards the end of Chapter 2. Importantly, previous studies have found that the absence of IL-23 leaves mice resistant to EAU (Luger et al. 2008; Sun et al. 2015).

IL-23p19 blockade has been proven to significantly modify certain human diseases that share key clinical and pathophysiological features with SpA, including psoriasis, PsA, and IBD. Significant disease modification has been seen in clinical trials of patients with active psoriasis, with Psoriasis Area and Severity Index (PASI)100 response rates between 50-70% following IL-23p19 inhibition (tildrakizumab) (Blauvelt et al. 2017; Reich et al. 2017; Papp et al. 2017). More modest improvements have also been recorded for PsA – both synovial and entheseal disease (Mease et al. 2020). In Crohn's disease, IL-23p19 inhibition (risankizumab) has demonstrated efficacy of disease modification in phase II and III trials (Feagan et al. 2017). Interestingly, despite all the disease associations and the shared underlying genetics , the most recent study of risankizumab in patients with active AS failed to meet the primary endpoint (Ankylosing Spondylitis Disease

Activity Score with an improvement of 40% (ASDAS40) at week 12), with no improvements in clinical or MRI outcomes compared with placebo (Baeten et al. 2018), whereas secukinumab (the inhibitor targeting the IL-17 cytokine which is downstream of IL-23) was demonstrated to have efficacy in disease modification of AS (Baeten et al. 2015).

Clinical trials have so far pointed towards the non-efficacy of the anti-IL-17A agent, secukinumab when administered subcutaneously in patients with non-infectious uveitis (Dick et al. 2013; Letko et al. 2015). However, when secukinumab was administerd intravenously at 30 mg/kg and 10 mg/kg it produced statistically higher responder and remission rates. In addition, ustekinumab, which targets the p40 subunit that is shared by both IL-23 and IL-12, has been reported to have effectively controlled uveitis in 2 patients treated for either coexisting severe PsA and plaque psoriasis, or Behçet's disease (Baerveldt et al. 2013; Mugheddu et al. 2017). Together these clinical trials highlight the important role of both IL-23 and IL-17A signalling in non-infectious uveitis. The Letko et al. (2015) study also raises the issue that biodistribution may be key to getting efficacy in the eye. Unless drugs reach the specific location needed within the eye in order to act, they may have limited efficacy which might account for why subcutaneous doses of secukinumab did not work. Unless one shows that a specific drug gets to the right site(s) and engages its target there, one can't be sure that a negative clinical outcome is not simply attributable to a problem with drug biodistribution. How high does an IV dose have to be administered before the concentration within the eye reaches a level that has efficacy? This answer could be achieved in potential future clinical trials by measuring the concentration of secukinumab or ustekinumab in the aqueous humour of patients.

Despite the close relationship of IL-23 and IL-17, similar responses to IL-23 and IL-17 inhibition are not always observed in human diseases. Several diseases report efficacy of both IL-12/23 and IL-17A inhibitors. Very good results were obtained using either the anti-IL-23 (p19) agent guselkumab, the anti-IL-23 (p40) agent ustekinumab, and secukinumab an IL-17 inhibitor in psoriasis trials (Gordon et al. 2015; Thaçi et al. 2015). Other studies have reported positive results for both skin and joint disease in PsA with guselkumab, and the anti-IL-17A agents, secukinumab and ixekizumab (Mease et al. 2015; Mease et al. 2017; Deodhar et al. 2018). However, in Crohn's disease, moderate efficacy was observed with either ustekinumab or the anti-IL23 (p19) agent, risankizumab (Feagan et al. 2016; Feagan et al. 2018), whereas poor efficacy, or even worsening of disease, was observed if these patients were treated with secukinumab (Hueber et al. 2012). Two further placebo-controlled trials in AS, one with ustekinumab (Deodhar et al. 2019) and one with risankizumab (Baeten et al. 2018), did not show efficacy for the IL-23 blocking agents above those of placebo on disease activity, despite the IL-17 inhibitors, secukinumab and ixekizumab being quite effective for the treatment of AS (Baeten et al. 2015; van der Heijde et al. 2018).

The efficacy of IL-17 inhibitors in treating enthesitis has also been analysed, and positive effects over placebo have been reported using ixekizumab (Mease et al. 2017) and secukinumab (McInnes et al. 2015) in PsA trials. However, in trials of AS using ustekinumab (Deodar et al. 2019) it was interesting to note that this inhibitor was: (A) better than placebo at treating PsA-associated enthesitis (McInnes et al. 2013); (B) it was superior to tumor necrosis factor inhibitors (TNFi) in an open-label study for treating peripheral enthesitis (the choice of TNFi was dependant on individual patient's preferences related to the route and frequency of administration)

(Araujo et al. 2019); and (C) it was superior in reducing enthesitis (as measured by ultrasonography) in patients with psoriasis who had subclinical enthesitis (Savage et al. 2019). However, a prospective, double-blind controlled trial of an IL-23 inhibitor that includes patients with peripheral enthesitis and measures changes in enthesitis as a primary outcome criterion is needed to determine the effects of IL-23 blockade on enthesitis that are different from its effects on axial manifestations.

In psoriasis, monocytes produce IL-23 in the skin, thereby increasing local production of IL-17 by T cells (Noack, Ndongo-Thiam, and Miossec 2016). In this situation, blocking either IL-23 or IL-17 will be effective at the effector site, as is observed in the clinic. By contrast, at sites in the bone or synovium, the requirement for monocytes (and IL-23) is limited because they are not needed for the local production of IL-17. Thus, blocking IL-23 would be ineffective in this situation, unlike blocking IL-17. This hypothesis might imply that the biological effects of IL-23 on various tissues are mostly indirect via IL-17 release (Yago et al. 2007). In contention to this theory, it has been suggested that IL-23 is generated in the gut in response to microbiota in AS, which subsequently disseminates in the blood stream to the sterile axial entheses (Cua and Sherlock 2011). The controversial studies mentioned earlier - that show higher levels of IL-23 in the serum of patients with AS, support this theory.

With regards to eye disease, phase 3 clinical trials have so far pointed towards the non-efficacy of secukinumab in patients with non-infectious uveitis (Letko et al. 2015), whereas, ustekinumab has been reported to have effectively controlled uveitis in 2 patients treated for coexisting severe psoriatic arthritis and plaque psoriasis or Behçet's disease (Baerveldt et al. 2013; Mugheddu et al. 2017). The promising results of the effectiveness of ustekinumab in non-infectious uveitis are

being followed up in the ongoing phase 2 clinical trials: STELARA https://clinicaltrials.gov/ct2/show/NCT02911116) and STELABEC (https://clinicaltrials.gov/ct2/show/NCT02648581).

Together these findings have prompted the question of whether (and in what way) the IL-23–IL-17 pathway is a potential target for the treatment of chronic diseases including non-infectious uveitis. The microenvironment of the tissue-specific inflammation in each disease and the time point at which each tissue is studied in each disease are important when elucidating the differences in IL-23 and IL-17 function.

An important difference has been observed *in vitro* in the interactions between mesenchymal cells of different origins and IL-17-secreting cells. In the presence of bone marrow-derived or synovium-derived mesenchymal cells, the interaction between activated T cells and these mesenchymal cells is sufficient for the production of large amounts of IL-17 without an obvious need for monocytes or IL-23 (Noack et al. 2016a). By contrast, in interactions between skin-derived mesenchymal cells and activated T cells, the presence of monocytes and production of IL-23 is important for the production of IL-17 (Noack, Ndongo-Thiam, and Miossec 2016). In the latter study, the removal of monocytes (and consequently IL-23) resulted in reduced IL-17 production. This data suggests a differential contribution of monocytes (and IL-23) to the local production of IL-17 depending on the nature of cell–cell interactions present at different anatomical sites.

Data exist that suggest the possibility of a partial uncoupling of IL-23 and IL-17 secretion under certain circumstances. In a study in mice, IL-17A regulated the tight junction protein occludin during epithelial injury in the gut and had a protective

function (Lee et al. 2015). In this investigation, IL-17 was produced by local γδ T cells and its production was independent from IL-23. However, IL-23-dependent production of IL-17 by γδ T cells has also been described (Sherlock et al. 2012; Reinhardt et al. 2016). In another study, a mouse model of colitis was worsened by IL-17 inhibition, whereas IL-23 inhibition decreased colonic inflammation and enhanced regulatory T cell accumulation (Maxwell et al. 2015), providing further evidence of a possible uncoupling of IL-23 and IL-17 function (Moschen et al. 2019). In EAE, dual inhibition of IL-23 and IL-17 was more effective than targeting either cytokine alone (Mangan et al. 2015), indicating again that IL-23 and IL-17 production might be partly uncoupled.

Despite the strong genetic and clinical associations of uveitis with SpA, and the evidence that IL-23 is sufficient to drive inflammation at other distinct anatomical sites affected by disease associated with SpA in multiple animal models, the role of IL-23 and IL-23 responsive cells has not yet been shown within the eye.

IL-23 and IL-23R – structure and function

IL-23 is a heterodimer consisting of the subunits IL-23p19 and IL-12p40. IL-23p19 was discovered as a novel sequence in a computational screen performed by Oppmann and colleagues (2000). It is structurally similar (70% identical) to IL-12p35, IL-6 and granulocyte colony-stimulating factor (G-CSF). IL-23p19 only becomes biologically active when it combines with the IL-12p40 subunit. The cells most commonly associated with IL-23 production are dendritic cells (DCs) and macrophages, specifically in response to inflammatory or biochemical insult (Wohn et al. 2013; Arnold et al. 2016). Upon expression and released by the cells, IL-23 is recognised by its receptor IL-23R, also a heterodimer, consisting of the subunits IL-12Rb1 and IL-23R - also discovered by Oppmann and colleagues (2000).

Binding of IL-23 to its receptor, initiates a signalling cascade phosphorylating and activating janus kinase (Jak) 2, then signal transducer and activator of transcription (STAT) 3 (Levin and Gottlieb 2014) which forms a complex with retinoic acid-related orphan receptor gamma t (ROR-γt) and interferon regulatory factor (IRF) 4, ultimately leading to increased expression of the pro-inflammatory cytokines IL-17, and IL-22 **(Figure 1.6)** (Mathur et al. 2007; Zhou et al. 2007)

This signalling cascade also allows IL-23R to be regulated via a positive feedback loop, as STAT3 directly binds to the *IL-23R* locus (Hirahara et al. 2010; Ghoreschi et al. 2010; Zúñiga et al. 2013). Furthermore, IL-23 signalling can create its own positive feedback loop under specific conditions to maintain pathogenicity, as it induces expression of granulocyte-macrophage colony stimulating factor (GM-CSF) in T helper 17 (T_H17) cells and this GM-CSF then goes on to promote further IL-23 by antigen presenting cells (APCs) (El-Behi et al. 2011).

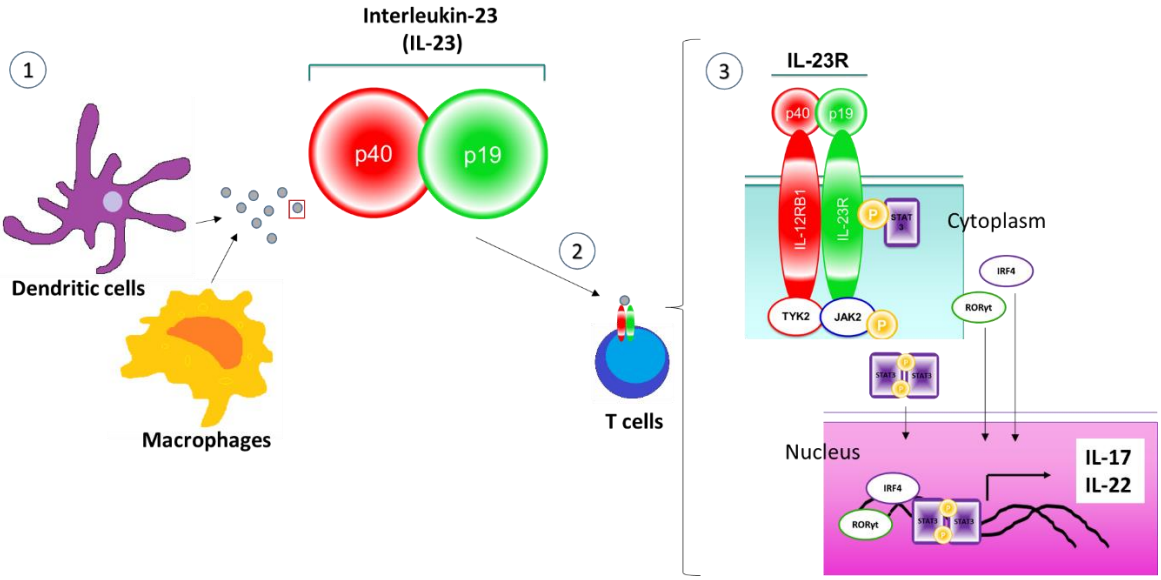


Figure 1.6: IL-23 signalling through IL-23R on T cells. Source of diagram - author's own work. The heterodimeric cytokine IL-23 (consisting of the subunits IL-23p19 and IL-12p40) is predominantly produced by dendritic cells and macrophages at barrier surfaces (1). IL-23 is recognised by its receptor IL-23R, also a heterodimer, consisting of the subunits IL-12Rb1 and IL-23R which among other cells is found on the surface of certain sub-populations of T cells (2). Binding of IL-23 to its receptor initiates (3) a signalling cascade phosphorylating and activating janus kinase (Jak) 2, then signal transducer and activator of transcription (STAT) 3 which forms a complex with retinoid-related orphan receptor-γt (ROR-γt) and interferon regulatory factor (IRF)-4, ultimately leading to increased expression of the pro-inflammatory cytokines IL-17, and IL-22

IL-23 expression profile

Due to the lack of availability of sensitive and specific antibodies against IL-23R in both mouse and human, Parham et al. (2002) used qPCR to determine the mRNA expression levels of the two IL-23R subunits in a number of human cell lines. Human *IL-23R* mRNA was expressed at a moderate level by human T_H1 and T_H0 clones as well as several NK cell lines and clones. cDNA libraries that were prepared from several cultured monocyte and dendritic cell populations expressed very low levels of *IL-23R* mRNA. In addition, relatively low but detectable human *IL-23R* mRNA levels were observed in EBV-transformed B cells and anti-CD3/anti-CD28/LPS-activated peripheral blood mononuclear cells (PBMC). Furthermore, very low levels of human *IL-23R* and *IL-12Rb1* mRNA were shown to be expressed individually or

co-expressed by bone-marrow derived macrophages under certain stimulatory conditions.

In a later study, Awasthi et al. (2009) generated and utilised IL-23R-GFP.KI reporter mice (where an IRES-GFP cassette was introduced after exon 8 in the endogenous IL-23R gene) to show for the first time that IL-23R is expressed by both adaptive and innate immune cells by flow cytometry. These IL-23R+ cells were observed in the spleen, lymph nodes and lamina propria (with ~3% of all CD45+ leukocytes in the lamina propria expressing IL-23R). Among adaptive immune cells, a small population of CD4+ T cells were shown to express IL-23R. Among innate immune cells, a large population of γδ T cells, a small fraction of CD11b+ macrophages/monocytes, CD11c+ DCs, and CD45+CD3-CD4+ cells [which the authors presumed to be lymphoid tissue inducer (LTi) cells], were shown to express IL-23R. In fact, 40% of γδ T cells in the lymph node and 65% of γδ T cells in the lamina propria, were IL-23R positive, indicating that IL-23R tends to be expressed by more cells in non-lympoid tissues as opposed to secondary lymphoid organs.

Other studies have shown IL-23R expression on αβ double-negative T cells (Sherlock et al. 2012), γδ T cells (Haas et al. 2009; Martin et al. 2009; Sutton et al. 2009), T_H17 cells (Aggarwal et al. 2003; Ghoreschi et al. 2010; McGeachy et al. 2009; Murphy et al. 2003), innate lymphoid cell type 3 ILC3s (Buonocore et al. 2010; Cuthbert et al. 2017), induced natural killer T (iNKT) cells (Satoh-Takayama et al. 2008; Cella et al. 2009; Luci et al. 2009; Sanos et al. 2009), NKp44+ natural killer (NK) cells and LTi-like cells (Cella et al. 2009; Crellin et al. 2010).

Although the focus of this study was to determine the presence of IL-23R on T lymphocytes in the eye, it is important to reinforce the point that the evidence of IL-

23R on myeloid cells is much more challenging and controversial than the well-known presence on lymphoid cells. Especially because myeloid cells are present in the mammalian eye (McMenamin 1997; McMenamin, Saban, and Dando 2019) and because myeloid cells are definitely indirect downstream responders to the IL-23 pathway activation (IL-23 induces IL-17 in lymphoid cells and IL-17 then causes elaboration of G-CSF from stroma which causes the bone marrow to produce more neutrophils). The original characterisation of IL-23R+ macrophages in mice by Awasthi et al (2009) was based on the observation of a IL-23R GFP+ CD11b+ subset residing in the lymph nodes. However, this phenotyping is insufficient to confirm that these cells are macrophages, since activated T cells, which are known to express IL-23R, can also express CD11b (Bullard et al. 2005). Furthermore, the same animal study confirmed that expression of CD11b by T cells is necessary for the pathogenesis of EAE.

More important than surface phenotyping of IL-23R is the observation of IL-23R functionality. Just because a reagent informs that cells are IL-23R+ it does not prove that a cell can respond to IL-23. Therefore, the observation of IL-23R+ CD11b+ cells by Awasthi et al. (2009) is not evidence that these cells have functional IL-23R activity. Confounding is an even greater aspect of the earlier work by Parham et al. (2002), especially seeing as just a small number of contaminating lymphoid cells could easily respond and confound the assay (using bulk PCR) if one didn't realise that there were lymphoid cells present.

Looking closely at cells with functionality of IL-23R, more recent studies have shown that; (A) ILC3s in the gut produce IL-22 in response to *in vivo* and *ex vivo* IL-23 stimulation (Cella et al. 2009; Sanos et al. 2009; Crellin et al. 2010; Chen et al. 2015); (B) mouse LTi cells strongly express *IL-23R* mRNA transcripts (Takatori et

al. 2009); (C) IL-23R expression on ILC3s is essential for IL-17A and IFNγ as well as the development of IL-23 mediated colitis in C57BL/6 $Rag1^{-/-}$ mice (Buonocore et al. 2010); (D) IL-23 induces *IL-23R* mRNA expression on peritoneal neutrophils from C57BL/6 mice (Chen et al. 2016); and (E) primary neutrophils freshly isolated from the bone marrow of C57BL/6 mice produce *il17a, il17f, and il22* mRNA in response to *in vivo* IL-23 stimulation (Li et al. 2018).

Before the discovery of IL-23 by Oppmann et al. (2000), it was believed that IL-12 was responsible for the response of T_H1 to intracellular viral and bacterial infections, through the specific production of interferon (IFN)-γ and was predicted to be the driving factor for autoimmune inflammation (Mosmann et al. 1986). However, it was also well recognised that IFN-γ and its receptor (IFN-γR) were not necessary for the development of EAE, a prototypical autoimmune model of brain inflammation (Ferber et al. 1996; Willenborg et al. 1996). Moreover, IFN-γ ablation or IFN-γR knockout in animal models showed significantly worse EAE pathology (Willenborg et al. 1996; Billiau et al. 1988; Lublin et al. 1993). To add to the confusion, it was reported that IL-12p40 was essential for EAE development, although the IL-12p35 subunit of the IL-12 heterodimer was not (Becher, Durell, and Noelle 2002). Blockade of IL-12 receptor subunit β2 (IL-12Rβ2) also did not ameliorate disease pathology (Zhang et al. 2003).

A seminal paper that highlighted the importance of IL-23 in inflammatory responses came almost 20 years ago from the utilisation of EAE murine model (Cua et al. 2003). Here, Daniel Cua and colleagues showed that Interleukin-23 rather than IL-12 is the critical cytokine for autoimmune inflammation of the brain. Furthermore, the importance of IL-23 in inflammatory arthritis was also shown in the same year (Murphy et al. 2003). Additional work using mice deficient in IL-12, IL-23 , or both,

also showed that EAE was dependent on IL-23, and polarizing of CD4 T cells to IL-17/IL-22 producing T_H17 cells (Parham et al. 2002). However, IL-23R expression on the presence of RAG2 independent cells is dispensable for the development of EAE which adds to the controversy of the presence and role of IL-23R on myeloid cells, dendritic cells and neutrophils (Awasthi et al. 2009).

Previous animal studies have also indicated that IL-23 is one of the key factors in the pathophysiology of diseases associated with SpA. Direct intradermal administration of IL-23, but not IL-12 in mouse skin, resulted in epidermal hyperplasia associated with parakeratosis, erythema, and mixed leukocyte dermal infiltrate resulting in the upregulation of a pro-inflammatory gene signature (IL-19 and IL-24), all of which are observations in human psoriasis (Chan et al. 2006). In addition, IL-23 overexpression in the mouse gut resulted in both T cell and ILCs mediated chronic intestinal inflammation, with accumulation of leukocytes within the lamina propria resulting in the upregulation of pro-inflammatory gene signature (IL-17, IL-6, IL-1β and TNFα) (Lee et al. 2004; Yen et al. 2006; Ciccia et al. 2009; Ahern et al. 2010; Buonocore et al. 2010). Furthermore, over-expression of IL-23 by hepatic injection of *IL23* minicircles, was shown to be sufficient to drive enthesitis and aortitis in mice through resident IL-23R+CD4-CD8-TCRγδ+ T cells (Sherlock et al. 2012; Reinhardt et al. 2016).

To date the critical role of IL-23 and IL-23 responsive T cells in the pathogenesis of anterior uveitis associated with SpA has not been fully investigated. Therefore, each subsequent chapter in this thesis will address the following research questions: (A) If IL-23 overexpression is sufficient to drive T cell mediated uveitis; (B) The phenotype and localisation of T cells in the anterior compartment of the eye; and (C) If the same IL-23–dependent γ/δ resident T cell population found in the axial

skeleton in mice is present in the anterior compartment of the eye in both mice and humans.

Chapter 2

IL-23 overexpression is sufficient to drive T cell mediated uveitis.

Introduction

Interleukin (IL)-23 - a link between uveitis and spondyloarthropathy

The uveitides are a heterogenous group of conditions characterised by inflammation of the uvea and its adjacent structures. Any portion of the uvea can become inflamed; this has resulted in multiple subtypes of uveitis being labelled according to anatomical location (Jabs et al. 2005). Subtypes can be further characterised based on whether disease is bilateral or unilateral, if disease is chronic or episodic, whether the onset was sudden or insidious, whether it is idiopathic, genetics, and patient age and gender (Rosenbaum et al. 2019). Furthermore, little is known about disease aetiology. The heterogeneity of uveitis has multiple implications in diagnosing disease and choosing the correct approach to therapy. It has been stated by senior opthalmologists that this has resulted in most forms of non-infectious uveitis being "approached with the use of a treatment algorithm that is not impacted by the cause of the uveitis" (Rosenbaum and Dick 2018). Heterogeneity of disease has impacted the ability to design clinical trials, such that uveitis cases of multiple aetiologies are usually eligible for recruitment into one trial (Dick et al, 2013; Letko et al. 2015; Nguyen et al. 2016; Tugal-Tutkun et al. 2017).

One particular subtype of uvieitis, non-infectious anterior uveitis, has strong genetic associations (HLA-B27 genotype and IL-23R polymorphisms) with a group of rheumatic diseases known as the spondyloarthropathies (SpA) (Brewerton et al. 1973; Rosenbaum 1989; Monnet et al. 2004; Duerr et al. 2006; Dong et al. 2013; Haroon et al. 2015; Hou, Kijlstra, and Yang 2015; Juanola, Loza Santamaría, and Cordero-Coma 2016; Jung et al. 2017). In addition, there is the clinical association of elevated levels of IL-23, although all of the studies supporting this finding have

caveats which will be discussed later in the chapter. (Cicca et al. 2009; Mei et al. 2011; Hou et al. 2015). The ability of IL-23, in the absence of any other inflammatory signal, to drive inflammation in many of the tissues associated with SpA (the axial skeleton, skin, and gut) has been shown in animal studies (Chan et al. 2006; Buonocore et al. 2010; Sherlock et al. 2012; Reinhardt et al, 2016). Inflammation in these animal studies also closely mimics the human pathology.

Systemic overexpression of IL-23 in mice has shown the accumulation of a small number of γδ T cells proximal to the anterior uvea (Reinhardt et al, 2016). Alternatively, the knock out of the unique IL-23 p19 subunit in mice confers protection to animals in EAU (Luger et al. 2008). Furthermore, ustekinumab, which targets the p40 subunit that is shared by both IL-23 and IL-12, has been reported to have effectively controlled uveitis in 2 patients treated for coexisting severe PsA and plaque psoriasis or Behçet's disease (Baerveldt et al. 2013; Mugheddu et al. 2017). These encouraging observations are being further investigated in the ongoing phase 2 clinical trials: STELARA (https://clinicaltrials.gov/ct2/show/NCT02911116) and STELABEC (https://clinicaltrials.gov/ct2/show/NCT02648581). Together this data encourages the investigation of an animal study that addresses the significance of IL-23 overexpression specifically within the eye to elucidate the role of this cytokine in non-infectious uveitis.

The cells which respond to IL-23 in animal studies vary with each tissue and show temporal segregation between innate (early response) and adaptive cells/infiltrating cells (during established disease). IL-23 overexpression results in both T_H17 and ILC3 mediated chronic intestinal inflammation (Wang et al. 2017). The same is true for psoriatic skin (Chan et al. 2006; Ward and Umetsu 2014). In contrast, entheseal inflammation at axial sites as a result of systemic IL-23 overexpression is mediated

by a rare population of resident CD4-CD8- T cells (Sherlock et al. 2012; Reinhardt et al, 2016).

Although extensive work has been done to characterize resident leukocyte populations within the uvea and its associated structures, revealing the presence of a diverse macrophage nomenclature, DCs and mast cells (McMenamin 1997, 1999), there has been no documentation of resident lymphoid cells in these tissues, and there is no evidence suggesting the presence of a sentinel cell that is capable of responding to IL-23. Evidence is limited to the few studies which have shown T cells trafficking through the healthy eye. CD4+ T cells have been imaged by fluorescent microscopy trafficking through the vessels of the choroid in the posterior compartment of normal mice (McMenamin, Saban, and Dando 2019). Another study has documented γδ T cells inside the vessels of the choroid in the posterior compartment in healthy human donor eyes (Zhao et al. 2017).

It is a well-established hypothesis that IL-23 is a unifying factor in the pathophysiology of SpA and suggest that targeting IL-23 may present a common approach to the treatment of diseases including psoriasis, PsA, IBD, and AS which often share clinical and genetic commonalities, I hypothesise that IL-23 is a factor that links non-infectious uveitis to SpA. However, due to the heterogeneity of uveitides it is would be very difficult to design a clinical trial to address this theory.

Animal studies allow the induction of disease in animals which follows the same aetiology, providing lots of tissue for analysis. Current animal models for the study of uveitis, such as EAU and EIU do not fit the seronegative immune response of SpA and do not address the specific IL-23 dysregulation linking SpA to uveitis. EAU is predominantly T-cell mediated but is antigen directed, and EIU is a simple LPS

innate stimulus used to mimic bacterial infection (reviewed in Bansal et al. 2015). Injection of IL-23 and systemic overexpression of IL-23 and in mice has been shown to be sufficient to replicate the clinical aspects of human SpA at barrier and junctional sites (Chan et al. 2006; Sherlock et al. 2012; Reinhardt et al, 2016). This approach represents a promising alternative to the animal models previously mentioned to study SpA pathology in the eye. Local injection of functional IL-23 into the inner eye would not be a suitable methodology as it would not remain in the eye for a long enough time or at a high enough concentration to trigger ocular disease due to its short half-life. Systemic IL-23 overexpression may also not be able to reach specific regions of the eye due to blood-occular barriers (one aspect of ocular immune privilege (Lugossy 1957; Shiose 1970; Smith 1971; Raviola 1974) and the effectiveness of the aqueous outflow system (Cunha-Vaz and Maurice 1967; Bito 1970, 1977). However, localised IL-23 overexpression had potential.

By establishing a new mechanism of endogenous, localised overexpression of IL-23 in the mouse inner eye, utilising gene transfer, I propose that IL-23 will be sufficient and necessary to drive uveitis - due to the presence of resident γδ T cells, which are similar in phenotype to those found within the musculoskeletal entheses (Sherlock et al. 2012; Reinhardt et al, 2016).

Gene Transfer

In this Chapter, gene transfer will be utilised to assess if endogenous, localised, IL-23 overexpression is necessary and sufficient to drive immune mediated inflammation of the mouse anterior uvea and its related structures. Gene transfer is the strategy of endogenously producing a target protein encoded by DNA (known as the transgene) in selected cells (Kaji and Leiden 2001). The eye is ideal for localised gene transfer – structurally it is easily accessible, highly

compartmentalised, and ‘relatively’ sequestered from the rest of the body by the blood–retinal and blood-aqueous barriers (Yücel et al. 2009). The compartmentalised nature of the eye and ‘relative’ biological independence of each eye also allows the contralateral eye to function as an effective experimental control tissue, limiting the number of mice that would need to be sacrificed. In addition, there are well-characterised animal disease models of the eye available – including EAU and endotoxin induced uveitis (EIU) (Bansal et al. 2015). Furthermore, there are non-invasive methods for imaging the eye and measuring changes in ocular function in mice (Lai 2021) allowing for longitudinal study.

The highly compartmentalised anatomy of the eye permits cells to be targeted effectively either by intravitreal injection or subretinal delivery of relatively modest doses of vector. In addition, ocular cell populations are typically very stable. The lack of cell division allows the use of non-integrating vector systems for sustained transgene expression without the risk of malignant transformation of cells following the use of integrating vector systems. However, the age and disease status of the retina itself can affect transduction patterns (Pang et al. 2006)

In the past gene transfer has been utilised extensively to investigate the overexpression of a number of genes associated with are inherited retinal diseases, generally of monogenic deficiency (autosomal recessive) in animals (Retinal Information Network: https://sph.uth.edu/retnet/sum-dis.htm#C-complex) (55 of which are reviewed in Liu et al. 2011). The mechanisms responsible for DNA transfer in the studies reviewed by Liu and colleagues (2011) differ, essentially viral vs non-viral (liposomes, plasmid electroporation etc). However, DNA transfer by viral vector is now more common, as it results in higher levels of expression and more persistent expression in general.

Selection of an appropriate viral gene delivery system is critical. Although the first reported study on the development of gene transfer for uveitis utilised a second-generation adenoviral vector to treat EAU in rodents, the utility of adenoviral vectors for this purpose was limited by the strong immune responses they elicited (de Kozak et al. 2002). The most promising vectors to date for use in the eye are those based on adeno-associated virus (AAV) and lentiviruses (Chu et al. 2012). HIV-1 based vectors have also been used to successfully transduce anterior segment structures in order to treat EIU (Trittibach et al. 2008). Various non-viral gene transfer techniques have been used in the eye, but thus far they are, without exception, inefficient and limited in duration compared with effective viral vectors. In experimental animal models of EAU, viral vectors have been used to deliver immunomodulatory genes including: IL-10, IL-1 receptor antagonist, interferon-alpha (IFNα), soluble TNFα receptors, and alpha-melanocyte stimulating hormone (MSH), which have resulted in the successful attenuation of disease (gene therapy) (reviewed in Chu et al. 2012).

Many variants (serotypes) have been identified for AAV, enhancing their desirability as a vector platform. Many of these variants have unique transduction characteristics, defined by their protein outer shell (capsid), that can be used to target different ocular cell types (Liu et al. 2011). The ShH10 serotype is an artificial AAV serotype based upon AAV6 generated by a technique of directed *in vivo* evolution, combined with a tyrosine to phenylalanine mutation in the capsid (Klimczak et al. 2009). It was chosen for use in this study as it has been shown to generate widespread transduction of both the posterior compartment (Muller cells) and anterior compartment (ciliary body epithelial cells) of the eye in a single intravitreal injection (Klimczak et al. 2009; Wu et al. 2020).

This study is not the first to utilise gene transfer to study the overexpression of target genes coding for pro-inflammatory cytokines within the eye (Da Cunha et al. 2018). However, to my knowledge this is the first study that uses gene transfer to model aspects of the pathogenesis of anterior uveitis using specifically IL-23 overexpression. Similar to IL-1β and TNFα (Da Cunha et al. 2018), I hypothesis that IL-23 is sufficient and necessary to drive ocular inflammation in the absence of any other inflammatory stimuli.

Aims

- To validate whether the ShH10 AAV vector encoding an IL-23 transgene leads to endogenous IL-23 expression following intravitreal administration.
- To demonstrate whether overexpression of IL-23 in the eye is sufficient to overcome mechanisms of immune privilege to drive inflammation via the recruitment of immune cells.
- To phenotype the populations of resident and infiltrating immune cells in the eye following local endogenous IL-23 overexpression.
- To determine whether a population of resident IL-23 responsive T cells is present.

Materials and methods

Animal strains and husbandry

Adult (6-8 week old) female C57BL/6J were purchased from Charles River Laboratories, Oxford. B10.RIII and B6.Cg-Thy1 (recombination activation gene (Rag)2 KO) were provided from established breeding colonies in the Animal Services Unit at Bristol University, Bristol. Mice were confirmed as negative for the Rd8 mutation (Mattapallil et al. 2012). All mice were housed under specific pathogen free conditions with food and water ad libitum. All procedures were conducted in concordance with the United Kingdom Home Office licence (PPL 30/3281) and were approved by the University of Bristol Ethical Review Group. The study also complied with the Association for Research in Vision and Ophthalmology (ARVO) Statement for Use of Animals in Ophthalmic and Vision research.

An overview of the ShH10 IL-23 AAV production process

Generation of adeno-associated virus (AAV) ShH10 serotype encoding IL-23 hyperkine (ShH10 IL-23 AAV) (curtesy of Dr Colin Chu) was conducted in collaboration with Professor Andrew Dick's research group at The University of Bristol within the Biomedical Sciences Department. The genomic ShH10 capsid and pHGTI helper plasmids were grown in DH5α bacteria, cultured for 16 hours in Miller's LB broth (Merck, UK) with ampicillin selectivity. DNA was isolated using an EndoFree Plasmid Mega Kit (Qiagen, Valencia, USA). The final vector was checked to be below 5 EU/ml using a LAL test during production.

Synthesis of mouse IL-23 sequence

The sequence was synthesized in collaboration with Professor Andrew Dick's research group at The University of Bristol within the Biomedical Sciences

Department. All synthesis was performed by GenScript, Piscataway, USA. Mouse IL-23 artificial hyperkine (a term coined by the DNAX Research institute that describes two protein subunits connected by a synthetic linker - GSGSSRGGSGSGGSGGGGSKL), consisting of mouse IL-12p40 and p19 as one sequence (Oppmann et al. 2000), shown below, with flanking restriction enzyme sites and ligated into a pD10-CMV plasmid **(Figure 2.1A)**. In an animal model this IL-23 hyperkine has been shown to drive pathology strongly resembling human autoimmune inflammatory conditions including psoriasis (Chan et al. 2006) and AS (Sherlock et al. 2012).

AATGTCTGCACTTCTGATCTTAGCTCTTGTTGGAGCTGCAGTTGCTGACTACAAAGACGATGA
CGACAAGCTTATGTGGGAGCTGGAGAAAGACGTTTATGTTGTAGAGGTGGACTGGACTCCCG
ATGCCCCTGGAGAAACAGTGAACCTCACCTGTGACACGCCTGAAGAAGATGACATCACCTGG
ACCTCAGACCAGAGACATGGAGTCATAGGCTCTGGAAAGACCCTGACCATCACTGTCAAAGA
GTTTCTGGATGCTGGCCAGTACACCTGCCACAAAGGAGGCGAGACTCTGAGCCACTCACATC
TGCTGCTCCACAAGAAGGAAAATGGAATTTGGTCCACTGAAATTTTGAAAAATTTCAAAAACAA
GACTTTCCTGAAGTGTGAAGCACCAAATTACTCCGGACGGTTCACGTGCTCATGGCTGGTGC
AAAGAAACATGGACTTGAAGTTCAACATCAAGAGCAGTAGCAGTTCCCCTGACTCTCGGGCA
GTGACATGTGGAATGGCGTCTCTGTCTGCAGAGAAGGTCACACTGGACCAAAGGGACTATGA
GAAGTATTCAGTGTCCTGCCAGGAGGATGTCACCTGCCCAACTGCTGAGGAGACCCTGCCCA
TTGAACTGGCGTTGGAAGCACGGCAGCAGAATAAATATGAGAACTACAGCACCAGCTTCTTCA
TCAGGGACATCATCAAACCAGACCCGCCCAAGAACTTGCAGATGAAGCCTTTGAAGAACTCA
CAGGTGGAGGTCAGCTGGGAGTACCCTGACTCCTGGAGCACTCCCCATTCCTACTTCTCCCT
CAAGTTCTTTGTTCGAATCCAGCACAAGAAAGAAAAGATGAAGGAGACAGAGGAGGGGTGTA
ACCAGAAAGGTGCGTTCCTCGTAGAGAAGACATCTACCGAAGTCCAATGCAAAGGCGGGAAT
GTCTGCGTGCAAGCTCAGGATCGCTATTACAATTCCTCGTGCAGCAAGTGGGCATGTGTTCC
CTGCAGGGTCCGATCCGTTCCTGGAGTAGGGGTACCTGGGGTGGGCCTGGCTGTGCCTAGG
AGTAGCAGTCCTGACTGGGCTCAGTGCCAGCAGCTCTCTCGGAATCTCTGCATGCTAGCCTG
GAACGCACATGCACCAGCGGGACATATGAATCTACTAAGAGAAGAAGAGGATGAAGAGACTA
AAAATAATGTGCCCCGTATCCAGTGTGAAGATGGTTGTGACCCACAAGGACTCAAGGACAACA
GCCAGTTCTGCTTGCAAAGGATCCGCCAAGGTCTGGTTTTTTATAAGCACCTGCTTGACTCTG
ACATCTTCAAAGGGGAGCCTGCTCTACTCCCTGATAGCCCCATGGAGCAACTTCACACCTCC
CTACTAGGACTCAGCCAACTCCTCCAGCCAGAGGATCACCCCCGGGAGACCCAACAGATGCC
CAGCCTGAGTTCTAGTCAGCAGTGGCAGCGCCCCCTTCTCCGTTCCAAGATCCTTCGAAGCC
TCCAGGCCTTTTTGGCCATAGCTGCCCGGGTCTTTGCCCACGGAGCAGCAACTCTGACTGAG
CCCTTAGTGCCAACAGCTTAAGC.

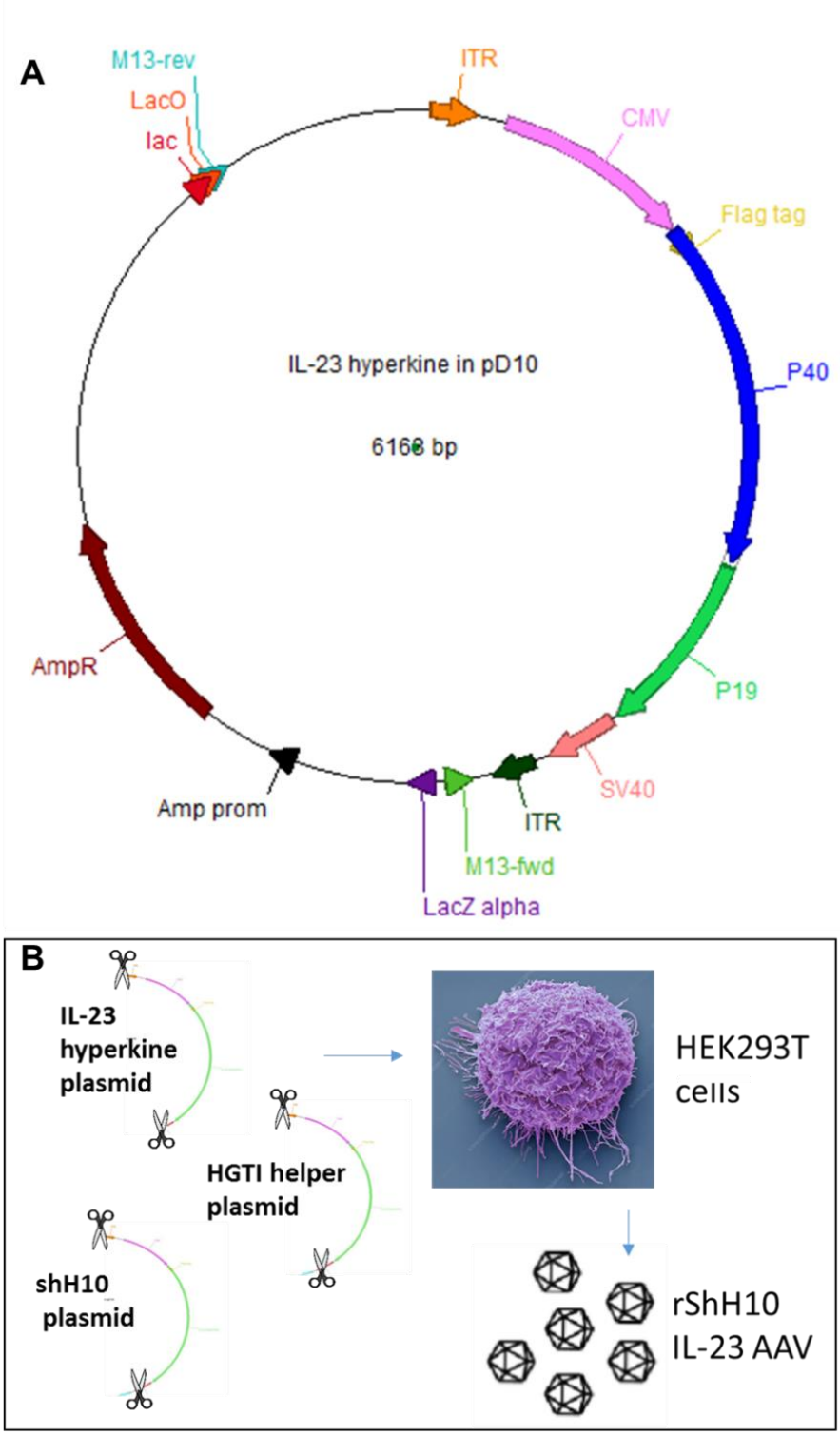


Figure 2.1: Recombinant (r)ShH10 IL-23 AAV production and purification process. Generation of adeno-associated virus (AAV) ShH10 serotype encoding IL-23 hyperkine (ShH10 IL-23 AAV) (curtesy of Dr Colin Chu) was conducted in collaboration with Professor Andrew Dick's research group at The University of Bristol Biomedical Sciences Department. (A) Schematic diagram of mouse IL-23 sequence (consisting of p40 and p19 subunits) ligated into a pD10-CMV plasmid. (B). HEK-293T cells seeded at $4.5x10^6$ in Dublecco's modified eagle medium (DMEM) with 10% Performance Plus Fetal Bovine Serum and 1x Antibiotic-Antimycotic (Invitrogen, life technologies, Paisley, UK) were simultaneously transfected with 10µg of pD10 genomic plasmid, 10µg of ShH10 capsid plasmid and 30µg of pHGTI helper plasmid per plate using Polyethylenimine (PEI). The cells were harvested after 72 hours and purified for viral ShH10 vector.

pCMV-eGFP, was also used in this study. pCMV-GFP was a gift from Connie Cepko (Addgene plasmid #11153; http://n2t.net/addgene:11153; RRID: Addgene_11153).

Recombinant ShH10 production

Twenty 15cm diameter Nunclon plates (Nunc, Thermo Fisher Scientific, Rochester, USA) were prepared per viral batch and seeded with HEK-293T cells at $4.5x10^6$ in Dulbecco's modified eagle medium (DMEM) with 10% Performance Plus Fetal Bovine Serum and 1x Antibiotic-Antimyocotic (Invitrogen, life technologies, Paisley, UK). These were simultaneously transfected with 10µg of pD10 genomic plasmid, 10µg of ShH10 capsid plasmid and 30µg of pHGTI helper plasmid per plate using Polyethylenimine (PEI) **(Figure 2.1B)**. The cells were harvested 72 hours after transfection by scraping, suspension in TD Buffer and frozen at -80°C. Prior to purification three-freeze that cycles are performed, and lysates were assured at below 2.5EU/mL endotoxin.

Purification of ShH10 vector

On the day of purification, the viral lysate was defrosted and 50 units of Benzonase nuclease (Sigma Aldrich, Dorset, UK) per mL of lysate incubated for 30 minutes at 37°C. A single spin at 18,000g for 30 minutes and 0.22µm filtration were performed to achieve debris-free supernatant. Lysate was diluted to 45mL with endotoxin-free PBS and passed into a disposable 1mL AVB affinity column (GE Healthcare, UK) at 2mL/min on a 0.5M sodium hydroxide sanitised AKTA prime plus FPLC machine. AAV was eluted with a solution of 50mM Glycine (pH2) into 1.5mL tubes containing 30µL of 1M Tris pH8.8 from Trizma base (Sigma Aldrich, Dorset, UK). The pooled aliquots corresponding to the peak of viral elution were diluted 1 in 2 with PBS and

concentrated with a Vivaspin 40 column (Sartorius, Germany) to a volume of 200µL. Aliquots of virus were then frozen at -80°C.

Limulus Amoebocyte Lysate assay

Single use gel-clot limulus amebocyte lysate assay tubes of 0.03EU/mL sensitivity (Pyrotell, Associates of Cape Cod, USA) were used to test samples for endotoxin. Briefly, samples were diluted with endotoxin-free PBS to achieve the desired threshold for testing e.g. 1:83 to test at 2.5EU/mL. 200 µL were added to each tube and incubated undisturbed at 37°C for one hour. A positive result is confirmed by static clot formation, despite inversion of the tube. Positive control tubes were used to detect the presence of any test inhibitors in all samples (Charles River, France).

Viral titre calculation using qPCR

Inverted terminal repeat (ITR) are DNA elements of the AAV virus that give it functional properties of packaging and transcription. There is one on each end and they form a secondary structure. Custom ITR primers (Table 2.1) were used with a bespoke fluorescein amidites (FAM) probe based assay (Sigma Aldrich, UK) to determine genome copy (gc) with a quantitative PCR thermal cycler 7900HT (Applied Biosciences, USA). Reaction master mix was from Roche Diagnostics, UK. Following initial denaturation at 95°C for 10 mins, all AAV capsids were lysed, exposing DNA to direct primer annealing. 40 cycles of 15sec at 95°C and 1min at 60°C annealing extension. From linearised pD10 plasmid of known concentrations, a standard curve was generated. For each sample, technical triplicates were performed over four serial two-fold dilutions. Stock preparations of ShH10 GFP AAV and ShH10 IL-23 AAV were titre matched at $5x10^{13}$gc/mL.

Table 2.1: ITR oligonucleotides sequences

Name	Sequence	Use
ITR_F	GGAACCCCTAGTGATGGAGTT	qPCR AAV titre
ITR_R	CGGCCTCAGTGAGCGA	qPCR AAV titre

Intravitreal administration of ShH10 AAV

Prior to anaesthesia, mouse pupils were dilated using topical tropicamide 1% w/v and phenylephrine 2.5% w/v (Minims; Chauvin Pharmaceuticals, Romford, UK). Mice were anaesthetised using intraperitoneal injection of 90 µL/10 g body weight of a mixture of Ketavet (Ketamine hydrochloride 100 mg/mL; Zoetis Ireland Ltd. Dublin, Ireland) and Rompun (Xylazine hydrochloride 20 mg/mL; Bayer PLC, Newbury, UK) mixed with sterile water in the ratio of 0.6:1:8.4, respectively.

A 2µL volume of ShH10 AAV at either $1x10^{9}$ genome copy (gc)/injection - low dose (LD), or $1x10^{11}$ genome copy (gc)/injection - high dose (HD), was delivered into the intravitreal space via the pars plana, using an operating microscope (Carl Zeiss, Jena, Germany) and a 33-gauge needle on a micro syringe under direct visualisation (Hamilton Company, Reno, NV). The contralateral eye of each animal received a control injection of phosphate buffered saline solution (PBS). Immediately following injection, 1% Chloramphenicol ointment (Martindale Pharma, Wooburn Green, UK) was applied topically, and the animals warmed on a heat-pad for recovery.

In vivo imaging techniques

Inflammation was monitored using the Micron IV: Retinal Imaging Microscope (Phoenix Research Labs, Pleasanton, CA), with an OCT1 attachment. Prior to imaging, the Micron IV and Optical Coherence Tomography (OCT) attachment were calibrated in accordance with the manufacturer's protocol. For brightfield fundus images, the gain was set to +3 dB, frames per second (FPS) to 15, and a 544/211 exciter filter with 700 nm shortpass emission filter was used. For fluorescence imaging, the brightness, gain, and FPS were adjusted so that (using the log histogram function of the Streampix software) the brightest non-dead pixels (representing the brightest spots of the fluorescently-labelled cells) were at an intensity just above 200: for green fluorescent protein (GFP) or fluorescein imaging this typically required maximum brightness, a gain of +15 dB, and FPS of 4. Gain-normalised settings were used to enable for comparison across a time-course for each retina.

For OCT, the parameters were defined according to the manufacturers protocol, and all scans were taken 30 times in rapid succession and averaged. Full-length line B-scans were taken horizontally and vertically with the optic disc centred; other features of interest, identified through fundal imaging, were also scanned. Full-length circle B-scans were taken centred around the optic disc **(Figure 2.2)**. Captured images were stored in the tagged image file format (TIFF).

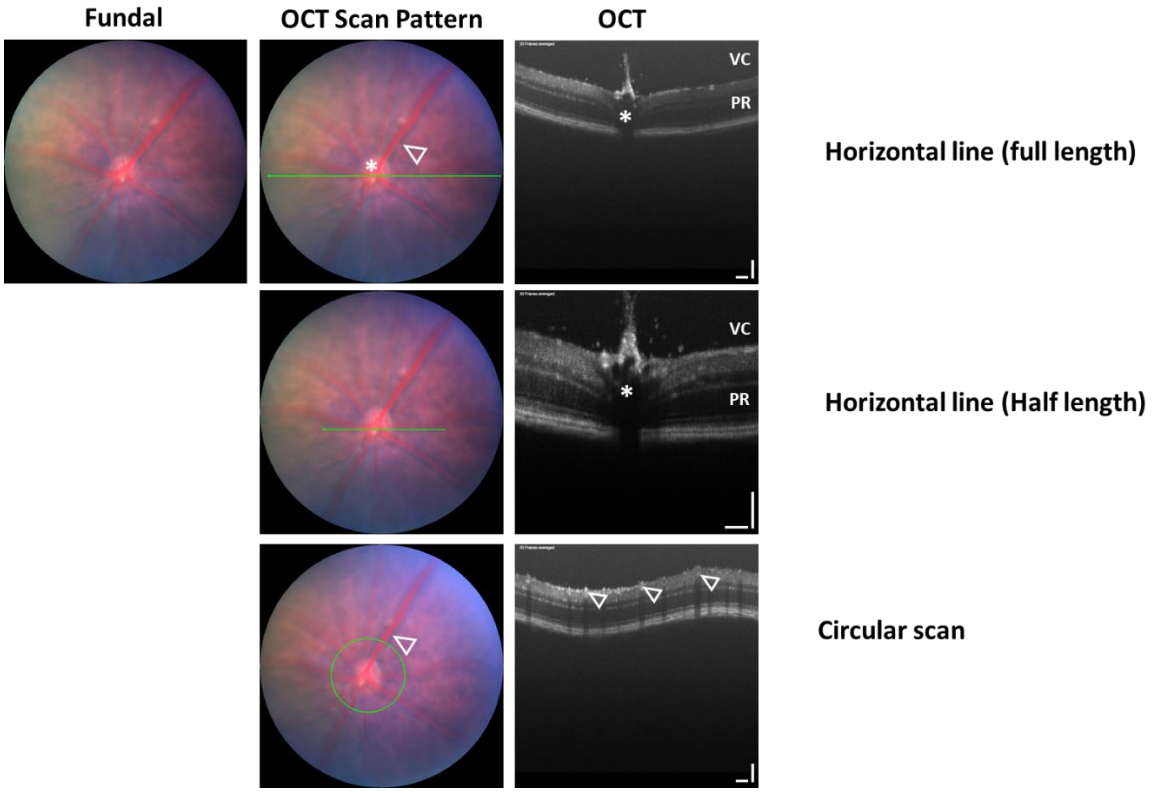


Figure 2.2 Micron imaging OCT scan patterns for methods. Image annotations: optic disc (*), retinal vessels (open white arrowhead), vitreous cavity (VC), and photoreceptor layer (PR). Scale bar 100um.

On selected days' post-injection of ShH10 virus (dpi), the pupils were dilated using a combination of topical eye drops; tropicamide 1% w/v, phenylephrine 2.5% before mice were anaesthetised (as described). Anaesthetised mice were transferred to the animal stage, and carbomer eye gel was administered for coupling to the objective lens. The mouse was positioned so the eye was perpendicular and near to the lens with the iris equidistant from pupil to sclera on the viewing plane on the computer monitor. Focus and illumination were adjusted (for brightfield – for fluorescent imaging, the settings are described above) to obtain a good colour balance and images were captured. Post-imaging, mice were monitored for vital signs (breathing, movement, heart rate, reflexes) and kept on a heated pad until recovered.

Dissection and extraction of non-ocular mouse tissues

Spleens were dissected using blunt, curved forceps and placed into D10 medium (Dulbecco's modified Eagle's medium (DMEM) + 10% fetal bovine serum (FBS) + L-glutamine (2 mM) + penicillin (100 U/mL) + Streptomycin (100 µg/mL)) on ice. Homogenisation was performed with the plunger of a 2mL disposable syringe, washed through a 70µm cell strainer (Corning, NY, USA) with PBS. Dependent upon subsequent application, red cell lysis was performed with Red Blood Cell Lysis Buffer (Sigma Aldrich, Dorset, UK) according to the manufacturer's instructions.

Dissection and extraction of ocular mouse tissues

Following enucleation, each eye was dissected in 100µL of PBS. Using a limbal incision the vitreous and retina were extracted. The anterior chamber (AC) was also opened and the contents washed into the dissecting fluid (PBS). The retina and PBS were completely aspirated and placed into a 1.5mL Eppendorf tube. If AC and posterior chamber separation was required, the AC was opened by clear corneal incision first, PBS removed, then replaced before the retina and vitreous were dissected.

Enzyme linked immunosorbent assay (ELISA)

A mouse IL-23 Quantikine ELISA kit (R&D systems, Minneapolis, USA) was used to quantify levels of IL-23 according to manufacturer's instructions. Homogenised ocular samples were spun at 13,000 rpm for 10 minutes and the supernatant typically diluted between 1:10 to 1:1000 prior to testing. Samples were analysed with technical triplicates unless limited material precluded this. Only results within the linear range of the standard curve were used. This assay has a detection range

of 15.6 - 1,000 pg/mL, and recognises natural and recombinant mouse IL-23. This assay does not recognize free p19 or p40 subunits.

Preparation of ocular tissues for analysis by flow cytometry

Mechanical cell dissociation of the retina was performed by rapping the Eppendorf tubes containing the retinal sample across a standard tube rack ten times. The iris, ciliary body and limbal sclera was first mechanically dissociated in a culture dish using scalpels in a scissoring motion, then enzymatically digested in DMEM containing 5 mg/mL type II collagenase (Worthington, # LS004202) and 0.2 mg/mL DNase I (Roche, #11284932001) for 120 minutes at 37°C undergoing constant, gentle agitation (Sherlock et al. 2012). Enzymatic digest was then washed with complete media and filtered twice through a 70µm cell strainer (Corning, # CLS431751-50EA). Viable cells were then counted by using trypan blue dye exclusion 5% w/v in water. All samples were filtered into a 96-well 60µm cell strainer plate (Merck Millipore, Watford, UK) and washed with 100µL of PBS. The plate was centrifuged at 300g for 5 minutes, 'retinal supernatants' collected, with the remaining cell pellet transferred into a sterile 96-well V-bottom plate.

- *Mouse surface antigen staining*

Cells were washed in the plate with 0.1%w/v bovine serum albumin (BSA) in PBS before resuspension in 0.5µL of neat Fc-block rat anti-mouse CD16/CD32 (BD Biosciences, Oxford, UK) diluted in 50µL 0.1% BSA in PBS. After 5 minutes, another 50µL was added containing a specific dilution of each neat primary conjugated antibody according to the manufacture's recommendations (Table 2.2). Following staining on ice for 20 minutes, cells were washed twice then incubated with viability dye (Table 4.1) for 30 minutes at room temperature. Following this, cells were

washed twice then placed into 200µL 0.1% w/v BSA in PBS in FACS tubes. Cells were analysed on a 4 laser (405nm, 488nm, 561nm and 640nm) BD LSR Fortessa X-20 flow cytometer (BD Biosciences) which was regularly maintained and used according to manufacturers' instructions. Medium or high flow rates were used. FACSdiva and FlowJo software (BD Biosciences) were used for analysis of data. Compensation was performed using OneComp eBeads (eBioscience, San Diego, USA, 01-1111-42) and an ArC Amine-reactive Compensation bead kit (Invitrogen Life Sciences, A10346) for the live-dead stain. unstained controls were used to determine gate position.

Table 2.2: Antibody panel and dilution

Antigen	**Flurochrome**	**Clone**	**Manufactuer**	**Dilution**
CD11c	af488	HL3	BD	1/200
F480	PE	T45-2342	BD	1/200
CD4	PE-Dazzle	GK1.5	Biolegend	1/100
CD45	PE-CY7	30-F11	BD	1/1500
CD11b	AF647	M1/70	BD	1/100
Ly6C	AF700	AL-21	BD	1/200
CD8	APC-CY7	53-6.7	Biolegend	1/20
Ly6G	BV421	1A8	BD	1/100
CD19	BV510	6D5	Biolegend	1/20
CD3	BV786	145-2C11	Biolegend	1/10
LIVE/DEAD	7AAD		Thermo Fisher	

Statistical analysis

Data were analysed using GraphPad Prism® software. For analysis between two groups variance was compared using an F-test. Data with equal variances were analysed using the unpaired Students two-tailed t-test. Non-parametric data were analysed with the Mann-Whitney U two-tailed test. For analysis between multiple groups variance was compared using Friedmann's test. Data with equal variances

were analysed using ordinary one-way ANOVA test with Tukey's multiple comparison test. Non-parametric data were analysed with the Kruskal-Wallis test with Dunn's multiple comparisons test. Significance was set at * $p \leq 0.05$, ** $p \leq 0.01$, *** $p \leq 0.001$, and **** $p \leq 0.0001$.

Results

ShH10 serotype rapidly transduces retinal cells after intravitreal delivery

AAV with ShH10 serotype encoding GFP transgene (ShH10 GFP AAV) was used to validate widespread transduction of the ShH10 serotype, specifically, into cells of the posterior compartment (Muller cells). This used a constitutive CMV promoter, so any infected cells would express GFP. 2µL of vector suspension containing $1x10^{11}$gc ShH10 GFP AAV was injected into the vitreous cavity of a single eye, and 2µL of PBS was injected into the vitreous cavity of the contralateral eye as an experimental control, in a total of 9 mice. Both eyes were subsequently imaged at day 1, 3, 7, 9 and 12 post injection **(Figure 2.3)**.

No GFP signal was observed at the optic disc or peripheral retina of any mice on the same day as (1hr after) intravitreal delivery **(Figure 2.3A)**. Imaging at 3 days post-delivery revealed low expression of GFP at the optic disk and adjacent to the walls of superficial retinal vessels of the inner limiting membrane (ILM). Low expression of GFP was also found in small diffuse colonies between retinal vessels proximal to the optic disk **(Figure 2.3A)**. Imaging at 7 days post-delivery revealed moderate expression of GFP at the optic disk. Moderate expression of GFP was also captured adjacent to the walls of superficial retinal vessels of the ILM in regions closest to the optic disk. Expression of GFP was reduced adjacent to the walls of these vessels as they travel towards the peripheral retina. Moderate expression of GFP was also found in small diffuse colonies between retinal vessels proximal to the optic disk **(Figure 2.3A)**. Imaging at 9 days post-delivery revealed high expression of GFP at the optic disk and adjacent to the walls of superficial retinal vessels of the ILM in all regions. Moderate expression of GFP was also captured

adjacent to the walls of deep retinal vessels in all regions. High expression of GFP was also found in small diffuse colonies between retinal vessels **(Figure 2.3A)**. Imaging at 12 days post-delivery **(Figure 2.3B)** revealed a similar expression pattern of GFP to day 9 in all mice. Furthermore, no GFP expression could be seen in the contralateral eye of any mouse at this final time point.

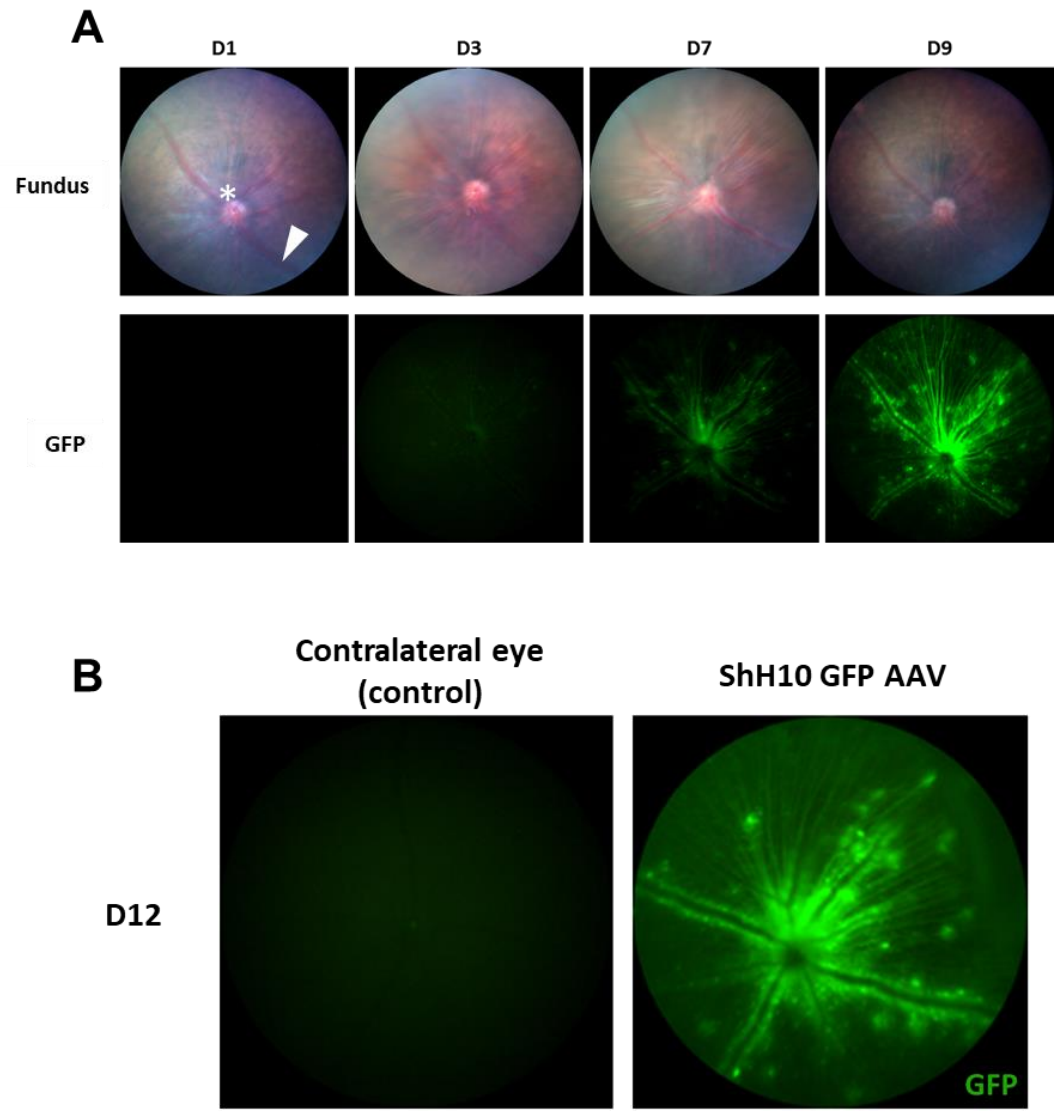


Figure 2.3: ShH10 serotype adeno-associated virus (AAV) efficiently transduced muller glia following Intravitreal Injection. 1x10^{12} genome copies (gc) of recombinant (r)ShH10 serotype AAV encoding green fluorescent protein (GFP) transgene driven by a CMV promoter in a volume of 2µL were injected into the vitreous cavity of a single eye of 9 mice. (A) Retinal transduction of ShH10 was examined by *in vivo* fundal fluorescence angiography (FA) at day D1, D3, D7, and D9 post-delivery in a representative mouse. The optic disc (white asterix) and a retinal vein (white arrowhead) are indicated on corresponding fundus images for that time point. (B) Retinal transduction of ShH10 was examined by *in vivo* fundal (FA) at day D12 in a representative mouse in comparison to its contralateral eye injected on the same day with 2µL of PBS (experimental control).

IL-23 is sufficient to drive inflammation of the inner eye *in vivo* in the absence of any other inflammatory signal

For IL-23 to be sufficient to drive uveoretinitis then it must be able to drive ocular inflammation in the absence of any other inflammatory signal. To elucidate this, two viral titres were utilised: low dose (LD) titre $1x10^9$ gc and high dose (HD) titre $1x10^{11}$ gc in a total of 2µL PBS, to assess if either titre of ShH10 serotype encoding IL-23 transgene was sufficient to induce intraocular inflammation. Viral vector was delivered into a single eye. A sham injection of 2µL PBS into the contralateral eye of a single mouse used for the PBS control (WT). Paired eyes are not technically statistically or immunologically independent, but often used with this caveat. Additionally, it was important to measure the degree of inflammatory changes as a response to control AAV transfection. To elucidate this ShH10 GFP AAV was used once again.

It was also important to choose the correct mouse strain. Mice of the H-2r haplotype (B10.RIII) are highly susceptible to whole IRBP or to its dominant pathogenic murine epitope (residues 161-180) in EAU (Silver et al. 1995). C57BL/6 (H-2b) strain is only moderately susceptible to IRBP or its component peptide IRBP(1-20) (Avichezer et al. 2000), but C57BL/6 is the background on which most knockout and transgenic mice are available, and so it is an important strain for basic studies. Here, I tested the susceptibility of C57BL/6 mice to ShH10-IL-23-AAV-induced uveoretinitis and compared the number of infiltrating immune cells between C57BL/6 and B10.RIII mice.

The effect of IL-23 on retinal structural changes was assessed at 12 days' post Intravitreal delivery of ShH10 IL-23 AAV is shown by fundus and OCT in both

C57BL/6 and B10.RIII mice strains. Based on the fact that HD titre elicits clinical signs of inflammation, vitreous condensation, disc swelling and vascular changes, in C57BL/6 mice **(Figure 2.3)**, I wished to examine the response of this dose further. Therefore, a time-course imaging assessment was conducted to examine long-term IL-23 mediated inflammatory changes with direct comparison to a GFP control vector.

Fundus and OCT imaging was performed on mouse eyes on days 1, 3, 5, 7, 12, 20, 30, and 49 **(Figure 2.4)**. I observed that retinal structural changes were rapidly induced in mice after intravitreal delivery of HD ShH10 IL-23 AAV, as early as 3 days' post intravitreal delivery **(Figure 2.4 C)**, beginning with a small amount of vitreous condensation that is highly localised to the optic disc. No other retinal structural changes were observed at this time point. However, by 5 days post intravitreal delivery, vitreous condensation was also observed at the peripheral retina **(Figure 2.4 D)**. Peak disease appears to have occurred by day 12, which is when vascular dilation and swelling of the optic disk were observed due to inflammation-induced tissue oedema **(Figures 2.3 and 2.4)**. This provided the rationale for a subsequent focus on Day 12. All retinal structural changes persisted and did not resolve by day 49 **(Figure 2.4 C and D)**. Over the course of 49 days the timing and severity of changes were highly consistent between animals.

Fundus and OCT imaging also permitted *in vivo* detection of changes in anterior chamber pathology after Intravitreal delivery of HD ShH10 IL-23 AAV. At day 12, when peak retinal disease is observed, aqueous condensation could also be seen **(Figure 2.5)**. However, changes in anterior chamber pathology were only visible in some animals, with timing and severity being variable. Fundus and OCT clinical imaging revealed no significant pathological changes in either the posterior or

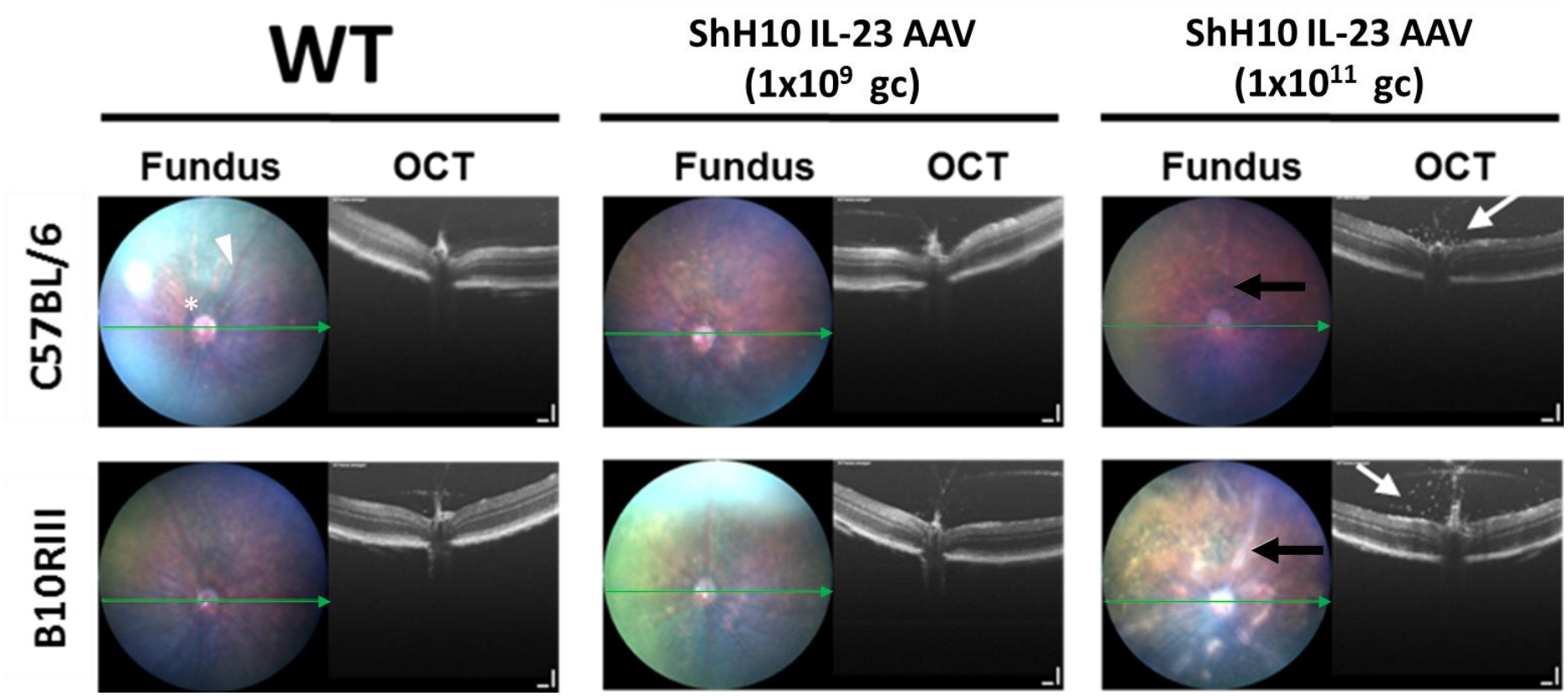


Figure 2.3: Fundus and OCT imaging detected changes in retinal pathology after intravitreal delivery of high titres of ShH10 serotype encoding IL-23 transgene. Two different viral titres of ShH10 IL-23 AAV were prepared, $1x10^9$ gc and $1x10^{11}$gc in a total of 2µL PBS and delivered by intravitreal injection into a single eye of both C57BL/6 and B10.RIII mice. A sham injection of 2µl PBS was utilised as an experimental control (WT). Representative fundus and OCT images of at least 3 independent experiments are represented for each condition 12 days post-delivery. The optic disc (white asterix) and a retinal vein (white arrowhead) are indicated. Green arrows indicate the orientation and position of the OCT scan. WT control eyes of both strains demonstrated little or no effect on fundus and OCT scans. $1x10^9$ gc in both strains have normal fundus and OCT scans. The higher titre ($1x10^{11}$ gc) in both strains showed corresponding disc swelling and vascular changes (black arrows) by fundus and vitreous opacities (white arrows) by OCT. OCT scale bars: 100µm.

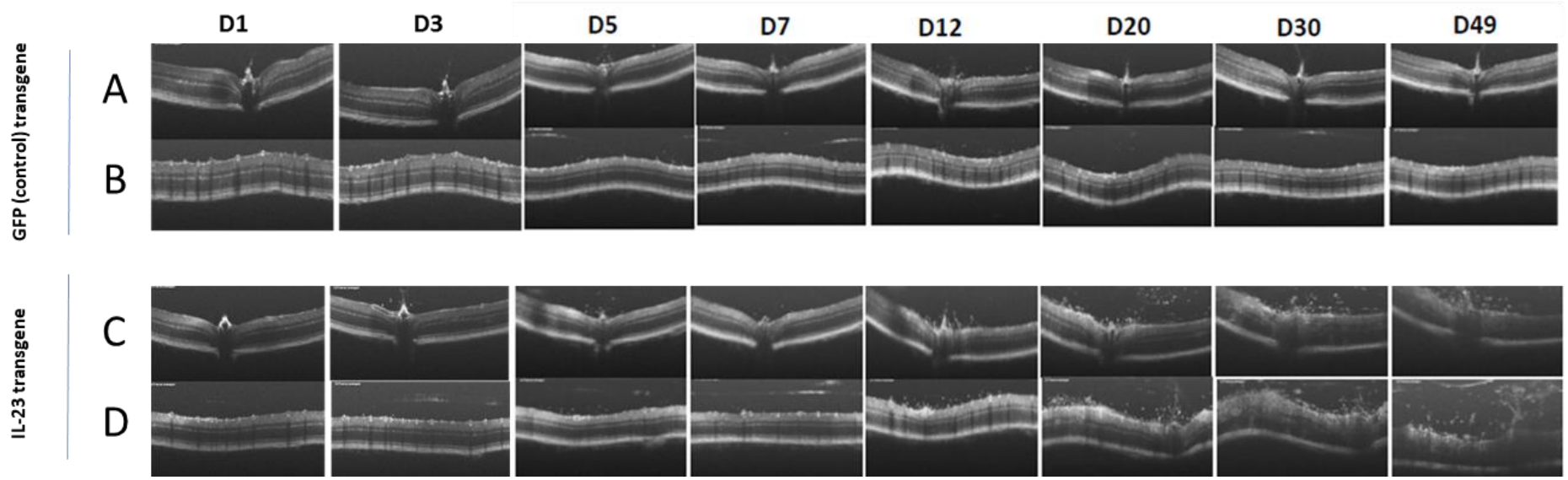


Figure 2.4: Intravitreal delivery of ShH10 IL-23 AAV leads to the rapid development of retinal pathology. ShH10 IL-23 AAV and ShH10 GFP AAV were prepared, $1x10^{11}$gc in a total of 2µL PBS, and delivered by intravitreal injection into a single eye of C57BL/6 mice. Each row illustrates the development of retinal tissue changes at specific regions, line scans (A and C) and circular scans (B and D), from the same eye of adult C57BL/6 mice. Time points at 1, 3, 5, 7, 12, 20, 30, and 49 days post-delivery of ShH10 with either IL-23 or GFP transgene are shown. Note that vitreous infiltrate could be seen as early as day 3 in mice after intravitreal delivery of ShH10 IL-23 AAV.

anterior compartment after ShH10 GFP AAV transfection in comparison to sham injection (WT) eyes.

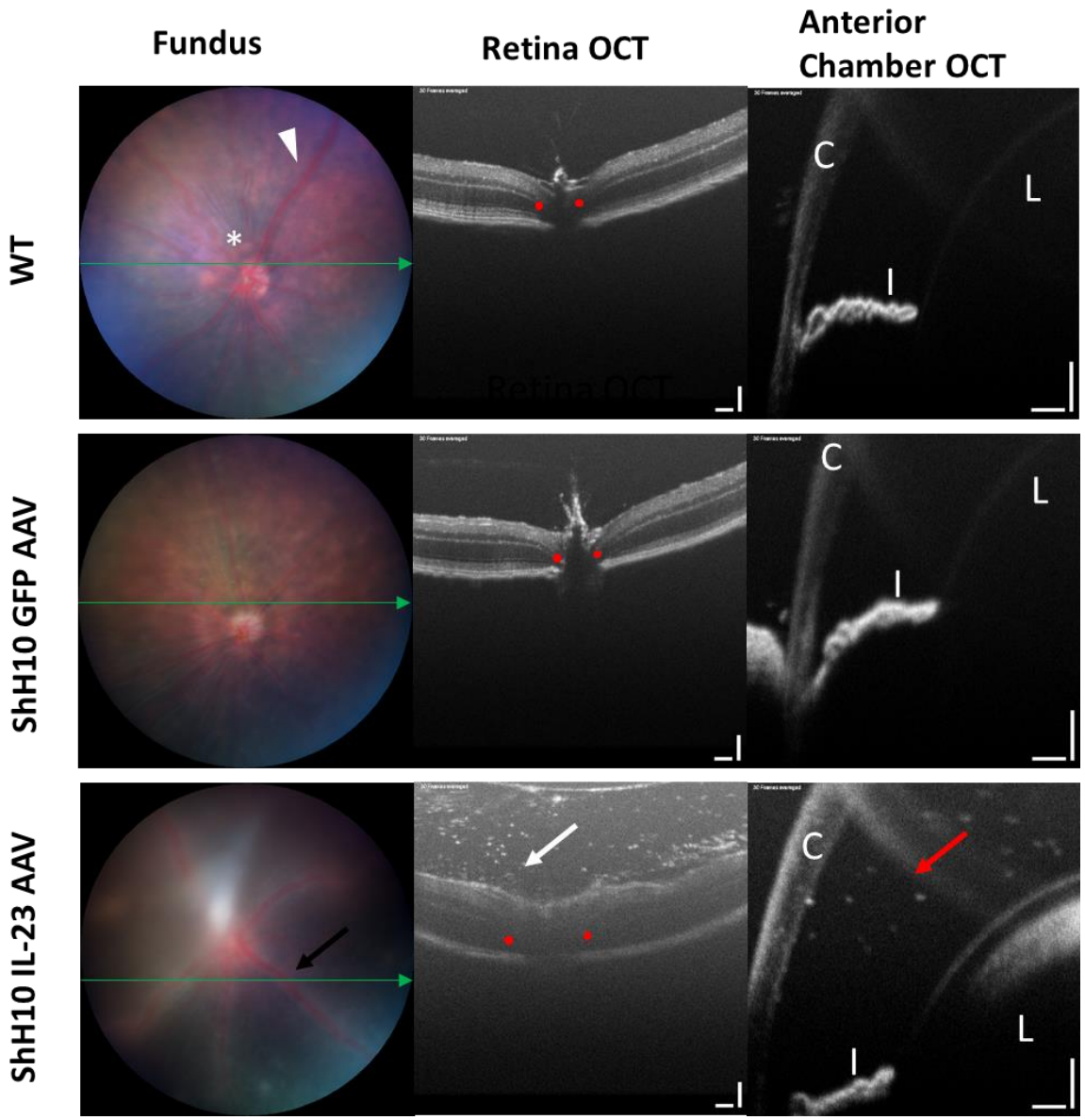


Figure 2.5: Fundus and OCT imaging detected changes in anterior chamber pathology after intravitreal delivery of high titres of ShH10 serotype encoding IL-23 transgene. ShH10 IL-23 AAV and ShH10 GFP AAV were prepared, $1x10^{11}$gc in a total of 2µL PBS, and delivered by intravitreal injection into a single eye of C57BL/6 mice. Representative fundus and OCT images of at least 7 mice were taken for each condition at 12 days post-delivery. The optic disc (white asterix) and a retinal vein (white arrowhead) are indicated. Green arrows indicate the orientation and position of the retinal OCT scans. Red dots indicate where the discrete signal from the outer plexiform layer became obscured by disc enlargement, as a landmark for comparison between eyes. WT eyes and ShH10 GFP AAV eyes demonstrated normal fundus and OCT scans for both retina and anterior chamber. ShH10 IL-23 AAV eyes revealed corresponding disc swelling and vascular changes by fundus (black arrows) and vitreous (white arrow) and aqueous (red arrow) opacities by OCT. In addition, there was enlargement of the optic disk. C = cornea, I = iris, L = lens. OCT scale bars: 100µm.

FACS analysis at 12 days post-delivery with LD titre of ShH10 IL-23 AAV revealed no significant differences in the total number of $CD45^+$ leukocytes in the retina of 6 week old naïve B10.RIII mice compared to naïve C57BL/6 mice (317.2 ± 15.8 for WT vs 378 ± 51.6 respectively; *P*>0.05; **Figure 2.6**). There was no significant increase in the total number of $CD45^+$ leukocytes in the retina of 6 week old B10.RIII mice at 12 days' post injection with LD titre of ShH10 IL-23 AAV compared to naïve B10.RIII controls (500 ± 151.2 for LD ShH10 IL-23 AAV vs 317.2 ± 15.8 for naïve; *P*>0.05; **Figure 2.6**). Furthermore, analysis at 12 days' post injection with HD titre of ShH10 IL-23 AAV revealed no significant increase in the total number of $CD45^+$ leukocytes in the retina of 6 week old B10.RIII mice compared to naïve B10.RIII controls (2611 ± 257.3 for HD ShH10 IL-23 AAV vs 317.2 ± 15.8 for naïve; *P*>0.05; **Figure 2.6**). Although a trend showing an increase was present. There was also no significant increase in the total number of $CD45^+$ leukocytes in the retina of 6 week old C57BL/6 mice at 12 days' post injection with LD titre of ShH10 IL-23 AAV compared to naïve controls (1119 ± 503 for LD ShH10 IL-23 AAV vs 378 ± 51.6 for naïve; *P*>0.05; **Figure 2.6**). Although a trend showing an increase was present. Importantly, the total number of $CD45^+$ leukocytes in the retina of 6 week old C57BL/6 mice increased significantly further at 12 days' post injection with HD of ShH10 IL-23 AAV (3562 ± 462 for HD ShH10 IL-23 AAV vs 378 ± 51.6 for naïve; *P*<0.001; **Figure 2.6**). Supporting the trend showing an increase in the total number of $CD45^+$ leukocytes in the retina of 6 week old B10.RIII mice at 12 days' post injection with HD titre of ShH10 IL-23 AAV compared to naïve B10.RIII controls – there was no significant difference between the total number of $CD45^+$ leukocytes in the retina of 6 week old B10.RIII and C57BL/6 mice at 12 days' post

injection with LD titre of ShH10 IL-23 AAV (2611 ± 257.3 for B10.RIII vs 3562 ± 462 for C57BL/6; *P*>0.05; **Figure 2.6**).

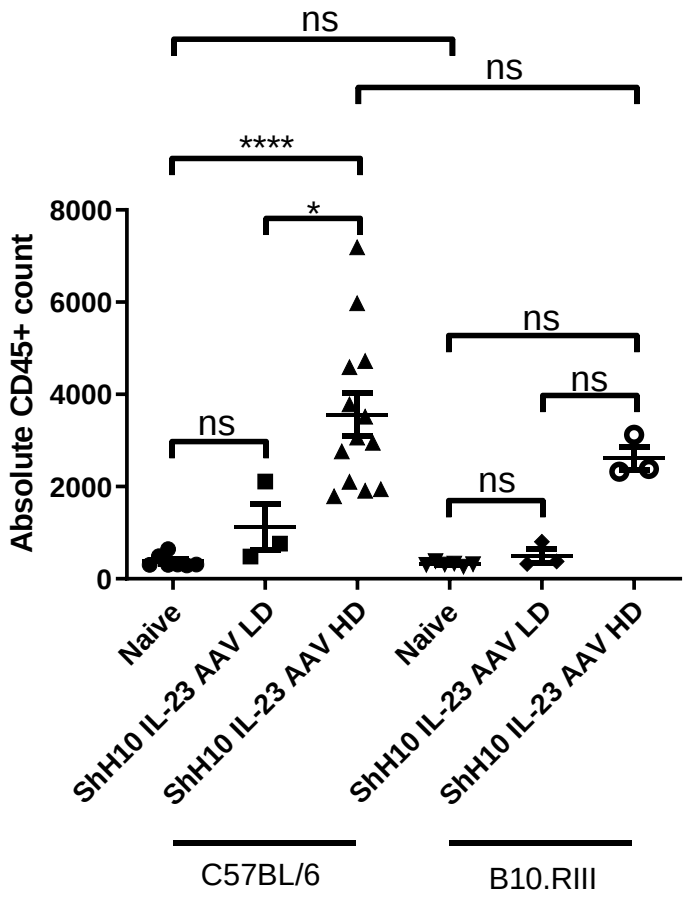


Figure 2.6: Flow cytometry reveals that IL-23 overexpression by Intravitreal delivery of ShH10 serotype drives retinal inflammation in a dose dependent manner. Two different viral titres of ShH10 IL-23 AAV were prepared, $1x10^{9}$ gc (LD) and $1x10^{11}$gc (HD) in a total of 2µL PBS and delivered by intravitreal injection into a single eye of both C57BL/6 and B10.RIII mice. A sham injection of 2µL PBS into the contralateral eye was utilised as an experimental control (naïve). A minimum of 3 mice were used for each condition. Immunophenotyping by flow cytometry was performed on retinal cells of the affected eye 12 days after delivery. Mean count is represented by the central line with error bars showing SEM. ns= not significant, * =*P*<0.05and **** = *P*<0.0001 (ordinary one-way ANOVA with Tukey's multiple comparison test).

In Addition, FACS analysis of C57BL/6 mice eyes at 12 days' post transfection (HD) revealed a significant increase in the total number of $CD45^{+}$ leukocytes in both the retina (1907 ± 166.6 vs 436.5 ± 81.5 for WT; *P*<0.001; **Figure 2.7**) and anterior chamber (684.8 ± 55.4 vs 78 ± 2.6 for WT; *P*<0.05; **Figure 2.7**) compared to

experimental controls. Furthermore, expression of control GFP virus alone was not sufficient to drive the pathological changes caused by the IL-23 virus. Analysis at 12 days' post injection with the IL-23 virus revealed a significantly greater increase in the total number of $CD45^+$ leukocytes compared to the control virus in both the retina (3562 ± 462 vs 1907 ± 166.6, respectively; *P*<0.001; **Figure 2.7**) and anterior chamber (2399 ± 329.4 vs 684.8 ± 55.4, respectively; *P*<0.05; **Figure 2.7**).

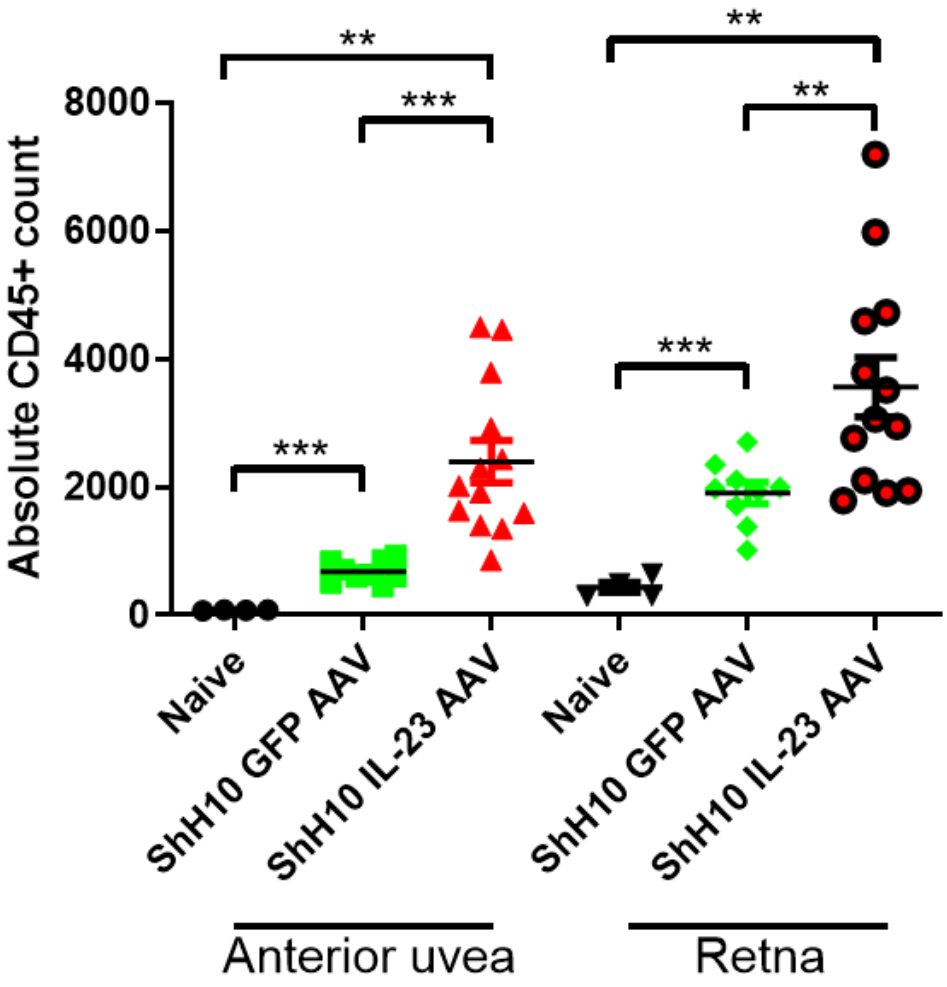


Figure 2.7: Flow cytometry data revealed that IL-23 overexpression by intravitreal delivery of ShH10 serotype drives inflammation of both the posterior and anterior compartment. ShH10 IL-23 AAV and ShH10 GFP AAV were prepared at $1x10^{11}$gc in a total of 2µL PBS, and delivered by intravitreal injection into a single eye of C57BL/6 mice. A sham injection of 2µL PBS into the contralateral eye was utilised as an experimental control (naive). Immunophenotyping by flow cytometry was performed on retinal cells, or cells of the anterior uvea from experimental eyes 12 days after delivery. Mean count is represented by the central line with error bars showing SEM. ** = *P*<0.01 and *** = *P*<0.001 (Non-parametric data were analysed with the Kruskal-Wallis test with Dunn's multiple comparisons test).

Inflammatory infiltrate significantly correlated with retinal pathology (OCT score) **(Figure 2.8A)**. In addition, inflammatory infiltrate and retinal pathology was restricted to the injected eye. **(Figure 2.8B)**. To address the issue of variability in inflammatory infiltrate and retinal pathology between animals, mouse (mIL-23) cytokine levels were measured by ELISA from homogenisation supernatants of the different compartments of the eyes, 12 days after intravitreal delivery of ShH10 IL-23 AAV (HD). Homogenisation supernatant from the uninfected contralateral eye was used as an experimental control. As expected, IL-23 levels varied between animals **(Figure 2.8C)**. Interestingly, higher IL-23 titres were recorded within the supernatant of anterior compartment compared to the retina (posterior compartment). Higher titres of IL-23 significantly correlated with leukocyte infiltration in both the anterior and posterior compartment **(Figure 2.8C)**, showing that higher titres of IL-23 exacerbate disease pathology. In addition, a significant correlation was observed between CD3+ infiltrate and IL-23 titre **(supplementary figure 2.1)**. This is an important finding, as in entheseal studies looking at IL-23 overexpression in mice, it is a resident sub-population of T cells expressing IL-23R that initially responds to IL-23 (Sherlock et al. 2012; Reinhardt et al, 2016), this early inflammation establishes an inflammatory milieu of cytokines that drives the infiltration and proliferation of other adaptive immune cells seen in established inflammation.

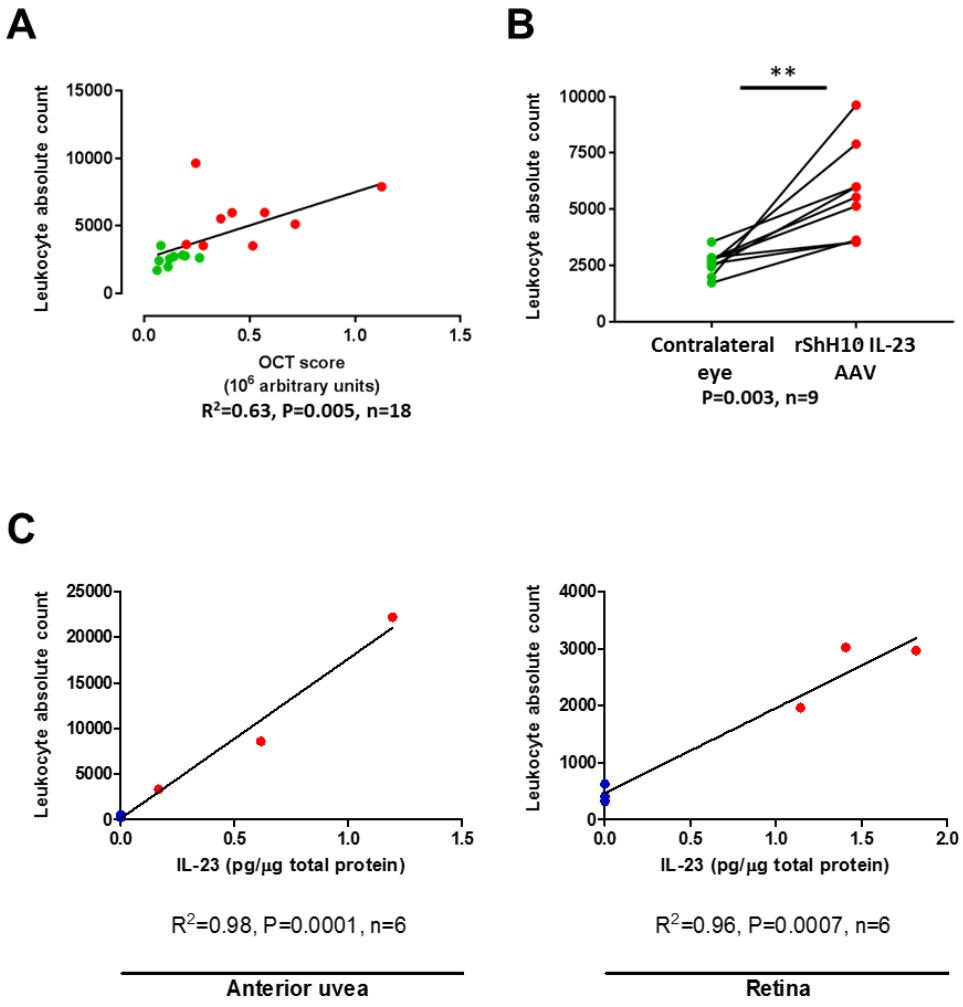


Figure 2.8: Leukocyte infiltration correlates with clinical disease score and IL-23 titre in the eye injected with ShH10 IL-23 AAV. ShH10 IL-23 AAV was prepared at $1x10^{11}$gc in a total of 2µL PBS, and delivered by intravitreal injection into a single eye of C57BL/6 mice (green dots). A sham injection of 2µL PBS into the contralateral eye was utilised as an experimental control (green/blue dots). (A) Linear regression shows that Leukocyte infiltration correlates significantly with OCT disease score. (B) leukocyte count is significantly higher in the eye injected with ShH10 IL-23 AAV, indicating that infiltration is restricted to the eye injected with ShH10 IL-23 AAV. (C) leukocyte infiltration into the anterior uvea and retina significantly correlates with IL-23 titre in a dose dependent manner. FACS analysis was used to quantify absolute leukocyte counts and ELISA was used to quantify IL-23 cytokine titres from homogenisation supernatants.

Flow cytometry data revealed that IL-23 overexpression in a single eye, by intravitreal delivery of ShH10 IL-23 AAV, drives a low level of leukocyte infiltration within the retina of the contralateral (uninjected) eye. This is higher than the total number of leukocytes recorded in the contralateral eye of viral control ShH10 GFP AAV mice (435.1 ± 49.31 vs 227 ± 11.45, respectively; *P*<0.001; **Figure 2.9A**). However, the same analysis of

the anterior uvea revealed no differences at day 10 (102.8 ± 28.6 vs 145.3 ± 88.9, respectively; Figure 2.9B).

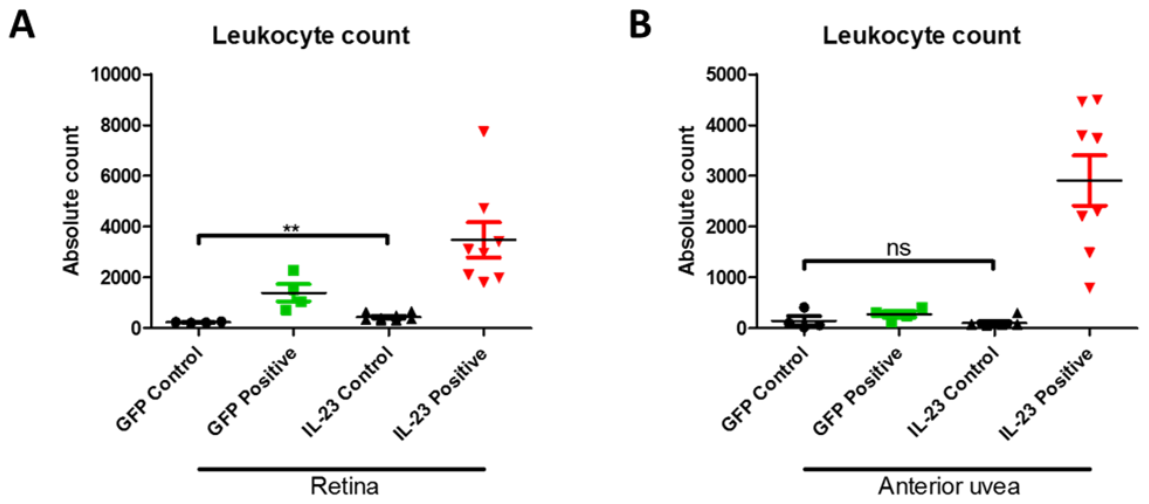


Figure 2.9: Flow cytometry data revealed that IL-23 overexpression by Intravitreal delivery of ShH10 serotype drives a low level of leukocyte infiltration within the retina of the contralateral (un-injected) eye. ShH10 IL-23 AAV and ShH10 GFP AAV were prepared at $1x10^{11}$gc in a total of 2µL PBS, and delivered by intravitreal injection into a single eye of C57BL/6 mice. A sham injection of 2µL PBS into the contralateral eye was utilised as an experimental control (GFP Control and IL-23 Control). A minimum of 7 mice were used for each condition. Immunophenotyping by flow cytometry was performed on (A) retinal cells or, (B) cells of the anterior uvea, 12 days after delivery. Mean count is represented by the central line with error bars showing SEM. Ns= not significant, and ** = P<0.01 (unpaired Student's two-tailed t-test).

IL-23 promotes the infiltration of immune cells into the anterior and posterior compartments of the eye.

As an increase in the number of CD45+ leukocytes was observed in both the anterior uvea and retina of murine eyes after intravitreal delivery of adenovirus carrying the IL-23 transgene, it was important to phenotype the individual populations that comprised the infiltrate. FACS analysis was performed initially on naive mice to phenotype the major sub-populations of CD45+ leukocytes that are resident or trafficking through the anterior uvea and retina **(Figure 2.10)**. Both the anterior uvea and retina were found to contain small numbers of CD3+ T cells, CD19+ B cells, CD11c+ Dendritic cells (DCs), CD11b+ monocytes, F4/80+ macrophages, and CD45low F4/80+ microglia.

This correlates with the histological studies of McMenamin (1997;1999a), with the exception that no T cells were observed. The very low numbers of microglia in the anterior compartment are most likely an artefact of dissection.

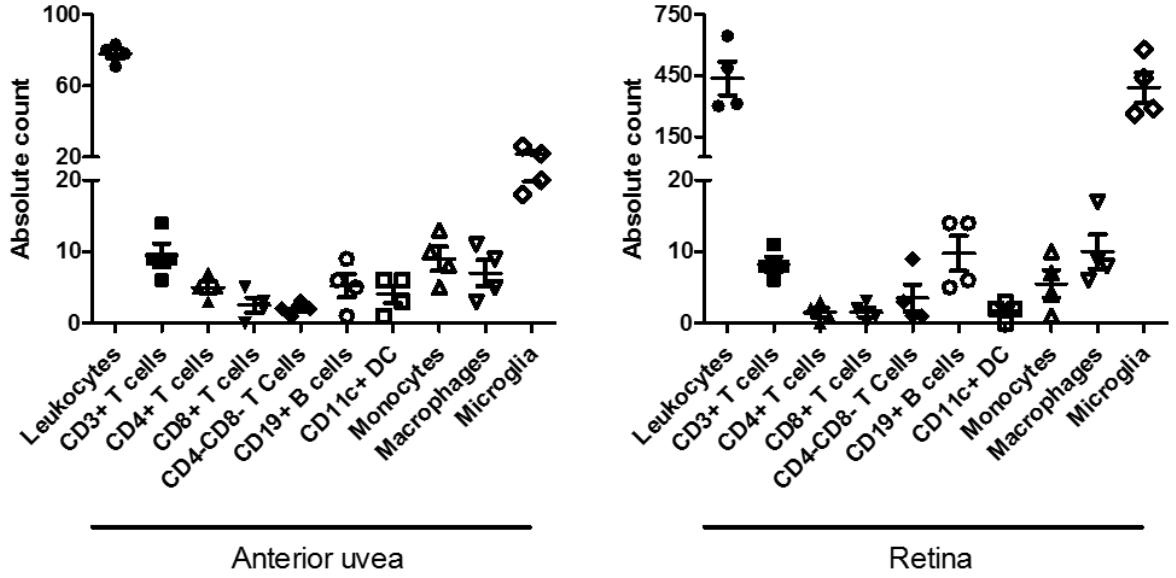


Figure 2.10: The inner eye of normal C57BL/6 mice is home to a diverse array of CD45+ leukocytes. The anterior uvea was dissected from the anterior compartment of the eye under a dissecting microscope and consisted of iris, ciliary body, trabecular meshwork, and anterior choroid. The retina was carefully dissociated from the choroid in the posterior compartment under a dissecting microscope. Both the anterior uvea and retina were found to contain small numbers of CD3+ T cells, CD19+ B cells, CD11c+ Dendritic cells (DCs), CD11b+ monocytes, F4/80+ macrophages, and CD45low F4/80+ microglia. In both tissue samples microglia represented the dominant CD45+ population in the untreated eye.

Flow cytometry was also used to phenotype cells dissociated from the anterior uvea and retina of C57BL/6 mice 12 days after intravitreal injection with either ShH10 IL-23 AAV or ShH10 GFP AAV. Frequencies of infiltrating cells were compared to those found in naïve mice. Interestingly, CD3+ T cells form the majority of the adaptive lymphocyte population which were resident/trafficking through the eye of naïve mice **(Figure 2.10)**. ShH10 GFP AAV was able to drive a low, but statistically significant, level of infiltration of CD3+ T cells into the anterior uvea (197.3 ± 23.77 vs 9.5 ± 1.7 for untreated controls; *P*<0.0001; **Figure 2.11A**) and retina (206.6 ± 43.7 vs 8.3 ± 1 for untreated controls; *P*<0.05; **Figure 2.11A**). ShH10 IL-23 AAV was able to drive

significantly higher CD3+ T cell infiltration in addition to that caused by the virus carrying the control transgene, in both the anterior uvea (715.9 ± 114.1 vs 197.3 ± 23.77, respectively; *P*<0.001; **Figure 2.11A**) and retina (457.6 ± 77.8 vs 206.6 ± 43.7, respectively; *P*<0.05; **Figure 2.11A**).

CD19+ B cells were also found in the normal eye **(Figure 2.10)**. ShH10 GFP AAV was able to drive a low, but statistically significant, level of infiltration of CD19+ B cells into the anterior uvea (32.67 ± 4.3 vs 5.3 ± 1.7 for untreated controls; *P*<0.001; **Figure 2.11B**). However, only a trend towards an increase was noted in the retina (24 ± 4.3 vs 9.8 ± 2.5 for untreated controls; **Figure 2.11B**). ShH10 IL-23 AAV was able to drive significantly higher CD19+ B cell infiltration in addition to that caused by the virus carrying the control transgene, in the anterior uvea (66.31 ± 8.3 vs 32.67 ± 4.3, respectively; *P*<0.001; **Figure 2.11B**), but again only a trend towards an increase was observed in the retina (46.4 ± 9.5 vs 24 ± 4.3, respectively; **Figure 2.11B**). B cells do not respond to IL-23 and this increase in B cells is likely due to their infiltration during the delayed adaptive immune response.

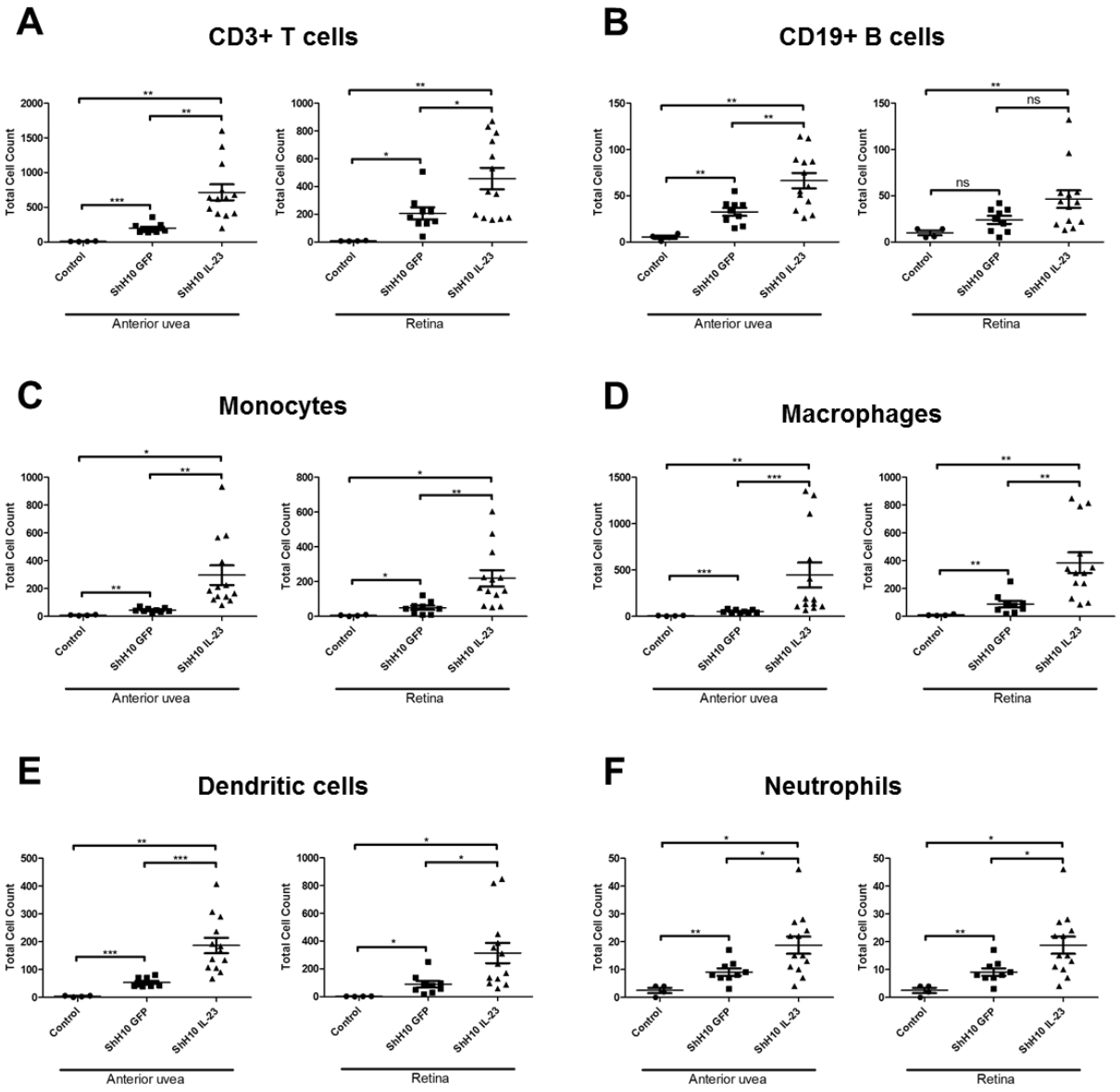


Figure 2.11: Characterisation of immune infiltrates in the eyes of C57BL/6 mice after IL-23 overexpression. ShH10 IL-23 AAV and ShH10 GFP AAV were prepared at $1x10^{11}$gc in a total of 2µL PBS, and delivered by intravitreal injection into a single eye of C57BL/6 mice. A sham injection of 2µL PBS into the contralateral eye was utilised as an experimental control (Control). A minimum of 7 mice were used for each condition. Immunophenotyping by flow cytometry was performed on retinal cells, or cells of the anterior uvea at 12 days after delivery for: (A) CD3+ T cells, (B) CD19+ B cells, (C) CD11b+F4/80- Monocytes, (D) CD11b+F4/80+ Macrophages, (E) CD11b+F4/80- Dendritic cells, and (F) Ly6G+ Neutrophils. Mean count is represented by the central line with error bars showing SEM. * = P<0.05, ** = P<0.01, and *** = P<0.001 (For analysis between multiple groups variance was compared using Friedmann's test. Data with equal variances were analysed using ordinary one-way ANOVA test with Tukey's multiple comparison test. Non-parametric data were analysed with the Kruskal-Wallis test with Dunn's multiple comparisons test).

Myeloid cells were also phenotyped by flow cytometry in naïve mice **(Figure 2.11)**.

ShH10 GFP AAV was able to drive a low, but statistically significant, level of infiltration

of monocytes into the anterior uvea (44.9 ± 5.2 vs 9 ± 1.7 for untreated controls; *P*<0.001; **Figure 2.11C**) and retina (49.7 ± 12.2 vs 5.5 ± 2 for untreated controls; *P*<0.05; **Figure 2.11C**). ShH10 IL-23 AAV elicited significantly higher monocyte infiltration in addition to that caused by the virus carrying the control transgene, in both the anterior uvea (296.8 ± 70.2 vs 44.9 ± 5.2, respectively; *P*<0.001; **Figure 2.11C**) and retina (220 ± 46.6 vs 49.7 ± 12.2 respectively; *P*<0.05; **Figure 2.11C**). It is important to note that this is the number of undifferentiated monocytes and that many more monocytes may have entered both eye compartments that have already differentiated under local conditions.

Many monocytes will differentiate into macrophages when drawn into a local tissue milieu (reviewed in Italiani and Boraschi 2014), such as those specialised sentinel macrophages found in the naive eye known as clump cells (Wobmann and Fine 1972) and microglia **(Figure 2.10)**. Monocytes infiltrating into the eye during established disease are expected to differentiate into macrophages in the same way. ShH10 GFP AAV generated a low, but statistically significant, level of infiltration of F4/80+ macrophages into the anterior uvea (53.7 ± 5.3 vs 7 ± 1.8 for untreated controls; *P*<0.0001; **Figure 2.11D**) and retina (88.7 ± 23.6 vs 10 ± 2.4 for untreated controls; *P*<0.001; **Figure 2.11D**). Furthermore, the total number of infiltrating F4/80+ macrophages were significantly higher than that found after 12 days of ShH10 GFP AAV in both the anterior uvea (447 ± 135.4 vs 53.7 ± 5.3, respectively; *P*<0.001; **Figure 2.11D**) and retina (385.5 ± 74.5 vs 88.7 ± 23.6, respectively; *P*<0.001; **Figure 2.11D**). All these macrophages were $CD45^{high}$ and do not include the $CD45^{low}$ microglia population.

DCs also represent a small portion of the total leukocytes found in the naïve C57BL/6 mouse eye **(Figure 2.10)**. ShH10 GFP AAV was able to drive a low, but statistically

significant, level of infiltration of CD11c+ DCs into the anterior uvea (53.7 ± 5.3 vs 4 ± 1.2 for untreated controls; *P*<0.0001; **Figure 2.11E**) and retina (88.7 ± 23.6 vs 1.8 ± 0.6 for untreated controls; *P*<0.05; **Figure 2.11E**). ShH10 IL-23 AAV generate significantly higher CD11c+ DC to that caused by the virus carrying the control GFP transgene, in both the anterior uvea (186.7 ± 27.6 vs 53.7 ± 5.3, respectively; *P*<0.001; **Figure 2.11E**) and retina (313.6 ± 72.5 vs 88.7 ± 23.6, respectively; *P*<0.001; **Figure 2.11E**).

Granulocytes in the naïve mice eye have been described as extremely rare (McMenamin 1997). This matches up with the findings of this study. The motile granulocytes known as eosinophils and neutrophils remain in the blood for 6-12 hours before emigration into the extravascular connective tissues, where they remain for at least few days (Spry et al. 1992). Under physiological conditions, there are believed to be around 200 times more eosinophils located in tissues than in the circulation, and these cells are more commonly associated of being tissue resident cells (Spry 1971). Neutrophils are commonly seen in the bone marrow and circulating in the blood (Summers et al. 2010). Greater neutrophil numbers are seen in ocular tissues of EAU mice (reviewed in (Németh, Mócsai, and Lowell 2016). ShH10 GFP AAV was able to elicit a low, but statistically significant, level of infiltration of Ly6G+ granulocytes (neutrophils/eosinophils) into the anterior uvea (9.1 ± 1.3 vs 2.5 ± 1 for untreated controls; *P*<0.001; **Figure 2.11F**) and retina (8.7 ± 1.2 vs 1.8 ± 0.6 for untreated controls; *P*<0.001; **Figure 2.11F**). This count was significantly higher than that which was generated in response to ShH10 GFP AAV in both the anterior uvea (18.7 ± 3 vs 9.1 ± 1.3, respectively; *P*<0.05; **Figure 2.11F**) and retina (17.6 ± 2.5 vs 8.7 ± 1.2, respectively; *P*<0.001; **Figure 2.11F**).

ShH10 IL-23 AAV driven uveoretinitis requires a Rag2-dependent cell

I next explored whether T helper (T_H) 17 cells or ILC3s were responsible for the early response to localised endogenous IL-23 overexpression as both of these cells are known to express functional IL-23 receptors (Parham et al. 2002; Awasthi et al. 2009; Buonocore et al. 2010). Expression of Rag2 is essential for the formation of the T cell receptor (Mombaerts et al. 1992). T cells without a functional T cell receptor have arrested development at an early stage and do not differentiate into mature T cells. ILC3s do not require Rag2 expression so by using $Rag2^{-/-}$ mice I was able to identify which cell was responsible.

$Rag2^{-/-}$ mice also show no clinical signs of inflammation 12 days after injection with ShH10 GFP AAV or ShH10 IL-23 AAV when assessed by fundus and OCT imaging. Retinal structural changes, such as vitreous condensation localised to the optic disc, vascular dilation and swelling of the optic disk, that were rapidly induced in mice after intravitreal delivery of ShH10 IL-23 AAV were ablated in $Rag2^{-/-}$ mice **(Figure 2.12A)**.

To assess subclinical inflammation, FACS analysis was performed on cells dissociated from the anterior uvea and retina of mice 12 days after intravitreal injection with ShH10 Adenovirus vector carrying either the IL-23 or GFP control transgene, and compared with those of untreated littermates in wild type (WT) and $Rag2^{-/-}$ mice. Fundus and OCT imaging was used to assess clinical inflammation in the same cohorts.

The presence of a RAG dependent cell is required for intraocular cellular responsiveness to IL-23, as $RAG2^{-/-}$ eyes did not show the same influx of CD45+ leukocytes as seen in WT mice after intravitreal injection of ShH10 IL-23 AAV in either the anterior uvea (230 ± 27.8 vs 3399 ± 329.4, respectively; $P<0.0001$; **Figure 2.12B**)

or retina (786.3 ± 59.1 vs 3562 ± 462, respectively; *P*<0.0001; **Figure 2.12B**). The total number of CD45+ leukocytes in Rag2$^{-/-}$ eyes after intravitreal injection of ShH10 IL-23 AAV were in fact comparable to untreated Rag2$^{-/-}$ eyes in the anterior uvea (230 ± 27.8 vs 165.8 ± 36.1, respectively**; Figure 2.12B**) and retina (786.3 ± 59.1 vs 710.3 ± 25.5, respectively; **Figure 2.12B**). In addition, there was no difference in the total number of CD45+ leukocytes in Rag2$^{-/-}$ eyes after intravitreal injection of ShH10 GFP AAV in comparison to untreated Rag2$^{-/-}$ eyes in the anterior uvea (157.2 ± 18.9 vs 165.8 ± 36.1, respectively; **Figure 2.12B**) and retina (660.5 ± 55.2 vs 710.3 ± 25.5, respectively; **Figure 2.12B**).

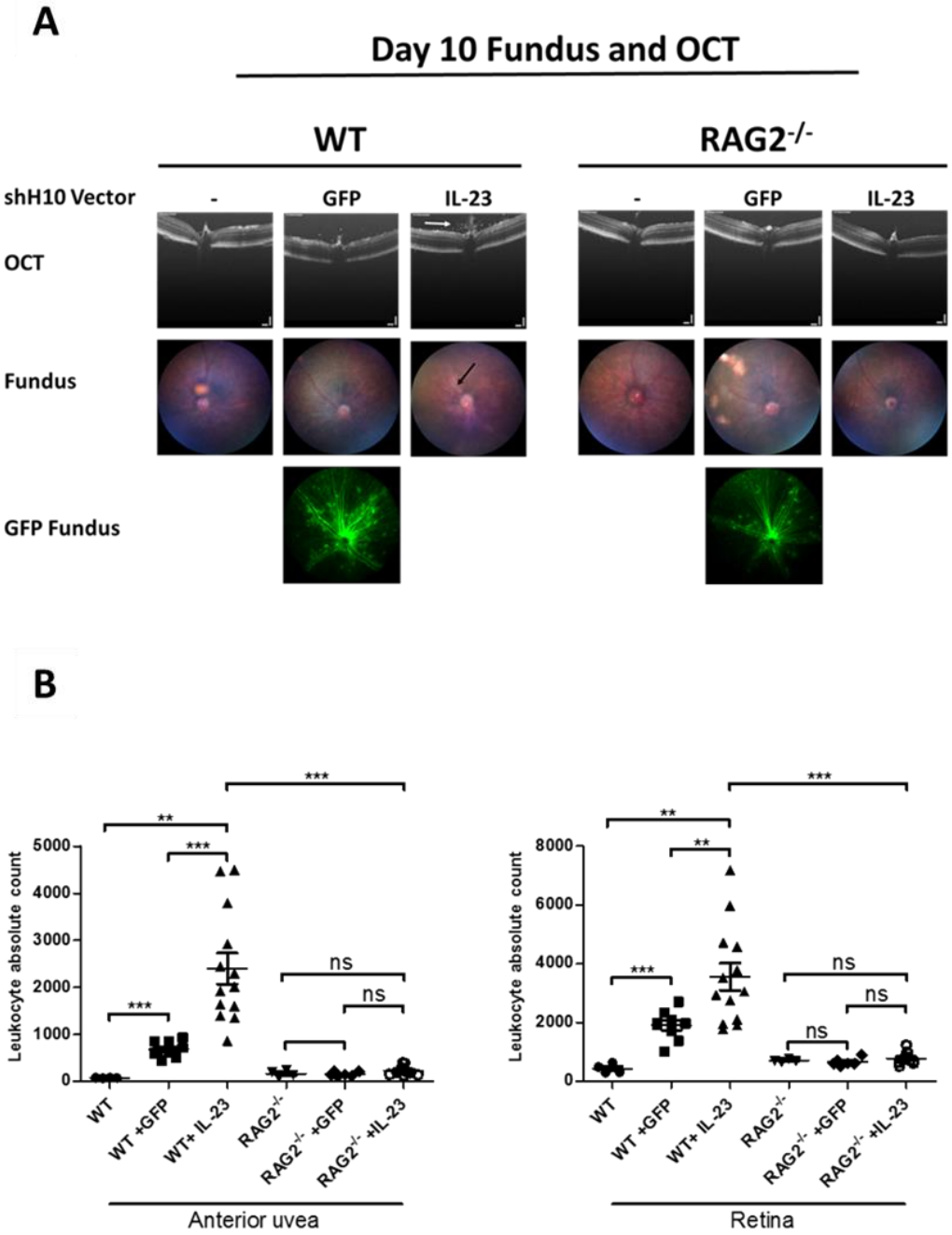


Figure 2.12: Resident ocular T cells are necessary for the clinical inflammation driven by localised IL-23 overexpression. (A) Fundus and OCT images show clinical inflammation (white and black arrows) of the posterior compartment 12 days after injection with ShH10 IL-23 AAV (1 x 10^{11} gc) in C57BL/6 mice but not in Rag2$^{-/-}$ mice. No clinical inflammation is seen in C57BL/6 mice or Rag2$^{-/-}$ mice 12 days' post injection with high titres of rShH10 GFP AAV virus particles. Representative images of at least 4 repeats of each condition. (B) Flow cytometric analysis of homogenised anterior uvea and retina for the absolute count of live CD45^{+} leukocytes in WT C57BL/6 mice (n = 4; data obtained from 2 independent experiments), or 12 days post injection of ShH10 GFP AAV (1 x 10^{11} gc; n = 9; data obtained from 2 independent experiments) or with high virus particle titres of ShH10 IL-23 AAV (2 x 10^{8}; n =13; data obtained from 3 independent experiment), in comparison to untreated RAG$^{-/-}$ C57BL/6 mice (n = 4; data obtained from 2 independent experiments), or 12 days post injection of high virus particle titres of ShH10 GFP AAV (1 x 10^{11}; n = 6; data obtained from 2 independent experiments) or with high virus particle titres of ShH10 IL-23 AAV (2 x 10^{8}; n = 11; data obtained from 2 independent experiment). Mean count is represented by the central line with error bars showing SEM. Ns= not significant, ** = P<0.01 and *** = P<0.001 (Kruskal-Wallis test with Dunn's multiple comparisons test).

Discussion

The pro-inflammatory cytokine IL-23 is known to be critically involved in the pathogenesis of disease in both animal models of chronic inflammation and in some human chronic inflammatory diseases that are collectively known as the spondyloarthropathies (SpA). Here, I used ShH10 AAV vector as a delivery vehicle to overexpress for up to 49 days the cytokine IL-23 in the eye of WT C57BL/6 mice in order to establish the pathogenicity of IL-23 without other factors contributing to disease. I have also used the same delivery system to overexpress IL-23 in the eye of B10.RIII mice which are highly susceptible to Interphotoreceptor retinoid binding protein (IRBP) the major uveitogenic retinal antigen eliciting EAU in mice (Cortes et al. 2008)

Using fundus and OCT imaging techniques, I found that the overexpression of IL-23 induced significant retinal vascular leakage as well as retinal degeneration. Vascular leakage was also observed in the anterior chamber of the anterior compartment in some but not all cases. This variability is highly likely due to technical limitations preventing me from accurately imaging the anterior chamber with the available equipment. When comparing a low ($1x10^9$ gc) and a high ($1x10^{11}$ gc) dose of IL-23 expressing virus, only the high dose resulted in retinal vascular leakage and retinal degeneration by day 10. When comparing two different strains of mice, both B10.RIII and C57BL/6 showed retinal vascular leakage and retinal degeneration by day 10 after receiving the high dose of IL-23 expressing virus. Both strains showed no signs of pathology by 10 after receiving the low dose. Furthermore, when using the high dose in C57BL/6, retinal vascular leakage was observed as early as day three. Whilst OCT permits *in vivo* imaging and is a good proxy to immunohistochemistry (IHC) and immunofluorescence (IF) it does not provide the same resolution and ability to

immunophenotype cells. Unfortunately, due to time limitations, I was unable to examine the effect of continuous overexpression of IL-23 on ocular tissues using IHC /IF. As part of future work I plan to incorporate these assays into my time course assay as they will be vital to confirm stages of infiltration, retinal degeneration, and disruptions to tissue morphology in the anterior compartment and posterior compartments.

In contrast, by using flow cytometry and even in the low dose treated eyes evidence of subclinical inflammation was observed with an increased number of CD45+ immune cells present in C57BL/6 mice 10 days after receiving the low dose compared to a normal naïve eye. A similar but non-significant trend was also observed in the B10.RIII strain. The extent of leukocyte infiltration was significantly elevated in both strains receiving the high ShH10 IL-23 dose, indicating a dose dependent response. Furthermore, assessment by ELISA of IL-23 levels in retinal supernatants from eyes receiving the same dose highlighted that despite administration of the same dose, there was variability in expression levels. Interestingly, there was a positive correlation between the IL-23 expression levels in the retina and the severity of inflammation (clinical disease score and number of infiltrating CD45+ cells) **(see Figure 2.8)**. As uveitis associated with SpA is predominantly anterior uveitis (Pepple and Lin 2018), I wanted to see if the same effects were similar in the anterior compartment. In agreement, mice with higher titres of IL-23 in the anterior compartment had greater levels of leukocyte infiltration into the anterior uvea.

Furthermore, the data demonstrates the previously unreported finding that IL-23 transgene expression and not the viral capsid (ShH10) was responsible for driving intraocular inflammation. Although flow cytometry revealed a subtle level of sub-clinical pathology in the eyes of injected with the control vector (IL-23 replaced with

GFP), no clinical pathology was revealed by clinical imaging. This was expected because although systemic AAV (AAV2) administration ($1x10^{10-11}$) gc in human clinical trials generates robust cytotoxic CD8+ T-cell responses, mouse models do not reflect this, and mice rarely develop T-cell responses to AAV, unless persistently re-challenged (Chan et al. 2021).

Previous *in vivo* animal studies in mice and rats have shown that IL-23, in the absence of any other inflammatory signal, can drive inflammation in many of the tissues associated with SpA (Buonocore et al. 2010; Chen et al. 2020; Reinhardt et al. 2016; Sherlock et al. 2012). These include the axial skeleton, skin, and gut. Mice with systemic IL-23 overexpression achieved through DNA mini-circle injection, using the same IL-23 hyperkine sequence as in this study, also developed mild psoriatic skin lesions with epidermal thickening, aortic valve inflammation, an accumulation of γ/δ T cells at the entheseal tissue in spine and ankle joints, aortic valve and root, and most interesting to this study within the anterior compartment of the eye (Reindhardt et al. 2016). Although it is not very clear from their reported imaging data, these cells appear to be within either the ciliary body or limbal sclera of the anterior chamber. These findings were observed at much later time points (between 21-30 days) to those observed by flow cytometry in this study. However, amongst those leukocyte populations observed infiltrating the anterior compartment by flow cytometry at day 10, a significant population was CD3+ T cells. The specific location of these T cells within tissues of the anterior compartment is covered in more detail in Chapter 3, and the specific phenotype of these cells, including γδTCR and IL-23R expression, is shown in chapter 4.

IL-23 overexpression models have been shown to be physiologically relevant to both AS and uveitis. Elevated levels of IL-23 have been identified in serum of AS patients

in a number of studies. Mei and colleagues (2011) showed by ELISA (assay range: 125 - 8000 pg/mL; p19 and p40 both need to be detected) that AS patients with either more active (n=26) and less active (n=24) disease (BASDAI, ESR, CRP, and HLAB27) had higher titres of IL-23 in their serum (3414.4+/-1423.5 pg/mL and 2861.9+/-1106.7pg/mL respectively) compared to healthy controls (n=43; 2399+/-719.6pg/mL). Chen and colleagues (2012) showed by ELISA (assay range: 15.6-2,000 pg/mL; p19 only) that AS patients with active (n=28) and less active (n=21) disease (BASDAI, BASFI, BAS-G, ESR, CRP, and HLAB27) had higher titres of IL-23 in their serum (215.36 pg/mL and 202.49 pg/mL respectively) compared to healthy controls (n=25; 121.12 pg/mL). Ugur and colleagues (2015) showed by ELISA (assay range: 15.6-2,000 pg/mL; p19 only) that AS patients with both active (n=6) and inactive (n=14) disease (BASDAI, BASFI, BASMI, ESR, CRP, and HLAB27) had around double the titre of IL-23 in their serum (383.24+/-218.48 pg/mL and 315+/-158.21pg/mL respectively) compared to healthy controls (n=20; 166.49+/-177.50pg/mL). In the eye IL-23A gene copy number variants greater than 2 in the peripheral blood have been associated with Behçet's disease uveitis and Vogt–Koyonagi–Harad uveitis (Hou et al. 2015). Increased levels of IL-23 have been discovered in the serum (measurement not disclosed) (Przepiera-Bedzak et al. 2016) and vitreous fluid (IL-23 >500pg/mL) (Velez et al. 2016) of patients with uveitis. The study by Velez and colleagues (2016) specifically shows an elevated level of IL-23 protein in a HLAB27 positive patient compared to healthy controls. Alternatively, the absence of IL-23 leaves otherwise susceptable animal models resistant to EAU (Luger et al. 2008; Sun et al. 2015).

Examination of this literature reveals a number of issues with IL-23 serum data in these studies. First was the variance in the recorded amount between studies. The study by Mei and colleagues (2011) measured around 10 times more IL-23 in the serum of

patients with active AS than the studies by Chen and colleagues (2012) and Ugar and colleagues (2015). In addition, the level of Il-23 measured in the serum of healthy controls in the study by Mei and colleagues (2011) was about 8 times higher than the level of IL-23 in patients with active AS in the studies by Chen and colleagues (2012) and Ugar and colleagues (2015). This variance could likely have been caused by the type of ELISA kit used by each study. Both Chen and colleagues (2012) and Ugar and colleagues (2015) use the same ELISA kit from eBioscience which detects the p19 subunit of IL-23, whereas Mei and colleagues (2011) use an ELISA from R&D which needs both the p19 and p40 subunit of IL-23 to be present. None-the-less, all these studies individually show an increase in the serum level of IL-23 in patients with either active or inactive AS compared to healthy control. When it comes to the eye, the data on IL-23 serum and vitreous fluid is even weaker. Although the study by Przepiera-Bedzak and colleagues (2016) state a significant increase in the level of serum IL-23 in patients with acute anterior uveitis and use a large sample size, they do no state in their paper the exact measurement of IL-23 in pg/mL. On the other hand, the data in the study by Velez and colleagues (2016) are limited by very small sample sizes.

In this study I measured IL-23 levels to be 361.9+/-127.9 pg/mL in the supernatant of the anterior compartment and 1032+/-264.4 pg/mL the posterior compartment at 12 days post injection with high dose ShH10 IL-23 AAV which is between the values measured for physiological serum levels of IL-23 in patients with active AS (Mei et al. 2011; Chen et al. 2012; Ugur et al. 2015).

IL-23 is produced by antigen-presenting Langerhans cells (Yoshiki et al. 2014), dendritic cells (Wohn et al. 2013) and monocytes/macrophages (Arnold et al. 2016). However, the stimulatory ligands (infection, stress, cytokines) responsible for IL-23 induction in disease are still debated. Bacterial and fungal ligands, such as

lipopolysaccharides (LPS), mannan, and zymosan, are known to activate pathogen-associated molecular pattern (PAMPS) such as toll-like receptor (TLR) 4 and induce IL-23. In Reactive arthritis (ReA), which has a strong association with HLA-B27, IL-23 induction usually occurs as a result of infection, such as Chlamydia or Salmonella (Colmegna, Cuchacovich, and Espinoza 2004; Weiss 2012). In the SKG model of murine arthritis (Sakaguchi et al. 2006), where a single point mutation in the ZAP-70 gene leads to reduced T-cell signalling – promoting the selection of highly self-reactive T cells (Sakaguchi et al. 2003), IL-23 induction also relies on induction from bacterial and fungal adjuvants (Benham et al. 2014). However, both anterior uveitis associated with SpA and the prototypical AS are not caused by infection.

A key theory for IL-23 overexpression in these diseases has arisen based on HLA-B27 misfolding within the endoplasmic reticulum with subsequent increased ER stress (Turner et al. 2005; Colbert et al. 2009) termed the UPR and can inhibit protein translation, upregulated ER chaperone molecules, and activate transcription factors. This is thought to result in IL-23 secretion (Colbert et al. 2009; DeLay et al. 2009; Neerinckx, Carter, and Lories 2014; Rezaiemanesh et al. 2017; Ambarus, Yeremenko, and Baeten 2018). However, associations between IL-23 expression and the UPR are controversial as Zeng et al. (2011) showed increased production of IL-23 by macrophages in AS patients in response to LPS occurred without induction of significant UPR, and Ciccia et al. (2014) reported that HLA-B27 misfolding in the gut of patients with AS is accompanied by activation of autophagy rather than a UPR. Other factors which are known to promote IL-23 expression in diseases associated with SpA include the IL-36 family cytokines (IL-36α, IL-36β, and IL-36γ) (Parsanejad et al. 2008; Chi et al. 2017; Ding et al. 2018) and prostaglandins (Shi et al. 2015). Nonetheless, the physical origin of IL-23 (locally or distally, at barrier sites such as the

gut and skin), and cellular origin remain unclear at sterile entheseal sites involved in SpA disease.

Recently AAV gene transfer was utilised also to look at the role of some other key pro-inflammatory cytokines, IL-1β, IL-6, IL-17A, and TNF, in the eyes of wildtype mice for up to 5 weeks (Da Cunha et al. 2018). These cytokines are known to regulate the recruitment of inflammatory cells to the eye in uveits (Xu et al. 2020). They found that the overexpression of IL-1β caused an increase in IL-6, IL-17A, KC (CXCL1), MCP-1, MMP-9, VCAM-1, and VEGFA, while the overexpression of TNF increased IL-1β, MCP-1, and VCAM-1 levels in the eye. Surprisingly, overexpressing IL-6 or IL-17A had minimal or no effects on the level of other cytokines and inflammatory mediators. The induction of additional pro-inflammatory mediators by the overexpression of IL-1β or TNF led to an influx of cellular infiltrates to the retina and resulted in retinal pathology. Interestingly, IL-17A but not IL-6 together with IL-1β or TNF tended to further decrease human retinal microvascular endothelial cells (HRMECs) impedance (ability to maintain barrier function), suggesting an additive pro-inflammatory effect of IL-17A. Their results suggest that, similar to other tissue-specific inflammatory conditions, there is a hierarchical order of pro-inflammatory cytokines in the eye and that IL-1β and/or TNF may be the key nodes in the initiation of ocular inflammation. However, this study did not look at the downstream effects of IL-23 and had a number of limitations: (A) it only documents late time points; (B) it did not utilise single cell flow cytometry data, only showing imaging and protein data (ELISA); and (C) it did not look at the effects of the empty virus vector.

In my study I have evaluated the effect of the IL-23 transgene at much earlier time points and clearly shown that IL-23 is sufficient to drive inflammation in both anterior and posterior compartment of the eye in the absence of IL-1β and/or TNF. Moreover,

my data show that IL-23 is sufficient to drive inflammation of both the anterior and posterior compartment and supports the findings of IL-23 inhibition efficacy, in non-infectious uveitis, by Baerveldt and colleagues (2013) and Mugheddu and collegues (2017). Through the use of RAG2 knockout mice, this study has also shown that T cells and not ILC3s are responsible for the chronic responsiveness to IL-23 over expression. This is a very interesting finding as the presence of a resident population of T cells in the eye has not yet been elucidated. The location and phenotype of these T cells is further explored in Chapters 3 and 4.

Chapter 3

The phenotype and localisation of T cells in the anterior compartment of the eye.

Introduction

In the previous chapter I resolved that a subset of T cells was responsible for initiating an inflammatory response to interleukin (IL)-23 as early as three days after an IL-23 transgene was overexpressed by viral transduction within the inner eye. This is an important finding as it implies: (a) that IL-23 is sufficient to drive inflammation of the uveal tract (uveitis) and retina (retinitis); and (b) is consistent with the hypothesis that a resident IL-23R+ T cell is able to drive the local ocular inflammation - as 3 days is too early for an adaptive immune response to occur whereby infiltrating T cells could propagate inflammation.

In disease models of the eye, such as EAU, the presence and role of T cells is well understood. Here, autoreactive antigen-specific T cells activated systemically home to the eye and encounter antigen presented by local antigen presenting cells resulting in a break-down of the ocular barriers and allows the free movement of T cells into the inner chambers of the eye (Kerr et al. 2008; Raveney et al. 2008; Copland et al. 2012). It is also known that during ACAID, T cells are permitted entry into the extravascular tissue of the eye to provide immunity against intraocular pathogens. However, studies have not demonstrated the presence of extravascular T cells in health healthy ocular tissue, neither have they described the fate of T cells that enter the eye during the resolution stages of injury and disease and how long do T cells persist in extravascular tissue before being filtering out through the known pathways. In this chapter, I show for the first time that T cells are present in multiple tissues of the healthy human and mouse anterior eye segment. We achieved this by using multiple high-resolution fluorescent imaging techniques in combination with multicolour fluorescence cytometry, which would not have been available in earlier studies.

Ocular immune privilege

The eye has been considered to have unique immunological features ever since the first successful human corneal transplant was performed in 1905 (Armitage, Tullo, and Larkin 2006). The term ‘ocular immune privilege’ was coined in 1948 when Peter Medawar published a paper demonstrating that skin allografts placed in the anterior chamber of the eye or the brain were tolerated in contrast to other tissues such as the skin where they were rejected (Medawar 1948). Important to this finding was that tolerance persisted even when the recipients were systemically immunised against the alloantigen. However, tolerance of grafts was lost if there was any vascular leakage into the anterior chamber. This showed the importance of the blood ocular barriers. This tolerance has been attributed to the avascular nature of the central cornea (Forrester et al. 2021), and the absence of a traditional lymphatic drainage systems within most of the tissues of the inner eye (Chen 2009).

The ability shown by the inner chambers of the eye to sequester antigen from the rest of the body has falsely generated the impression to some that the inner anterior segment of the eye is devoid of all immune cells and immune responses. However, Immune privilege in the inner eye is a real phenomenon (Aspelund et al. 2015; Louveau et al. 2015, 2016; Rua and McGavern 2018), achieved through the combined efforts of multiple protective mechanisms, including sequestration of the eye from the immune system through physical barriers, Anterior chamber-associated immune deviation (ACAID), and the maintenance of an immunosuppressive milieu by local stroma; expanded on in more detail below.

Sequestration of the eye from the immune system

Although the anterior uvea is highly vascular, physical barriers exist to prevent free movement of cells and macromolecules in and out of the eye (Bill 1973). Briefly, there

are two types of physical barrier. The first type of barrier are the blood ocular barriers (blood-aqueous and blood-retina barriers), baring entry into the posterior chamber and posterior compartment, that were first shown to be vital for tolerance of tissue grafts placed in the anterior chamber in the late 1940's (Medawar 1948). In ophthalmology clinics today, the integrity of the blood-retina barrier is routinely assessed using fluorescein - providing a widely accepted measure of ocular health (Spaide et al. 2018; Wylęgała, Bolek, and Wylęgała 2020). The second barrier is recognised as the absence of functional afferent lymphatics within the eye. This barrier is now controversial after lymphatic structures were identified by one group of investigators in the ciliary body (Yücel et al. 2009), and that various tracers injected into the anterior chamber can drain to the ipsilateral submandibular (Tam et al. 2011, 2013) and cervical lymph nodes (Yucel et al. 2018). In addition, other researchers have identified lymphatics in tissues of the CNS homologous to the choroid, collectively known as the leptomeninges (Aspelund et al. 2015; Louveau et al. 2015; Louveau et al. 2016; Rua and McGavern 2018). Regardless of these physical barriers, the idea of sequestration of the eye from the immune system is challenged by the phenomenon known as anterior chamber associated immune deviation (ACAID).

The distribution of immune cells in the uveal tract of the normal eye

The uveal tract is home to many innate immune cells, including resident tissue macrophages, retinal microglia, dendritic cells and mast cells (Forrester et al. 2010; McMenamin 1997, 1999). In contrast, information regarding T cells is limited. In the EAU mouse model, inflammation is propagated by infiltrating activated Th1 and Th17 cells, through secretion of inflammatory cytokines including TNF-α, IL17, and IL6 (Amadi-Obi et al. 2007; Caspi 2010). However, no reports have documented the presence of T cells within the extravascular tissue of the anterior uvea in control mice,

which has previously been referred to as ‘devoid’ of T cells (Forrester and Xu 2012). This view is supported by the early imaging study of McMenamin (1997).

More recently, a small number of T cells have been described proximal to the limbal sclera in the normal mouse eye and the accumulation of γ/δ T cells has been observed in this region after the systemic overexpression of IL-23 (Reinhardt et al, 2016). CD4+ T cells have also been imaged by fluorescent microscopy trafficking through the vessels of the choroid in the posterior compartment of naive mice (McMenamin, Saban, and Dando 2019). In addition, γ/δ T cells inside the vessels of the choroid in the posterior compartment in healthy human donor eyes (Zhao et al. 2017). It is also possible that a small number of T cells could remain in the eye as sentinel cells after the resolution of an ACAID immune response (Wilbanks and Streilein 1990; Faunce and Stein-Streilein 2002; Jiang et al. 2009; Paunicka, Chen, and Niederkorn 2012; Hsu et al. 2014). However, post infectious resident immune cells represent a general paradigm and the aim of this study is to identify cells that are resident independent of infection. Nonetheless, none of these studies identify the presence of resident T cells within the normal extravascular tissue of the anterior uvea, and no study has yet proposed how a resident IL-23 responsive T cell could escape the mechanisms maintaining ocular immune privilege.

Aims

- To assess if CD3+ T cells are trafficking through vasculature or reside in extravascular tissues surrounding the anterior compartment of the eye in both mice and in humans.
- To assess if CD3+ T cells are escaping the blood aqueous barriers in healthy human eyes.
- To quantitate the relative frequency of the main CD3+ T cell subpopulations within the tissues surrounding the anterior compartment of human eye, and to assess if CD3+ T cells are trafficking through vasculature or reside in extravascular tissues surrounding the anterior compartment of the eye in both mice and in humans.
- To assess if CD3+ T cells are utilising structures of the aqueous outflow system in healthy human eyes to travel through the eye?

Materials and Methods

Animal strains and husbandry

Adult (6-8 week-old) female *C57BL/6J* were purchased from Charles River Laboratories, Oxford. *B6(Cg)-Tyrc-2J/J* (Albino C57BL/6J) were provided from established breeding colonies in the Animal Services Unit at Bristol University, Bristol. Mice were confirmed as negative for the *Rd8* mutation (Mattapallil et al. 2012). All mice were housed under specific pathogen free conditions with food and water *ad libitum*. All procedures were conducted in concordance with the United Kingdom Home Office licence (PPL 30/3281) and were approved by the University of Bristol Ethical Review Group. The study also complied with the Association for Research in Vision and Ophthalmology (ARVO) Statement for Use of Animals in Ophthalmic and Vision research.

Human ocular tissue

Healthy globes were obtained from NHS Blood and Transplant Services eye bank, Filton, Bristol, where deceased individuals had donated their eyes for corneal transplant material. The partial globes obtained, post corneal removal, were considered waste tissue that was specific and of high enough quality to be included in this study. These samples were collected from male and female individuals. Corneal removal took place within 24hours of death. Globes were transferred into Roswell Park Memorial Institute (RPMI) 1640 media complete with L-glutamine (Gibco, #21875-034) with 10% heat inactivated foetal bovine serum (FBS; Gibco, #10500-064) and 1% penicillin-streptomycin (P/S; Gibco, #15140-122) (complete media) post corneal removal to preserve cell viability and transported by express courier to the Botnar

Research Centre, Oxford University, for processing. Any patient with a known inflammatory or infected condition of the entheses were excluded from the study.

Dissection and Isolation of ocular leukocytes from human ocular tissue

Partial globes were transported and processed within 36 hours from time of death. Briefly, the entire anterior uvea was removed by cutting around the circumference from the choroid to the base of the ciliary body (avoiding any sclera and retinal attachment from the ora serrata; **Figure 3.2**). Following this, a ~2mm cut around the circumference of the limbal sclera was made (which included any muscular attachment sites; **Figure 3.2**). Both tissues were washed twice in Dulbecco's Modified Eagle's Medium (DMEM; Gibco, #41965-039), cut into small ~1mm^3 pieces and enzymatically digested in DMEM containing 5 mg/mL type II collagenase (Worthington, # LS004202) and 0.2 mg/mL DNase I (Roche, #11284932001) for 120 minutes at 37°C undergoing constant, gentle agitation. The digest was then washed with complete media and filtered twice through a 70μm cell strainer (Corning, # CLS431751-50EA). Viable cells were then counted by using trypan blue dye exclusion 5% w/v in water. Single cell suspensions were immediately stained with the Zombie NIR™ Fixable Viability KIT (780nm of excitation; Biolegend, #423106) at a 1/250 dilution in Cell Staining Buffer (Biolegend, #420201) for 20 minutes at 4°C.

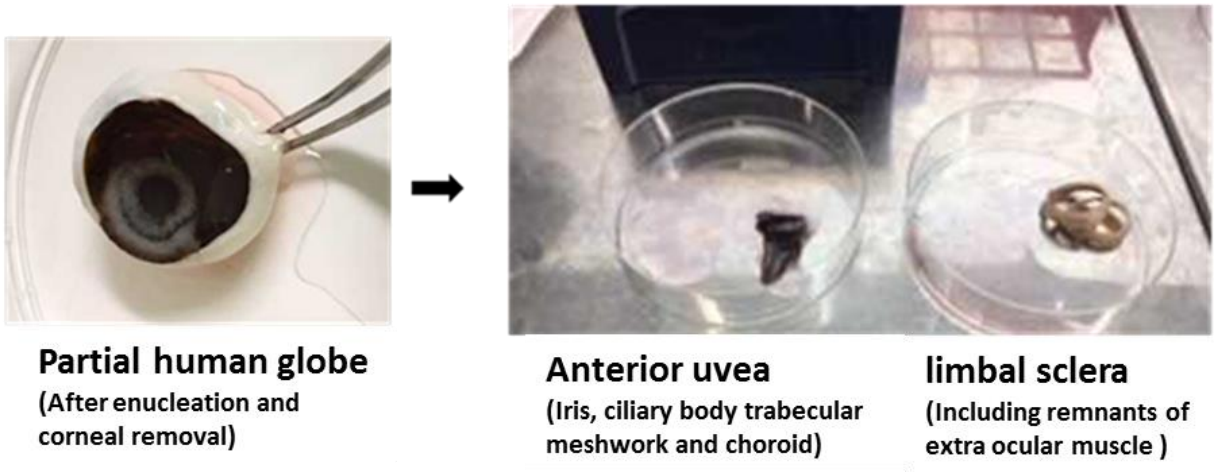


Figure 3.2. Dissection of human ocular tissue from partial globes. Photographic images demonstrating isolation of human anterior uvea (including iris, ciliary body, and choroid) and limbal sclera (including remnants of extra ocular muscle attachment sites). Globes were obtained from deceased individuals with no history of disease, sourced from Filton Eye Bank after corneal removal.

This protocol was adapted from my supervisors Nature Medicine paper (Sherlock et al. 2012) for use on larger samples. Optimisation of the digestion protocol for downstream analysis of cells by flow cytometry can be seen in **Supplementary Figures 3.1 and 3.2**, showing; (a) the comparison of mechanical homogenisation alone vs combined mechanical and enzymatic homogenization; (b) the use of different collagenases; and (c) a range of enzymatic incubation times. These optimisation experiments assessed the number of cells retrieved and the degree of surface marker cleavage cause by homogenisation.

Flow Cytometry

Cells were incubated with Zombie NIR viability dye (Biolegend) for 30 minutes at room temperature. Following this, cells were washed in Cell staining buffer (Biolegend) before resuspension in Human TruStain FcX™ blocking agent at a 1:50 dilution in a residual 50µL volume of cell staining buffer for 20 minutes at 4°C. All primary conjugated antibodies were diluted 1/20 in Cell staining buffer for a total volume of 50µL per sample (Table 3.1), this was then directly added to cells without washing.

Following staining on ice for 20 minutes, cells were washed twice then placed into 400µL cell staining buffer in FACS tubes. Compensation controls were made using UltraComp eBeads (eBioscience). Cells were analysed on a 3 laser (405nm, 488nm, and 640nm) BD LSR Fortessa X-20 flow cytometer (BD Biosciences) where both FACSdiva and FlowJo software (BD Biosciences) were used for analysis.

Table 3.1: Flow cytometry antibody panel, source, and dilution

Antigen	Fluorophore	Clone	Host species	reactivity	Manufacture
CD45	BV695	H130	Mouse	Human	BioLegend
CD3	AF647	HIT3a	Mouse	Human	BioLegend
CD14	FITC	M5E2	Mouse	Human	BioLegend
CD68	PE-CY7	Y182A	Mouse	Human	BioLegend
CD11B	BV421	ICRF44	Mouse	Human	BioLegend
CD4	AF700	RPA-T4	Mouse	Human	BioLegend
CD8	PER CP CY-5.5	RPA-T8	Mouse	Human	BioLegend
CD20	PE	2H7	Mouse	Human	BioLegend

Immunohistochemistry and Immunofluorescence

Human and perfused mouse ocular tissue were immersed in 10% buffered formalin and left for about 0.5 mm/hour. For immunohistochemistry and immunofluorescence samples were processed using a Leica ASP300S tissue processor and embedded in paraffin wax. Tissues were sectioned at 4 µm using a rotary RM2135 microtome (Leica

Microsystems Ltd.) onto adhesive glass slides (Leica, # 3800050) and baked at 60°C for 30 mins and then at 37°C for a further 60 mins.

- *Immunohistochemistry*

For antigen retrieval, slides were incubated at 60°C for 60 min, and tissue sections were obtained through deparaffinization and target retrieval steps (heat-mediated antigen retrieval at pH 6) using an automated PT Link instrument (Dako). Antibody staining was performed using the EnVision FLEX visualization system with an Autostainer Link 48 (Dako). Antibody binding was visualized using FLEX 3,3′-diaminobenzidine (DAB) substrate working solution and haematoxylin counterstain (Dako, UK) as per protocols provided by the manufacturer. Primary antibodies against human CD3 (1:100; #A045229-2) and CD68 (1:400; #M0876) were obtained from Dako, UK. Images were acquired using an inverted microscope (Axiovision software - Zeiss). Due to extremely small sample size of the specimens, only four images were acquired; two at x20 and two at x40 magnification.

- *Immunofluorescence of albino C57BL/6f mouse eyes for co-localisation of T cell markers*

Segments of anterior uvea were snap frozen in Jung tissue-freezing medium (Leica Microsystems) using 2-methylbutane (C_5H_{12}) (Sigma-Aldrich) super cooled in liquid nitrogen. Seven micrometre cryosections of each tissue were prepared on Superfrost Plus slides (Fisher Scientific), air dried for 2 hours at room temperature, and fixed in acetone (C_3H_6O) (Sigma-Aldrich) for 10 minutes. Fixed cryosections were then blocked with 150ml of 20% normal horse serum (PAA Laboratories Inc) for 15 minutes at room temperature (25°C) in a humidified chamber. Blocked sections were then incubated with 150µL of AlexaFluor 647 conjugated rat anti-mouse CD3 antibody

(17A2 clone, Biolegend) diluted 1/100 in PBS/0.1% bovine serum albumin (BSA), for 1 hour. Nuclei were counterstained with µl/ml DAPI (Invitrogen) for 10 minutes. Stained Cryosections were washed and mounted with Vectashield® mounting medium (Vector Labs). Images were captured at x20 magnification on an Olympus BX51 microscope using Micro-Manager software (Vale Laboratory).

- *Immunofluorescence of human eyes for co-localisation of T cell markers*

This protocol was adapted from my previous paper (Dakin et al. 2017). Briefly, after antigen retrieval steps, tissues were blocked in 5% normal goat serum (Sigma-Aldrich) in PBS for 60 min in a humid chamber at room temperature. After removal of blocking solution, sections were incubated with the primary antibody cocktail diluted in 5% normal goat serum in PBS for 2 hours at room temperature. Details of primary antibodies used for immunofluorescence are listed in Table 3.2. All primary antibodies were diluted at 1:200 unless stated otherwise, except for CD45 which was used without any dilution. When primary antibodies were stained simultaneously with CD45 the antibodies were diluted into the CD45 solution.

Table 3.2: Immunofluorescence antibody panel and dilution

Antigen	Clone	Isotype	Host Species	Reactivity	Manufacturer
CD45	2B11 + PD7/26	IgG1	Mouse	Human	Dako
CD34	3C8G12	IgG2B	Mouse	Human	Proteintech
CD3	POLY	IgG	Rabbit	Human	Dako
CD3	F7.2.38	IgG1	Mouse	Human	Dako
PDPN	18H5	IgG1	Mouse	Human	Abcam
Col T1	COL-1	IgG1	Mouse	Human	Abcam
Col T4	POLY	IgG	Rabbit	Human	Abcam
Col T6	6B3	IgG1	Mouse	Human	Abcam
VCAM-1	EPR5047	IgG	Rabbit	Human	Abcam

After incubation with the primary antibody, sections were washed three times with PBS–Tween 20 (PBST) for 5 min. Slides were incubated in the secondary antibody cocktail, each diluted 1:200 in 5% normal equine serum (Sigma-Aldrich) in PBS for 2 hours, and shielded from light. The secondary antibodies were Alexa Fluor goat anti-mouse IgG2a or IgG2b or goat anti-rabbit IgG (Life Technologies) and goat anti-mouse IgG1 (Southern Biotech). After washing with PBST, sections were incubated in 2 μM POPO-1 nuclear counterstain (Life Technologies) diluted in PBS containing 0.05% saponin (Sigma-Aldrich) for 20 min. After washing with PBST, tissue autofluorescence was quenched with a solution of 0.1% Sudan Black B (Applichem) in 70% ethanol for 10 min. After washing, slides were mounted using fluorescent mounting medium (VectaShield), sealed, and stored at 4°C until image acquisition. For negative controls,

the primary antibody was substituted for universal isotype control antibodies: cocktail of mouse IgG1, IgG2a, IgG2b, IgG3, and IgM (Dako) and rabbit immunoglobulin fraction of serum from non-immunized rabbits, solid-phase absorbed (Dako).

Lightsheet imaging

Following euthanasia 8-week old *B6(Cg)-Tyrc-2J/J* mice underwent cardiac perfusion with 4% Paraformaldehyde. Eyes were enucleated and the anterior segment isolated by dissection along the ocular equator. The anterior segments were then placed overnight in 1:4 dilution of BD Cytofix/Cytoperm in PBS at 4°C . The following day this was washed once in PBS then incubated for 24 hours at room temperature in 1x BD Wash Perm buffer with 5% normal goat Serum (Jackson Immunolabs). This was then replaced with 1x BD Wash Perm buffer alone, or a 1:100 dilution of AlexaFluor 647 conjugated rat anti-mouse CD3 antibody (17A2 clone, Biolegend) and incubated for 3 days at room temperature. The tissue was washed for 4 hours then placed into Ce3D clearing medium (available now from Biolegend) overnight. The tissues were then mounted in Ce3D medium and imaged on a Z1 Lightsheet system (Zeiss) acquiring the preset 633nm and 488nm channels. Images underwent 3D reconstruction using Imaris version 8.0 (Oxford Instruments).

Statistical analysis

Data were analysed using GraphPad Prism® software. For analysis between multiple groups variance was compared using Friedmann's test. Data with equal variances were analysed using ordinary one-way ANOVA test with Tukey's multiple comparison test. Significance was set at * $p \leq 0.05$, ** $p \leq 0.01$, and *** $p \leq 0.001$.

Results

Extravascular T cells are present in the anterior eye compartment in mice

We assessed the limbal region of the anterior compartment in albino (B6(Cg)-Tyrc-2J/J) mice where three important vascular structures are closely located: limbal blood vessels, limbal lymphatic vessels, and the Schlemm's canal of the anterior chamber angle. Perfused eyeballs were optically cleared, stained with DAPI and immunolabeled with CD3, a pan-T cell marker **(Figure 3.3 A-D)**. The 3D rendered image was captured and can be rotated in 360°, allowing analysis to be performed at various planes to locate T cells at a specific region or spot. This capacity allows accurate tracking of T cells within the multiply microstructures that make up the anterior compartment (peripheral cornea, sclera, ciliary body, ciliary processes, iris, trabecular meshwork, and Schlemm's canal), and from different respective views.

3D rendered images were obtained from a cross section through the left of the anterior chamber, the front of the peripheral cornea and limbal sclera, and an internal view of the anterior compartment, reflecting the original spatial locations of T cells in the extravascular tissue **(Figure 3.3 A-D)**. A cross section through the left of the anterior compartment best shows off all the structures that make up the anterior compartment **(Figure 3.3 A and C)**. Here, T cells can be seen in clusters within the limbal episclera, limbal scleral stroma, peripheral cornea, ciliary body proximal to ciliary muscle and processes, trabecular meshwork proximal to Schlemm's canal and iris root, and the ciliary zone of the iris. Serial cross sections of the anterior compartment of the mouse eye confirm that these CD3+ cells co-express CD45, a pan-Leukocyte marker **(Figure 3.4 A and B)**.

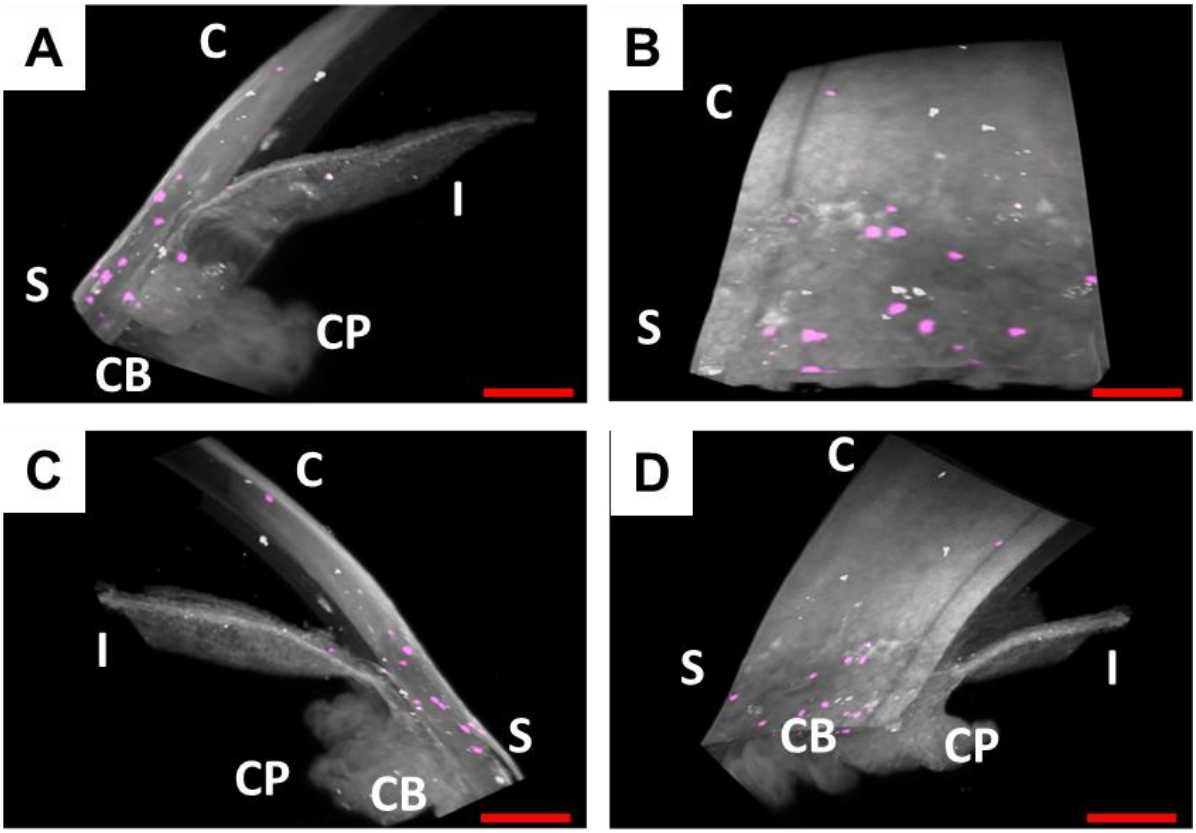


Figure 3.3: CD3+ cells are present in multiple tissues surrounding the anterior chamber in C57BL/6 mice. (A) Lightsheet Z.1 acquired, immunofluorescent whole mount imaging, of a perfused and cleared steady state albino C57BL/6 mouse eye, (B) rotated 90°, (C) rotated 180°, and (D) rotated 270°. 3D rendered image shows expression of tissue autofluorescence (white) and CD3 (purple). Co-expression of CD3 and nuclei can be seen in the sclera, peripheral cornea, ciliary body and cornea. Images captured at x10 magnification. Red scale bar: 100 µm. CP – ciliary process, CB – ciliary body, S – sclera, I – iris, and C – cornea.

Although low magnification Lightsheet imaging allowed a large region of the full anterior chamber configuration to be imaged at once, this made it difficult to identify the exact location of T cells around smaller structures such as the trabecular meshwork and Schlemm's canal without the help of additional markers **(Figure 3.3 A-D)**. In contrast, serial sections of the anterior compartment in the transverse or sagittal plane allow easy identification of these smaller structures even at low magnification **(Figures 3.4 and 3.5)**. Here T cells were observed proximal to the inner wall the JCR.

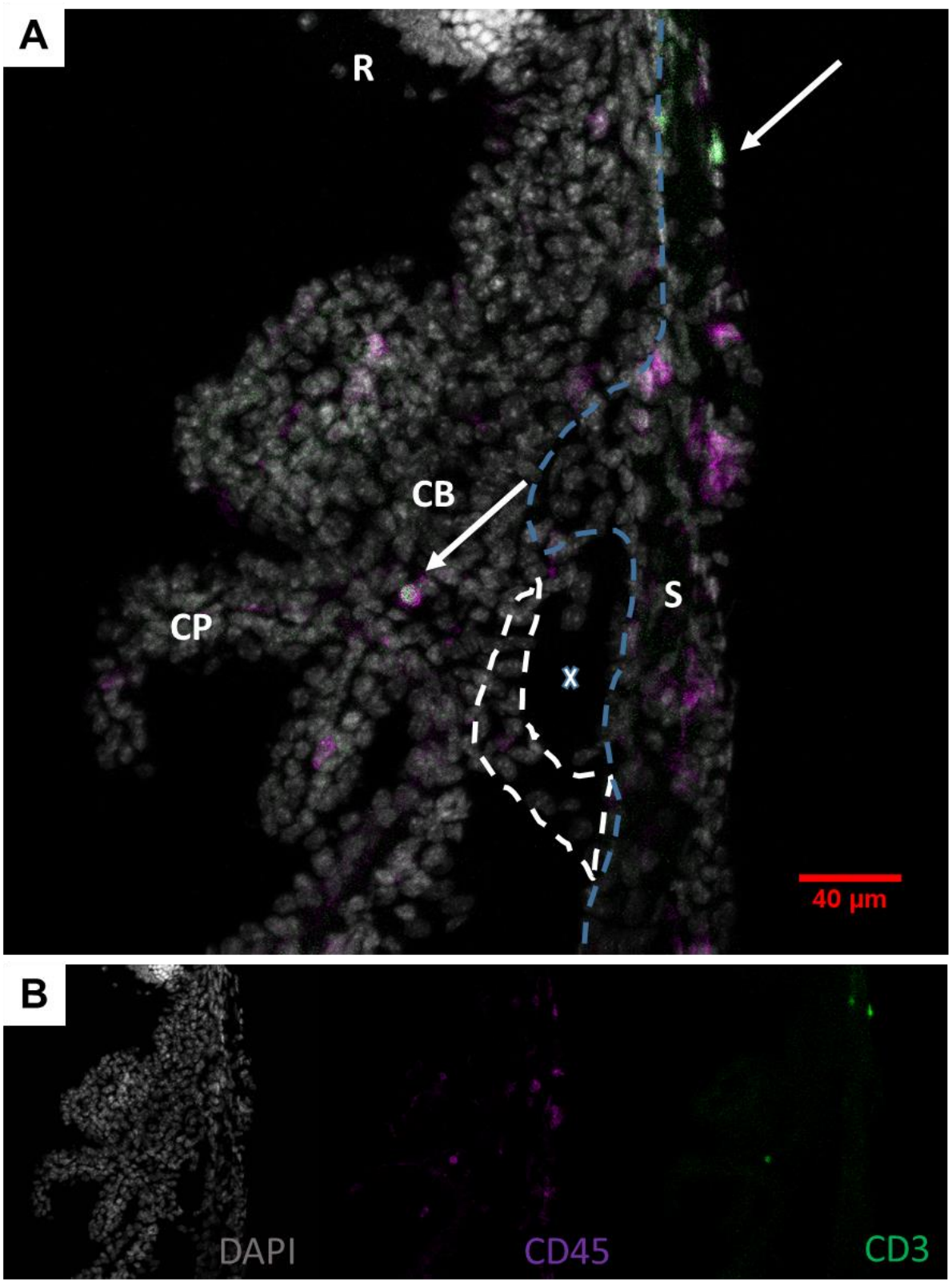


Figure 3.4: CD3+ T cells reside in the extravascular tissues of the anterior uvea and sclera in C57BL/6 mice. (A) Representative immunofluorescence image showing expression of nuclei (grey), CD45 (purple), and CD3 (green) within the anterior compartment, in a perfused, albino C57BL/6f mouse eye after lens removal. White arrows indicate the presence of CD3+ T cells. (B) Individual expression of nuclei (grey), CD45 (purple), and CD3 (green). All images were captured at x20 magnification. Dashed blue line – the inner limit of the sclera, dashed white line – trabecular meshwork, X – Schlemm's canal, CP – ciliary process, CB – ciliary body, S –sclera, and R – retina.

We next assessed the limbal region of the anterior compartment in C57BL/6J mice for T cell sub-types within the extravascular tissue. These included CD4+CD8- T helper cells (T_H cells), CD4-CD8+ cytotoxic T cells (CD8+ T cells), and CD4-CD8- T cells.

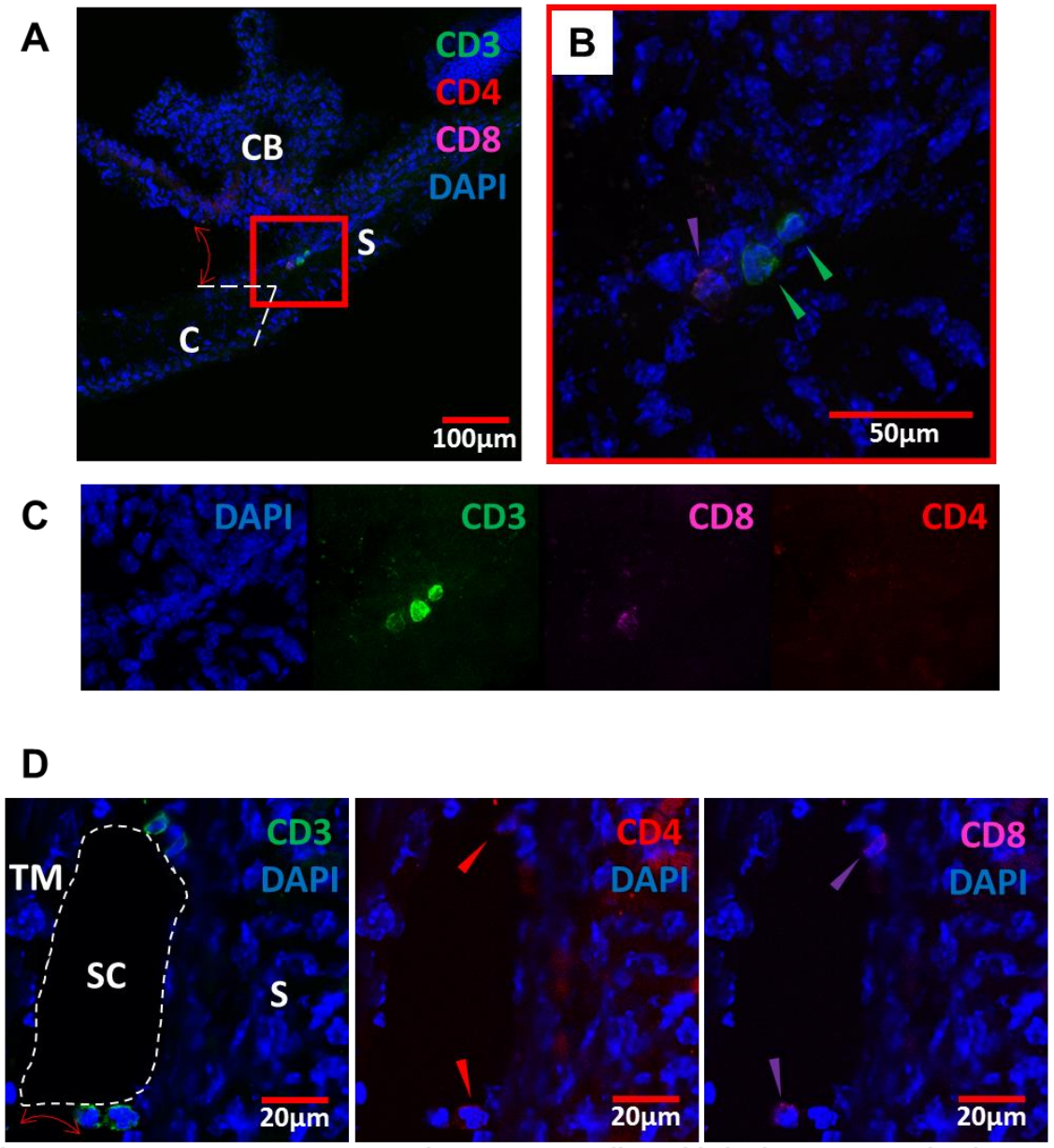


Figure 3.5: CD4+CD8-, CD4-CD8+, and CD4-CD8- T cells reside in the extravascular tissue of the sclera in C57BL/6J mice. (A) Representative immunofluorescence image within the anterior compartment and the limbal sclera (dashed white line). in a perfused, healthy, albino C57BL/6f mouse eye after lens removal. (B) Magnification of the red square region shown in A. Coloured arrows indicate the presence of CD3+ T cell subtypes (C) Individual expression of DAPI (nuclei) (blue), CD3 (green), CD4 (red), and CD8 (purple) T cells. (D) Representative immunofluorescence images showing co-expression of either CD3 (green), CD4 (red), or CD8 (purple) with nuclei (blue) in the tissues surrounding Schlemm's canal. Dashed white line highlights the walls of Schlemm's canal. All images were captured at x20 magnification. Red double-headed arrow – Irideocorneal angle, ▲ – CD3+ T cell, ▲ – CD8+ T cell, ▲ – CD4+ T cell, CB – ciliary body, S –sclera, C – cornea, TM – trabecular meshwork, and SC – Schlemm's canal.

Both CD8+ and CD4-CD8- T cells were found in the region of tissue closest to the irideocorneal angle **(Figure 3.5 A-C)**. Both T_H cells and CD8+ T cells were found in the JCR of the trabecular meshwork proximal to the inner wall of Schlemm's canal **(Figure 3.5 D)**. The anatomical location of these cells was easily identified due to the large lumen presented by Schlemm's canal in serial sections and is estimated at being proximal to the JCR of the trabecular meshwork and limbal sclera.

Only CD4-CD8- T cells were identified in the region of ciliary body proximal to the limbal sclera (Figure 3.6 A and B). These cells were found in much lower frequencies than those found closer to the irideocorneal angel, often residing as a single cell other than a cluster of cells **(Figure 3.6 B)**, and were present in both the ciliary body and sclera parallel to both the *pars plana* and *pars plicata* of the ciliary body. No T cells were found in any part of the sclera other than at this region. This is interesting as this region of tissue can be considered entheseal tissue based on the border enthesis idea (McGonagle and Georgouli 2008).

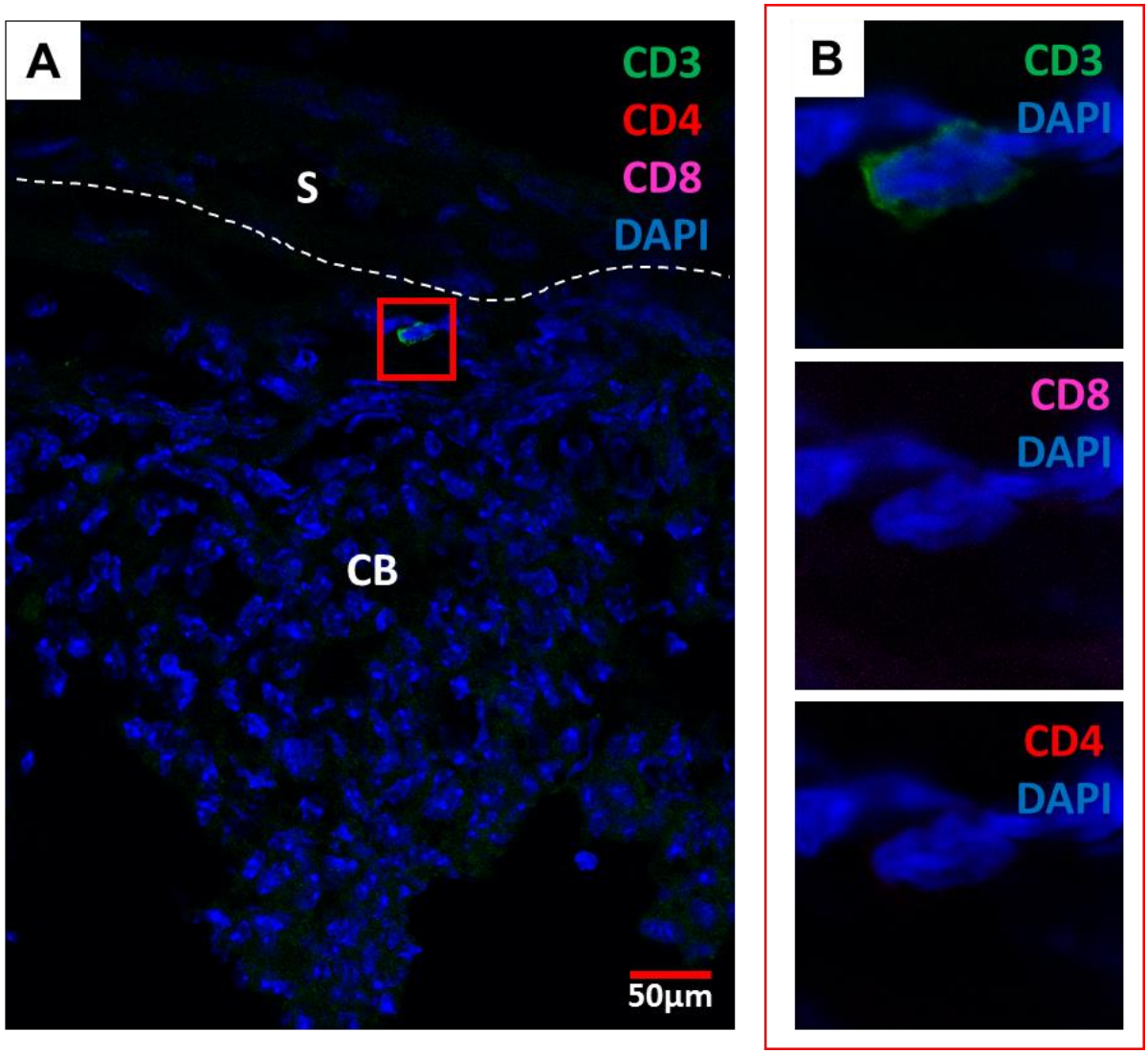


Figure 3.6: CD4-CD8- T cells reside in the extravascular tissue of the ciliary body in C57BL/6 mice. (A) Representative immunofluorescence image showing expression of nuclei (blue), CD3 (green), CD4 (red), and CD8 (purple) within the anterior compartment of a perfused, healthy, albino C57BL/6f mouse eye after lens removal. Dashed white line highlights the lamina fusca separating sclera (S) from ciliary body (CB). Red square highlights the region of tissue magnified in B. (B) Representative immunofluorescence images showing co-expression of either CD3 (green), CD4 (red), or CD8 (purple) with nuclei (blue).

T cells are resident within tissues surrounding and dividing the anterior and posterior chamber of the anterior cavity in the human eye

Following the above observations in the mouse, I then investigated the presence of T cells in different compartments of the human eye, including the anterior uveal tract and the limbal sclera.

- *The anterior uveal tract*

FACS analysis was performed on healthy human globes to phenotype the major CD45+ leukocytes that are resident or trafficking through the anterior uveal tract **(Figure 3.6 A and B)**. As described previously **(see Figure 3.2)**, the entire anterior uveal tract was dissected from the sclera.

Similar to what was found in steady state mouse in Chapter 2 the human anterior uveal tract contained CD3+ T cells (sub divided into CD4+CD8-,CD4-CD8+, and CD4-CD8- T cells), CD20+ B cells, CD14+ monocytes, and CD68+ macrophages (sub divided into CD11b+ and CD11b- Macrophages). In addition, a population of large/high complexity (based on light scatter) CD11b+CD68- cells was found. Consistent with published data (McMenamin 1997; McMenamin, Saban, and Dando 2019) macrophages represented the dominant CD45+ population in the healthy anterior uveal tract. However, these were not further sub divided to identify microglia.

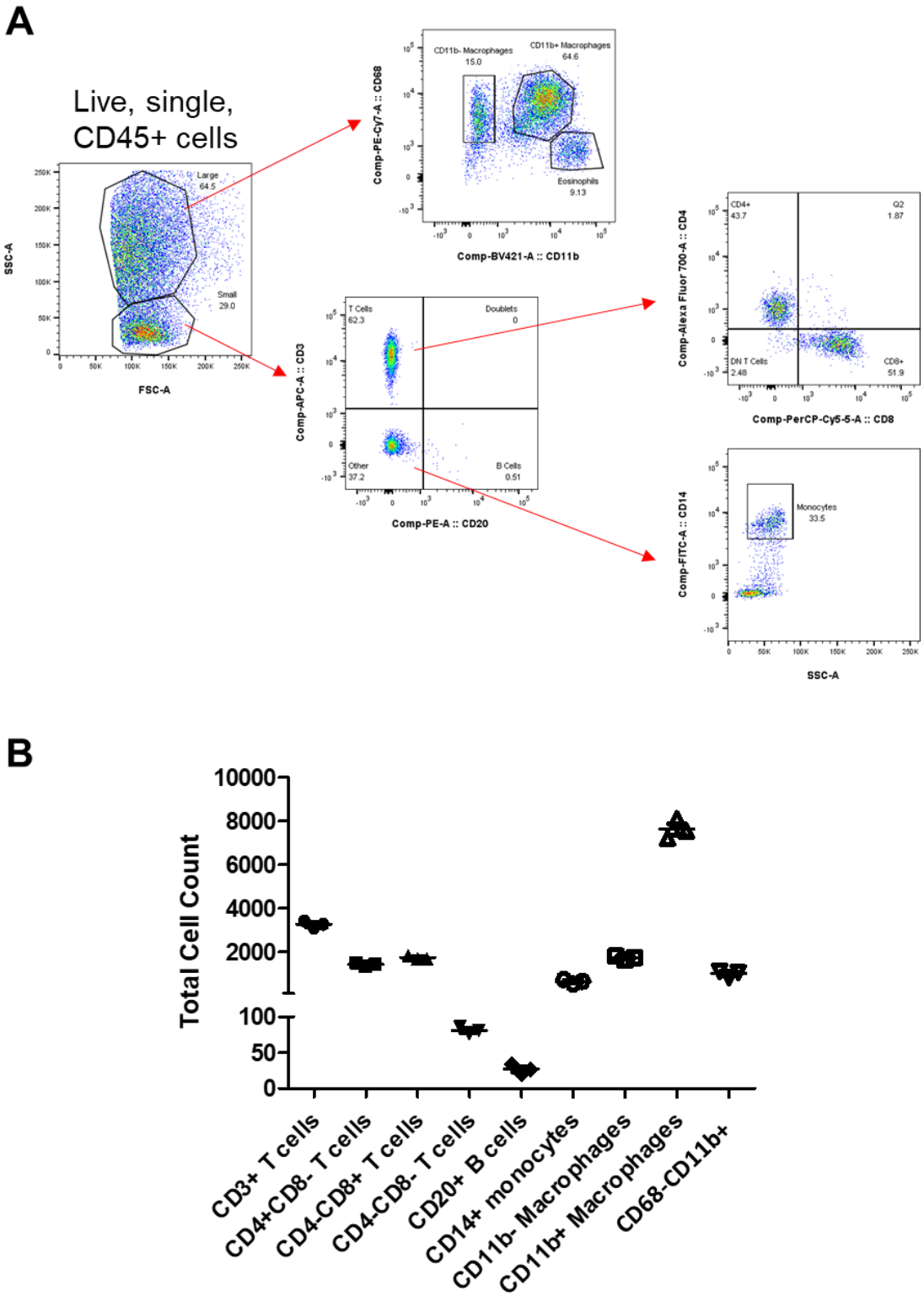


Figure 3.7: The healthy human anterior uvea is home to a diverse array of CD45+ leukocytes. The anterior uvea was dissected from the anterior compartment of the eye and consisted of iris, ciliary body, trabecular meshwork, and anterior choroid. (A) Representative plots of 3 repeats show FACS gating strategy for sub populations of uveal CD45+ leukocytes. (B) Sub populations include CD3+ T cells (sub divided into CD4+CD8-,CD4-CD8+,and CD4-CD8- T cells), CD20+ B cells, CD14+ monocytes, CD68+ macrophages (sub divided into CD11b+ and CD11b- Macrophages), and large/high complexity (based on light scatter) CD11b+CD68- cells.

T cells were found at frequencies around 50 times higher than B cells **(Figure 3.7 B)**. However, unlike in mice, healthy human anterior tissue was not perfused prior to FACS analysis, which could result in peripheral blood contaminants affecting these results.

The cellular architecture of the dissected anterior uveal tract can be observed in coronal sections by H&E staining **(Figure 3.8 A and B)**. Here, H&E staining has been performed on a section at a depth in the coronal plane more posterior than the iris root. This is easily identifiable as the iris no longer forms one continuous structure with the ciliary body. Although a small portion of the iris, known as the iris root, was absent when sections were imaged at this depth, it permitted a way to image both the posterior pigmented epithelium of the iris and the inner most folds of epithelial tissue within the ciliary body tissue, known as the major ciliary processes. Both epithelial tissues were in fact continuous at the iris root.

Using a validated anti-human CD3 clone **(Supplementary Figure 3.3)**, T cells were observed throughout the iris in healthy human tissue **(Figure 3.8 C and D)**. The iris can be distinguished from the rest of the anterior uveal tract through the high expression of Podoplanin (PDPN) by iris stroma (Birke et al. 2010). Large numbers of diffusely spaced T cells were found throughout PDPN+ stromal cells. T cells were also observed throughout the ciliary body in healthy human tissue **(Figure 3.8 E and F)**. Like within the ECM of the iris, these T cells were found diffusely spread in large numbers. T cells were identified in smaller numbers towards the folds of the ciliary body but not within the dual epithelial layers. Unfortunately, in coronal sections of this tissue it was not possible to accurately identify the regional presence of T cells within the ciliary body, although T cells were present in coronal sections of tissue at a depth where ciliary folds were much less prominent. It was also not possible to image T cells at specific regions such as

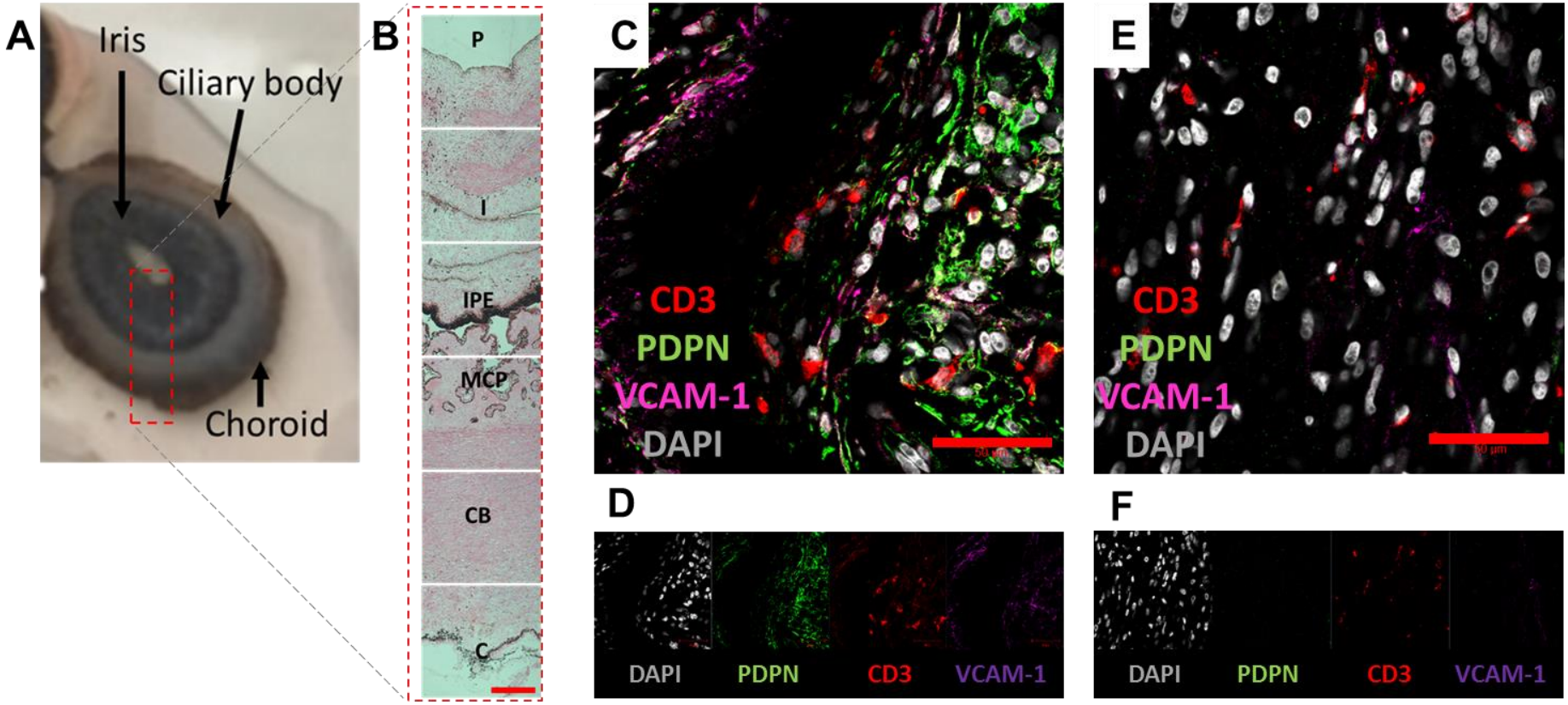


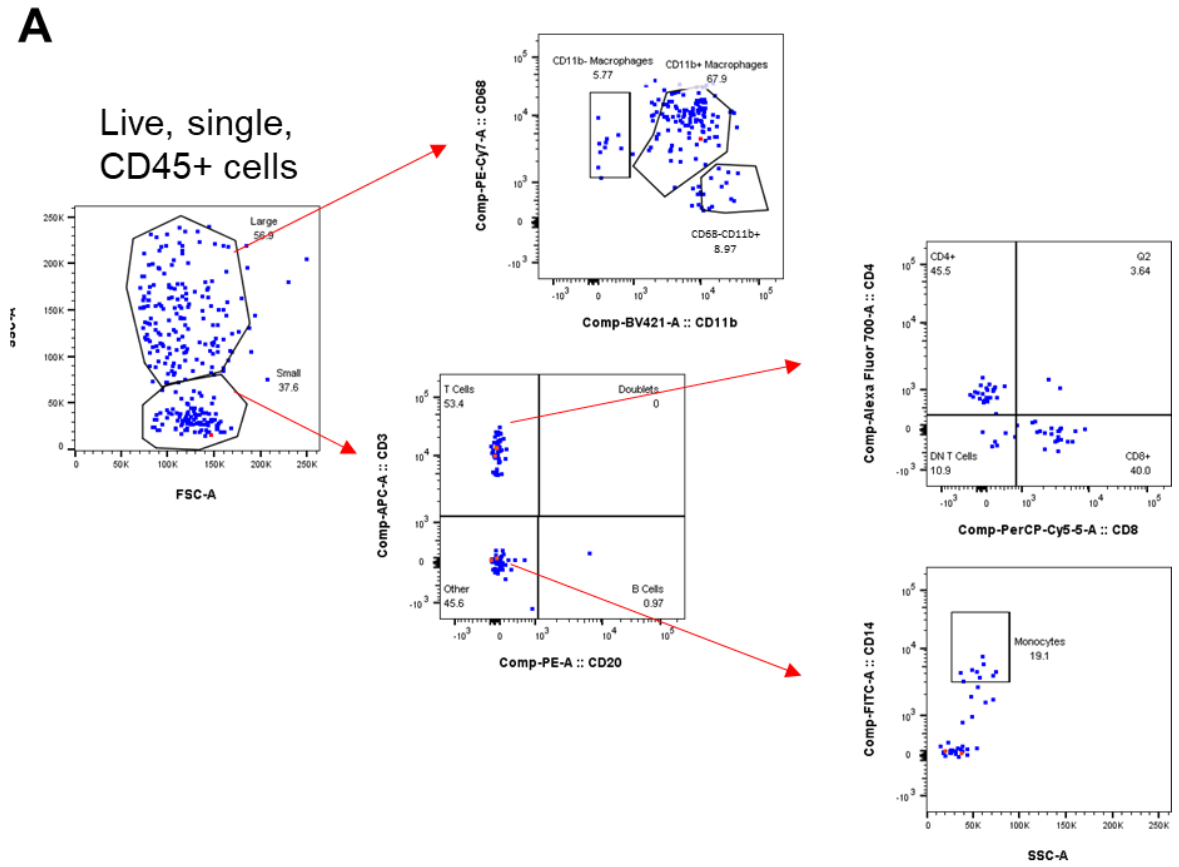
Figure 3.8: CD3+ T cells are present in the anterior uveal tract of healthy human eyes. (A) Photographic image of healthy human anterior uvea showing the different compartments including the iris and the ciliary body. (B) H&E staining of healthy human anterior uvea. Tile scan formed of 6 individual images captured at x10 magnification from the same sample. P – pupil, I – iris, IPE – iris pigmented epithelium, MCP – major ciliary processes, CPE – ciliary pigmented epithelium, CB – ciliary body, and C – choroid, red scale bar indicates 200µm. (C) Representative immunofluorescence image showing merged expression of nuclei (grey), CD3 (red), PDPN (green), and VCAM-1 (purple) within the iris. Image captured at x40 magnification. Red scale bar indicates 50µm. (D) Representative immunofluorescence images showing individual expression of either nuclei (grey), CD3 (red), PDPN (green), and VCAM-1 (purple) within the iris. (E) Representative immunofluorescence image showing merged expression of nuclei (grey), CD3 (red), PDPN (green), and VCAM-1 (purple) within the ciliary body. Image captured at x40 magnification. Red scale bar indicates 50µm. (F) Representative immunofluorescence images showing individual expression of either nuclei (grey), CD3 (red), PDPN (green), and VCAM-1 (purple) within the ciliary body.

the trabecular meshwork and Schlemm's canal due to uveal detachment from the sclera made during corneal removal.

- *-The limbal sclera*

FACS analysis was then also performed on healthy human limbal sclera to phenotype the major CD45+ leukocytes that are resident or trafficking through this tissue. A large amount of tissue was used for this analysis (~2mm cut was made around the circumference of the limbal sclera, which included any muscular attachment sites; **see previously described Figure 3.2**). Here we found a small population of T cells in the human. However, the total count of each individual leukocyte sub-populations in the limbal sclera was dramatically reduced compared to the anterior uvea **(Figure 3.9 A and B)**.

Sclera taken from healthy human eyes for use in FACS analysis was not deemed of good enough quality for histological examination. During the process of corneal removal for transplantation the anatomy of the limbal sclera was too significantly disrupted - resulting in the absence of vital regions of interest to this study. These regions included: the trabecular meshwork (TM), Schlemm's canal, the iridocorneal angle, iris root, supracoroidal lamina, supraciliary space, scleral spur and lamina fusca. Therefore, from this point forwards - histological examination of the anterior compartment was performed on intact, morphologically normal, sections of the human



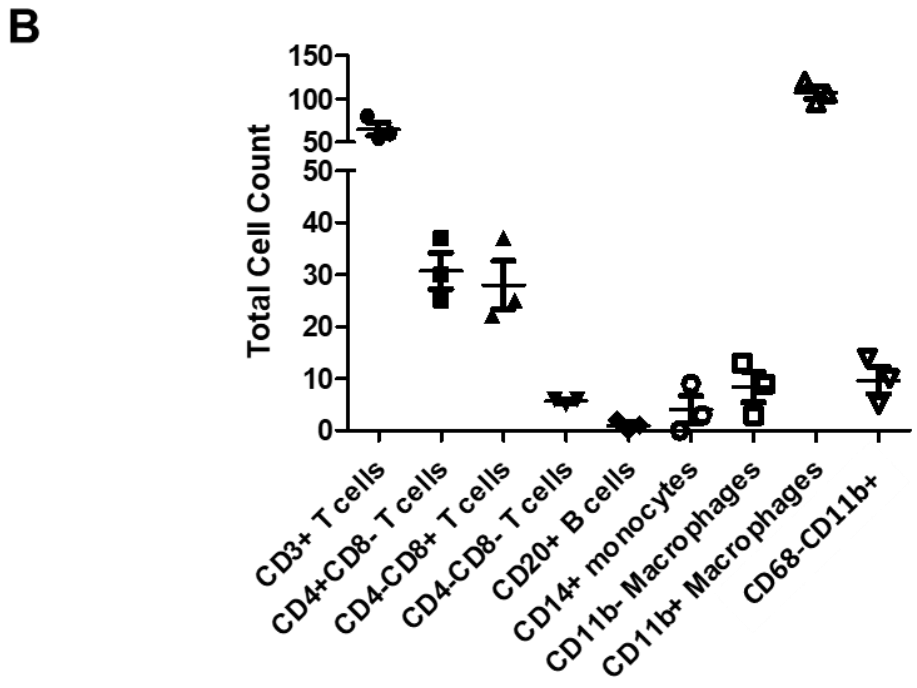


Figure 3.9: The healthy human limbal sclera is home to a diverse array of CD45+ leukocytes. The limbal sclera was dissected from the anterior compartment of the eye and consisted of sclera and extra ocular muscle enthesis. (A) Representative plots of 3 repeats show FACS gating strategy for sub populations of limbal sclera CD45+ leukocytes. (B) Sub populations include CD3+ T cells (sub divided into CD4+CD8-, CD4-CD8+, and CD4-CD8- T cells), CD20+ B cells, CD14+ monocytes, CD68+ macrophages (sub divided into CD11b+ and CD11b- Macrophages), and large/high complexity (based on light scatter) CD11b+CD68- cells.

anterior compartment (**Supplementary Figure 3.4)**, in eyes enucleated due to the presence of melanoma in the posterior compartment.

The entire cellular and extracellular architecture of the morphologically normal anterior compartment can be seen in equatorial transverse sections of the human eye. This was visualised by generating a tile scan image of multiple low magnification (10 times magnification) images **(Figure 3.10)**. As in mice T cells were observed throughout the anterior compartment. Comparable to the disrupted coronal sections of healthy human anterior uvea **(see Figure 3.8)**, T cells were also captured throughout the iris and ciliary body in the intact transverse sections. In contrast to coronal sections, transverse sections permitted the visualisation of T cells in both the *pars plana* and the *pars plicata* of the ciliary body. In both regions T cells were diffusely spread but in large numbers **(Figure 3.10)**. In addition, T cells were present at the iridocorneal angle where the trabecular meshwork forms a bridge between the iris root, scleral spur and the posterior limiting lamina (Desçemet's membrane) of the peripheral cornea (Figure 3.9).

T cells were captured throughout all layers of the sclera, from the outer vascular episclera to the most internal lamina fusca region, and even within the scleral spur **(Figure 3.10 and Figure 3.11)**. Interestingly T cells are found in both limbal sclera and peripheral cornea.

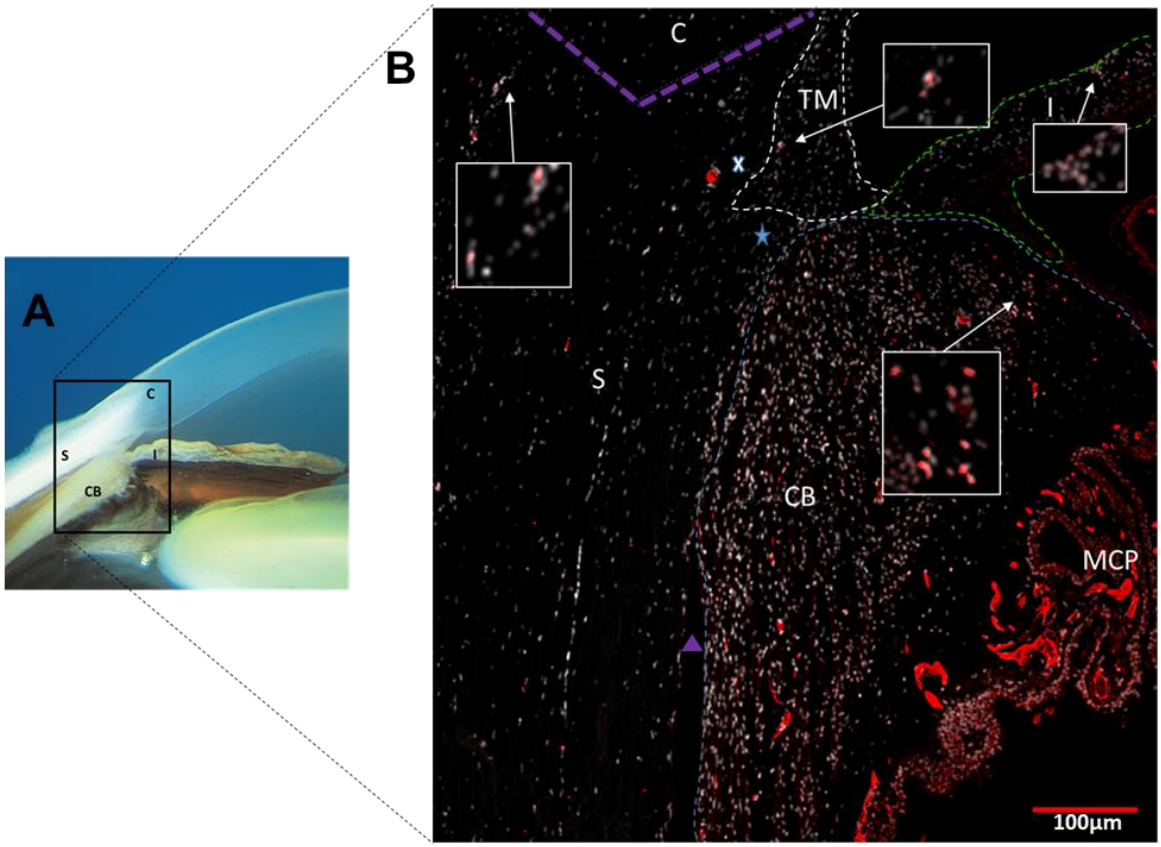


Figure 3.10: T cells are found throughout the anterior compartment of the human eye (A) Photographic image of the tissues surrounding the anterior cavity of the human eye: C – cornea, S – sclera, CB- corneoscleral limbus in globes from deceased individuals obtained from Liverpool Eye Bank (B) Immunofluorescent staining of human anterior eye FFPE section for nucleus (grey) and CD3+ (red) T cells. White arrows and boxes show areas of T cell clusters under digital magnification. Tile scan composed of 4 x 4 individual images. Images captured at x10 magnification. C – cornea, S – sclera, purple line – corneoscleral limbus, 'TM' and white line – trabecular meshwork, 'X' – Schlemm's canal, blue star – scleral spur, purple triangle - supraciliary space, 'I' and green line – iris, 'CB' and blue line – ciliary body, and MCP – major ciliary processes. Red scale bar indicates 100µm.

The transitional region where cornea stops and sclera begins, known as the surgical limbus, was estimated through identification of key landmarks: Schwalbe's line (defining the end of the trabecular meshwork), and the terminating region of Bowman's membrane. A V-shaped line pointing peripherally was then drawn between these structures representing the surgical limbus **(Figures 3.10B and 3.11B)**. Low numbers of diffusely spread, T cells were captured throughout the width of the peripheral cornea). These were found at a much lower frequency to the sclera. No T cells were observed in the central (anterior) cornea.

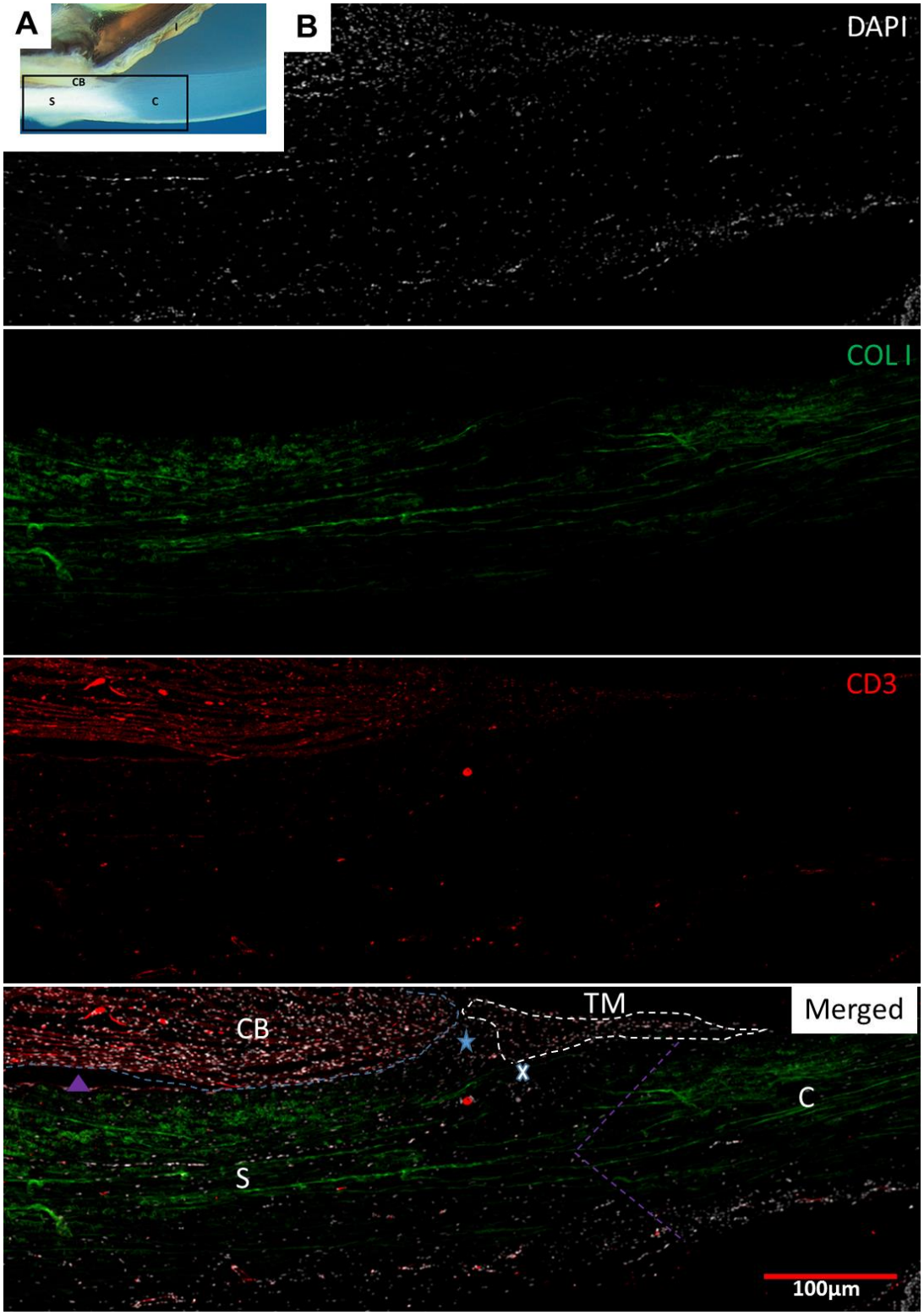


Figure 3.11: T cells are present in the human limbal sclera and less frequently within the peripheral cornea. (A) Photographic image of the tissues surrounding the anterior cavity of the human eye: C – cornea, S – sclera, CB- corneoscleral limbus. (B) Immunofluorescent staining of human anterior eye FFPE section for nucleus (grey), collagen type 1 (Col1; green), and CD3 (red) from cadaver eyes obtained from Liverpool Eye Bank. Tile scan composed of 4 x 4 individual images. Images captured at x10 magnification. C – cornea, S – sclera, purple line – corneoscleral limbus, 'TM' and white line – trabecular meshwork, 'X' – Schlemms canal, blue star – scleral spur, purple triangle - supraciliary space, 'CB' and blue line – ciliary body, and MCP – major ciliary processes. Red scale bar indicates 100µm.

T cells can be seen at the peripheral termination of the trabecular meshwork, but not in Descemet's membrane.

The highest frequency of T cells was captured proximal to the episclera where the density of collagen type 1 was low. In contrast, a much lower frequency of T cells was captured amongst the thick stromal layer where the ECM is rich in collagen type 1 **(Figure 3.11B)**. Low resolution CD3 signal was also captured on both sides of the scleral spur within the trabecular meshwork and ciliary body which indicated an absence of collagen type 1 in their ECM. The frequency of T cells increased in these tissues in sharp contrast to the end of collagen type 1 signal. T cells could not be captured in the outermost layers of the corneoscleral coat (Tenon's membrane, extraocular muscles, and conjunctiva), as these were removed/dissociated from the samples made available to this study, during the process of enucleation. In contrast to the ciliary body, T cells morphology was much more elongated and flatter within the dense collagenous matrix of the sclera **(Figure 3.12B)**.

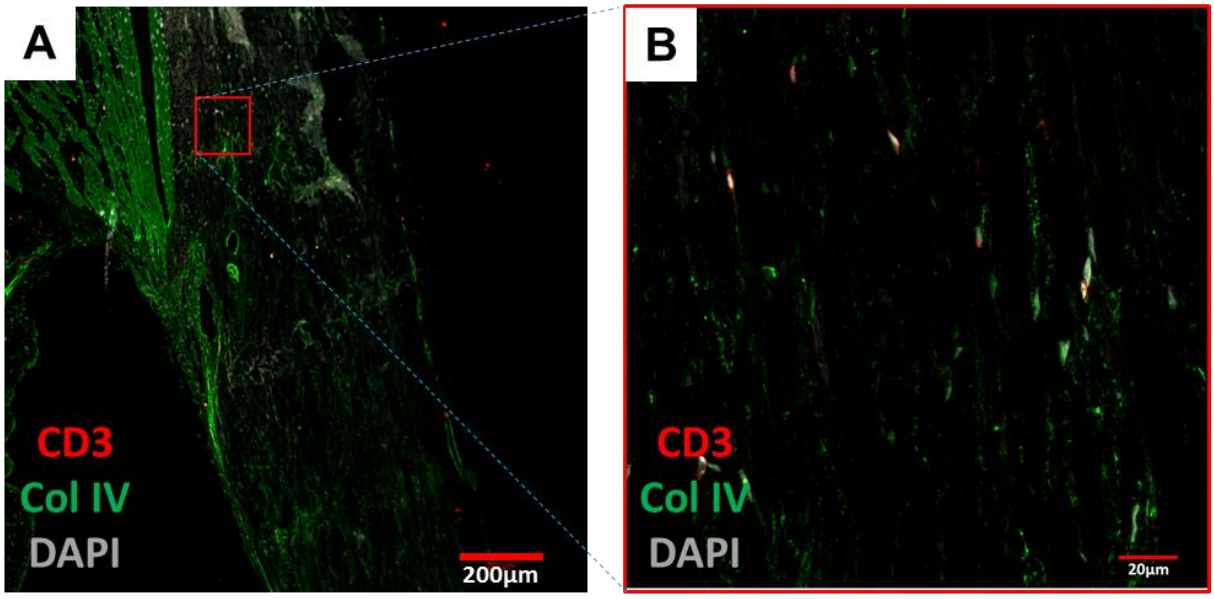


Figure 3.12: T cell morphology appears flat and elongated within the dense ECM of the sclera. A) Representative immunofluorescence image showing expression of nuclei (grey), CD3 (red), and Collagen type 4 (Col IV) (green) within the morphologically normal human anterior compartment. Red square highlights the region of tissue magnified in B. (B) Representative immunofluorescence image showing expression of nuclei (grey), CD3 (red), and Collagen type 4 (Col IV) (green) within the sclera.

Low magnification imaging (x10 magnification) of T cells that reside in the tissues surrounding the anterior cavity was hindered by the unwanted generation of autofluorescence signal **(Figures 3.10 and 3.11)**. This signal emanated from blood vessels and both iris and ciliary epithelium. This meant that T cells could not be captured proximal to these structures when images were acquired at x10 magnification. CD3 signal was detected using a primary rabbit anti-human polyclonal antibody (Abcam; #ab5690) and a secondary goat anti-rabbit IgG (H+L) conjugated to Alexa Fluor™ 633 (AF633), which had an emission spectrum wavelength between 610-800nm and an emission max of 647nm when excited at 632nm. Furthermore, a high voltage was applied to the 632nm laser to excite and make the CD3 signal visible at such a low magnification. The band pass filter used to detect CD3 signal was 670/30 which meant that the false-positive signal, also known as autofluorescence, arising from the blood vessels and epithelium were being emitted between 655 and 685nm when these cellular structures were excited at a high voltage 632nm wavelength.

There is an inverse ratio of CD4 to CD8 T cells in human anterior uvea and sclera samples compared to PBMCs

I first assessed if the immune composition of leukocytes in the anterior uveal tract and sclera was different to that which is found in peripheral blood. FACS analysis revealed a statistically significant decrease in the relative frequency of $CD45^+$ cells that were identified as lymphocytes (based on SSC-A and FSC-A) in the anterior uvea (AU) compared to control PBMCs (52.3 ± 3.7% for AU vs 88.1 ± 4% for PBMCs; *P* <0.001; **Supplementary Figure 3.5**). However, this result was expectedly skewed due to the presence of larger leukocytes such as macrophages and mast cells that known to reside in the extravascular tissue of the anterior uveal tract and were not found in peripheral blood. No significant differences in the relative frequency of $CD45^+$ cells that were lymphocytes (based on SSC-A and FSC-A) in the limbal sclera (LS), was noted compared to control PBMCs (68.6 ± 11.8% for LS vs 88.1 ± 4% for PBMCs; *p*<0.05; **Supplementary Figure 3.5**). However, a trend could be seen indicating a decrease in the relative frequency of lymphocytes in the LS compared to PBMCs. Interestingly, a statistically significant decrease in the relative frequency of $CD3^+$ T cells was observed in the AU compared to control PBMCs (61 ± 3% for AU vs 76.9 ± 3.2% for PBMCs; *p*<0.01; **Supplementary Figure 3.6**). This finding was also observed in the LS (57.2 ± 7.9% for LS vs 76.9 ± 3.2% for PBMCs; *p*<0.05; **Supplementary Figure 3.6)**.

Further investigation by FACS analysis revealed differences in the relative frequency of AU and LS T cell subsets compared to those found in control PBMCs. Strikingly, a statistically significant 31% decrease in the relative frequency of

$CD45^+CD3^+CD4^+CD8^-$ (CD4) T cells was observed in the AU compared to control PBMCs (33.8 ± 2.4% for AU vs 64.2 ± 3.4% for PBMCs; *p*<0.001; **Figure 3.13 A and B**). This finding was also observed in the LS (37 ± 3.2% for LS vs 64.2 ± 3.4% for PBMCs; *p*<0.001; **Figure 3.13 B**). In contrast, a statistically significant 29% increase in the relative frequency of $CD45^+CD3^+CD4^-CD8^+$ (CD8) T cells was observed in the AU compared to control PBMCs (58 ± 2.4% for AU vs 29 ± 2.8% for PBMCs; *p*<0.001; **Figure 3.13 A and C**). This finding was also observed in the LS (49.8 ± 6% for LS vs 29 ± 2.8% for PBMCs; *p*<0.001; **Figure 3.13 A and C**).

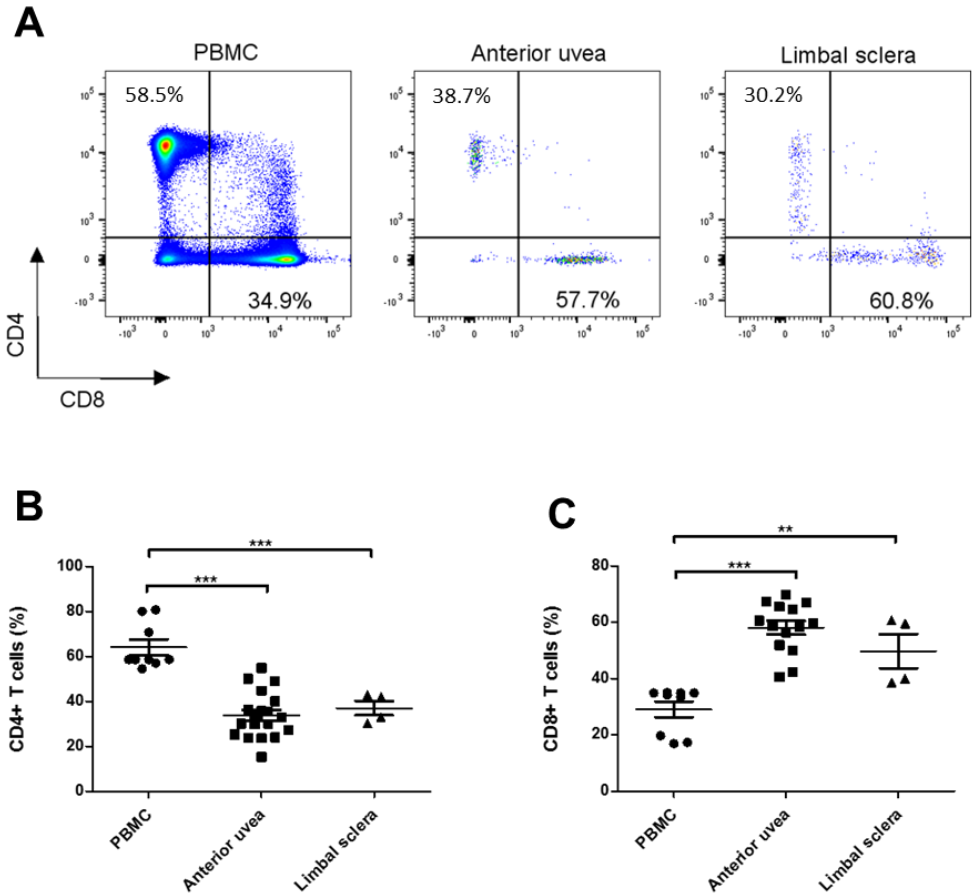


Figure 3.13: Analysis of the human anterior uvea and limbal sclera by flow cytometry shows an inverse relative frequency of CD4+ to CD8+ T cells to that found in Peripheral blood mononuclear cells (PBMCs). (A) Representative plots show flow cytometric analysis for uveal and sclera CD3+ T cells that are either CD4+ or CD8+ in contrast to those isolated from peripheral blood mononuclear cells (PBMCs). (B) FACS compiled frequency data for the percentage of live CD3+ T cells that are CD4 and (D) CD3+ T cells that are CD8+ in healthy anterior uvea (n = 19; data obtained from 7 independent experiments), limbal sclera (n = 4; data obtained from 2 independent experiments), and control blood (n = 9; data obtained from 4 independent experiments). Mean percentage is represented by the central line with error bars showing SEM ** = P<0.01 and *** = P<0.001 (ordinary one-way ANOVA test with Tukey's multiple comparison test).

The relationship of resident T cells with vascular and aqueous outflow structures of the anterior compartment

I next sought to assess the location of T cells in relation to vascular structures within the anterior compartment of the human eye. These vascular structures include blood vessels and vessels associated with the aqueous outflow and ACAID such as Schlemm's canal. In mice it was possible to locate tissue resident cells after perfusion of samples. However, in humans we achieved this by co-staining sections of the anterior compartment for CD3+ (T cells), CD34 (vascular endothelium), and PDPN (lymphatic endothelium).

It was also very important to this study to confirm that the architecture of tissue remained intact, and that all the joining regions (entheseal regions) of the multiple tissues that make up the anterior compartment were not disrupted. H&E staining of sequential transverse sections **(Supplementary Figure 3.4B)** confirmed that: (a) the enthesis formed between the corneoscleral coat and anterior uveal tract remained intact; (b) the folds of the inner ciliary body known as the ciliary processes was unaffected by sectioning (the appositional ciliary non-pigmented epithelium (CNPE) and ciliary pigmented epithelium (CPE) of the *pars plana*, and ciliary vascular core could all be identified with no dissociation from each other); (c) the region of ciliary body known as the ciliary muscle was unaffected by sectioning (the concentric layers of ciliary muscle of the *pars plicata* and *pars plana*, separated from the sclera by the supraciliary space, and could be identified with no dissociation from each other; the Collagen IV+ connective tissue between the muscle fibre bundles were also previously demonstrated to be intact in the previously described **Figure 3.12A**); (d) the iris was presented as one continuous structure from the collarette to the iris root where it narrowed and merged with the ciliary body and trabecular meshwork at the

iridocorneal angle; (e) the concentric layers of the iris: anterior border layer, stroma and sphincter muscle, anterior epithelium and dilator muscles, and iris posterior pigmented epithelium (IPPE) could all be identified with no dissociation from each other; (f) the iridocorneal angle (ICA) analysed which connects the iris root, the trabecular meshwork, and the ciliary body was continuous across these tissues; and (g) the concentric layers of the trabecular meshwork were mostly intact with only a small loss of uveal trabeculae.

A transverse section tile scan image of the human anterior compartment (generated from multiple smaller 10X magnification images) was used as an overview to identify vascular structures and structures associated with aqueous outflow **(Figure 3.14B and C)**. Multiple CD34+ vascular structures were observed within the anterior uveal tract). The major vascular artery that feeds the ciliary body and iris was the MACI and could be identified as a cross section in the anterior inner *pars plicata* by CD34 **(Figure 3.14 B and C)**. Cross sections of various smaller vascular structures were also identified by CD34 in the ciliary muscle and processes of the *pars plicata, the iris, and the corneoscleral limbus.* The variance in shape and size of these smaller vascular structures was likely due to their orientation at the point of cross section. The trabeculae of the corneoscleral trabecular meshwork did not show the presence of integrated vascular structures by CD34. In the iridocorneal angle, the trabecular meshwork, was noted by a high expression level of PDPN **(Figure 3.14 B and C)**. The corneoscleral trabeculae, and the cells that envelope them, could be seen extending towards the ciliary muscle of the *pars plicata.* The endothelium-lined canal of Schlemm lied between the outer aspect of the corneoscleral trabecular meshwork and the corneoscleral coat. This structure was identified by CD34 as a long circumferential channel **(Figure 3.14 B and C)**.

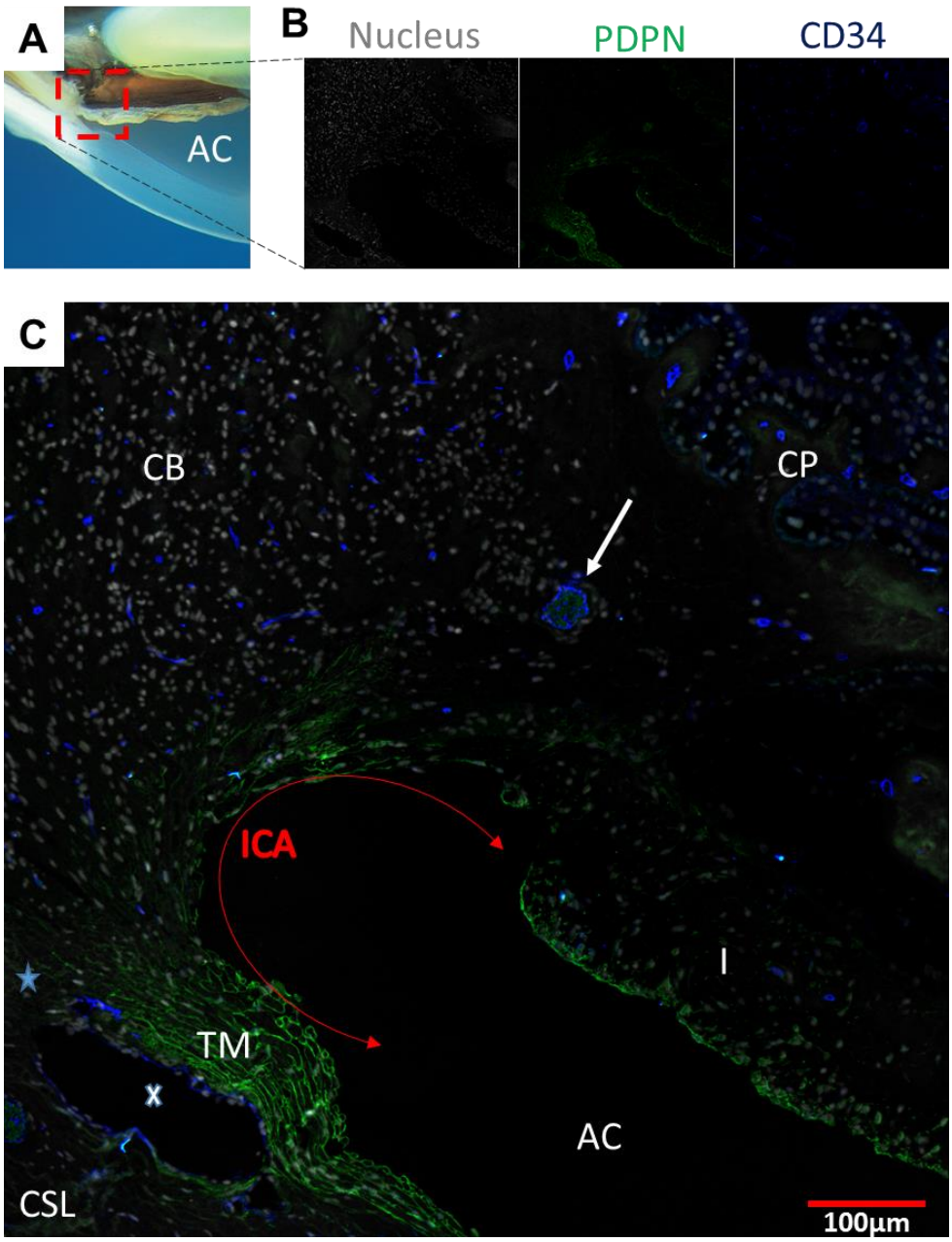


Figure 3.14: The anterior uvea is composed of a mixture of highly vascular and avascular tissues. (A) Photographic image of the tissues surrounding the anterior cavity of the human eye. (B) Representative confocal immunofluorescence (IF) images of a meridional section of the anterior uveal tract and anterior chamber from enucleated eyes with a healthy anterior chamber. Images show individual expression of Hoechst (nucleus) (grey), Podoplanin (PDPN; green), and CD34+ vascular structures (blue). (C) Representative confocal IF image of a meridional section of the anterior uveal tract and anterior chamber from enucleated eyes with a healthy anterior chamber. Image shows co-localisation of nucleus (grey), Podoplanin (green), and CD34+ vascular structures (blue). 4 by 4 tile scan images were stitched together, captured at x10 magnification. White arrow indicates a large vessel staining positive for CD34 and Podoplanin. Red scale bar indicates 100µm. CSL – corneoscleral limbus, TM – trabecular meshwork, X – Schlemm's canal, blue star – scleral spur, ICA and red arrow-headed line – the iridocorneal angle, CB - ciliary body, CP – ciliary process, I – iris, and AC – anterior chamber.

Although tile scans at 10X magnification generate an excellent overview of the vascular architecture within the anterior compartment, representative populations of

CD3+ T cells were poorly observed at this magnification **(Figure 3.14C)**. To demonstarte the relationship between CD3+ T cells, vascular structures, and aqueous outflow structures, transverse sections of the anterior compartment were analysed at a higher magnification (40X). Four regions of the anterior compartment were selected for high magnification imaging based on having high vascularity or association with aqueous outflow structures: (1) *pars plicata* ciliary body; (2) iris ciliary zone; (3) The irideocorneal angle; and (4) the corneoscleral trabecular meshwork.

T cells in the extravascular tissue of the ciliary body

Multiple CD34+ vascular structures were observed within the major ciliary processes **(Figure 3.15 A-C).** The CD34+ vascular structures varied in size and shape and were restricted to the core. No CD34+ vascular structures were evident past the basement membrane of the CNPE or within the CPE, as expected. T cells were observed throughout the core of the major ciliary process **(Figure 3.15B)**. Many of these T cells were found within the extravascular tissue, identified as being outside of vascular structures staining positive for CD34, or identified by second harmonic resonance **(Figure 3.16)**. The majority of extravascular ciliary process T cells appear

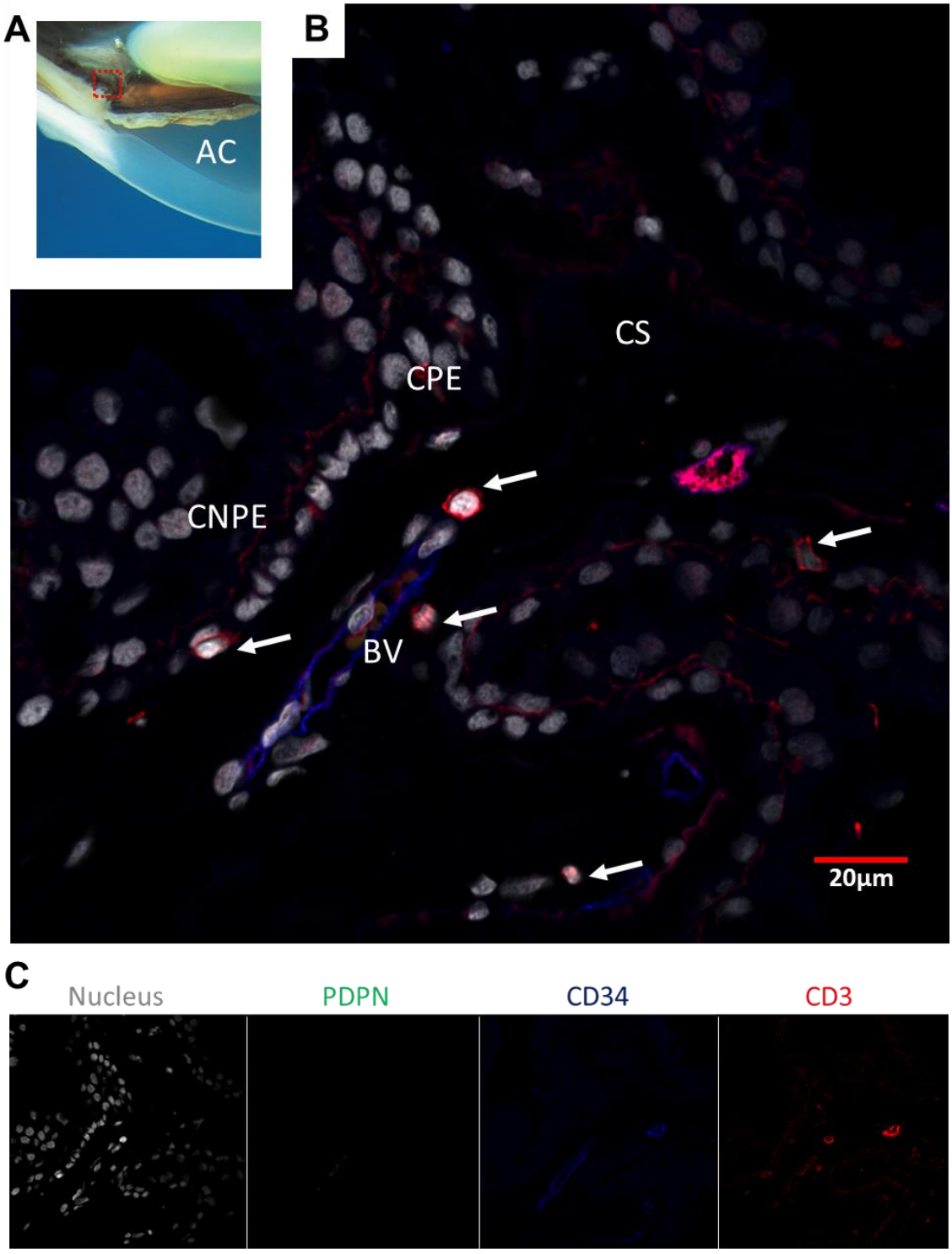


Figure 3.15: CD3+ T cells are found in the extravascular tissue of human ciliary processes. (A) Photographic image of the tissues surrounding the anterior cavity of the human eye. Red square highlighting the ciliary processes. (B) Representative confocal immunofluorescence (IF) image of a fold in the ciliary body known as a ciliary process. Section taken from an enucleated eye with a healthy anterior chamber. Image shows co-localisation of Hoechst (nucleus) (grey), Podoplanin (PDPN) (green) and CD34+ vascular structures (blue), and CD3+ T cells. Image captured at x40 magnification. White arrows indicate the presence of T cells outside of vascular structures. Red scale bar indicates 20µm. (C) Representative confocal IF images of a ciliary process. Section taken from an enucleated eye with a healthy anterior chamber. Images show individual expression of nucleus (grey), PDPN (green), CD34 (blue), and CD3 (red). AC – anterior chamber, CNPE – ciliary non-pigmented epithelium, CPE – ciliary pigmented epithelium, CS – ciliary stroma, and BV – blood vessel.

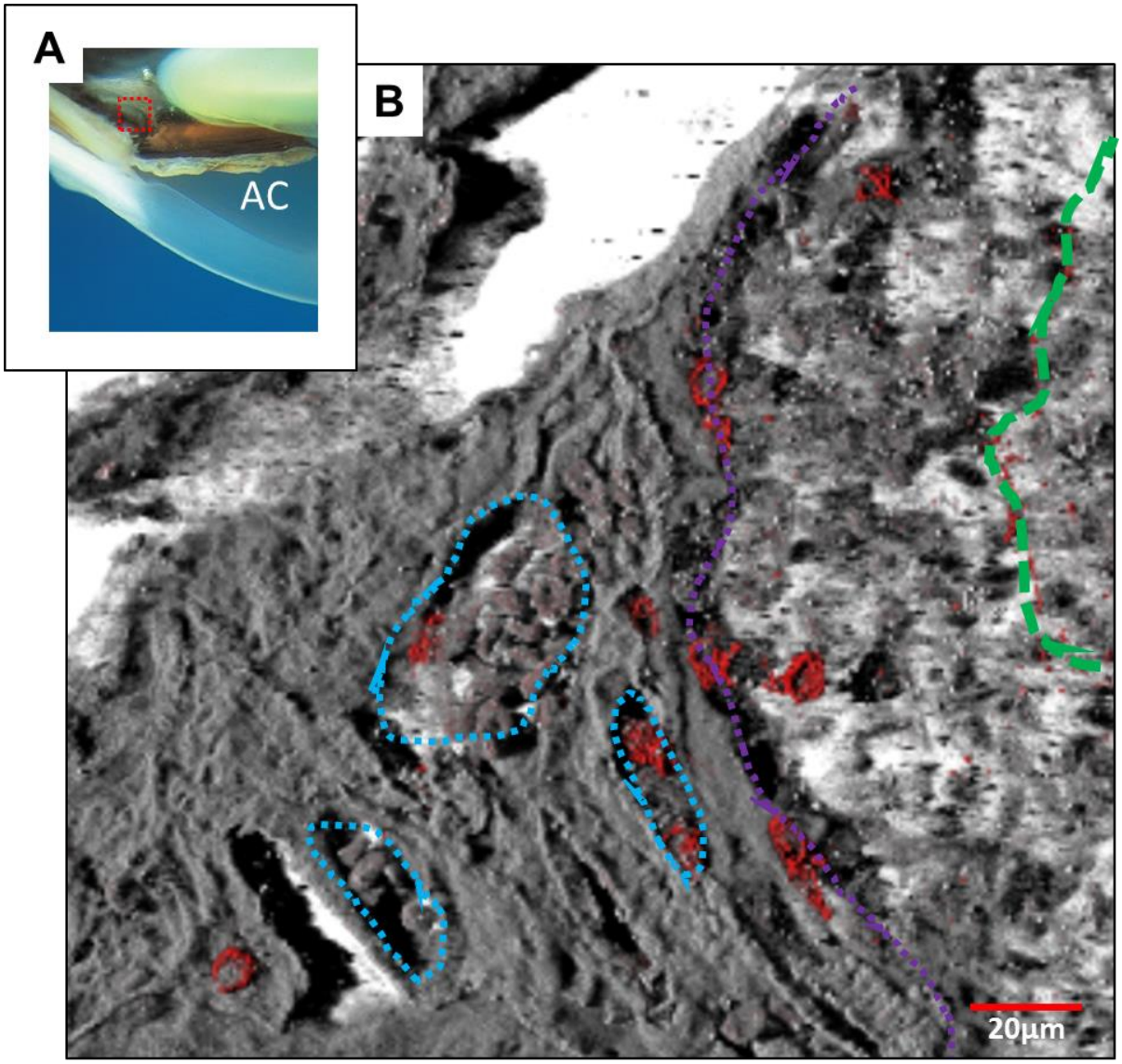


Figure 3.16: CD3+ T cells are found outside of vascular structures identified by second harmonic resonance in human ciliary processes. (A) Photographic image of the tissues surrounding the anterior cavity of the human eye. Red square highlighting the ciliary processes. (B) Representative confocal immunofluorescence (IF) image of a fold in the ciliary body known as a ciliary process. Transverse section taken from an enucleated eye with a morphologically normal anterior chamber. Image shows CD3+ (red) T cells outside of vascular structures visualised through second harmonic resonance (grey). Image captured at x40 magnification. Purple dashed line highlights the basement membrane of the ciliary pigmented epithelium (CPE); green dashed line highlights the division between CPE and ciliary non pigmented epithelium; blue dashed line highlights blood vessels filled with erythrocytes.

to be arranged closely to the basement membrane of the CPE **(Figure 3.15 and 3.16)**.

No T cells were observed in the CPE.

To assess the relationship between T cells, the collagenous vascular core of the ciliary processes, and the basement membrane of the CPE, high magnification multiphoton

imaging was utilised to generate second harmonic resonance images of collagen fibres in coronal sections of healthy tissue **(Figure 3.17 C-E)**. T cells were observed throughout the dense collagen cores of ciliary processes. They were identified by the co-localisation of CD3 around nuclei (signal generated as an artefact of second harmonic resonance generated by 488 wavelength). Most T cells were observed in the centre of the collagenous cores **(Figure 3.17 C and D)**. However, some T cells were proximal to fine collagen fibres inserting into the CPE **(Figure 3.17 E)**, beyond the basement membrane of the CPE but not the CNPE.

To further confirm that T cells in the CPE were not an artefact of sectioning in the coronal plane, whole mount imaging was performed on intact CD3 stained ciliary processes **(Figure 3.18 A-D)**. By repeating the second harmonic resonance process to visualise the dense collagen cores of ciliary processes we were still able to observe T cells on clusters of collagen fibres inserting into the CPE **(Figure 3.19 B, C and D)**.

It must be noted that a low level of autofluorescence emitted at the same wavelength as the fluorophore used to identify CD3+ T cells was detected from red blood cells inside the vascular structures, and a low level of autofluorescence emitted at the same wavelength as the fluorophore used to detect CD34+ vascular structures could be seen coming from the CNPE **(see previously described Figure 3.14)**. However, the autofluorescence signals were below the lower detection levels of CD3+ and CD34+ signals respectively.

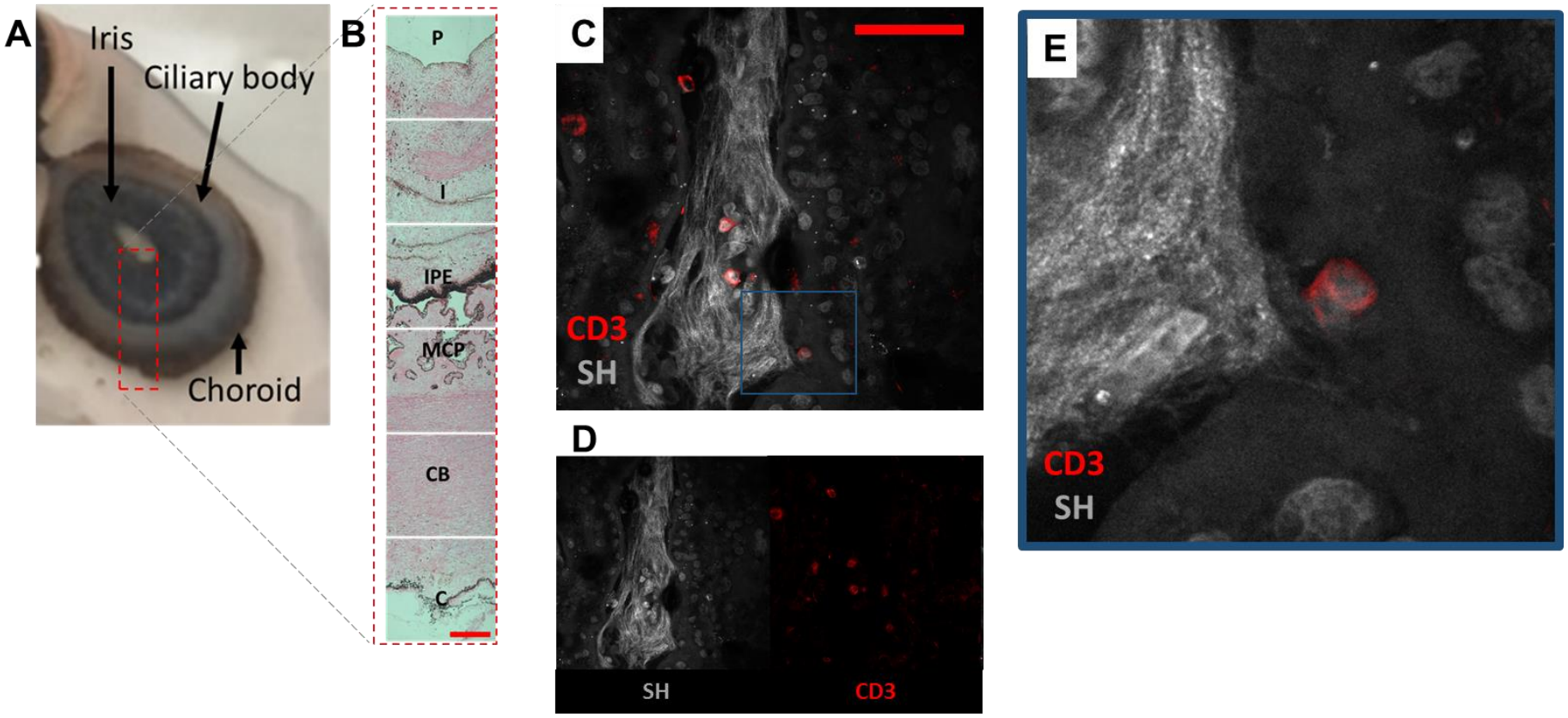


Figure 3.17: CD3+ T cells are associated with collagen fibres which insert into the ciliary pigmented epithelium of human eyes. (A) Photographic image of healthy human anterior uvea. (B) H&E staining of healthy human anterior uvea. Tile scan formed of 6 individual images captured at x10 magnification from the same sample. P – pupil, I – iris, IPE – iris pigmented epithelium, MCP – major ciliary processes, CB – ciliary body, and C – choroid, red scale bar indicates 200µm. (C) Representative immunofluorescence image showing merged expression of second harmonic resonance collagen fibres and nuclei (grey), and CD3 (red) within a major ciliary process. Blue square highlights the region magnified in E. Image captured at x40 magnification. Red scale bar indicates 50µm. (D) Representative immunofluorescence images showing individual expression of either second harmonic resonance collagen fibres and nuclei (grey), or CD3 (red) within a major ciliary process (E) Representative immunofluorescence image showing merged expression of second harmonic resonance collagen fibres and nuclei (grey), and CD3 (red) within a major ciliary process. Image captured at x40 magnification.

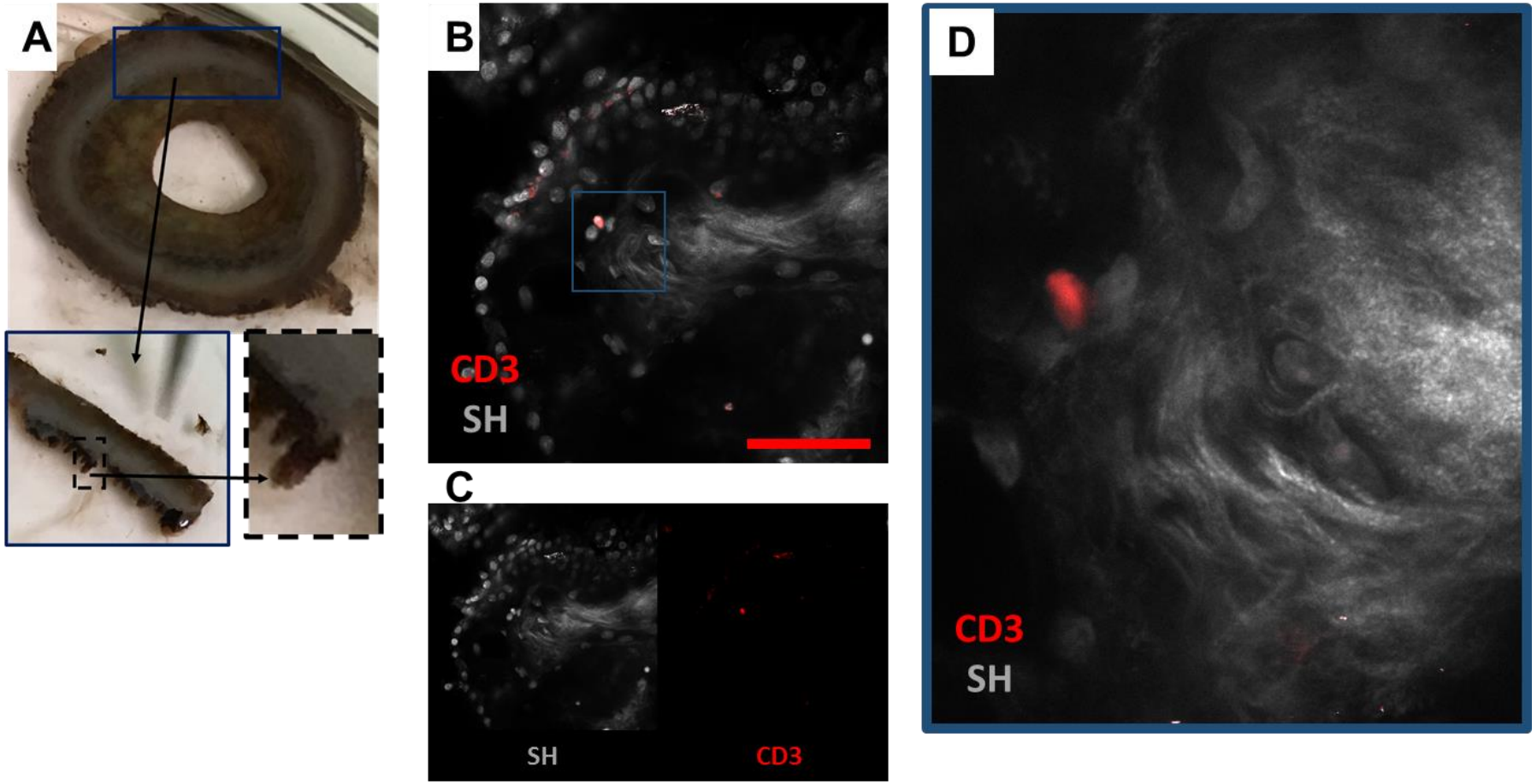


Figure 3.18: CD3+ T cells inserted into the ciliary pigmented epithelium by collagen fibres of the vascular core are not artefacts of sectioning in healthy human eyes. (A) Photographic image showing dissection of a major ciliary process from healthy human anterior uvea. (B) Representative whole mount fluorescence image showing merged expression of second harmonic resonance collagen fibres and nuclei (grey), and CD3 (red) within a major ciliary process. Blue square highlights the region magnified in D. Image captured at x40 magnification. Red scale bar indicates 50µm. (C) Representative whole mount fluorescence images showing individual expression of either second harmonic resonance collagen fibres and nuclei (grey), or CD3 (red) within a major ciliary process (D) Representative whole mount fluorescence image showing merged expression of second harmonic resonance collagen fibres and nuclei (grey), and CD3 (red) within a major ciliary process. Image captured at x40 magnification.

Multiple T cells were also observed outside of CD34+ vascular structures in the ciliary muscle region of ciliary body **(Figure 3.18 A- C)**. It must be noted that a low level of autofluorescence emitted at the same wavelength as the fluorophore used to identify CD3+ T cells and CD34+ vascular structures can be seen coming from the ciliary muscle and connective tissue **(Figure 3.18 C)**. However, the autofluorescence signals are below the lower detection limits of CD3+ and CD34+ signals respectively. Also previously confirmed was that PDPN positive cells of the trabecular meshwork are anchored onto the ciliary muscle within the anterior *pars plicata* **(see previously described Figure 3.13)** but not in the intermediate and posterior *pars plicata.* As the region of ciliary muscle shown in **Figure 3.18** did not contain any PDPN cells, the region shown was either from the intermediate or posterior *pars plicata* ciliary body.

T cells in the extravascular tissue of the iris

T cells were observed outside of CD34+ vascular structures in the iris ciliary region **(Figure 3.19 A-C)**. T cells were mostly seen proximal to the anterior epithelium and dilator muscles of the posterior border layer (**Figure 3.19 B**), but rarely seen proximal to the PDPN high anterior border layer. This was even more evident when looking at intermediate - posterior coronal sections of the iris (see previous described **Figures 3.7 C and D**).

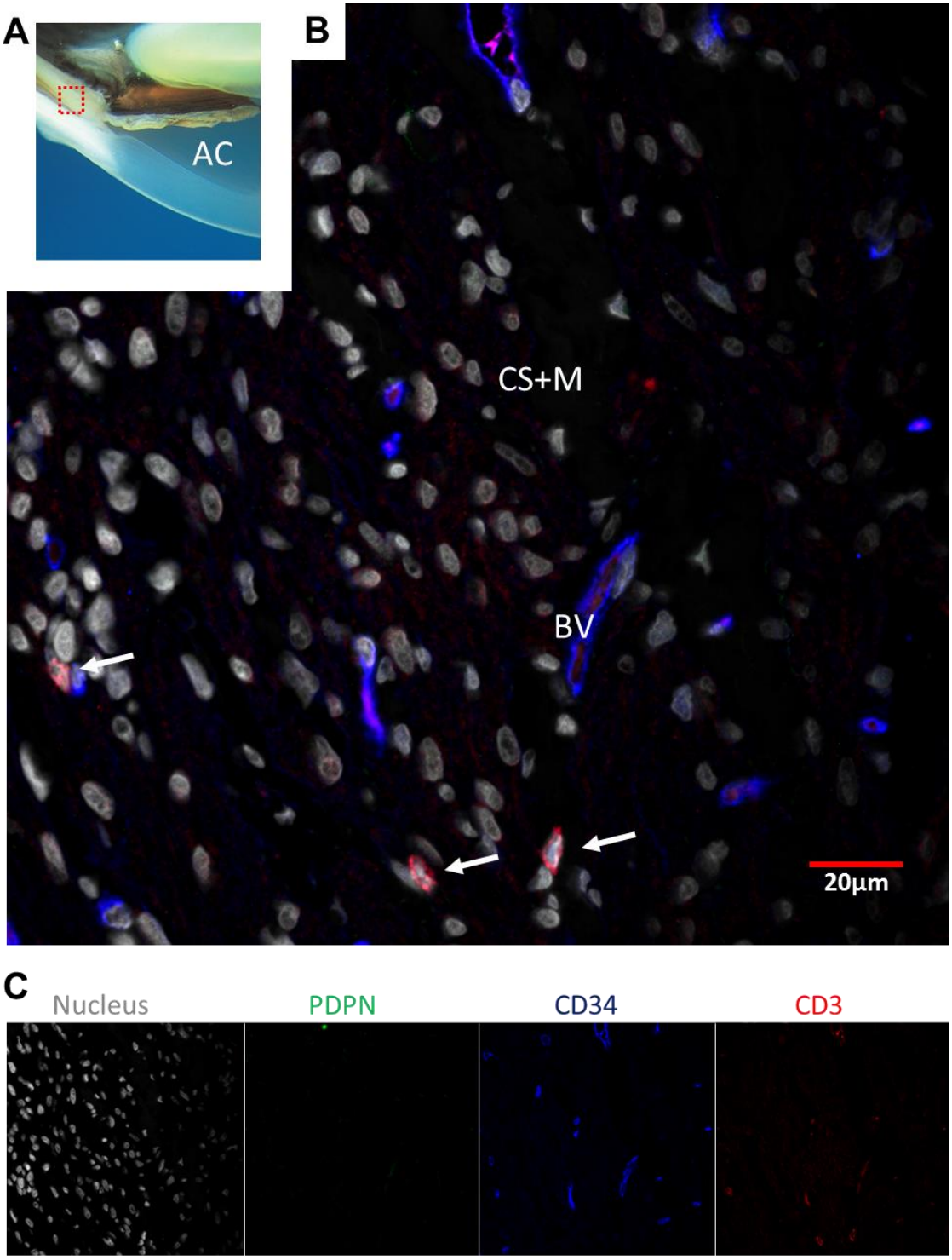


Figure 3.19: CD3+ T cells are in the extravascular tissue of morphologically normal human ciliary body. (A) Photographic image of the tissues surrounding the anterior cavity of the human eye. Red square highlighting the muscular region of ciliary body known as the *pars plicata*. (B) Representative confocal immunofluorescence (IF) image of *pars plicata*. Section taken from an enucleated eye with a healthy anterior chamber. Image shows co-localisation of Hoechst (nucleus) (grey), Podoplanin (green) and CD34+ vascular structures (blue), and CD3+ T cells. Image captured at x40 magnification. White arrows indicate the presence of T cells outside of vascular structures. Red scale bar indicates 20µm. (C) Representative confocal IF images of the *pars plicata*. Section taken from an enucleated eye with a healthy anterior chamber. Images show individual expression of nucleus (grey), Podoplanin (green), CD34 (blue), and CD3 (red). AC – anterior chamber, CS+M – ciliary stroma and muscle, and BV – blood vessel.

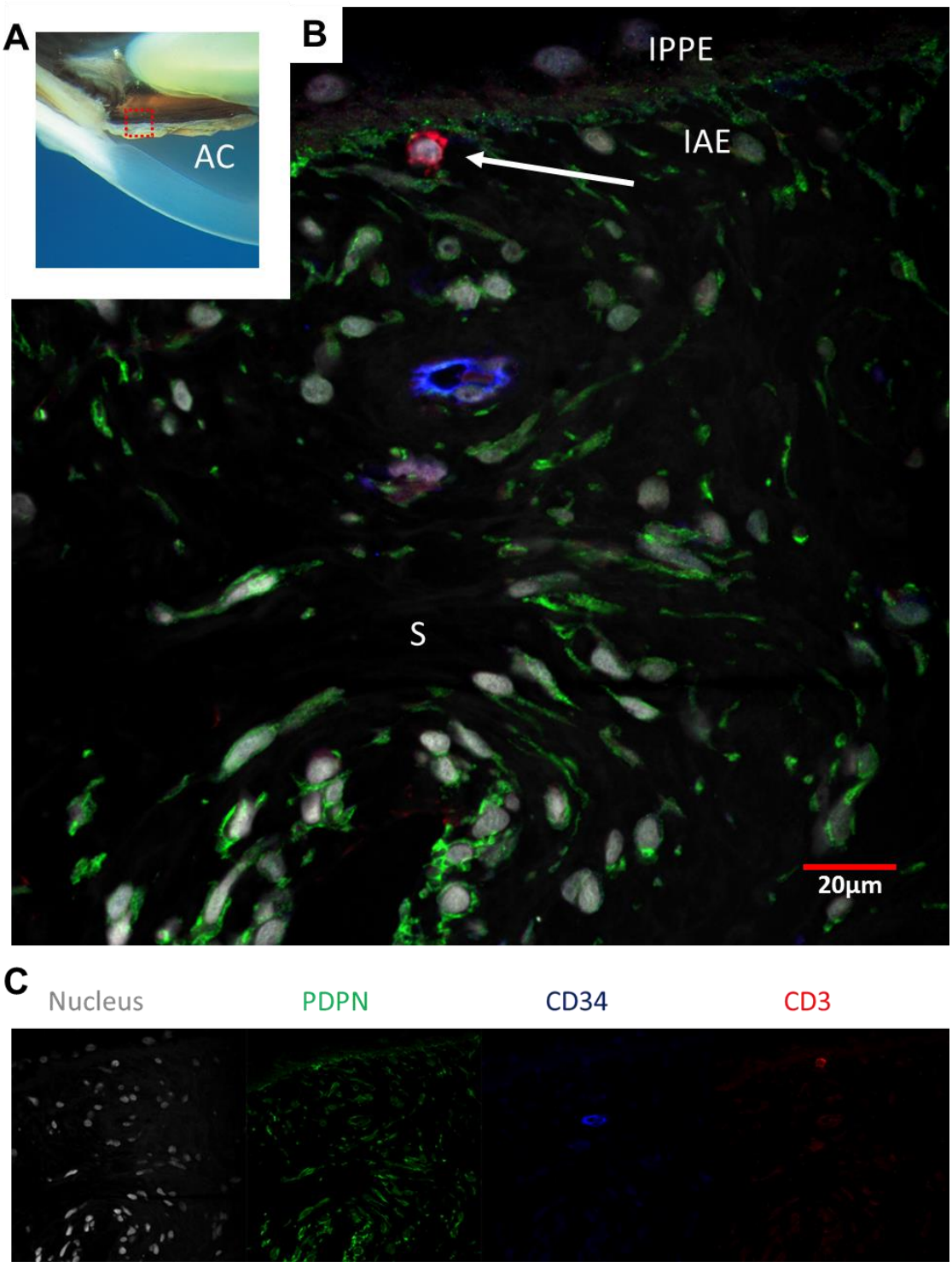


Figure 3.20: CD3+ T cells are in the extravascular tissue of the iris in morphologically normal sections of the human anterior eye compartment. (A) Photographic image of the tissues surrounding the anterior cavity of the human eye. Red square highlighting the posterior region of the iris. (B) Representative confocal immunofluorescence (IF) image of the posterior region of the iris. Section taken from an enucleated eye with a healthy anterior chamber. Image shows co-localisation of Hoechst (nucleus) (grey), Podoplanin^{+} (green) and CD34^{+} vascular structures (blue), and CD3^{+} T cells. Image captured at x40 magnification. White arrow indicates the presence of a T cell outside of vascular structures. Red scale bar indicates 20µm. (C) Representative confocal IF images of the posterior iris. Section taken from an enucleated eye with a healthy anterior chamber. Images show individual expression of nucleus (grey), Podoplanin (green), CD34 (blue), and CD3 (red). AC – anterior chamber, IPPE – iris posterior pigmented epithelium, IAE – iris anterior epithelium, and S – stromal layer.

T cells in the extravascular tissue of the iridocorneal angle (ICA)

The ICA was largely formed of PDPN positive cells of the trabecular meshwork branching into the ciliary body and inserting into the scleral spur or longitudinal ciliary muscle fibres and contained very few CD34+ vascular structures. 40x magnification imaging of the ICA confirmed that T cells were observed outside of CD34+ vascular structures **(Figure 3.20 A-C)**. These T cells were found in large frequencies right at the border of the ICA and arranged alongside PDPN+ trabeculae cells. No T cells were observed within the estimated region of the scleral spur (represented by the star symbol). It is also important to note that it was impossible to observe T cells in the aqueous of the anterior chamber in transversely sectioned tissue. This is because all aqueous fluid would have been lost during processing and sectioning of tissue.

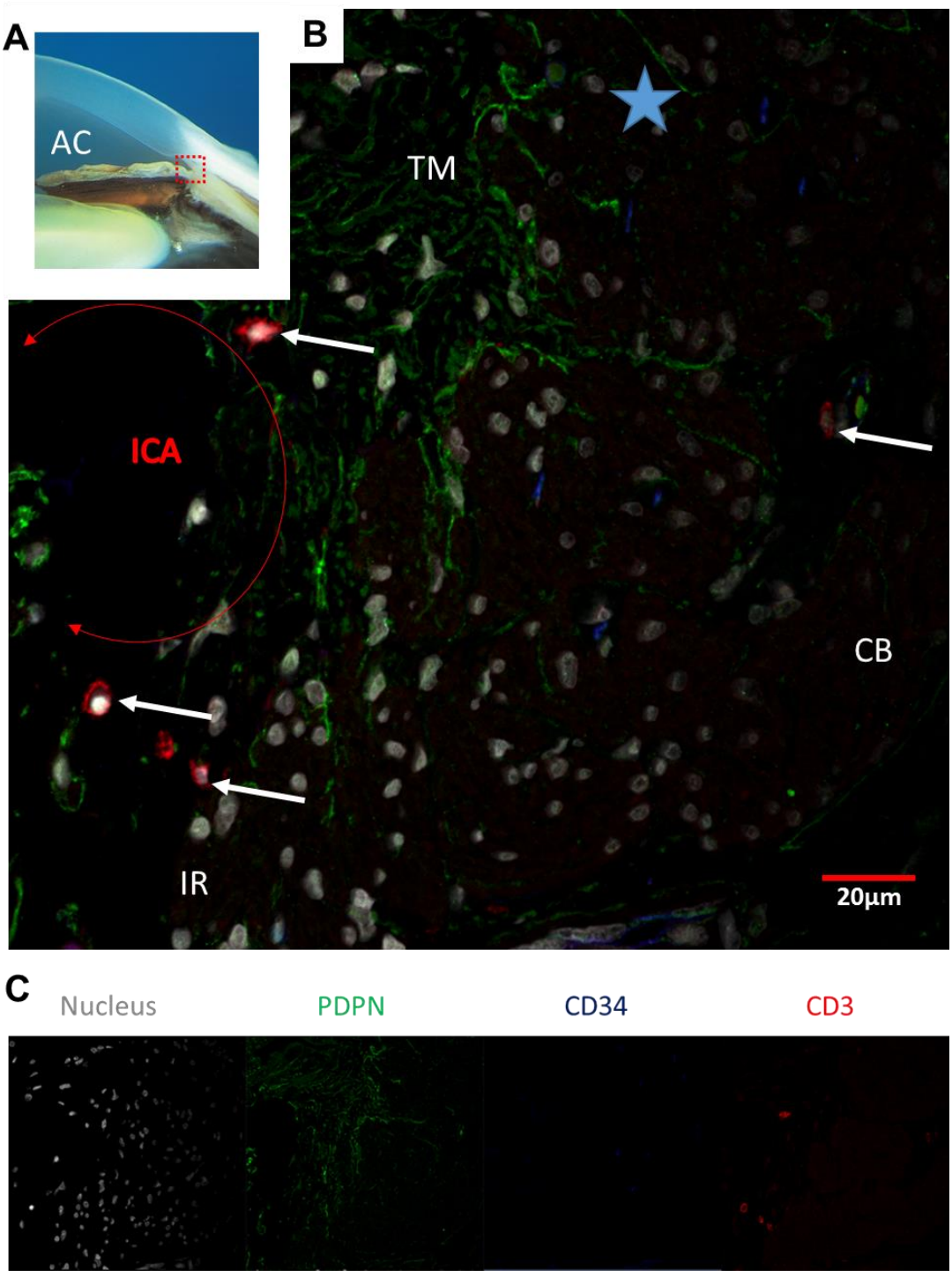


Figure 3.21: CD3⁺ T cells are located proximal to podoplanin+ (PDPN) cells organised along trabeculae fibres at the iridocorneal angle. (A) Photographic image of the tissues surrounding the anterior cavity of the human eye. Red square highlighting the structures forming the iridocorneal angle. (B) Representative confocal immunofluorescence (IF) image of the iridocorneal angle. Section taken from an enucleated eye with a healthy anterior chamber. Image shows co-localisation of Hoechst (nucleus) (grey), PDPN⁺ (green) and CD34⁺ vascular structures (blue), and CD3⁺ T cells. Image captured at x40 magnification. White arrows indicate the presence of a T cells outside of vascular structures. Red scale bar indicates 20µm. (C) Representative confocal IF images of the iridocorneal angle. Section taken from an enucleated eye with a healthy anterior chamber. Images show individual expression of nucleus (grey), PDPN⁺ (green), CD34 (blue), and CD3 (red). AC – anterior chamber, ICA and red arrow-headed line – iridocorneal angle, TM – trabecular meshwork, blue star – scleral spur, CB – ciliary body, and IR – iris root.

T cells in the trabecular meshwork

The trabecular meshwork was chosen as a region of interest as it filters and modulates the flow of all aqueous fluid exiting the anterior chamber via Schlemm's canal (the canonical route of aqueous outflow in the eye). Potentially, any T cells that might be in the aqueous fluid of the eye would be directed towards and pass through the trabecular meshwork. Additionally, the trabecular meshwork can be considered an entheseal tissue as it forms tendon like connections between the cornea, sclera and longitudinal muscles. This was confirmed in the previously described **Figure 3.13 C** where PDPN+ Trabeculae were seen branching from Schwalbe's line to either the ciliary body, the anterior border layer of the iris, or to the scleral spur.

The three anatomical zones of the trabecular meshwork were estimated based on the density and location of PDPN+ trabeculae **(Figure 3.21 B)**: (1) the uveal meshwork; (2) the corneoscleral meshwork; (3) the cribriform meshwork. Schlemm's canal is bridged by the trabecular meshwork and easily identifiable by CD34+ inner and outer wall endothelium surrounding a very large lumen. 40x magnification imaging of the trabecular meshwork confirmed that T cells were located in the cribriform layer adjacent to the inner wall of Schlemm's canal **(Figure 3.21 B and C)**. No T cells were observed in the uveal meshwork or corneoscleral meshwork except where trabeculae merge with the iris root and penetrate the ciliary body at the iridocorneal angle **(Figure 3.20 B)**.

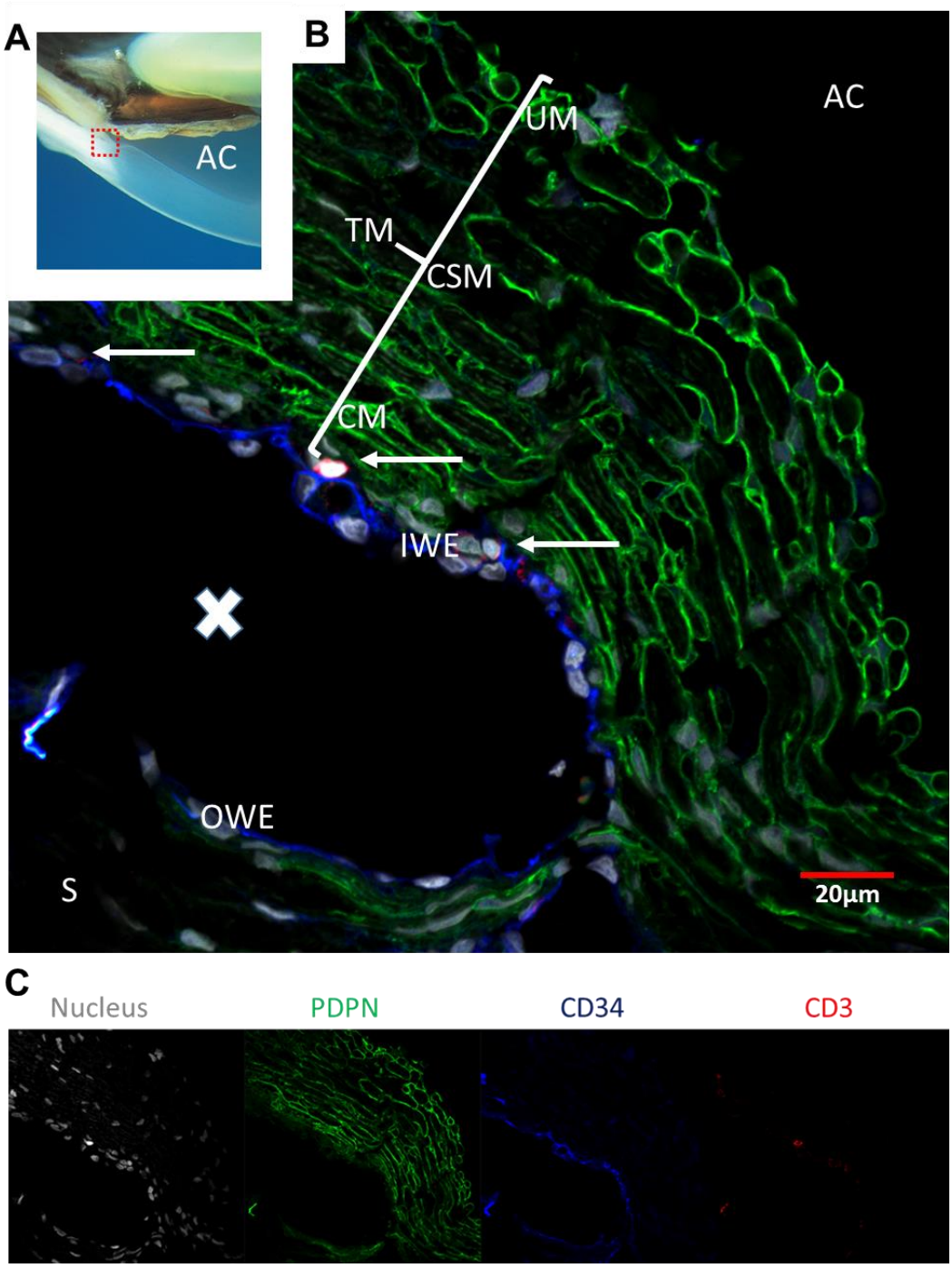


Figure 3.22: CD3⁺ T cells are located outside of Schlemm's canal - proximal to the inner wall epithelium running adjacent to the cribriform meshwork. (A) Photographic image of the tissues surrounding the anterior cavity of the human eye. Red square highlighting the trabecular meshwork and Schlemm's canal. (B) Representative confocal immunofluorescence (IF) image of the trabecular meshwork and Schlemm's canal. Section taken from an enucleated eye with a healthy anterior chamber. Image shows co-localisation of Hoechst (nucleus) (grey), Podoplanin⁺ (PDPN) (green) and CD34⁺ vascular structures (blue), and CD3⁺ T cells. Image captured at x40 magnification. White arrows indicate the presence of a T cells outside of Schlemm's canal. Red scale bar indicates 20µm. (C) Representative confocal IF images of the trabecular meshwork and Schlemm's canal. Section taken from an enucleated eye with a healthy anterior chamber. Images show individual expression of nucleus (grey), PDPN (green), CD34 (blue), and CD3 (red). AC – anterior chamber, TM – trabecular meshwork, UM – uveal meshwork, CSM – corneoscleral meshwork, CM – cribriform meshwork, IWE – inner wall epithelium of Schlemm's canal, OWE – outer wall epithelium of Schlemm's canal, 'X' – the lumen of Schlemm's canal, and S – sclera.

Discussion

In the previous chapter, I found that IL-23 was sufficient to drive inflammation of the uveal tract (uveitis) and retina (retinitis) in C57BL/6 mice, and that IL-23 associated uveoretinitis was dependent on a resident or infiltrating RAG dependent cell, presumed to be a T cell. As inflammation was seen as early as day 3 in these mice, it is highly likely that the T cells in question must be resident within the tissue where inflammation originates as there would not have been enough time for an adaptive, antigen specific immune response to be initiated and the resultant cells recruited to the eye. Evidence shown in this chapter unequivocally shows the presence of CD4 T_H cells, CD8 expressing cytotoxic T cells, and CD4-CD8- T cells in the extravascular tissue of the normal C57BL/6 mouse eye anterior chamber. This is the first study that extensively documents the exact location of CD3+ T cells in each of the tissues that make up the anterior compartment of the mouse and human eye.

IL-23 responsive T cells have been previously identified in the entheseal tissue of the axial skeleton in mice, which is the area where inflammation arises in the prototypical SpA AS in humans (Sherlock et al. 2012; Reinhardt et al. 2016). Moreover, IL-23 responsive T cells have also been identified within the lamina propria of the gut in mice associated with IBD. Further evidence regarding involvement of IL-23 at peripheral sites was reported by Sherlock et al. (2012) and further confirmed by Reinhardt et al. (2016) who demonstrated that T cells accumulate within the aortic valve and at a region proximal to the sclera of the eye in mice after systemic IL-23 overexpression. Therefore, it is likely that an IL-23 responsive T cell could be resident at a proximal location to the anterior uvea of both the mouse and human eye. In this Chapter I have also identified T cells at a number of tissue junctions of the anterior inner eye that can be considered entheseal in nature.

Lymphocytes were originally reported to be absent or scant in the normal uveal tract of rodents (Williamson, Bradley, and Streilein 1989) and in the human iris (Wakefield, McCluskey, and Palladinetti 1992). Personal observations in a later review by McMenamin (1997) also concluded that there are no γδ T cells in the extravascular tissue of the uveal tract. Each of the studies mentioned above had their own limitations (see below) which may have resulted in no T cells being documented specifically in the extravascular tissue of the anterior uvea.

Williamson et al. (1989) looked at both the anterior and posterior compartments of the eye individually in BALB/c mice. However, they only used an antibody against the Thy-1 molecule (clone not stated; obtained from Becton-Dickinson) to phenotype for T cells using epifluorescent microscopy and flow cytometry (Epics V, Coulter Electronics, Hialeah, FL). By not using the pan specific T cell marker CD3, this may have resulted in not identifying all of the T cells within the anterior compartment. In addition, only tissues from the ciliary body and iris were included in their analyses, so any T cells in the limbal sclera and trabecular meshwork could have been missed.

Wakefield et al. (1992) analysed iris biopsy samples from ten patients with uveitis (8 of which were idiopathic) and 12 subjects who were undergoing cataract surgery without a history of inflammatory eye disease. Samples were sectioned (depth was not stated) and analysed by microscopy at 25X magnification for the binding of primary antibodies against the T cell markers CD2, CD4, CD8, and CD25 (clones not stated; signal identified by secondary antibody immunoperoxidase staining). As in the Williamson et al. (1989) study, Wakefield et al. (1992) failed to phenotype CD3+ cells, and although they examined for the expression of CD4+ and CD8+ T cells, any identification of the CD4-CD8- subtype was omitted.

In addition, Wakefield et al. (1992) extracted iris biopsies from three different eye operations; trabeculectomy, iridectomy, or planned extracapsular cataract extraction. This is not ideal because of potentially a number of limitations; e.g. a) cellular variability from different sites; b) variations in operative technique; c) estimation on exact location (ciliary body vs iris root vs trabecular meshwork) of biopsies were taken from; and d) size of biopsies. The National Survey of Trabeculectomy I (Edmunds et al. 1999) and The National Survey of Trabeculectomy II (Edmunds et al. 2001) report considerable variation in practice and operative technique. Variation in operative technique has also been confirmed by our ophthalmologist colleagues who carried out the surgeries at the University of Bristol and University of Oxford Eye Hospitals (*personal communication*). My own data, shown in **Supplementary Table 3.1** and **Supplementary Figure 3.5**, confirmed that there were significant variations in mass of tissue and the number of leukocytes phenotyped between individual iris and scleral biopsies.

To date only a few reports have specifically documented the presence of T cells within the anterior compartment and posterior uveal tract of the eye in mammals; immunohistochemical staining of wholemount normal rat uveal tissue using antibodies against the CD5 antigen (only expressed on T cells in rat) revealed the density of T cells to be around 16 ±6 cells/mm^2 in the iris and 16 ±7 cells/mm^2 in the choroid (Butler and McMenamin 1996). Another report by Reinhardt et al. (2016) showed low-resolution images of γ/δ T cells in tissue proximal to the limbal sclera of B10RIII mice, but without any reference to the vasculature. Others have documented the presence of γ/δ T cells inside the vessels of the choroid in the posterior compartment in healthy human donor eyes (Zhao et al. 2017). More recently, McMenamin et al. (2019) demonstrated higher resolution images of CD4+ T cells inside vessels of the choroid

in DPE-GFP mice. However, these studies also have their own individual limitations (see below).

In Butler and McMenamin (1996), horseradish peroxidase labelled CD5+ T cells were visualized by light microscopy in whole mount tissue samples of iris and choroid by addition of 3-amino-9-ethyl carbazole substrate. However, the intensity of the staining in the representative image of the iris shown in their study was quite weak and almost comparable to background staining. Moreover, no representative image of the choroid was shown, and the exact location of the cells was unclear (in or outside the vascular endothelium). Additionally, the iris and choroid were separated from the sclera further preventing the identification of the exact location of T cells; either within the sclera, entheseal, or ciliary body region.

Reinhardt et al. (2016) used 2-photon microscopy and flow cytometry to analyze entheseal lymphocytes in the eye of B10.RIII Tcrd-H2BeGFP mice. However, the precise identification of γδ T cells in the anterior compartment, was significantly limited by the intensity of autofluorescence from the local tissue into the GFP detection channel. They also failed to provide evidence about the exact location of T cells (inside or outside of the vascular endothelium).

Zhao et al. (2017) performed immuno-labelling on adjacent sections of the choroid, that were prepared from patients with AMD or age-matched healthy controls. They labelled vascular endothelium with lectin and co-stained with either CD3 or TCRγδ to show T cell and γδ T cell localisation. However, in healthy controls they only showed T cells in the posterior and not anterior compartment, and did not specifically verify that any of these T cells were resident as opposed to being inside of blood vessels.

McMenamin et al. (2019) looked at choroidal wholemounts from DPE-GFP mice for the presence of perivascular macrophages. In these mice GFP is expressed under the control of the CD4 enhancers and promoter. They co-stained tissues with either collagen IV - to identify larger vascular structure, or Iba1 – to identify myeloid cells. The authors found a population of macrophages previously reported to express CD4 in higher amounts than T cells (Abtin et al. 2014). Unfortunately, they completely disregarded the heterogeneity of CD4 expressing cells in the vascular and extravascular tissue, as some of the small round CD4+ cells shown in the representative figure could have been T cells and not myeloid cells.

In this chapter I aimed to overcome some of the limitations outlined above by; a) imaging at high resolution; b) using the pan human and mouse T cell marker - CD3; c) use of the most appropriate CD3 clone; d) use of optimum titration of CD3 antibody; and e) using multicolour fluorescent microscopy to stain for multiple parameters on the same tissue sample and improving on the T cell phenotype shown in previous studies, by identifying cell subtypes (through the co-localisation of CD3 and CD4 or CD8), and revealing their proximity to other cells and structures.

Expanding on the above, I also used perfused tissue in C57BL/6 mice to exclude blood derived cells and included the CD34 marker for vascular endothelium to assess if T cells reside in the extravascular tissues of the uveal tract. I also included the PDPN marker for lymphatic endothelium (Astarita, Acton, and Turley 2012) and epithelium of the trabecular meshwork (Birke et al. 2010), and I included markers for various collagen types (I, III, and IV) to distinguish regions of the anterior compartment such as the sclera and ciliary body (Marshall, Konstas, and Lee 1993). I also imaged sections of tissue from the anterior compartment that had not been dissociated from any of its adjacent structures to keep entheseal regions intact. Furthermore, I included

light sheet imaging of wholemount stained human and mouse anterior compartment tissue to remove any artefacts that might have been generated by sectioning of these tissues.

I was able to show, for the first time, that T cells are present in the anterior chamber of the perfused normal mouse eye suggesting that these cells are resident, not only in the specific tissues of the anterior uvea (iris and ciliary body), but also in regions of the limbal sclera and the trabecular meshwork. Although, cross sections of the mouse anterior uvea revealed only low numbers of T cells by confocal imaging, using high depth Lightsheet imaging of cleared whole mount stained tissue, I was able to observe that the majority (~95%) of the T cells were localised in the sclera and the ciliary body. This validated the hypothesis formed in Chapter 3 that a resident population of differentiated T cells is present in the normal mouse eye; capable of recognising local IL-23, and rapidly inducing an immune response (as described in Chapter 2).

One of the limitations of using mouse specimens was the small size and width of the anterior uvea samples. To overcome this, I decided to use the much larger anterior uvea specimens from human cadavers, where the presence of T cells was substantiated by confocal microscopy. Moreover, using the vascular staining markers; CD34 and PDPN, and second harmonic resonance, I was also able to locate these T cells outside of blood vessels **(see Figures 3.15 - 3.22)**, as was the case in perfused mice **(see Figure 3.3)**.

Within the human ciliary body, I found extravascular T cells diffusely spread throughout the stroma, proximal to the ciliary muscle, within the core of the ciliary folds (ciliary processes), adjacent to the ciliary pigmented epithelium (CPE), but not within the ciliary non-pigmented epithelium (CNPE). Similarly, within the iris, I also found T cells

at the anterior border layer, throughout the width of the iris stroma, proximal to the anterior epithelium, but not within the iris pigmented epithelium (IPE).

The above observation is not surprising as previous studies have shown; (A) the existence of barriers within the iris and ciliary epithelial layers that stop the movement of cells from the anterior uvea into the posterior chamber (Shiose and Oguri 1969; Raviola 1971, 1977; Raviola and Raviola 1978; Noske et al. 1994; Sonsino et al. 2002; Gabelt et al. 2003); (B) that there are no barriers which could prevent the movement of cells into the anterior chamber; (C) that the flow of aqueous fluid moves in a single direction from the posterior compartment towards the anterior compartment (Bill 1973; Eichhorn, Inada, and Lütjen-Drecoll 1991; Gabelt et al. 2003; Krause and Raunio 1969; Raviola 1977; Raviola and Raviola 1978); (D) that the iris, which separates the posterior and anterior chambers is in a constant state of contraction and relaxation in a motion similar to the squeezing out of a sponge (Fine and Yanoff 1979), which could add to the forced movement of cells into the anterior chamber from the extravascular tissue; (E) that the canonical route of exit for aqueous fluid from the anterior chamber is through Schlemm's canal (Ashton and Smith 1953; Braakman et al. 2016; Ethier 2002; Goel et al. 2010), which is first filtered through the trabecular meshwork; and (F) that there exists a potential chemokine gradient directing the movement of T cells towards the anterior chamber (Ugorski, Dziegiel, and Suchanski 2016; Kodati et al. 2014). However, it is not known whether T cells that I found in my study are directed towards Schlemm's canal by the circulation of aqueous fluid alone, by the mechanical contraction of the iris, through a chemokine gradient generated by PDPN+/CCL21+ cells, or a combination of all of the above described mechanism **(Figure 3.23)**.

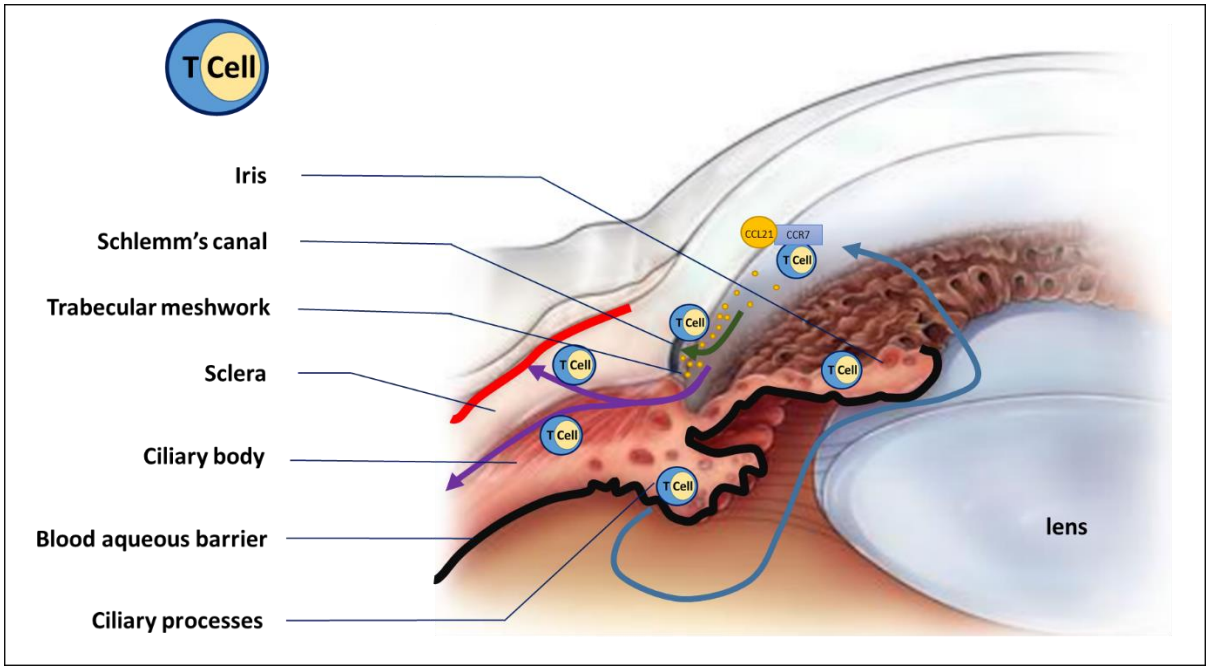


Figure 3.23: The association between the loci of T cells found in the human anterior compartment with aqueous outflow pathways and potential chemokine gradients. T cells can enter the anterior uvea through blood vessels and are prevented from moving into the posterior chamber due to the presence of the blood-aqueous barrier (black line). The Blue arrow describes the flow of aqueous humour from the posterior to anterior chamber. Green arrow shows the outflow of aqueous by the canonical outflow pathway (filtered through the trabecular meshwork into Schlemm's canal). The purple arrow shows the outflow of aqueous by the non-canonical pathways, first through the ciliary body (ciliary muscle), then into the supraciliary space, where it can then flow towards the vortex veins of the choroid, or through the collagen dense stromal layer of the sclera towards the vascular episclera (red line).There is a potential chemokine (CCL21) gradient being produced by the PDPN+ epithelial cells of the trabecular meshwork which might be directing CCD7+ T cells caught in the aqueous outflow current towards the canonical outflow pathway. I generated this diagram from a stock footage image of the anterior eye obtained from alamy.com.

The T cells I observed in the limbal sclera could be the same T cells that have been found at certain entheseal regions of the axial skeleton in mice by Sherlock et al. 2012 and Reinhardt et al. 2016. In both these studies systemic IL-23 overexpression has been shown to initiate inflammation within the entheses of the axial skeleton in mice, similar to what I observed in the anterior uvea of the eye in Chapter 2. A potential reason that these two distal anatomic sites could be affected in the same way is that the tissues are structurally similar and that the same T cells are present at both sites (Sherlock et al. 2012; Reinhardt et al. 2016). In the eye, the extraocular muscles attach to the limbal sclera. These attachment sites can be considered entheseal sites

similar to the attachment sites of tendons to bones in the musculoskeletal system, and would be considered to be under constant mechanical stress. Therefore, the resident T cells I found in the limbal sclera could be assisting in the maintenance and repair of this tissue caused by such mechanical stress, as resident T cells have been described to have such a role in the musculoskeletal entheseal tissue (Jacques et al. 2014).

In summary, the findings in this chapter that T cells are resident in the anterior uvea and limbal sclera of the eye in both mouse and human eye although unexpected/ surprising are welcome. This is because tissue resident cells are usually associated with members of the innate immune system, and with barrier surfaces such as the skin or the gut, where microbiota is abundant and plays a symbiotic role in maintaining immune homeostasis. These T cells are associated with the ability to express IL-23R receptor and are directly responsible for initiating inflammation in response to IL-23 cytokine (Reinhardt et al. 2016; Sherlock et al. 2012). Therefore, in the next chapter I perform phenotyping of T cells in the mouse eye for their ability to express of IL-23R and other T_H17 related markers, and assess if any of the T cells I have found in the anterior chamber are similar in phenotype (CD45+CD3+CD4-CD8-gdTCR+IL-23R+) to the T cells documented as being capable of responding to IL-23 in the entheseal tissues of the mouse axial skeleton (Sherlock et al. 2012; Reinhardt et al, 2016). I also perform functional assays to test the ability of human T cells to respond to IL-23 *in vitro*. It is plausible to speculate that a sub-population of the resident T cells I have shown in this chapter do express IL-23R, as the mouse eye was rapidly (within 3 days) able to responded to IL-23 after localised overexpression (as shown in Chapter 2). In addition, I explore the limits of phenotyping T_H17 T cells by FACS in small surgical samples, to assess if these samples can be utilised in future clinical studies. Finally, I

assess if frequencies of T cells increase in certain regions of the human anterior compartment increase in patients that have presented with clinical uveitis.

Chapter 4

Identification of a novel resident Interleukin-23–dependent γδ T cell population in the anterior uvea in mice and humans

Introduction

In the previous two results chapters I have shown for the first time that localised IL-23 overexpression is sufficient to drive T cell dependant pan-uveitis in the eyes of C57BL/6 mice, and that T cells are present in the extravascular tissues of the anterior chamber and limbal sclera of the mouse and human eye. In mice these were shown to be a heterogeneous population of CD4+, CD8+ and CD4-CD8- T cells. These populations were found at many junctional (entheseal) sites within the anterior compartment including: (A) the connections formed between the transverse ciliary muscles the scleral spur, and the trabecular meshwork; (B) the region of tissue connecting the iris stroma to the iris radial and longitudinal muscles; (C) the anchorage site of zonule fibers to the ciliary epithelium; (D) The bridge between the longitudinal muscles and the supracoroidal lamina (fibres that bridge the choroid with the inner sclera); and (D) the region of limbal sclera where proximal to the attachment site of the extraocular muscles to Tenon's capsule. The focus of this chapter is to look at the T cells found in these entheseal sites and see if any of these cells are capable of responding to IL-23.

The T-helper (T_H) 17 cell

The T-helper (T_H) 17 cells lie at the apex of the IL-23/IL-17 inflammatory axis (Gaffen et al. 2014). First identified in 2005, T_H17 cells are named for their signature cytokine, IL-17, which they produce in abundance once activated. They are an important subpopulation of CD4+ T_H cells which expanded upon the prior T_H1 versus T_H2 paradigm of T_H cell subpopulations (Tesmer et al. 2008). IL-17 –expressing cells are characterised by the transcription factor RORγt and an activated JAK-STAT intracellular signalling pathway (Goepfert et al. 2017).

The cytokine environment in which naïve T cells are exposed to their cognate antigen helps determine what type of T cell it will differentiate into. Low levels of transforming growth factor (TGF)-β is able to synergise with inflammatory cytokines such as IL-6 to promote the expression of RORγt and development of T_H17 cells from naive CD4+ T cells (Mangan et al. 2006; Weaver et al. 2006; Zhou et al. 2008). However, higher levels of TGF-β also plays a critical role in the expression of the transcription factor FoxP3 and the extrathymic generation of immunosuppressive regulatory T cells (Tregs) (Chen et al. 2003; Kitani et al. 2003). Interestingly animal studies have shown that FoxP3 can also inhibit RORγt functionality through a direct protein-protein interaction, and can suppress *il17a* transcription through a mechanism involving DNA binding (Ichiyama et al. 2008; Zhou et al. 2008). Therefore, TGF-β plays an important role in the maintenance of equilibrium of T cell immunology. Nonetheless, TGF-β independent differentiation of naïve T cells into T_H17 cells capable of expressing IL-17 has also been described through the synergy of IL-23 with IL-1 and IL-6 (Ghoreschi et al. 2010).

Although IL-23 is not necessary for the initial stages of T_H17 differentiation, the absence of IL-23 signalling results in abrogated T_H17 cell maturation, reduces the ability of T_H17 cells to proliferate, and hinders the ability of T_H17 cells to become memory cells able to perform secondary recall responses (McGeachy et al. 2009; Ghoreschi et al. 2010; Haines et al. 2013). IL-23 also maintains this phenotype by upregulating the expression of its own receptor (IL-23R) (McGeachy et al. 2007). Additionally, IL-23 has been identified as key checkpoint cytokine in deciding the fate of naïve T cells in becoming homeostatic T_H17 or pathogenic T_H17 effector cells (Luger et al. 2008). An environment where IL-23 is expressed preferentially drives the developing T_H17 cells into the highly inflammatory pathogenic subtype. Interestingly

and an elevated ratio of T_H17 to regulatory T cells has been correlated to disease activity in patients with human leukocyte antigen HLA-B27 associated uveitis (Zhuang et al. 2017). If HLA-B27 misfolding and the UPR is responsible for increased expression of IL-23 (as discussed in Chapter 1) then this increase in IL-23 could be responsible for the greater commitment to the T_H17 lineage seen in (Zhuang et al. 2017).

T_H17 cells are heterogeneous and function both in autoimmunity and in mucosal immunity to protect the body from pathogens such as fungi, bacteria, and viruses (Korn et al. 2009). They have been described to have both pathologic and homeostatic functions, segregated within at least 2 distinct subpopulations (Nian et al. 2012). One subpopulation of T_H17s is highly pathogenic, identifiable by the co-expression of IL-17, IFN-γ, GM-CSF and IL-6. The second group has beneficial homeostatic functions, identifiable by the co-expression of IL-17 and IL-10. Although defined as two distinct subpopulations of T_H17, the relationship between them is in reality more complex and fluid. A recent publication showed the trans differentiation of pathogenic T_H17 cells into IL-10 expressing regulatory cells in the small intestine during resolution of inflammation in a selection of murine experimental models (Gagliani et al. 2015). In the absence of disease, the majority of naïve T_H17 progenitor cells reside in the intestines where their development is induced by the presence of certain types of commensal bacteria, such as SFB (Lee et al. 2015; Littman and Rudensky 2010). Once induced they will help maintain a healthy mucosal barrier by interacting with intestinal epithelial cells. The importance of these T_H17 cells has been highlighted in the clinical setting, as patients with deficiencies of the key factors of T_H17 biology developed infections, such as chronic mucocutaneous candidiasis (McDonald 2012).

In the case of autoimmunity, pathogenic T_H17 cells drive destructive tissue inflammation. One of the main pathologic roles of T_H17 cells is to produce and release IL-17. IL-17 is likely a key amplification cytokine in entheseal inflammation, as it is known to initiate the synthesis of several other inflammatory mediators such as granulocyte-macrophage colony stimulating factor (GMCSF), prostaglandin (PGE)2 and IL-8, which promote the recruitment of, for example, neutrophils to the site of inflammation, which in turn increase the inflammatory cascade through the release of proteases and reactive oxygen species (Ye et al. 2001; Yu et al. 2007). As IL-17 producing γδ T cells (Sherlock et al. 2012; Reinhardt et al. 2016) and ILC3 (Cuthbert et al. 2017; Cuthbert et al. 2019) have been shown to reside in entheseal structures, it is probable that IL-17 is locally produced in the entheses and elicits site-specific attraction of effector cells. In addition, both IL-17 and IL-23 have profound osteoclastogenic properties (Adamopoulos et al. 2011; Adamopoulos et al. 2015). Which explains the systemic bone remodelling in the context of PsA and SpA (Neumann et al. 2018; Simon et al. 2019). While most studies have focussed on IL-17A as the main mediator driving enthesitis within the IL-17 family of cytokines, it may well be that other variants, such as IL-17F, exert similar actions and augment localised entheseal inflammation as well.

Less informative to disease initiation and of more interest to disease modification, is the observation that the T_H17 subtype is enriched in the musculoskeletal entheses and peripheral blood of patients with AS (Shen, Goodall, and Hill Gaston 2009; Kenna et al. 2012). Of specific interest is the observation that an expanded T_H17 expressing subpopulation able to recognise HLA-B27 homodimers (KIR3DL), particularly sensitive to IL-23, has also been observed as being enriched in the musculoskeletal entheses and peripheral blood of patients with AS (Bowness et al. 2011). T_H17 cells

have also been phenotyped within the eyes of mice with establishes disease in EAU (Caspi 2010). Furthermore in other animal models of uveitis, disease severity has been correlated to the total burden of intraocular T_H17 cells (Yazid et al. 2015). In addition, T_H17 cells have been identified in the peripheral blood of patients with scleritis and active uveitis (Amadi-Obi et al. 2007).

Tγδ17 cells

CD4+ T_H17 cells are not the only type of T cell that are capable of producing IL-17. γδ T cells are part of the three evolutionary conserved lymphocyte lineages (with αβ T cells and B cells) that undergo somatic gene rearrangement for the generation of antigen receptors (Hirano et al. 2013), and are also capable of producing IL-17. Unlike αβ T cells, which develop in the thymus from CD4-CD8- to CD4+CD8+ eventually yielding CD4+ or CD8+ single positive αβT-cells (Chien, Zeng, and Prinz 2013; Fehling et al. 1995), γδ T cells develop following a single γδ-selection step mediated by the γδTCR, do not progress through to a CD4+CD8+ stage, and most γδ T cells remain CD4-CD8- (Ciofani and Zúñiga-Pflücker 2010). Whereas αβT-cells leave the thymus as naïve cells and acquire their effector function in the periphery, γδ T cells are able to commit to an effector phenotype during development in the thymus. This pre-activation in the thymus permits γδ T cells to become early innate-like responders to infection and tissue-damage, without the delay that is required for αβT-cell responses. It is important to note that some γδ T cells are permitted to exit the thymus as naïve cells and acquire their effector function following activation in the periphery; these are referred to as “inducible” γδ T cells (Zeng et al. 2012; Chien, Zeng, and Prinz 2013). Like αβT-cells, ILCs, and other lymphocyte lineages, γδ T cells can be phenotyped into effector subsets based on the expression of either T-bet/IFNγ (Tγδ1) or RORγt/IL-

17A (Tγδ17) (Narayan et al. 2012; In et al. 2017; Sumaria et al. 2017; Zuberbuehler et al. 2019).

In addition, the fate decisions of developing thymocytes during fetal life impacts the adult reservoir of innate-like γδ T cell effectors. Effector γδ T cell subsets differentiate during development in functional waves incorporating different TCR repetoirs: Vγ5+Vδ1+ dendritic epidermal T cells (DETCs), Vγ6+ γδ T cells, and NKT γδ T cells, which are also partially associated with Vγ usage (Prinz, Silva-Santos, and Pennington 2013). Specifically, DETCs preferentially produce IFNγ, and Vγ6+ γδ T cells largely produce IL-17A (Turchinovich and Hayday 2011). Later waves, where Vγ4 and Vγ1 are generated, are more heterogeneous in their ability to produce effector cytokines. Although IL-17A production is not restricted to a specific Vγ subset, innate-like Tγδ17 cell generation is limited to a period of ontogeny during fetal life, approximately E16 to birth, that enriches for Vγ6+ and Vγ4+ γδ T cell subsets (Haas et al. 2012).

A number of surface markers have recently been shown to distinguish between the Tγδ1 and Tγδ17 subsets. Tγδ1 cells typically express CD27, CD122, NK1.1, and high levels of CD45RB, while Tγδ17 cells lack expression of CD27, CD122, and NK1.1 but usually express CCR6 and low levels of CD45RB (Haas et al. 2009; Ribot et al. 2009; Turchinovich and Hayday 2011). Another study by Sumaria et al. (2017), showed that CD44 is also able to distinguish between effector lineages: CD44hiCD45RB^{lo} γδ T cells express high levels of RORγt and IL-7Rα and are committed to IL-17A production, whereas CD44+CD45RB+ γδ T cells express T-bet, but lack RORγt or IL-7Rα expression and are committed to IFNγ production. Functional IL-23R has also been shown to be expressed by these cells in the spleen, colon and fat tissue, using GFP reporter mice (Wei et al. 2015).

Interestingly, the entheseal tissue of the axial skeleton and aortic root in mice contains a mixture of αβTCR+ and γδTCR+ CD4−CD8−ROR-γt+IL-23R+ T cells (Sherlock et al. 2012). Moreover, systemic IL-23 overexpression in B10.RIII mice, is sufficient to elicit enthesitis and joint disease with histological and bone remodelling features that were reminiscent of human ankylosing spondylitis. This pathology was dependent on the presence of CD3+CD4−CD8−IL-23R+ROR-γt+ T cells (as disease was absent in Rag2−/− mice) but did not require $T_H17$cells (as depletion of CD4+ T cells, using a CD4 specific antibody, did not modify the disease state). In addition, Reinhardt et al. (2016) showed the presence of γδ T cells proximal to the limbal sclera in naïve B10.RIII mice. However, the resolution and relative autofluorescence of samples meant that the precise location of these cells could not be determined. More recently, Cuthbert and colleagues (2019) identified the presence of tissue resident Vδ1 and Vδ2 γδ T cells within the human spinous entheseal soft tissue. Interestingly, although both populations were capable of producing IL-17, IL-22, RORC and CCR6 transcripts following PMA or CD3/CD28 stimulation, only the Vδ2 subsets expressed a high relative abundance of IL-23R suggesting that the Vδ1 subsets induce IL-17A independently of IL-23R expression. This suggests for the first time that there may be heterogeneity amongst entheseal γδ T cells.

Presumably due to the difficulties in obtaining the correct ocular tissues, to my knowledge no resident T_H17 cells or other IL-23R+ T cells have been documented as being present in the anterior compartment of healthy mammalian eyes. In this Chapter, I show for the first time, the presence of Tγδ17 in the anterior compartment of the naïve C57BL/6 mouse eye and is also the first study that shows the presence of IL-23R+ T cells in the anterior compartment of the human eye.

Aims

- To assess if the anterior compartment of healthy murine and human eyes contains an IL-23R+ γδ T-cell population.
- To assess if murine and human anterior compartment-resident γδ T cells show a pre-activated effector phenotype.
- To assess if murine and human anterior compartment γδ T cells are capable of producing downstream pro-inflammatory cytokines in response to IL-23 and in the absence of any other pro-inflammatory mediators.
- To characterise T cells in biopsies samples of the human anterior compartment.
- To assess if the anterior compartment of the human eye is primed to respond to IL-17A produced by IL-23R γδ T cells.

Materials and Methods

Animal strains and husbandry

Adult (6-8 week-old) female *C57BL/6J* were purchased from Charles River Laboratories, Oxford. IL-23R-eGFP (previously described in Awasthi et al. 2009) were provided from an established breeding colony at the University of Oxford, Oxford. Mice were confirmed as negative for the *Rd8* mutation (Mattapallil et al. 2012). All mice were housed under specific pathogen free conditions with food and water *ad libitum*. All procedures were conducted in concordance with the United Kingdom Home Office licence (PPL 30/3281) and were approved by the University of Bristol Ethical Review Group. The study also complied with the Association for Research in Vision and Ophthalmology (ARVO) Statement for Use of Animals in Ophthalmic and Vision research.

Dissection of mouse ocular tissue

Following enucleation, each eye was dissected in 100µl of PBS. Using a limbal incision, the vitreous and retina were extracted. The anterior chamber (AC) was also opened and the contents washed into the dissecting fluid. The retina and PBS were completely aspirated and placed into a 1.5mL Eppendorf tube. If AC and posterior chamber separation was required, the AC was opened by clear corneal incision first, PBS removed, then replaced before the retina and vitreous were dissected.

Preparation of mouse ocular tissues for analysis by flow cytometry

Mechanical cell dissociation of the retina was performed by rapping the Eppendorf tubes containing the retinal sample across a standard tube rack ten times. The iris, ciliary body and limbal sclera was first mechanically dissociated in a culture dish using scalpels in a scissoring motion, then enzymatically digested in DMEM containing 5

mg/mL type II collagenase (Worthington, # LS004202) and 0.2 mg/mL DNase I (Roche, #11284932001) for 120 minutes at 37°C undergoing constant, gentle agitation as described in Sherlock et al. (2012). Enzymatic digest was then washed with complete media and filtered twice through a 70µm cell strainer (Corning, # CLS431751-50EA). Viable cells were then counted by using trypan blue dye exclusion 5% w/v in water. All samples were filtered into a 96-well 60µm cell strainer plate (Merck Millipore, Watford, UK) and washed with 100µL of PBS. The plate was centrifuged at 300g for 5 minutes, 'retinal supernatants' collected, with the remaining cell pellet transferred into a sterile 96-well V-bottom plate.

- *Mouse surface antigen staining*

Cells were washed in the plate with 0.1%w/v bovine serum albumin (BSA) in PBS before resuspension in 0.5µL of neat Fc-block rat anti-mouse CD16/CD32 (BD Biosciences, Oxford, UK) diluted in 50µL 0.1% BSA in PBS. After 5 minutes, another 50µL was added containing a specific dilution of each neat primary conjugated antibody according to the manufacture's recommendations (Table 4.1). Following staining on ice for 20 minutes, cells were washed twice, and then incubated with viability dye (Table 4.1) for 30 minutes at room temperature. Following this, cells were washed twice then placed into 200µL 0.1% w/v BSA in PBS in FACS tubes. Cells were analysed on a 4 laser (405nm, 488nm, 561nm and 640nm) BD LSR Fortessa X-20 flow cytometer (BD Biosciences) which was regularly maintained and used according to manufacturers' instructions. Medium or high flow rates were used. FACSdiva and FlowJo software (BD Biosciences) were used for analysis of data. Compensation was performed using OneComp eBeads (eBioscience, San Diego, USA, 01-1111-42) and an ArC Amine-reactive Compensation bead kit (Invitrogen Life Sciences, A10346) for the live-dead stain. unstained controls were used to determine gate position.

- *Mouse Intracellular cytokine staining*

Intracellular cytokine staining of T-cells was performed by stimulating cell suspensions for 2 hours with 50 ng/ml phorbol myristate acetate (PMA) and 500 ng/ml Ionomycin then for a further 2 hours with the addition of 1 mg/ml Brefeldin and Monensin (all from Sigma Aldrich, Dorset, UK) in D10 medium. Following surface antigen staining, the Transcription Factor Buffer Set (BD Biosciences, Oxford, UK) was used according to the manufacturer's protocol for intracellular staining. A specific dilution of each primary conjugated antibody was used according to the manufactures recommendations (Table 4.1). Following this, cells were washed twice then placed into 200µL 0.1% w/v BSA in PBS in FACS tubes.

Table 4.1: Mouse flow cytometry antibodies and panels

Antigen	**Fluorophore**	**Clone**	**Manufactuer**
PANEL 1 - IL-23R			
IL-23R	eGFP	N/A	N/A
gdTCR	BV421	GL3	BIOLEGEND
CD45	PE-Cy7	30-F11	BD
CD3	BV786	145-2C11	BIOLEGEND
CD4	APC	GK1.5	BIOLEGEND
CD8	PE-CF594	53-6.7	BIOLEGEND
Viability dye	7AAD	N/A	THERMO FISHER
PANEL 2 - IL-17A ICC			
gdTCR	af488	GL3	BIOLEGEND
CCR6	PE	29-2L17	BIOLEGEND
CD4	PE-Dazzle	GK1.5	BIOLEGEND
CD45	PE-Cy7	30-F11	BD
IL-17	AF647	TC11H10.1	BIOLEGEND
AF700	CD44	IM7	BIOLEGEND
CD8	APC-C7	53-6.7	BIOLEGEND
CD27	BV421	LG.3A10	BIOLEGEND
CD3	BV786	145-2C11	BIOLEGEND
IFNy	BV711	XMG1.2	BIOLEGEND
CD62L	PERCP-Cy5.5	145-2C11	BIOLEGEND
Viability dye	BV510	N/A	BIOLEGEND

GFP Immunofluorescence

Murine eyes were snap frozen in Jung tissue-freezing medium (Leica Microsystems) using 2-methylbutane (C_5H_{12}) (SIGMA-ALDRICH) super cooled in liquid nitrogen. Seven micrometer cryosections of each tissue were prepared on Superfrost Plus slides (Fisher Scientific), air dried for 2 hours at room temperature, and fixed in acetone (C_3H_6O) (SIGMA-ALDRICH) for 10 minutes. Fixed cryosections were then blocked with 150ml 20% normal horse serum (PAA Laboratories Inc) for 15 minutes at room temperature (25°C) in a humidity chamber. Nuclei were counterstained with 2µg/ml DAPI (Invitrogen) for 10 minutes. Stained Cryosections were washed and mounted with Vectashield® mounting medium (Vector Labs). Images were captured at x10 magnification on an Olympus BX51 microscope using Micro-Manager software (Vale Laboratory).

Human ocular tissue

Healthy human eyes were obtained from the Filton Eye Bank, Bristol, where deceased individuals had donated their eyes for corneal transplant material. The partial globes obtained, post corneal removal, were considered waste tissue that was specific and of high enough quality to be included in this study. These samples were collected from male and female individuals. Corneal removal took place within 24 hours of death. Globes were transferred into Roswell Park Memorial Institute (RPMI) 1640 media complete with L-glutamine (Gibco, #21875-034) with 10% heat inactivated foetal bovine serum (FBS; Gibco, #10500-064) and 1% penicillin-streptomycin (P/S; Gibco, #15140-122) (complete media) post corneal removal to preserve cell viability and transported by express courier to the Botnar Research Centre, Oxford for processing. Exclusion criteria for this study included any patient with a known inflammatory or

infected condition of the enthesis. Partial globes were transported and processed within 36 hours from time of death.

Preparation of human ocular tissues for analysis by flow cytometry

For homogenisation of anterior compartment tissues see Chapter 2, Materials and methods.

- *Ex-vivo stimulation of human ocular cell suspensions*

Anterior uvea and limbal sclera digests and cultured overnight on filters (Millipore, #PICM0RG50) in IMDM alone or with recombinant human (rh)IL-23 (100ng/ml; Peprotech, #200-23). Following this, cells were washed twice then placed into 200µL 0.1% w/v BSA in PBS in FACS tubes.

- *Human surface antigen staining*

Cells were washed in Cell staining buffer (Biolegend) before resuspension in Human TruStain FcX™ blocking agent at a 1:50 dilution in a residual 50µL volume of cell staining buffer for 20 minutes at 4°C. 50µL containing a specific dilution of each neat primary conjugated antibody (Table 4.2) was then directly added without washing. Following staining on ice for 20 minutes, cells were washed twice then placed into 400µL cell staining buffer in FACS tubes. Compensation controls were made using UltraComp eBeads (eBioscience). Cells were analysed on a 3 laser (405nm, 488nm, and 640nm) BD LSR Fortessa X-20 flow cytometer (BD Biosciences) which was regularly maintained and used according to manufacturers' instructions. Medium or high flow rates were used. FACSdiva and FlowJo software (BD Biosciences) were used for analysis of data. Compensation was performed using OneComp eBeads (eBioscience, San Diego, USA, 01-1111-42) and an ArC Amine-reactive

Compensation bead kit (Invitrogen Life Sciences, A10346) for the live-dead stain. unstained controls were used to determine gate position.

- *Human intracellular cytokines staining*

Intracellular cytokine staining of T-cells was performed by stimulating cell suspensions for 2 hours with 50 ng/ml phorbol myristate acetate (PMA) and 500 ng/ml Ionomycin then for a further 2 hours with the addition of 1 mg/ml Brefeldin and Monensin (all from Sigma Aldrich, Dorset, UK) in D10 medium. Following surface antigen staining, the Transcription Factor Buffer Set (BD Biosciences, Oxford, UK) was used according to the manufacturer's protocol for intracellular staining. A specific dilution of each primary conjugated antibody was used (Table 4.2). Following this, cells were washed twice then placed into 200µL 0.1% w/v BSA in PBS in FACS tubes.

Table 4.2: Human flow cytometry antibodies and panels

Antigen	Fluorophore	Clone	Manufactuer
PANEL 1 - Uvea and sclera ICC			
γδTCR	BV421	B1	BD Pharmingen
CD45	BV605	HI30	Biolegend
CD3	AF647	HIT3a	Biolegend
CD4	PE	RPA-T4	Biolegend
CD8	BV510	sk1	Biolegend
tnfa	PERCP-Cy5.5	MAB11	BD Pharmingen
IL17A	FITC	ebio64DEC17	Biolegend
IFNg	PE-CY7	B27	BD Pharmingen
Viability	APC Cy7	N/A	Biolegend
PANEL 2 - Trabeculectomy			
CCR6	PE-CY7	G034E3	Biolegend
CD45	BV605	HI30	Biolegend
CD3	AF700	OKT3	Biolegend
CD4	PE	RPA-T4	Biolegend
CD161	BV711	DX12	BD Horizon
CCR6	FITC	G034E3	Biolegend
Viability	APC Cy7	N/A	Biolegend
PANEL 3 - Stabismus			
CD45	BV605	HI30	Biolegend
CD3	BV421	OKT3	Biolegend
CD4	PE	RPA-T4	Biolegend
CD8	BV510	sk1	Biolegend
CD161	BV711	DX12	BD Horizon
CCR6	PE-Cy7	G034E3	Biolegend
γδTCR	PERCP-Cy5.5	B1	BD Pharmingen
αβTCR	APC	T10B9.1A-31	BD Pharmingen
CD20	AF700	2H7	Biolegend
Viability	APC Cy7	N/A	Biolegend

Modified ViewRNA assay

Due to the lack of reliable antibodies against human IL-23R, IL-23R messenger transcripts were instead phenotyped histologically using ViewRNA technology (Affymetrix). Furthermore, due to the rarity and highly localized anatomical location of human IL-23R+ entheseal cells a modification needed to be made to the ViewRNA

assay (Affymetrix, #QVT0012) manufacturers protocol that would allow large, un-sectioned samples to be hybridized with ViewRNA probes. Day 1: following sample preparation, specimens were washed 3 times with phosphate buffered saline (PBS) and treated with Pre-treatment solution at 85°C for 20 minutes. Following this, samples were washed once with double distilled (dd)H_20 and twice with PBS. Samples were then treated with proteinase K (5µg/ml; Sigma, #P6556) for 20 minutes at 37°C. Following this, samples were washed twice with PBS, fixed in 10% buffered formalin for 4 minutes, washed an additional time with PBS, and then placed in a 24 well plate. Probes against IL-23R (type 1; #VA1-16191), scrambled IL-23R (type 1; # VA1-12629) and RPL13A (type 1; #VA1-13100) human mRNA transcripts were purchased from Affymetrix. Probes were diluted 1:40 in probe diluent pre warmed to 40°C and incubated with sample overnight at 40°C. Day 2: Samples washed twice with Wash Buffer, then cover samples with Pre-amplification Buffer pre-wared to 40°C, and incubate at 40°C for 90 minutes. Following this, samples were washed twice with Wash Buffer, then covered and incubated for 100 minutes at 40°C with pre-warmed Amplification Buffer. Afterwards, samples were washed twice with Wash Buffer and incubated with pre-warmed Label Probes, diluted 1/100 with Label Probe Diluent, for 100 minutes at 40°C. Finally, samples were washed twice in PBS and incubated with Hoescht (Life Tech, #H3570) nuclear counterstain (1/5000 in PBS 0.5% saponin) for 5 minutes in the dark. Images were acquired on a Lightsheet Z.1 microscope using ZEN software (both Zeiss). As many images were acquired as possible until the cells of interest were found. Images were acquired at both x10 and x20 magnification.

Statistical analysis

Data were analysed using GraphPad Prism® software. For analysis between two groups variance was compared using an F-test. Data with equal variances were

analysed using the unpaired Students two-tailed t-test. Non-parametric data were analysed with the Mann-Whitney U two-tailed test. For analysis between multiple groups variance was compared using Friedmann's test. Data with equal variances were analysed using ordinary one-way ANOVA test with Tukey's multiple comparison test. Non-parametric data were analysed with the Kruskal-Wallis test with Dunn's multiple comparisons test. Significance was set at * $p \leq 0.05$, ** $p \leq 0.01$, and *** $p \leq 0.001$.

Results

The anterior compartment of healthy murine eyes contains an IL-23R+ γδ T-cell population

I used IL-23R–eGFP heterozygous reporter mice to investigate the presence of IL-23R+ cells that are capable of responding locally to IL-23 within the anterior compartment of murine eyes. An evaluation of CD45+ anterior compartment cells from naive mice using flow cytometry revealed that the IL-23R–eGFP+ fraction expressed CD3 and represented approximately 13% of the total T cell pool in un-perfused eyes (although eyes should ideally have been perfused, they were taken as waste tissue from mice undergoing another experiment and thus tissue could not be perfused) **(Figure 4.1A-D)**, with as many as 250 IL-23R–eGFP+ T cells being present in a single anterior chamber. A very small number of CD45+, IL-23R–eGFP+, CD3- cells with a similar FSCA and SSCA profile can also be seen, representing less than 10% of the total IL23R+ expressing cells within the anterior compartment **(Figure 4.1A)**. This cell population could potentially represent ILC3s.

To show the exact anatomical location of these cells, I performed fluorescence microscopy on intact, live, un-manipulated tissue from naive mice. I found that IL-23R–eGFP+ cells are located at the outer wall of Schlemm's canal proximal to the cribriform meshwork **(Figure 4.1D)**, at the limbal sclera **(Figure 4.2A and B)** specifically within the scleral stroma proper and not the vascular episclera **(Figure 4.2C and D)**, and within both the ciliary processes **(Figure 4.2E and F)** and ciliary muscle **(Figure 4.2G and H)**. These cells are absent from the prepupillary cornea and pupillary region of the iris.

Furthermore, the IL-23R itself appears to functionally regulate the IL-23R+ T cell phenotype within the anterior uvea. By comparing the IL-23R-eGFP heterozygous mice to IL-23R-eGFP homozygous mice (which lack a functional IL-23R)

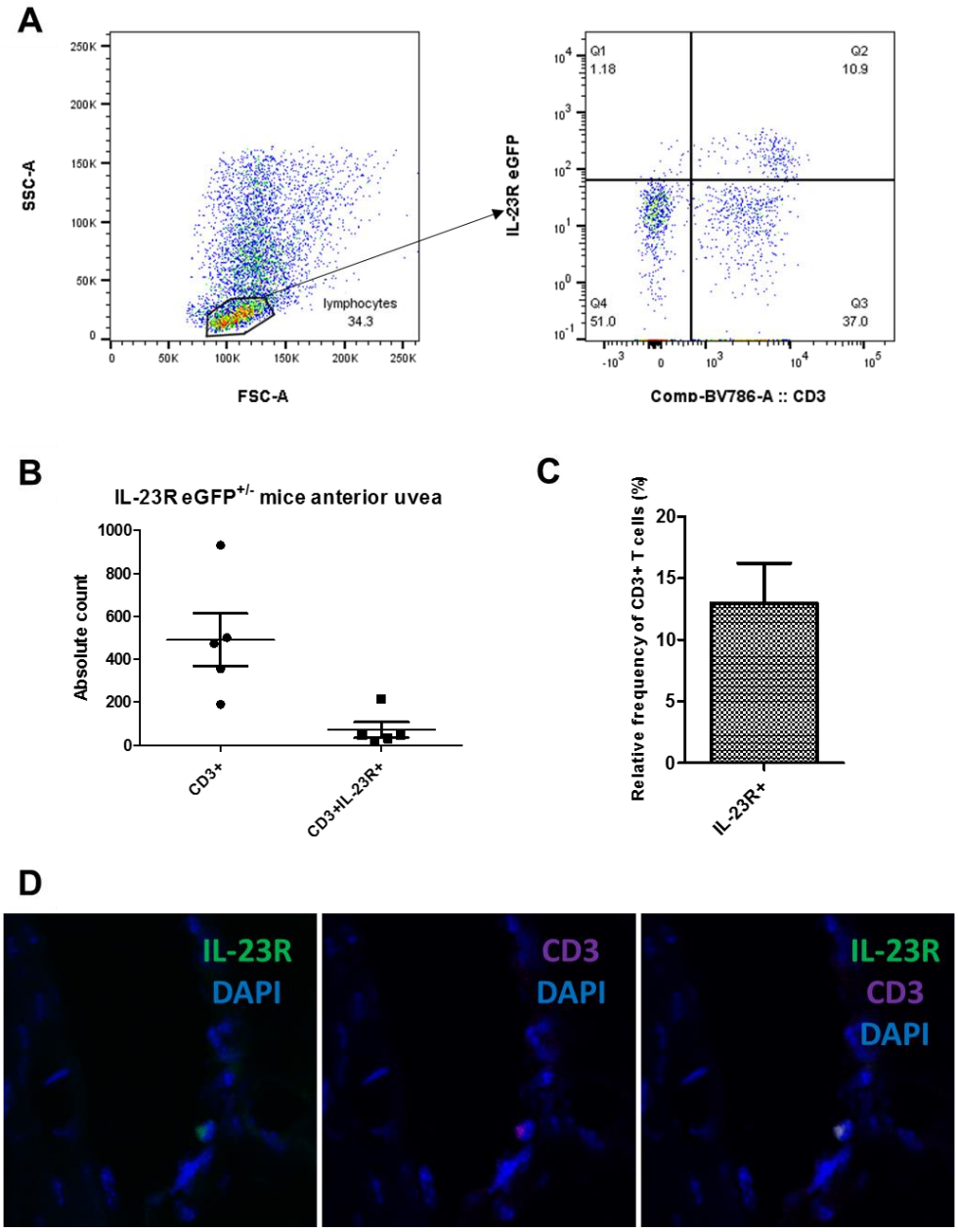


Figure 4.1: Il-23R+ T cells are located in the anterior uvea of healthy murine eyes. (A) Flow cytometry of anterior uvea cell suspensions from naive IL-23R–eGFP+/- reporter mice. The initial plot (left) was gated on CD45+ cells, the second plot (right) was gated on small (FSCAlow) low complexity ($SSCA^{lo}$) cells (lymphocytes). (B) Compiled frequency plot showing the absolute count of CD3+ (T) cells and IL-23R+ T cells. (C) The frequency of IL23R+ cells amongst T cells. (D) Representative immunofluorescence image showing the individual and merged expression of nuclei (blue), CD3 (purple), and IL-23R-eGFP (green) within the Trabecular meshwork. All images were captured at x20 magnification.

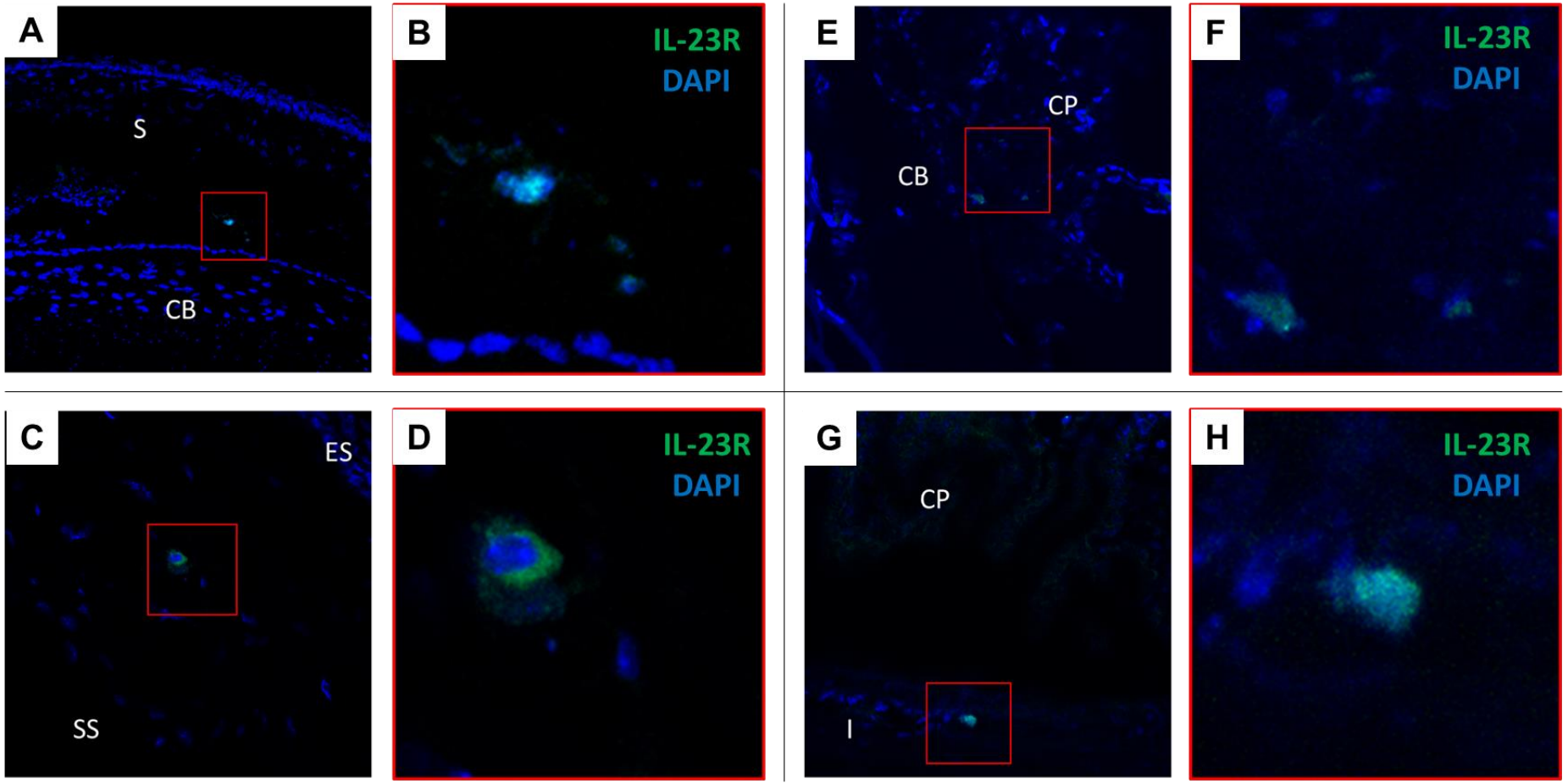


Figure 4.2: IL-23R+ cells are found in multiple tissues of the anterior compartment in naïve mice. Representative confocal immunofluorescence images of intact anterior compartment tissues including the sclera (S), ciliary body (CB), and iris (I). (A and B) The transitional region of sclera to ciliary body. (C and D) The transitional region from episclera (ES) to stromal sclera (SS). (E and F) The folding of the inner ciliary body to become ciliary process (CP). (G and H) the transitional region where ciliary body becomes iris. Nuclei (blue) and IL-23R-eGFP (green).

(Awasthi et al. 2009), I noticed a comparable total numbers of T cells, and relative frequency of T cells compared to the total CD45+ leukocyte pool **(Figure 4.3A and B)**, IL-23R-eGFP homozygous mice have a significantly lower total number of IL23R+ T cells and relative frequency of IL-23R+ T cells relative to the total T cell pool compared with IL-23R-eGFP heterozygous mice **(Figure 4.3C and D)**.

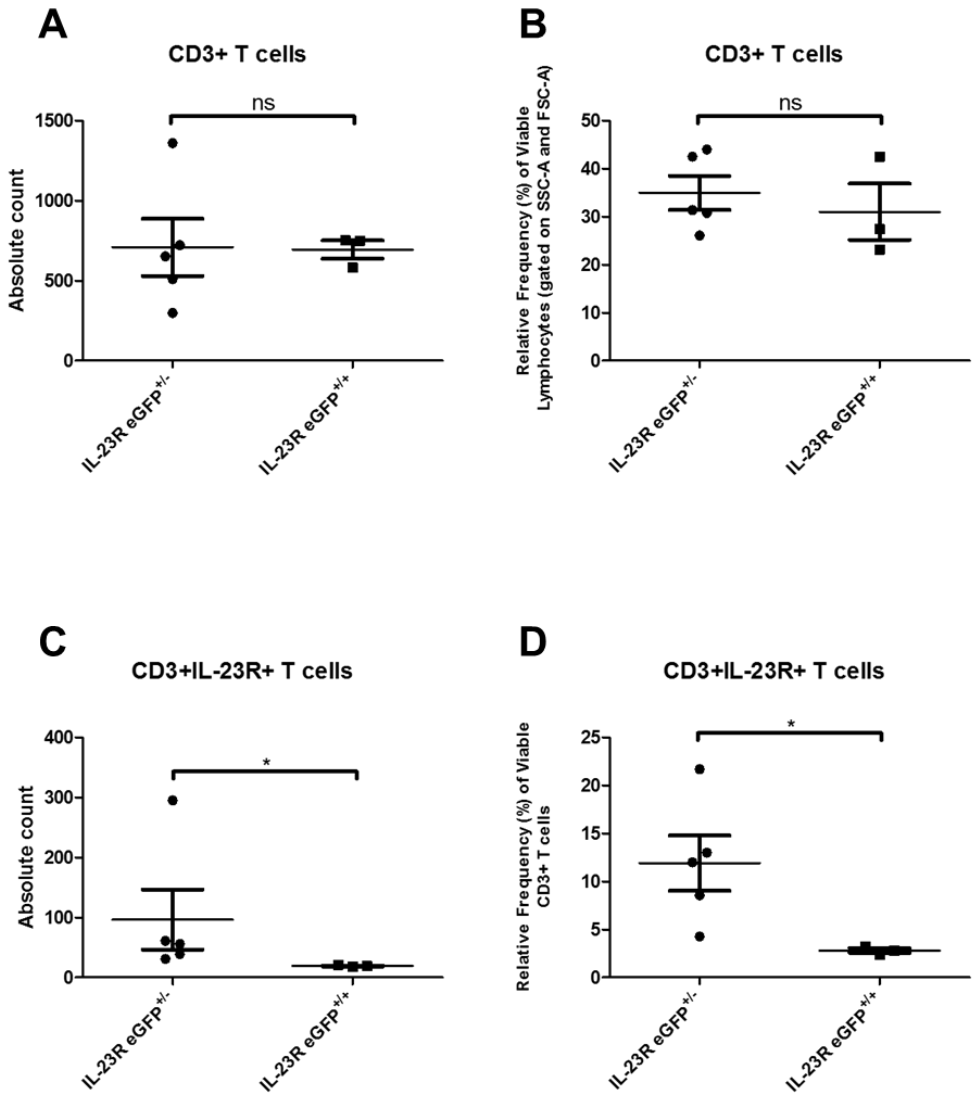


Figure 4.3: Functional IL-23R expression effects accumulation of CD45+CD3+CD4-CD8-TCRγδ+IL-23R+ T cells within ocular tissue. (A) FACS compiled frequency data of pooled left and right IL-23R eGFP$^{+/-}$ or IL-23R eGFP$^{+/+}$ C57BL/6 eyes (after lens removal; n = 5) for the absolute count of viable CD3^{+} T cells. (B) FACS compiled frequency data of pooled left and right IL-23R eGFP$^{+/-}$ or IL-23R eGFP$^{+/+}$ C57BL/6 eyes (after lens removal; n = 5) for the relative frequency of viable CD45^{+} lymphocytes (based on FSC-A and SSC-A) that are CD3^{+} T cells. (C) FACS compiled frequency data of pooled left and right IL-23R eGFP$^{+/-}$ or IL-23R eGFP$^{+/+}$ C57BL/6 eyes (after lens removal; n = 5) for the absolute count of viable CD3^{+}IL-23R^{+} T cells. (D) FACS compiled frequency data of pooled left and right IL-23R eGFP$^{+/-}$ or IL-23R eGFP$^{+/+}$ C57BL/6 eyes (after lens removal; n = 5) for the relative frequency of viable CD3^{+} T cells that are CD3^{+}IL-23R^{+} T cells. Line represents mean and error bars show SEM. ns = not significant and * = P<0.05 (unpaired Student's two-tailed t-test).

Consistent with the findings of Sherlock and colleagues (2012) and Reinhart and colleagues (2016) within musculoskeletal entheseal tissues – CD4-CD8- γδ T-cells, but not αβT cells, constituted the majority of all anterior compartment IL-23R+ T cells **(Figure 4.4A)**. Approximately 95% of IL-23R+ T cells were γδTCR+ and 100% were CD4-CD8- **(Figure 4.4B)**.

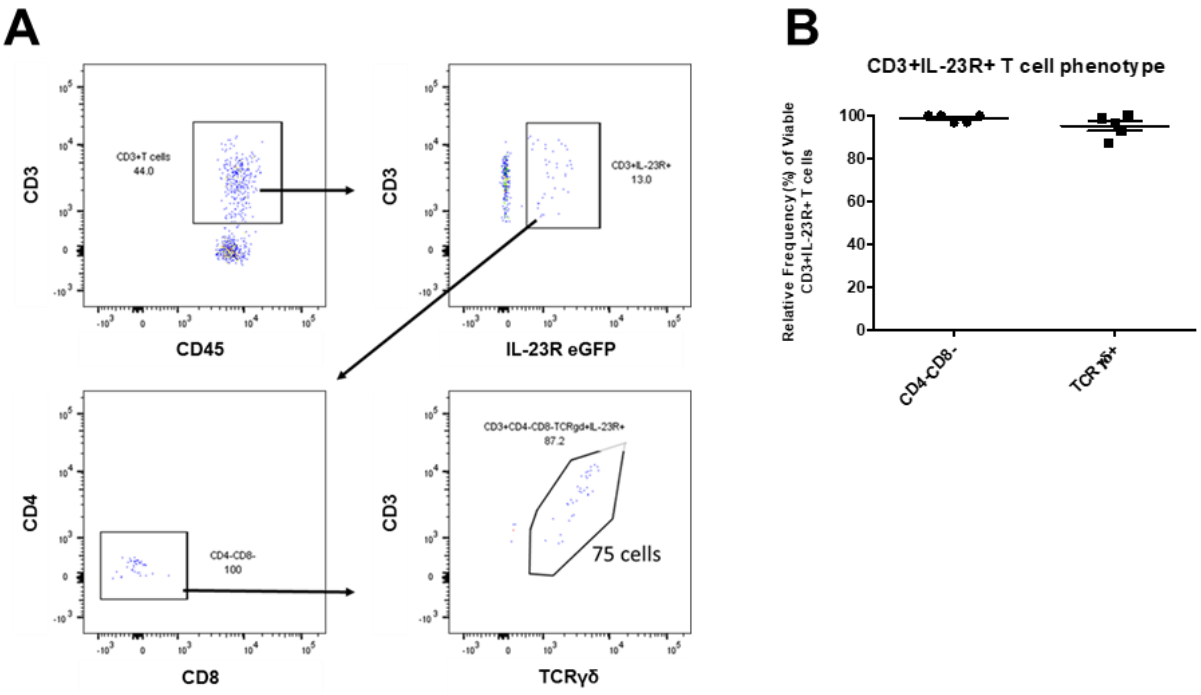
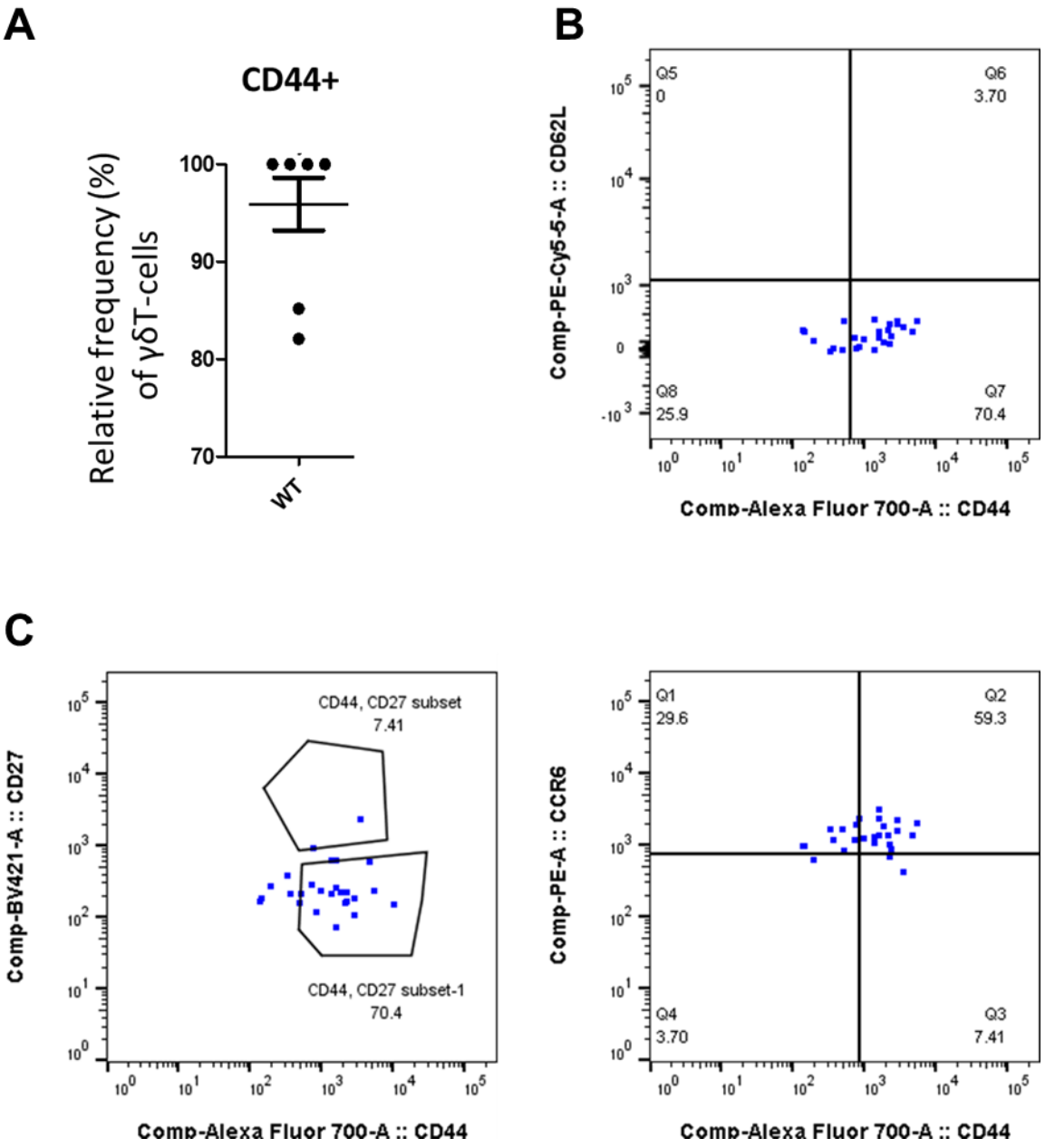


Figure 4.4: Fluorescence activated cell sorting (FACS) defines the mouse IL-23R+ cell population within the eye as CD45+CD3+CD4-CD8-TCRγδ+ T cells. (A) Representative plots show flow cytometric analysis gating strategy for $CD45^{+}CD3^{+}CD4^{-}CD8^{-}TCR\gamma\delta^{+}IL\text{-}23R^{+}$ T cells. Cells were isolated from left and right IL-23R $eGFP^{+/-}$ C57BL/6 eyes pooled together (after lens removal). (B) FACS compiled frequency data of pooled left and right IL-23R $eGFP^{+/-}$ C57BL/6 eyes (after lens removal; n = 5) for the relative frequency of viable $CD3^{+}Il\text{-}23R^{+}$ T cells that are $CD4^{-}CD8^{-}$ T cells and $TCR\gamma\delta^{+}$ T cells. Line represents mean and error bars show SEM.

Murine anterior compartment-resident γδ T cells show a pre-activated effector phenotype

Next, we characterized anterior compartment-resident γδ T cells in more detail using flow cytometry of anterior compartment cell suspensions from IL-23R-eGFP heterozygous reporter mice. Activated and functionally differentiated effector γδ T cells Have been shown to express high levels of CD44 (Prinz et al. 2013). In naive C57BL/6 mice, approximately 95% of all isolated anterior compartment-resident γδ T cells were $CD44^{high}$ **(Figure 4.5A)** and displayed a $CD44^{high}$CD62L− effector phenotype **(Figure 4.5B)**. Since CCR6 (Haas et al. 2009) and CD27 (Ribot et al.2009) are surface markers for functional discrimination between IL-17−producing and IFNγ-producing γδ T cells respectively, expression of both molecules on ocular γδ T cells was determined **(Figure 4.5C)**. Within the anterior compartment, approximately 60-70% of γδ T cells were pre-activated $CD44^{high}$CCR6+ or $CD44^{high}$CD27− cells, suggesting IL-17 production capacity. In summary, the population of entheseal γ/δ T cells was dominated by $CD44^{hi}$CD62L−CD27− activated effector memory cells.

To study anterior compartment resident γδ T cells in IL-23−induced inflammation, the IL-23 encoding modified adenovirus (ShH10 IL-23 AAV ($2x10^{10}$gc)) was intravitreally injected into C57BL/6 mice as described in Chapter 2. Overexpression of IL-23 in the inner eye in these mice leads to increased inflammatory infiltrate in the anterior compartment by day 10. A control group was injected with an GFP−encoding modified adenovirus control. At day 10, significantly higher numbers of γδ T cells were observed within the anterior uvea of ShH10 IL-23 AAV mice compared to controls **(Figures 4.6A and B)**. This was accompanied by an overall increase in the number of (infiltrating) T cells in ShH10 IL-23 AAV mice compared to controls **(Figures 4.6C)**.



.

Figure 4.5: Pre-activated effector cells dominate the pool of anterior compartment-resident γδ T cells. Results of flow cytometric analysis of γδ T cells isolated from the anterior compartment of *IL23R--eGFP* mice are shown. (A) Frequency of CD44^{high} cells among anterior compartment γδ T cells. Symbols represent individual mice; horizontal line shows the mean; error bars show SEM. Data from 2 independent experiments are shown. (B) Representative dot plot showing the expression of CD44 and CD62L on anterior compartment γδ T cells. (C) Representative dot plot showing the expression of CD44 CCR6, and CD27 on anterior compartment γδ T cells.

The relative frequency of γδ T cells with a pre-activated effector phenotype (CD44^{high}CD27−) remained unchanged in both ShH10 IL-23 AAV and ShH10 GFP IL-23 AAV mice at day 10 compared to naïve mice **(Figure 4.6D)**.

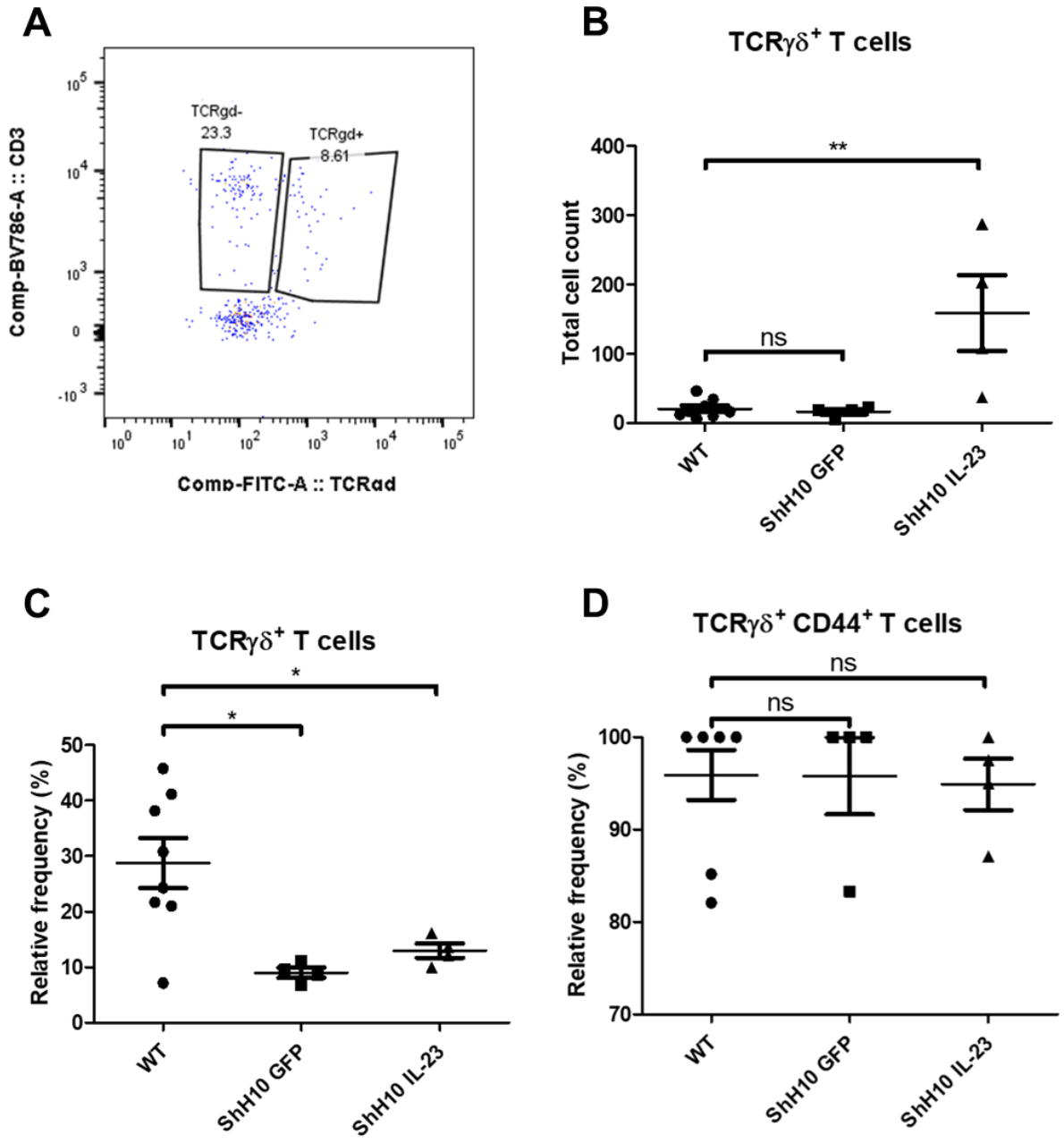


Figure 4.6: The relative frequency of γδ T cells with a preactivated effector phenotype in the anterior uvea is unaffected by IL-23 overexpression (ShH10 IL-23) in mice. Anterior compartment cell suspensions from naive mice 10 days after intravitreal delivery of ShH10 IL-23 AAV ($2x10^{10}$gc), control ShH10 GFP AAV ($2x10^{10}$gc), or sham injection of PBS (WT) were analysed by flow cytometry. (A) The anterior uvea of cell suspensions from naive mice was gated on CD45+, small ($FSCA^{low}$), low complexity ($SSCA^{lo}$) cells (lymphocytes). (B) Compiled frequency plot showing the absolute count of γδ T cells. (C) The frequency of γδ T cells amongst T cells. (D) The frequency of cells with a pre-activated effector phenotype (CD27-CD44high) amongst γδ T cells. For analysis between multiple groups variance was compared using Friedmann's test. Data with equal variances were analysed using ordinary one-way ANOVA test with Tukey's multiple comparison test. ns = not significant, * = $P<0.05$ and ** = $P<0.01$ (non-parametric data were analysed with the Kruskal-Wallis test with Dunn's multiple comparisons test).

Production of IL-17 within the murine anterior compartment by γδ T cells

Expression of IL-23R is hallmark of IL-17−producing lymphocytes, including γδ T cells (Sutton et al. 2009), Th17 cells (Zhou et al. 2007; Lochner et al. 2008; Awasthi et al. 2009) and ILC3s (Takatori et al. 2009; Sawa et al. 2010). As we had visualised the presence of IL23R+ γδ T cells in naïve IL-23R-GFP mice by 2-photon microscopy, consistent with, and expanding on the data published by Reinhardt and colleagues (2016), we were prompted to determine the abundance of IL-17A−producing IL-23R+ cells among anterior compartment-resident lymphocytes by flow cytometry.

We have already shown that γδ T cells, but not αβ T cells, constitute the majority of all anterior compartment-resident IL-23R+ cells and CD3+CD4−CD8− cells **(Figure 4.4)**. Our data also clearly shows that γδ T cells were the main IL-17A−producing anterior compartment resident cell type after *in vitro* stimulation with PMA/ionomycin in naïve mice **(Figure 4.7A)**. Furthermore, the majority of γδ T cells readily produced IL-17A after ex vivo stimulation, whereas only a minor population produced IFNγ **(Figure 4.7B)**. Almost all IL-17A producing CD4+ and CD8+ T cells express C-C chemokine receptor 6 (CCR6), and T cells expressing CCR6 have been shown to express 100-fold more IL-17A than CCR6- T cells (Satya et al. 2008). As expected, these anterior compartment-resident IL-17−producing γδ T cells were CCR6+ cells **(Figure 4.7C)**. Since anterior compartment-resident γδ T cells not only express key markers indicative of an IL-17−producing phenotype, but also possess the capacity to produce IL-17A ex vivo, they most likely represent the main IL-17−producing anterior compartment-resident lymphocyte population in naïve mice.

Next I determined if γδ T cells were still the main IL-17A−producing cells in the anterior compartment of ShH10 IL-23 AAV mice during established disease (Day 10).

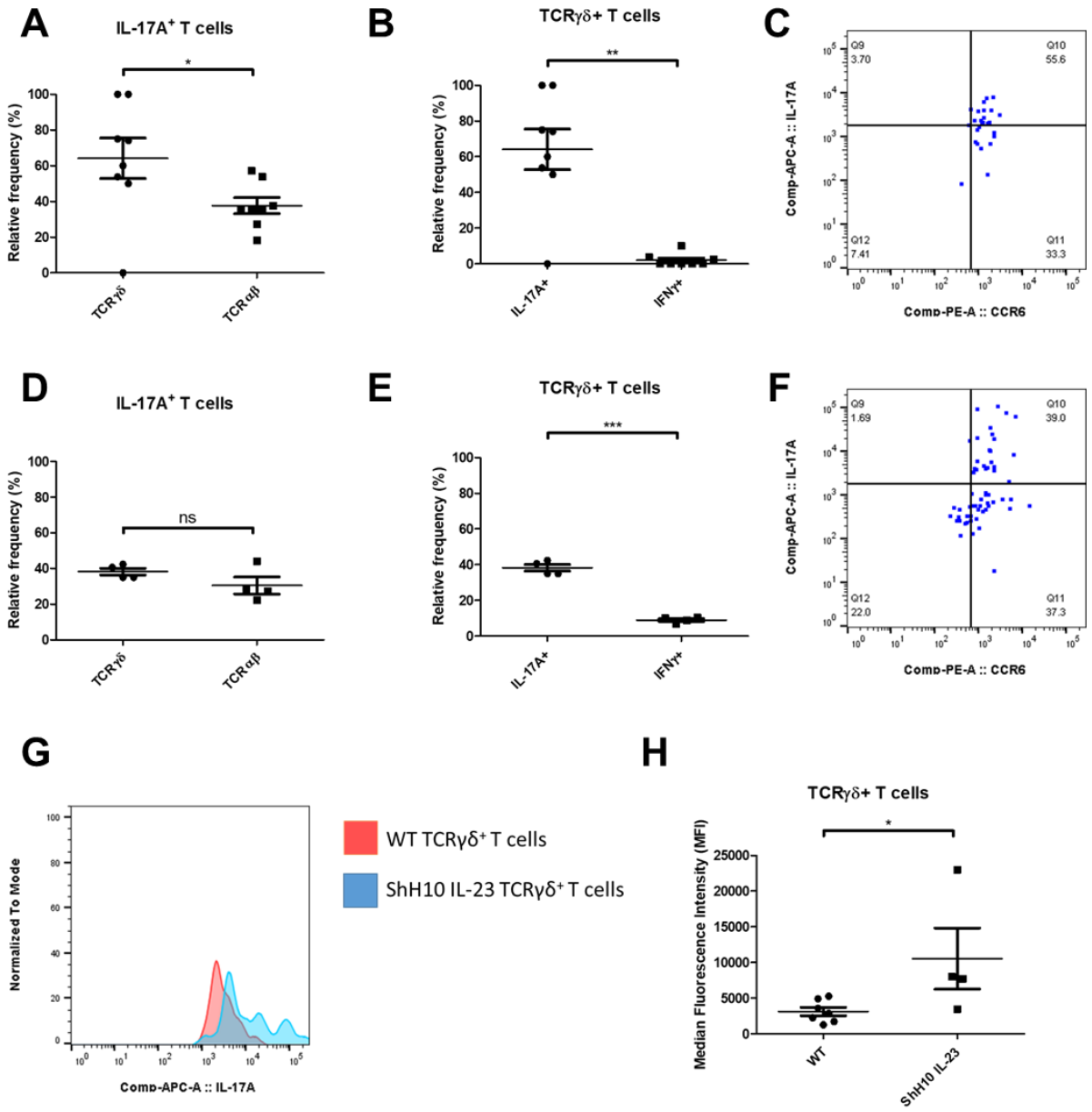


Figure 4.7: Anterior compartment-resident γδ T cells produce interleukin-17 (IL-17) and constitute the pool of IL-23R+ lymphocytes. Results of flow cytometric analysis of anterior compartment tissue taken from C57BL/6 mice at day 10 after sham injection of PBS (WT) (A-C) or intravitreal delivery of ShH10 IL-23 AAV ($2x10^{10}$gc) (D-F). Cells were stimulated with phorbol myristate acetate/ionomycin. Frequencies of αβ and γδ T cells among IL-17−producing CD3+ cells (A and D). IL-17 production by γδ T cells (B, E, G and H). CCR6 expression by IL-17−producing γδ T cells (C and F). In compiled frequency plots symbols represent individual mice; horizontal lines show the mean and error bars represent SEM. ns = not significant; ∗ = P < 0.05; ∗∗ = P < 0.01; ∗∗∗ = P < 0.001, by unpaired t-test.

Here, γδ T cells still represent the bulk of IL-17A−producing cells (~ 40%), but there was now a comparable frequency of IL-17A−producing αβ T cells within the anterior

compartment (~37%) **(Figure 4.7D)**, likely due to an increase in the total number of T cells, caused by infiltrating αβ T cells. The majority of γδ T cells (~68%) still readily produced IL-17A after ex vivo stimulation with PMA/ionomycin. However, a much larger population of γδ T cells now produced IFNγ (~11%) **(Figure 4.7E)**. Anterior compartment-resident IL-17−producing γδ T cells were still all CCR6+ **(Figure 4.7F)**. Interestingly, although the relative frequency of γδ T cells that were able to produce IL-17A after in vitro stimulation with PMA/ionomycin decreased in ShH10 IL-23 AAV compared to naïve mice, γδ T cells in ShH10 IL-23 AAV mice produced more IL-17 than naïve mice **(Figure 4.7F, G and H)**.

The anterior compartment of healthy human eyes contains an IL-23R+RORγt+ γδ T cell population

Following the above observations in the mouse, I then investigated the presence of IL-23R+ γδ T cells in the anterior compartment of the human eye, including the anterior uveal tract and the limbal sclera. In light of evidence suggesting that early experimental SpA, but not established disease, is dependent on IL-23 (Adams et al. 2015; Baeten et al. 2015; Dubash et al. 2019) I believed it was key to investigate the presence of IL-23R+ T cells in healthy human eyes that likely act as sentinels or early first responders for IL-23 signal. I have already shown in Chapter 3 that CD45+CD3+ T cells are present on multiple tissues of the healthy human anterior chamber, including the iris, ciliary body, and limbal sclera, but are not present in the prepupillary cornea.

I characterized the anterior uvea-resident T-cells using flow cytometry of anterior uvea cell suspensions from cadava eyes with no history of disease. Eyes were enucleated and phenotypes within 72 hours of death. In addition to CCR6 (Haas et al. 2009), CD161 is a highly up-regulated gene in human T_H17 cells that are actively able to

produce IL-17 (Cosmi et al. 2008). In the healthy human anterior uvea, approximately 11% of all isolated anterior compartment-resident T-cells were CCR6+CD161+ **(Figure 4.8A)** and approximately 12% of the CD3+CCR6+CD161+ were CD4-CD8- cells. I also observed that ~17% CD3+CCR6+CD161+ were CD4+ and a staggering ~64.3% were CD8+.

To show the exact anatomical location of these cells, I performed fluorescence microscopy on intact, live, un-manipulated tissue from naive mice. I found that IL-23R–eGFP+ cells are located at the outer wall of Schlemm's canal proximal to the cribriform meshwork **(Figure 4.1D)**, at the limbal sclera **(Figure 4.2A and B)** specifically within the scleral stroma and not the vascular episclera **(Figure 4.2C and D)**, and within both the ciliary processes **(Figure 4.2E and F)** and ciliary muscle **(Figure 4.2G and H)**. These cells are absent from the prepupillary cornea and pupillary region of the iris.

During the course of this study, none of the tested commercially available anti-IL-23R antibodies were able to effectively and repeatable stain for IL-23R in human tissue. This finding was consistent with the known technical difficulties of staining IL-23R, mostly likely due to very low expression levels of the protein. We instead found that repeatable and accurate labelling of *il23r* in control tissues was possible by fluorescence in-situ hybridisation (FISH) flow cytometry using the recently developed Invitrogen PrimeFlow RNA assay **(supplementary figure 4.1A and B)**. Unfortunately, this assay was proving problematic to produce repeatable evidence that distinguished *il23r* expressing T cells in our human ocular material. Although we did manage to show some data that suggests a large population of T cells in the Human anterior uvea express IL23R messenger transcripts **(supplementary figure 4.2A and B)**, time limitations and the cost of the assay prevented me from exploring this any further. We instead attempted to look for *il23r* expression in intact, fixed, whole mount tissue from

human anterior uvea **(Figure 4.8B)** by light sheet fluorescence microscopy (LSFM), using an optimised protocol described in my materials and methods section. *Consistent* with my findings in the naïve mice, I found that IL-23R expressing cells are located within the ciliary processes **(Figure 4.8C-E)**.

In addition to IL-23R, the expression of RORγt has also been identified as a hallmark of IL-17−producing lymphocytes, including γδ T cells (Sutton et al. 2009), T_H17 cells (Zhou et al. 2007; Lochner et al. 2008), and ILC3s (Takatori et al. 2009; Sawa et al. 2010). Therefore, I next analysed the folds of the ciliary body where we had previously identified IL-23R expression using high magnification 2-photon microscopy. In the healthy human ciliary body, I observed several RORγt+ T cells **(Figure 4.9)**. Consistent with the data published by Sherlock and colleagues (2012) these cells are associated with fine collagenous strands. Although many hours were spent looking for these cells, very few were found within the serial sections of human anterior uvea, highlighting their rarity. Although I did not include any epithelial markers for this part of the study, high magnification, multi-photon imaging does allow for speculation of the specific localisation of the RORγt+ T cells within the ciliary processes. RORγt+ T cells appear to be within the tissue of the ciliary pigmented epithelium outside of the blood vasculature **(Figure 4.9B)**.

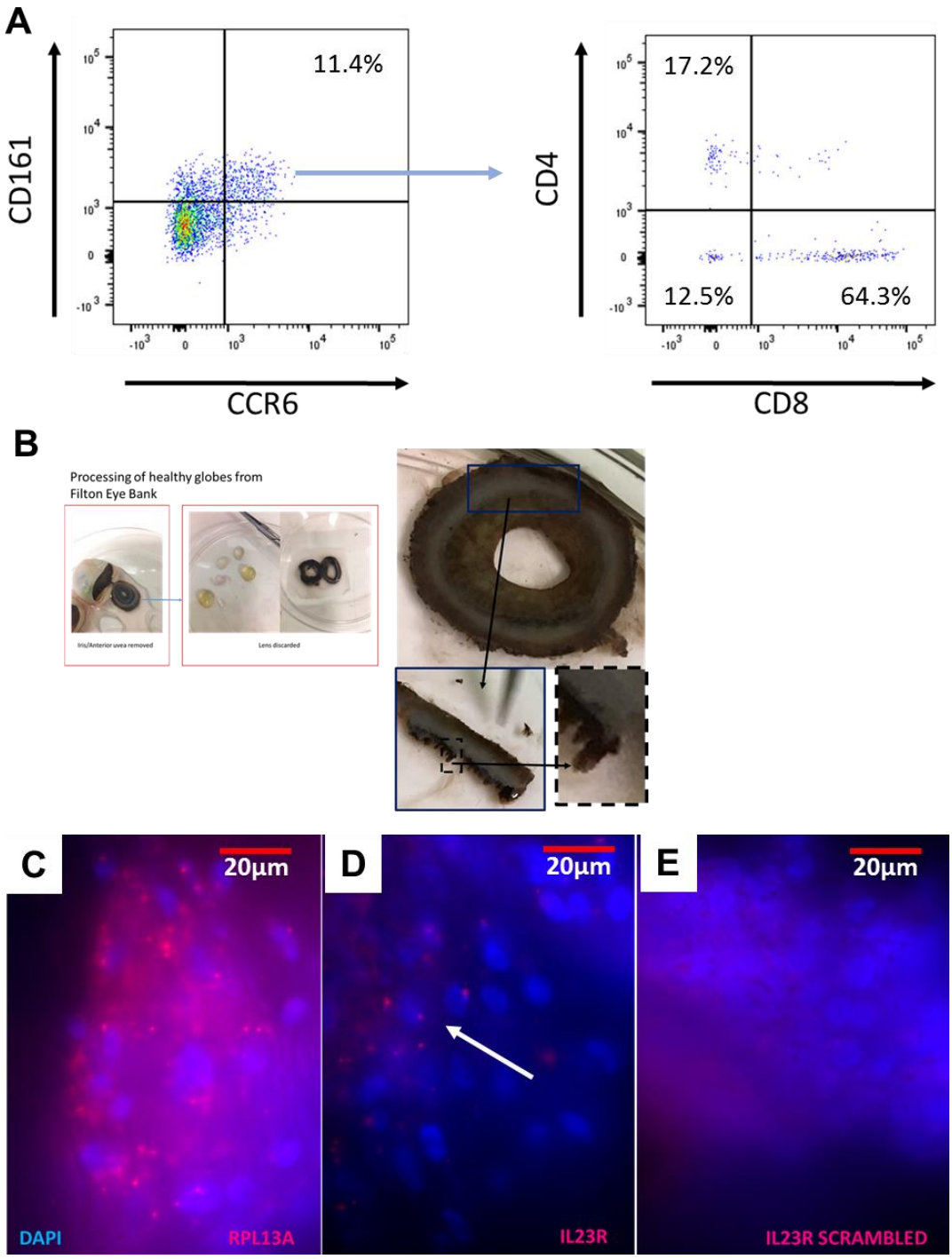


Figure 4.8: The healthy human anterior uvea contains an IL-23R+ cell population. (A) Representative plots show flow cytometric gating strategy for viable $CD3^+$ T cells that are $CD161^+CCR6^+$, and $CD3^+CD161^+CCR6^+$ T cells that are $CD4^+$, $CD8^+$ or $CD4^-CD8^-$ from healthy anterior uvea dissected from globes obtained from deceased individuals obtained from Filton Eye Bank after corneal removal. Percentages shown represent relative frequency of parent population. (B) Representative light sheet immunofluorescence images showing merged expression of nucleus (blue) and ribosomal RPL13A message (control) probe (purple) in sections of whole mount ciliary body. (C) Representative light sheet immunofluorescence images showing merged expression of nucleus (blue) and target IL-23R message probe (purple) in sections of whole mount ciliary body. (D) Representative light sheet immunofluorescence images showing merged expression of nucleus (blue) and reverse sequence (scrambled) IL-23R message probe (purple) in sections of whole mount ciliary body.

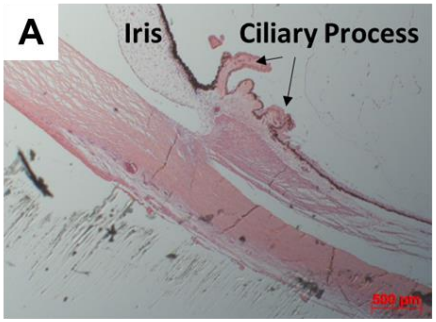
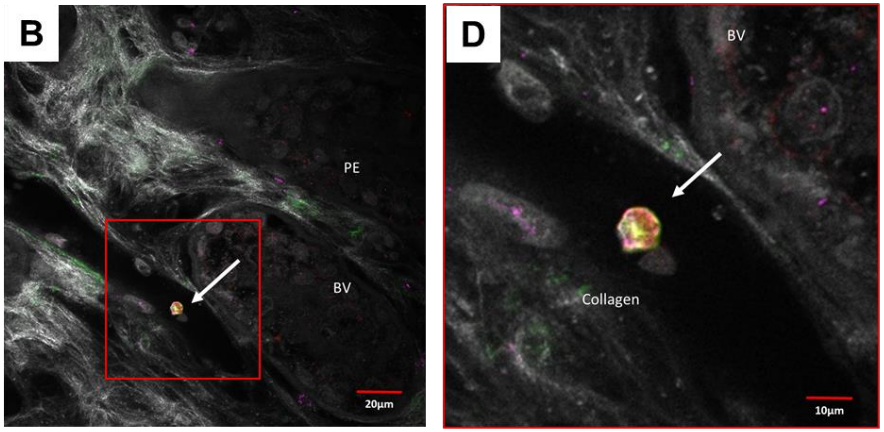
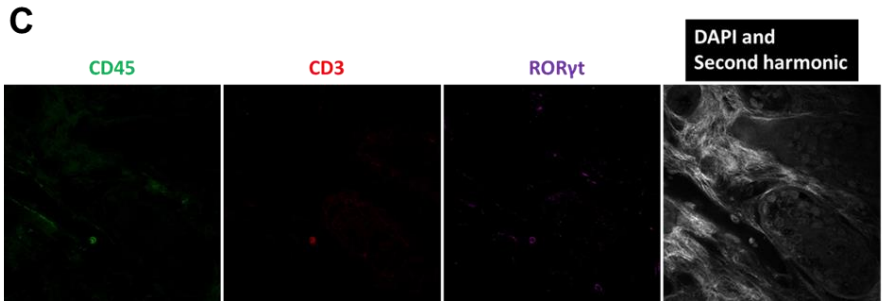
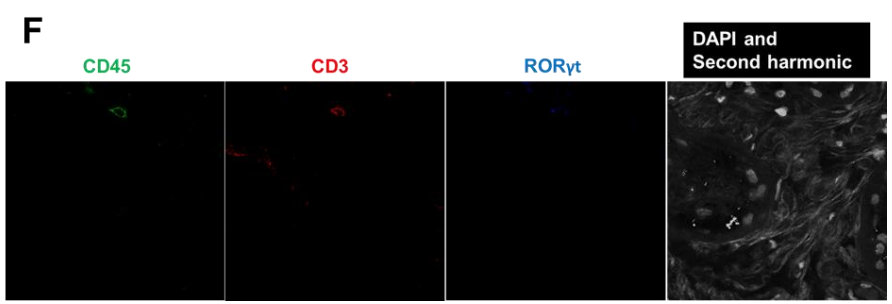


Figure 4.9: RORγt+ T cells are inserted into the ciliary pigmented epithelium by collagen fibres of the in healthy human eyes. (A) H&E staining of healthy human anterior compartment. (B and E) Representative immunofluorescence image showing merged expression of second harmonic resonance collagen fibres and nuclei (grey), CD3 (red), and RORγt (purple) within a major ciliary process. Red square highlights the region magnified in D and G respectively. (C and F) Individual expression of second harmonic resonance collagen fibres and nuclei (grey), CD3 (red), and RORγt (purple). (D) Magnification of the region shown in B and E respectively.







IL-23 promotes IL-17A expression ex-vivo in cells of the human anterior compartment

These findings prompted me to determine the abundance of IL-17A−producing T cells among human anterior compartment-resident lymphocytes by flow cytometry. My data clearly shows that a small fraction (~1.5%) of anterior uvea-resident T cells are IL-17A−producing cells after in vitro stimulation with PMA/ionomycin **(Figure 4.10A and B)**. A much larger fraction of the total T cell population was able to produce the T_H1 cytokine IFNγ and the majority were capable of producing TNFα.

Next we assessed the impact of a more physiological stimulus on anterior uvea-resident T cells using IL-1β and IL-23. Previous studies have shown that naive murine T cells which do not express IL-23R do not differentiate into T_H17 cells in response to IL-23 in vitro (Langrish et al. 2005, van Beelen et al. 2007). In contrast, IL-23 can expand Th17 cells from memory CD4+ T cells (Aggarwal et al. 2003). It has also been demonstrated that IL-1α or IL-1β synergizes with IL-23 to promote IL-17 production by murine T cells in the presence or absence of T cell receptor engagement (Sutton et al. 2006). This is not limited to Th17 cells as γδ T cells can also produce an important source of innate IL-17 when activated by IL-1β and IL-23 (Sutton et al. 2009).

Unlike PMA/ionomycin stimulation, no noticeable IL-17 production was observed by flow cytometry on cell suspension of human anterior uvea after overnight stimulation with IL-1β and IL-23. However, when ascertaining whether IL-17A protein was detectable using the highly sensitive ELISA, we could detect changes in IL-17A protein using IL-1β and IL-23 stimulation **(Figure 4.10C)**.

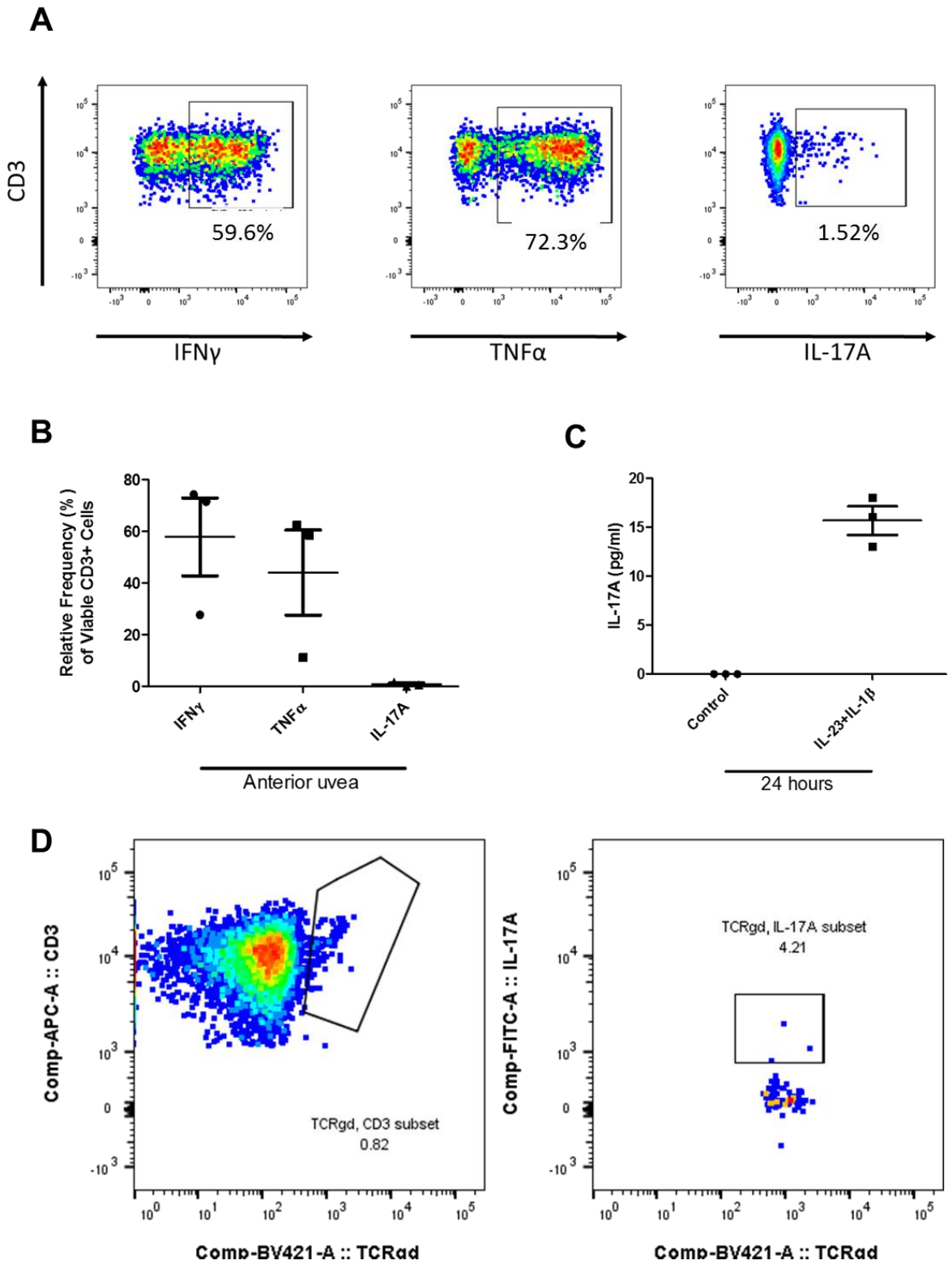


Figure 4.10: A small population of γδ T cells in the healthy human anterior uvea is capable of producing IL-17A. Anterior uvea cell suspensions from human cadavers were analysed by flow cytometry (A) Percentage of T cells that express IFNγ, TNFα, or IL-17A after 4 hours' stimulation with PMA and ionomycin. (B) Compiled frequency data (n=3) showing the relative frequency of viable $CD3^+$ T cells that are $IFN\gamma^+$, $TNF\alpha^+$, or IL-17A. Horizontal lines show the mean and error bars represent SEM. (C) Supernatant levels of IL-17A after 24 hours IL-1β and IL-23 stimulation. Horizontal lines show the mean and error bars represent SEM. (D) Percentage of γδ T cells that express IL-17A after 4 hours' stimulation with PMA and ionomycin.

As γδ T cells, but not αβ T cells, constituted the majority of all anterior compartment-resident IL-17A+ producing T cells in naïve mice, I wanted to ascertain if this was also the case in the human anterior uvea. My data shows that a much smaller fraction of the total T cell pool is made of γδ T cells in human anterior uvea cell suspensions (~1%) than in the mouse. In contrast to naïve mice, only a small population of γδ T cells (~4%) were IL-17A−producing cells after in vitro stimulation with PMA/ionomycin **(Figure 4.10D)**.

Previously in this chapter, Immunofluorescent imaging of limbal sclera in IL-23-eGFP mice revealed the presence of IL-23R+ γδ T cells. This data is supported by the findings of Reinhardt and colleagues (2016) that showed an accumulation of γδ T cells in the limbal sclera. In Chapter 3 I also showed by high resolution immunofluorescence imaging the presence of CD3 T cells in human limbal sclera. These findings prompted me to determine the abundance of IL-17A−producing T cells among human limbal sclera-resident lymphocytes by flow cytometry. In contrast to the human anterior uvea, the human limbal sclera contained an even lower fraction of IL-17A−producing T cells after in vitro stimulation with PMA/ionomycin **(Figure 4.11 A and B)**, and high sensitivity ELISA was unable to detect IL-17A protein using IL-1β and IL-23 stimulation. Furthermore, although the sclera had a slightly higher percentage of γδ T cells (~1.5%) **(Figure 4.11C)**, none of these cells were IL-17A−producing cells after in vitro stimulation with PMA/ionomycin **(Figure 4.11D)**.

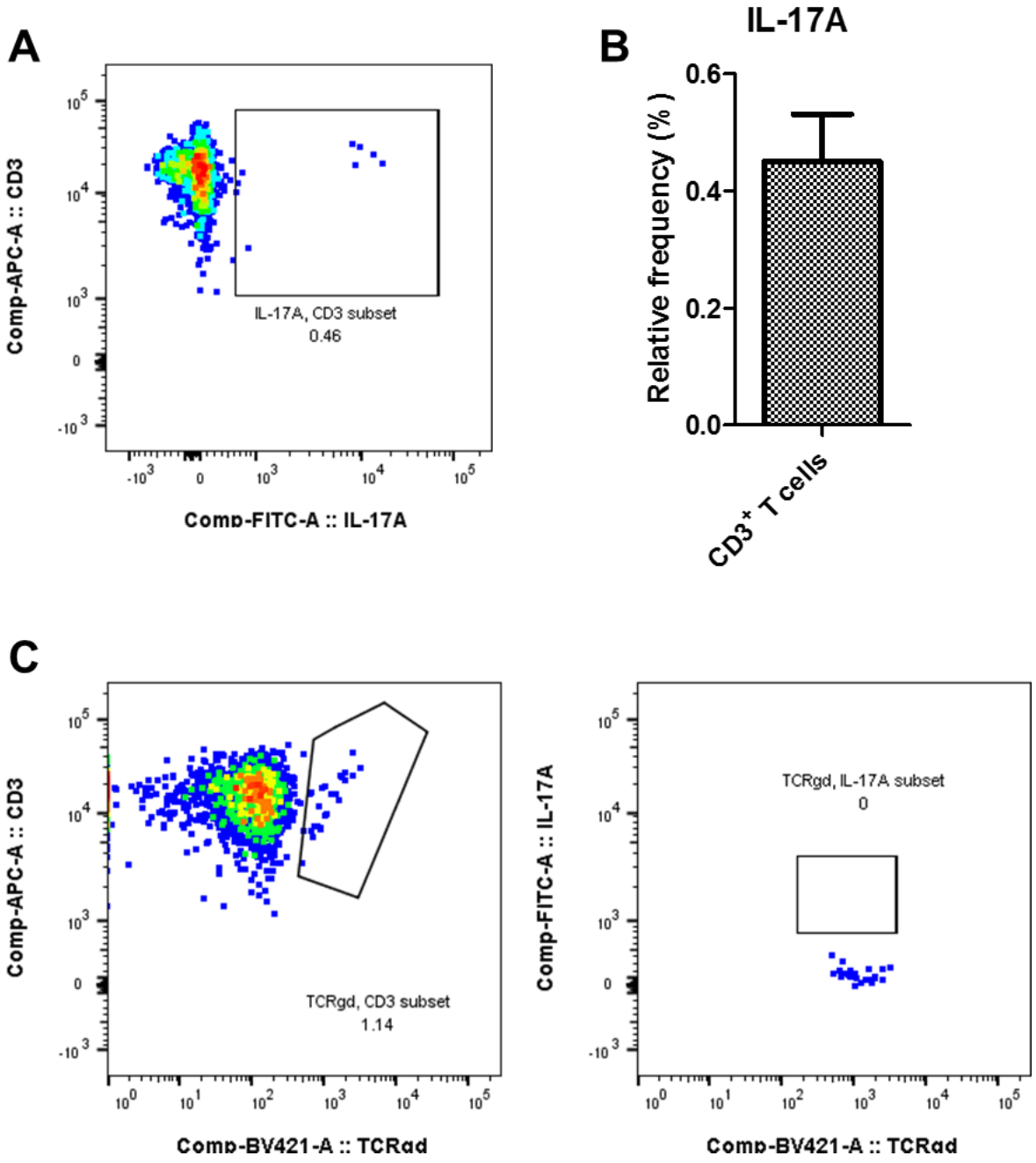


Figure 4.11: Data suggests a small population of CD3+ T cells in the healthy human limbal sclera is capable of producing IL-17A. limbal sclera cell suspensions from human cadavers were analysed by flow cytometry (A) Percentage of T cells that express IL-17A after 4 hours' stimulation with PMA and ionomycin. (B) Compiled frequency data (n=3) showing the relative frequency of viable $CD3^+$ T cells that are IL-17A. Horizontal lines show the mean and error bars represent SEM. (C) Percentage of γδ T cells that express IL-17A after 4 hours' stimulation with PMA and ionomycin.

Phenotypic characterisation of T cells in human anterior compartment biopsy samples

Access to research tissue from the anterior compartment of the human eye in human is very difficult, and is likely one of the main limitations that has prevented the identification of resident T cells involved in the IL-17/IL-23 axis in humans in the past. However, analysis of waste tissue produced as a result of routine trabeculectomy procedures, revealed that T cells can be isolated from such tissue. During trabeculectomy, a scleral flap is created approximately 4 × 4 mm in size with a thickness aimed at ½ to ¾ of the sclera. The eye's anterior chamber is then entered underneath the scleral flap and an iridectomy is taken. This usually results in 2 separate tiny ~1-2mm^2 pieces of waste tissue consisting of limbal sclera and iris root/ciliary body **(Figure 4.12A)**. These are the areas we have shown γδTCR+IL-23R+ T cells to be present in naïve mice and RORγt+ T cells to reside in humans. Clinically, reduction of intraocular pressure (IOP) remains the only proven treatment for glaucoma (Collaborative Normal-Tension Glaucoma Study Group, 1998; The Advanced Glaucoma Intervention Study (AGIS): 7, 2000; Lichter et al. 2001), the second leading cause of blindness and a commonly associated symptom of anterior uveitis (Panek et al. 1990). Therefore, IOP must be lowered by surgical means, such a trabeculectomy and minimally invasive glaucoma surgery (MIGS) techniques such as microstent (Theilig et al. 2020), If IOP-lowering medications are not effective, making this waste tissue readily available.

I decided to determine if the T cells phenotyped in larger cadaver samples could also be phenotyped in these much smaller trabeculectomy samples **(Figure 4.12B)** by flow cytometry to assess their suitability as a tissue for readout in potential future clinical trials investigating the IL-17/IL-23 axis. Using a modified digestion protocol for

digestion of small ocular samples I looked for the abundance of T cells with a Th17 phenotype among cell suspension of human trabeculectomy samples by flow cytometry. As expected, these samples contained cells with an IL-17−producing phenotype, furthermore CCR6+ T cells were present in both the scleral flap and iridectomy **(Figure 4.12 C and D)**. The percentage of T cells with a CCR6+ phenotype being ~3 and 4% respectively.

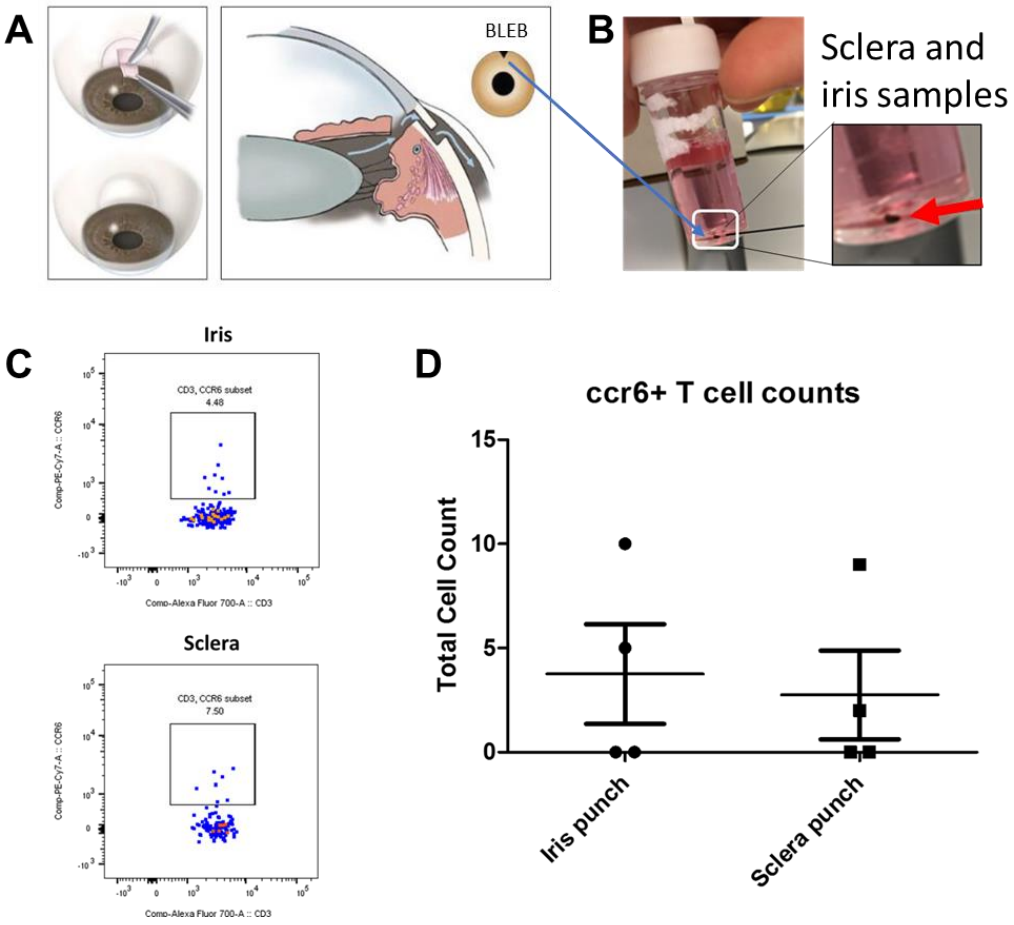


Figure 4.12. T cells with a Th17 phenotype can be recovered from trabeculectomy waste tissue. Trabeculectomy waste tissue cell suspensions were analysed by flow cytometry. (A) Illustrative diagram showing the trabeculectomy procedure, adapted from https://www.ophthalmologyexpertservices.com. Briefly, a scleral flap is created, approximately 4 × 4 mm in size with a thickness aimed at ½ to ¾ of the sclera (top left), the eye's anterior chamber is then entered underneath the scleral flap and an iridectomy is taken (right). The scleral flap is then sealed allowing fluid to drain away, a bleb is formed (bottom left and right). (B) photographic image of trabeculectomy waste tissue. (C) The percentage of T cells with a Th17 phenotype (CCR6+) in the iridectomy (iris) and scleral flap (sclera). (D) Compiled frequency data (n=4) showing the relative frequency of viable $CD3^+$ T cells that are CCR6+. Horizontal lines show the mean and error bars represent SEM.

T cells were phenotyped in both the naïve mouse and healthy human limbal sclera in chapter 3. Earlier in this chapter we have also shown the presence of IL-23R+ T cells in the stromal sclera layer of limbal sclera in the naïve mouse. Embedded and forming an enthesis just behind the region of limbal sclera are the extra ocular muscles (EOMs). I decided to determine if the T cells could also be phenotyped in entheseal EOMs. Tissue of this type is produced as waste as a result of strabismus surgery. Strabismus surgery is the gold standard for correction of squints.

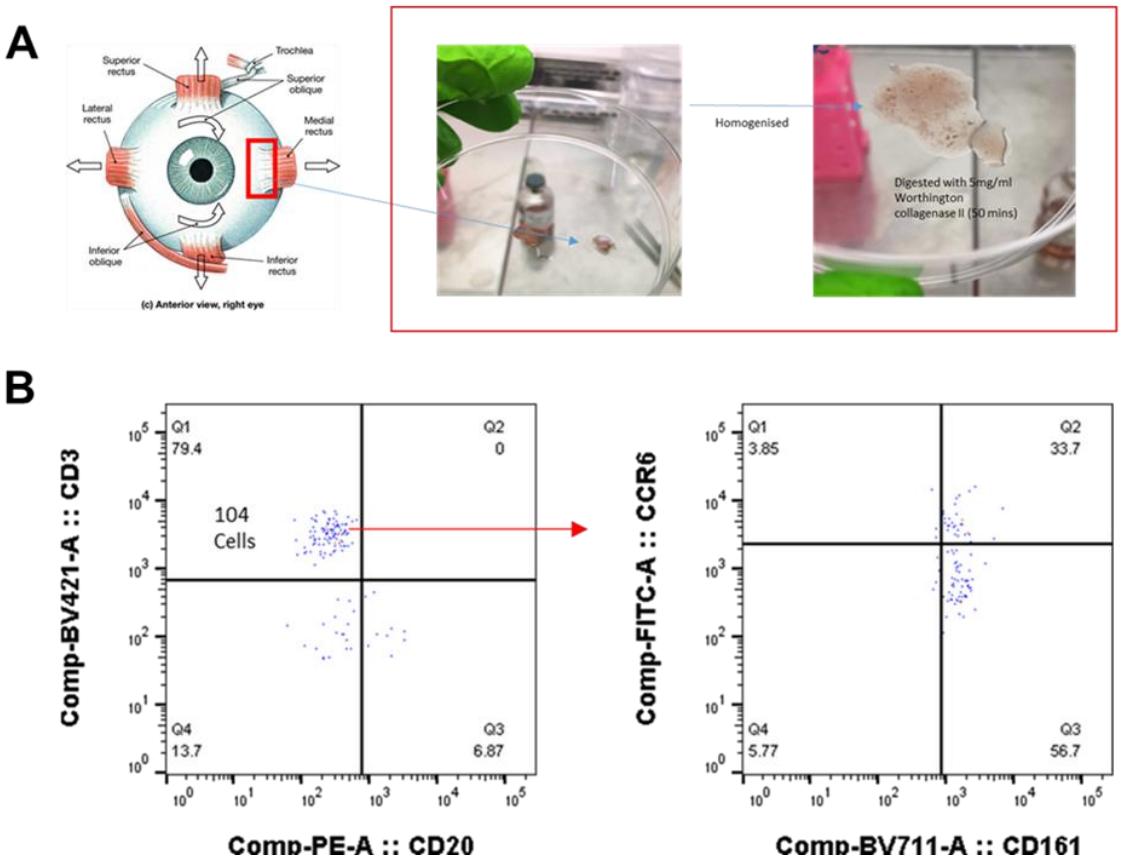


Figure 4.13. T cells with a Th17 phenotype can be recovered from strabismus surgery waste tissue. Strabismus waste tissue cell suspensions were analysed by flow cytometry. (A) Illustrative diagram showing the region of entheseal extra ocular muscle (EOM) removed during strabismus surgery. Approximately 5-10mm of the weaker EOM is removed. (B) photographic image of strabismus surgery waste tissue. (C) The percentage of T cells with a Th17 phenotype (CCR6+) in entheseal EOM. (D) Compiled frequency data (n=4) showing the relative frequency of viable $CD3^+$ T cells that are CCR6+. Horizontal lines show the mean and error bars represent SEM.

During this surgery a 5-10mm recession of the weaker EOM is made **(Figure 4.13A)**. I phenotyped cell suspensions of this tissue by flow cytometry for T cells involved in the IL-23/IL-17 axis. As expected, these samples contained cells with an IL-17−producing phenotype **(Figure 4.13B)**. 33.7% of T cells were found to be a CD161+CCR6+.

The anterior compartment of the human eye is primed to respond to IL-17A produced by IL-23R γδ T cells

Once secreted, IL-17A/F cytokines stimulate stromal cells and immune cells to promote inflammation (Bartlett et al. 2015; Bridgewood et al. 2019). IL-17 exerts its effects by binding to IL-17 receptors (IL-17R family). IL-17A/F stimulation requires the expression of IL-17RA and also IL-17RC receptor pairing (Hu et al. 2010). A recently published paper added further complexity to IL-17 receptor biology by finding that a receptor complex consisting of IL-17RA and IL-17RD was able to only bind specifically to IL-17A homodimers (Su et al. 2019). Previous studies have shown IL-17RA is expressed by retinal Muller cells (Qiu et al. 2016), and corneal and limbal superficial epithelial cells (Fang et al. 2010; Arranz-Valsero et al. 2012).

At the time of writing, no studies have shown the presence of IL-17RA expressing cells within the anterior uvea. To show if IL-17RA is expressed by cells of the anterior uvea and its connecting tissues, I performed fluorescence microscopy on intact, live, un-manipulated eyes from naive mice. I found that IL-17RA cells are located at the outer and inner walls of Schlemm's canal **(Figure 4.14A)**, throughout all layers of the trabecular meshwork **(Figure 4.14A)**, and at the anterior border layer of the human iris **(Figure 4.14B)**. IL-17RA cells within the trabecular meshwork and iris specifically are $PDPN^{high}$. IL-17RA cells are also present in the ciliary body **(Supplementary**

Figure 4.3 E), but are absent from the limbal sclera and peripheral cornea **(Supplementary Figure 4.3 A and B)**.

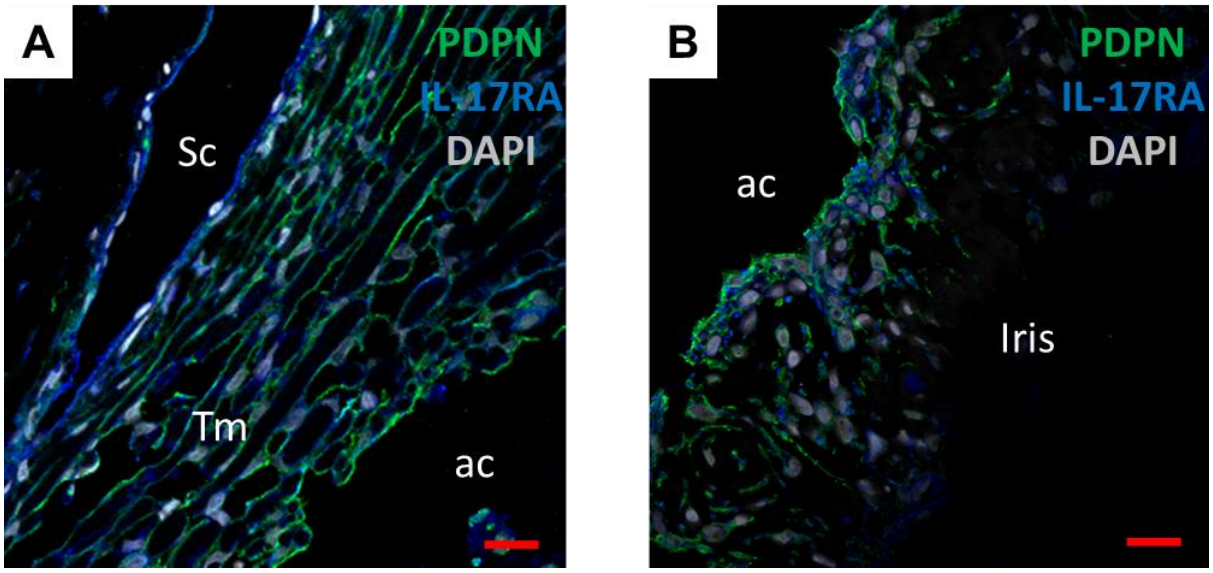


Figure 4.14: IL-17RA expression by cells of the healthy human trabecular meshwork, iris and Schlemm's canal. Representative immunofluorescence images showing merged expression of nuclei (grey), IL-17RA (blue), PDPN (green) within the trabecular meshwork (A) and iris (B). Image captured at x40 magnification. Red scale bar indicates 20µm.

Discussion

In the previous Chapter I found that the eyes of both the healthy subjects and naïve C57BL/6f mice contain multiple sub-populations of T cells. These T cells were located in tissues of the anterior compartment of the eye, including the iris, ciliary body, limbal sclera, and the trabecular meshwork. Sub-populations of T cells included CD4+, CD8+ and CD4-CD8-. In this Chapter I assessed the specific location of T cells expressing Th17 associated markers by histology and further phenotyped these subpopulations in healthy subjects, naïve C57BL/6f mice, and naïve IL-23R-eGFP mice by flow cytometry for expression of Th17-associated markers including IL-23R, RORγt, CCR6, CD161, and IL-17A. Finally, I assessed if the same sub-populations could be found in small clinical samples obtained from ophthalmic surgeries, such as trabeculectomy and strabismus, and determined if these samples could be a suitable material for phenotyping T cells in the anterior compartment from living humans in potential future clinical trials.

To the best of my knowledge, the findings of this Chapter, are the first to show a population of resident IL-23R+ γδ T cells in naïve mice that are present within the same regions of the eye that become inflamed in established human AAU (the ciliary body, limbal sclera and iris). These cells share the same phenotype as those T cells found in the naïve mouse axial skeleton entheses and aortic root in earlier studies, IL-23R+CD3+CD4-CD8-γδTCR+ (Reinhardt et al. 2016; Sherlock et al. 2012), and all have a pre-activated effector phenotype CCR6+CD44+CD27-CD62L- (Reinhardt et al. 2016). I have also shown that surgical procedures such as trabeculectomy and strabismus can provide relevant readout samples, usually discarded as waste material, for assessment of T cell populations within the anterior compartment by flow cytometry.

All be it with caveats, this study is also the first to show evidence that RORγt and IL-23R positive T cells exist within the anterior compartment of the human eye. Commercially available antibodies against RORγt and IL-23, such as those used in this study are known amongst T_H17 immunologists to be difficult to work with. RORγt staining often results in a large amount of non-specific staining. RORγt was observed in the ciliary processes of healthy human tissue by IF and was accompanied by CD3 staining encircling nuclei. In contrast IL-23R staining is often undetectable on human T_H17 cells, and believed to be due to the low expression of IL-23R. Although IL-23R signal was not detected in tissues of the anterior compartment by IF, *IL23R* messenger transcripts were detected within T cells of the anterior compartment of the healthy human eye by fluorescent *in-situ* hybridisation (FISH) flow cytometery. This methodology was validated on human T cells isolated from blood cones selected positively for Th17 (first separated by size (FSC-A vs SSC-A) using elutriation, followed by positive selection of CD3+CD4+CCR6+CD161+ T cells by fluorescence-activated cell sorting) but had limited success on T cells from human anterior uveal digests. The caveats of which are discussed in more detail below.

Although, *IL23R* messenger transcripts were detected within T cells of the anterior uvea which suggests that T cells in the eye are at least transcribing the receptor, a limitation of the results in this assay was that although exceptionally high expression was observed in the T cells identified as positively expressing *IL23R* messenger transcripts, all T cells showed background expression of *IL23R* above negative controls (no *IL23R* probe added) which suggests that fluorescence background was being induced in the negative population, adding an element of doubt to this finding. Nonetheless, the percent of T cells with *IL23R* messenger transcripts were consistent between biological repeats with anterior uveal samples showing approximately 25%

positivity and PBMCs showing 0.15% positivity. Although 25% is much higher than one would expect to find on cells in the blood, it could be the case for tissue specific cells which have been shown to be enormously enriched for IL-23R+ cells, as will be discussed below.

In the previous study by Sherlock et al. (2012), between 1-2% of CD45+ cells in the axial skeleton or aortic root of healthy naïve mice were shown to be IL-23R positive, and almost 100% of these cells were CD3+CD4-CD8- T cells. Although the number of times the experiment was repeated was very low (n=2), the study was strengthened by the larger number of RORγt-eGFP mice used (n=9), which showed a comparable percentage of CD45+ cells that are RORγt+ CD4-CD8- cells, although the study did not show that these cells were specifically (CD3+) T cells. Subsequent investigation by Reinhardt et al. (2016) substantiated these finding by providing evidence that approximately 75% of CD3+CD4-CD8-IL-23R+ T cells and about 60% of CD3+CD4-CD8-RORγt+ T cells were γδT-cells. Using flow cytometry in my study, I have demonstrated a similar number (~2%) of CD45+ cells in the anterior compartment of the eye are IL-23R+ using the same IL-23R-eGFP mice (n=5) as utilised in Sherlock et al. (2012) and Reinhardt et al. (2016). Additionally, I have demonstrated that 10% of lymphocytes (CD45+ cells with a small FSC-A and SSC-A) were IL-23R+ T cells and 1% of lymphocytes were IL-23R+CD3-. Furthermore, I showed that approximately 15% of T cells in the healthy naïve mouse anterior compartment of the eye, were IL-23R positive, and that almost 100% of IL-23R+ T cells are CD4-CD8-γδTCR+. Finally, even though results in Chapter 2 suggest that an IL-23R+ T cell is responsible for diving innate pathology in the anterior compartment of the eye in response to IL-23 overexpression, flow cytometry data produced in this Chapter suggest another

subtype of cells, other than T cells, does exist in the anterior compartment of the eye which express IL-23R **(Supplementary Figure 4.4)**.

Using immunofluorescence microscopy in the same IL-23R-eGFP mice, I showed that these cells are within the *pars plicata* of the ciliary body - both proximal to longitudinal ciliary muscle - and within the folds proximal to the ciliary epithelium, the iris, and within the stromal layer of the limbal sclera. This indicates that these regions of the eye may be primed to respond to IL-23. These sentinel IL-23R+ T cells are a key finding that could explain the results seen in Chapter 2 of this study; that *In vivo* exposure to IL-23 was sufficient to induce inflammation in the anterior compartment of the naïve mouse eye with rapid kinetics, and could potentially explain why the anterior region of the human eye became inflamed in AAU. These finding also suggests that only a fraction of the T cells found in the extravascular tissue of the anterior compartment in mice in Chapter 3, are the sentinel CD4-CD8-IL-23R+ T cells as a mixture of CD4+, CD8+ and CD4-CD8- subpopulations, were found throughout the anterior compartment of the healthy naïve mouse eye. IL-23R+ cells were also found in the healthy human anterior uvea by FISH histological methods, although time limitations prevented me from further phenotyping these cells.

It is also possible that there may be heterogeneity within the sentinel CD4-CD8-γδTCR+IL-23R+ T cell population within the anterior compartment. Typically, γδ T cells are classified according to the variable domain of the TCRγ (Vγ) chain (Carding and Egan 2002). A previous study by Reinhardt and colleagues (2016) showed that the Achilles tendon enthesis of mice contained γδ T cells displaying Vγ1, Vγ4, and Vγ6 chains. However, the majority of Achilles tendon enthesis γδ T cells were the Vγ6 subset. According to nomenclature reported by Heilig and Tonogawa in their 1986 Nature publication (Heilig and Tonegawa 1986), it is the Vγ6 subset that is the IL-17A

producing subset of γδ T cells. Although data produced by Reinhardt and colleagues (2016), confirmed that approximately 60% of Achilles tendon enthesis γδ T cells express IL-17A after IL-23 stimulation, they did not show that this was being produced by the Vγ6 subset specifically. Unfortunately, due to time limitations I was unable to phenotype Vγ chains on γδ T cells within the anterior compartment of the eye. Nonetheles, expression of RORgt and IL-23R, which I did manage to show on T cells in the healthy human and naïve mice eye, are also hallmarks of IL-17 producing T cells (Sutton et al. 2009).

I have shown for the first time that γδ T cells within the anterior compartment of the naive mice eye significantly dominated the pool of IL-17 producing T cells after *ex-vivo* stimulation with phorbol myristate acetate (PMA)/ionomycin. I presented that approximately 70% of IL-17A producing T cells in the anterior compartment of naïve mice were γδ T cells. Interestingly, this is similar to the percent of IL-17A producing T cells in the Achilles tendon enthesis of naïve mice that were found to be γδ T cells in the previous study by Reinhardt and colleagues (2016), although in this study these T cells were stimulated *ex-vivo* with the more physiologically relevant IL-23. Furthermore, I have shown that the percent of IL-17A producing T cells, in the anterior compartment of mice that were γδ T cells, were reduced after 12 days of highly localised ocular overexpression of IL-23. One could speculate that this decrease was due to the infiltration of αβ T cells with a Th17 phenotype following a breakdown in the blood ocular barrier (as shown to occur as early as 3 days after highly localised ocular overexpression of IL-23 in the C57BL/6 mice eye in Chapter 2).

CCR6 is involved in both homeostatic and inflammatory trafficking of leukocytes in barrier tissues, and is expressed by both T_H17 and Tγδ17 (Haas et al. 2009; Hirota et al. 2007). In a previous study by McKenzie et al. (2017), Tγδ17 cells in the dermis of

the skin were shown to constitutively express CCR6, believed to be imprinted during thymic development. The authors go on to speculate that this constitutive expression of CCR6 is what controls homeostatic γδT17 cell trafficking to the dermis where CCL20, the ligand for CCR6, is constitutively expressed. This is a very important finding and hypothesis, as γδT17 cells found in the anterior compartment of the naïve mouse eye all expressed CCR6. However, only very low concentrations of CCL20 have been detected by ELISA in the aqueous humor of the healthy human eye (Abu El-Asrar et al. 2019; Abu El-Asrar et al. 2016), which suggests this potential mechanism might not function in the eye as it does in the skin. However, one could argue that the findings in the fluid aren't relevant for the homing of cells to tissue. In this case one would need to look in the tissue, not the fluid, as chemokines are known to be incorporated into tissue matrices to form gradients, and so they are localised.

In this Chapter 1 found that approximately 12% of CCR6 expressing T cells in the healthy human anterior uvea were CD4-CD8-. Some of these T cells can be further localised to the iris root through homogenisation of small clinical samples obtained from trabeculectomy. In addition, CCR6 expressing T cells were found in the limbal sclera of trabeculectomy waste tissue, and the entheseal region joining the extraocular muscles to the anterior sclera in strabismus waste tissue. Data also produced in this Chapter suggests that there is a population of T cells in the anterior compartment of the healthy human eye that is capable of producing IL-17A after PMA/ionomycin stimulation. The anterior uvea and limbal sclera were dissected and homogenised from the same cadaver eyes. Interestingly, the anterior uvea showed a higher percent of IL-17A producing T cells than the limbal sclera, which was also shown to contain RORγt T cells found in the ciliary body by histology. Although the percent of T cells that could express IL-17A in the anterior uvea and limbal sclera, were consistent

across all three biological repeats, further experiments would strengthen this data. Furthermore, this finding was only shown by flow cytometry as qPCR of the same samples failed to show a fold change in *il17a* transcription between control and stimulated samples (in fact I failed to show consistent fold change in all of the genes I attempted to measure transcripts of by qPCR, even control genes such as GAPDH and beta actin). When troubleshooting, I later found that my qPCR was failing at a very early stage during cDNA synthesis, which we believe was due to the large amount of pigment in the sample preventing the amplification of RNA transcripts (this is why no qPCR data is included in this chapter).

It is important to mention that a limitation of this finding is that we are unable to know if the IL-17A producing T cells originated from within the blood or were resident within the tissue. Another limitation of this assay is that stimulation with PMA and ionomycin will only show what a cell can produce under a non-physiologically relevant condition. A more physiologically relevant way that T cells can be made to induce IL-17A production is through stimulation with IL-1β and IL-23 (Khan and Ansar Ahmed 2015). Unfortunately, when I stimulated T cells from the same samples under these *ex vivo* conditions, I was only able to measure IL-17A at just above the minimum detection threshold by ELISA in the anterior uvea and not in the limbal sclera. I speculate that although IL-17A is detectable in the small numbers of cells by FACS, this is only made possible through the induced the intracellular accumulation of IL-17A made possible by the presence of monensin and brefeldin that was also in the stimulation master mix. However, due to the relevantly low numbers of cells that were capable of producing IL-17A, the IL-17 may have been secreted but diluted so much in the supernatants tested, that its concentration were lower than the detection limits of the ELISA kit.

It is important to note, although we show in this Chapter that IL-23 stimulation is able to drive IL-17A expression by anterior compartment γδ T cells *in vivo* in mice and *ex-vivo* in humans, IL-17A production by γδ T cells has been demonstrated to be independent of IL-23 at other entheseal sites associated with SpA. In a recent study where entheseal γδ T cells were isolated from human spinous processes entheseal soft tissue and peri-entheseal bone, and phenotyped based on the their variable delta (Vδ) chain (Cuthbert et al. 2019), it was observed that: (a) resident spinal entheseal γδ T cells are a mixture of Vδ1 and Vδ2 subsets; (b) Vδ2 cells expressed high relative abundance of IL-23/17-associated transcripts including IL-23R, RORC and CCR6, and produced IL-17A in response to IL-23; (c) the Vδ1 subset lacked detectable IL-23R transcript and produced IL-17A independently of IL-23R expression. Due to time limitations I was unable to phenotype Vδ chain subsets of T cells, but I have shown the presence of IL-17A producing IL-23R+ γδ T cells within the anterior compartment of the eye, and it is probable that these are the Vδ chain subset.

The question arises of why these IL-23R+ γδ T cells might be present in entheseal tissue of healthy mice and humans. Entheseal organs are permanently exposed to mechanical forces and microdamage and are hence constantly switching between anabolic and catabolic processes (Thomopoulos et al. 2006; Benjamin et al. 2007; Jacques et al. 2014). Thus, it is conceivable that enthesis-resident γδ T cells interfere with bone metabolism to control tissue homeostasis in rodents and humans. Almost every region of tissue where γδ T cells were found in the anterior area of the eye can be associated with a degree of mechanical involvement. Jacques and colleagues (2014) identified the importance of biomechanical stress in the induction of enthesitis in mice, as hind limb unloading prevented enthesitis in generally highly susceptible TNF-transgenic mice. Since tissue-resident γδ T cells within the skin or intestines are

known to rapidly respond to either cytokine stimulation or stromal and epithelial cell stress-induced molecules, one could speculate that entheseal microdamage could activate enthesis-resident γδ T cells and trigger production of proinflammatory cytokines such as IL-17A. Whether genetic factors including HLA−B27 or polymorphisms in the IL-23R decrease the threshold for microdamage-induced γδ T cell activation, or just alter activated γδ T cells responses remain an important open question. Furthermore, I have shown in this Chapter that certain epithelial tissues of the anterior uvea are primed to respond to IL-17A. regions of the trabecular meshwork and iris anterior boarder layer all showed positive staining for IL-17 receptor A (IL-17RA). This suggests a greater involvement of IL-17A, downstream of IL-23, in the pathology of IL-23 induced ocular inflammation.

In summary the anterior compartment of the eye can be considered a functional IL-23–responsive anatomic site that, like the axial skeleton, skin, aortic root and lung. Although populations of αβ and γδ T cells found in the anterior compartment of the mouse eye were both capable of producing IL-17A, γδ T cells represented the larger sub-population and matched the phenotype of other IL-23 responsive γδ T cells found in entheseal tissue of the axial skeleton. It appears likely that the accumulation of IL-23R γδ T cells in some of the precise anatomical regions (eye and axial skeleton) where inflammation is observed in SpA represents a common IL-23−driven mechanism of pathology. Furthermore, the regions of the anterior chamber of the eye where γδ T cells were phenotyped in both mice and humans (iris, ciliary body, trabecular meshwork and limbal sclera) contain multiple muscle attachment sites and are subjected to considerable mechanical stress making these tissues similar in structure and function in to entheseal tissues of the axial skeleton.

Chapter 5

Final Discussion, concluding remarks, and proposed future studies

In this thesis I set out to address the following three research questions: (a) Is IL-23 overexpression sufficient to drive T cell mediated uveitis? (b) What is the phenotype and localisation of T cells in the anterior compartment of the eye? and (c) Is the same IL-23–dependent γ/δ resident T cell population found in the axial skeleton in mice is present in the anterior compartment of the eye in both mice and humans? In this final chapter I will discuss my findings and comment on any limitations I encountered as well as potential future work which I plan to conduct.

Previous animal studies have shown IL-23 to be sufficient to drive the pathophysiology of diseases associated with SpA in multiple tissues, including the skin (Chan et al. 2006), the gut (Lee et al. 2004; Yen et al. 2006; Ciccia et al. 2009; Ahern et al. 2010; Buonocore et al. 2010), the musculoskeletal enthuses, and the heart (Sherlock et al. 2012; Reinhardt et al. 2016). To my knowledge this is the first study that has specifically shown that IL-23 overexpression is sufficient to drive the pathophysiology of anterior uveitis in the mouse eye. More specifically, I have shown that localised IL-23 overexpression within the posterior compartment of the eye of C57BL/6 mice is sufficient to drive T cell mediated pan-uveitis. This observation was reached by utilising viral gene transfer of IL-23 with an ShH10 capsid, previously shown to generate widespread transduction of both the posterior compartment (Muller cells) and anterior compartment (ciliary body epithelial cells) of the eye in a single intravitreal injection (Klimczak et al. 2009; Wu et al. 2020), and validated in this study by funduscopy and through measuring IL-23 protein titres within the supernatant of homogenised ocular tissue. Pan uveitis was determined by fundal imaging of the posterior compartment, OCT scans of both the anterior and posterior compartments, and through flow cytometric analysis of cells within the posterior compartment (retinal homogenates) and anterior compartment (trabecular meshwork, iris, ciliary body,

choroid, limbal sclera). Unfortunately, due to time limitations, I was unable to repeat these experiments and utilise the tissue for histological examination. In future experiments I plan to score disease after IL-23 overexpression at different time points using H&E stained tissue and CD68 DAB staining (macrophage staining).

I am also confident that IL-23 overexpression specifically and not just AAV is responsible for driving pan uveitis. AAV generally elicits minimal immune responses in non-inflamed eyes compared to vectors such as adenovirus and most do not efficiently transduce antigen presenting cells, making them potentially ideal for gene transfer in the eye (Nayak and Herzog 2010). However, intravitreal administration has been shown to result in systemic capsid-directed immune responses in animal models (Chu, 2014), and trigger an immune response through Toll-like receptor 9 (TLR9), a receptor that senses foreign DNA, in both mice and humans (Chan et al. 2021). In this study, I looked at the effect of AAV with a null transgene (GFP) on C57BL/6 mice, and although I did not find any clinical signs of uveitis by fundal imaging, I did observe a low level of subclinical inflammation in both the posterior and anterior compartments of the eye by flow cytometry. Nonetheless this low level of subclinical inflammation was found to be significantly less than the subclinical inflammation induced by IL-23 overexpression.

This study is not the first to utilise gene transfer to study the overexpression of target genes coding for pro-inflammatory cytokines within the eye (Da Cunha et al. 2018). I have now added IL-23 to the list of cytokines (IL-1β and TNFα) that are sufficient to drive uveitis in the absence of any other factors. Interestingly IL-23 is upstream of IL-1β and TNFα. IL-23 promotes the expansion of cells that directly express IL-17A and TNFα, whilst engagement of IL-17A on IL-17R expressing cells (including stroma, epithelial and endothelial cells, and a population of myeloid cells (Kolls and Lindén

2004)) promotes the expression of IL-1β and TNFα (Langrish et al. 2005; McGeachy, Cua, and Gaffen 2019; McKenzie, Kastelein, and Cua 2006). Together, the purpose of these pro-inflammatory cytokines is to rapidly recruit neutrophils to the site of infection.

The conclusion that IL-23 overexpression is sufficient to drive, specifically, T cell mediated pan-uveitis, was reached by using Rag2 KO mice. Here I document that Rag2 KO mice were protected against IL-23 induced pan-uveitis. This conclusion was reached as Rag2 KO mice don't have T or B cells (Mombaerts et al. 1992), of which only T cells have been shown to express IL-23R functionality (Parham et al. 2002; Aggarwal et al. 2003; Murphy et al. 2003; Awasthi et al. 2009; McGeachy et al. 2009; Ghoreschi et al. 2010; Sherlock et al. 2012; Reinhardt et al. 2016). In addition, clinical signs of IL-23 mediated inflammation were observed as early as 3 days in C57BL/6 which suggests the presence of a resident T cell, as 3 days is too soon for an adaptive immune response to have occurred.

Prior to this study, information regarding T cells in the anterior compartment of the eye was limited. Immunohistochemical staining of wholemount normal rat uveal tissue using antibodies against the CD5 antigen (only expressed on T cells in rat) revealed the density of T cells to be around 16 ±6 cells/mm^2 in the iris and 16 ±7 cells/mm^2 in the choroid (Butler and McMenamin 1996). A small T cell cluster has been described proximal to the limbal sclera in the normal mouse eye and the accumulation of γδ T cells has been observed in this region after the systemic overexpression of IL-23 (Reinhardt et al, 2016). CD4+ T cells have also been imaged by fluorescent microscopy trafficking through the vessels of the choroid in the posterior compartment of normal mice (McMenamin, Saban, and Dando 2019). In addition, γδ T cells have been reported inside the vessels of the choroid in the posterior compartment in healthy

human donor eyes (Zhao et al. 2017). However, no reports have documented the presence of T cells within the extravascular tissue of the anterior uvea in control mice, which has previously been referred to as ‘devoid’ of T cells (Forrester and Xu 2012). This view is supported by the early imaging study of McMenamin (1997). Furthermore, no study has yet proposed how a resident IL-23 responsive T cell could escape the mechanisms maintaining ocular immune privilege within the eye.

I was able to show, for the first time, that T cells are present in the anterior chamber of the perfused normal mouse eye suggesting that these cells are resident, not only in the specific tissues of the anterior uvea (iris and ciliary body), but also in regions of the limbal sclera and the trabecular meshwork. Although, cross sections of the mouse anterior uvea revealed only low numbers of T cells by confocal imaging, using high depth Lightsheet imaging of cleared whole mount stained tissue, I was able to observe that the majority (~95%) of the T cells were localised in the sclera and the ciliary body. This strengthens the hypothesis that a resident population of differentiated T cells is present in the normal mouse eye; capable of recognising local IL-23 (T_H17), and rapidly inducing an immune response (as described in Chapter 2). T cells were also observed outside of vascular structures in the iris, ciliary body, TM, and limbal sclera of the normal human eye. Furthermore, I was able to phenotype T cells in the normal human eye as being a mixture of CD4+, CD8+, CD4-CD8-, αβTCR+, and γδTCR+ cells. However, due to time limitations I was unable to phenotype which of these subtypes of T cells existed outside of the blood vasculature in the normal human eye. I have described in detail in Chapter 3 how I have improved on the methodologies of past studies that were unable to identify the presence of T cells in these tissues.

I have also provided evidence by IF and flow cytometry that IL-23R+CD3+CD4-CD8-γδTCR+ T cells are resident in the anterior compartment of the naïve C57BL/6 mice

eye. This population of T cells shares the same phenotype as entheseal resident T cells (IL-23R+CD3+CD4-CD8-) previously documented as being present within the axial skeleton and aortic root of mice (Sherlock et al. 2012; Reinhardt et al. 2016). In addition, both the IL-17 producing γδ T cells in this study and those shown in Reinhardt et al. (2016) had a pre-activated effector phenotype ($CD44^{high}CD27-$). Although I did not have time to show this in my study, Reinhardt et al. (2016) also revealed that the majority of tissue resident γδ T cells in the muskculoskeletal entheses were Vγ6+ and Vγ4+ .This population of γδ T cells matches the previously described innate-like Tγδ17 cells (Narayan et al. 2012; In et al. 2017; Sumaria et al. 2017; Zuberbuehler et al. 2019).

Although IL-17A production is not restricted to a specific Vγ subset, innate-like Tγδ17 cell generation is limited to a period of ontogeny during fetal life, approximately E16 to birth, that enriches for Vγ6+ and Vγ4+ γδ T cell subsets (Haas et al. 2012). Innate-like γδ T cells leave the thymus and are able to carry out their effector functions early during ontogeny, consequently they do not require clonal expansion or differentiation from a naïve cell for their effector responses (Chien, Zeng, and Prinz 2013; Muñoz-Ruiz et al. 2017). Importantly, innate-like γδ T cells have the four key characteristics of tissue-resident lymphocytes; (A) self-renewal and long-term maintenance, (B) abundance at barrier tissues, (C) sensing of microbial products, cytokines, alarmins, and stress ligands, and (D) rapid effector responses (Fan and Rudensky 2016). These hallmark properties combined with early seeding during fetal life enable innate-like γδ T cells to act as a first line of defense in the skin, gut, and reproductive tract while other lymphocytes are still being developed.

In a future study I would like to assess if the IL-23R+CD3+CD4-CD8- γδTCR+ T cells are resident in the anterior compartment of the naïve C57BL/6 mice eye are the same

Vγ6+ and Vγ4+ γδ T cell subsets found in the axial skeleton and aortic root. Evidence of the same subpopulation of Tγδ17 cells in multiple entheseal tissues involved in disease associated with SpA (the anterior compartment of the eye, the axial skeleton, and the aortic root) suggest that this cell could be the critical component that links all of these sterile sites to other barrier tissues (skin and gut) associated with SpA and critically to IL-23.

Nonetheless, IL-23R+CD3+CD4-CD8- γδTCR+ T cells were not the only subtype of T cells found in the extravascular tissues of the anterior compartment of the eye. This in itself is a novel discovery. The question then arises of how T cells are able to escape the mechanisms of immune privilege within the eye and remain resident. The eye has been considered immunologically different ever since the first successful human corneal transplant was performed in 1905 and was not rejected. In contrast, the first successful kidney transplant did not occur until 49 years later (Merril et al. 1956). Ocular immune privilege was not officially recognised until 1948 when Peter Medawar demonstrated that skin allografts placed in the anterior chamber of the eye or the brain are not rejected, in contrast to other tissues such as the skin (Medawar 1948). This occurred even when the recipients were systemically immunised against the alloantigen. However, tolerance of grafts was lost if there was any vascular leakage into the anterior chamber, signifying the importance in maintaining the blood ocular barrier.

For a long time, it was assumed that, with the exception of the limbus, there were no lymphatics in the eye. To date this remains true for most ocular tissues, including the cornea, lens, iris, retina, choroid and sclera which are heterogeneously void of lymphatic vessels (reviewed in Chen 2016). The alymphatic mechanism of the cornea, the tissue most subjected to lymphatic investigation in the eye, was only uncovered in

the last 10 years by Albuquerque and colleagues (2009). They showed that a soluble VEGFR-2 form is secreted by corneal epithelial cells that selectively suppress the physiologic growth of lymphatic vessels. In addition, this was the first identification of a specific lymphangiogenesis inhibitor. In contrast, extraocular tissues, such as the eyelids, lacrimal glands, conjunctiva, optic nerve sheath, extraocular muscles, and connective tissues of the extraocular muscle are rich in lymphatics. The conjunctiva is the most lymphatic-developed tissue in the eye.

A renewed search using lymphatic endothelium markers combined with intracamerally injected tracer studies led to the discovery of lymphatic vessels in the ciliary body of the sheep and human eye (Yücel et al. 2009; Kim et al. 2011). The lymphatic endothelium markers used were the D2-40 antibody for podoplanin and LYVE-1 antibody. These were detected in meridional sections of steady state ciliary body by Immunofluorescence confocal microscopy. Lymphatic vessels in the conjunctiva were used as positive control. In addition, D2-40 and LYVE-1-positive lymphatic channels in the ciliary body had a distinct lumen, were negative for the blood vessel endothelial cell marker CD34, and were surrounded by either discontinuous or no collagen type IV-positive basement membrane. Further studies of ocular lymphatic drainage involving mouse models, pursued due to having similar aqueous dynamics (Aihara et al. 2003; Millar et al. 2015) and pharmacology to humans (Crowston et al. 2004; Boussommier-Calleja et al. 2012), have revealed that tracer injected into the anterior chamber drains to ipsilateral submandibular (Tam et al. 2011; Tam et al. 2013) and cervical lymph nodes (Yucel et al. 2018) in a manner independent to that of conventional aqueous fluid outflow. This alternate route for aqueous fluid outflow has been termed the uveolymphatic pathway.

Evidence supporting the existence of lymphatics in the normal ciliary body and uveolymphatic pathway remains controversial (Schroedl et al. 2014). Although vessels in the ciliary body were found, they were only detected by one group (Yücel et al. 2009) and not detected by others under normal physiological conditions (Birke et al. 2010; Kaser-Eichberger et al. 2015). In addition, there were limitations of the tracer studies used to validate the uveolymphatic pathway, as they did not take into account tracer that may have left the anterior chamber via the uveoscleral route (Bill 1966) towards the conjunctiva where lymphatic vessels are plentiful (Lohrberg and Wilting 2016). Tracer studies are also limited by the assumption that no tracer is retained or trapped in the tissue, due to variables such as size of tracer molecules used (Pederson and Toris 1987), and that all tracer enters tissue by flow of aqueous humor rather than diffusion. Furthermore, when reviewing these studies, I was only able to see evidence of D2-40 and LYVE-1-positive lymphatic channels in the outer *pars plicata* most proximal to the longitudinal ciliary muscles. Maruyama and colleagues (2005) showed the novel finding that LYVE1+ macrophages alone were capable of forming tube-like structures that expressed markers of lymphatic endothelium such as LYVE-1 and podoplanin. These structures originate in the prepupillary corneal stroma and proceed to link up with the existing lymphatics at the limbus. The iris (Birke et al. 2010), choroid (Schroedl et al. 2008), sclera (Trost et al. 2018). and optic nerve sheath (Trost et al. 2018) also lack LYVE-1+ lymphatics, but presented with a high number of single cells co-stained for CD68 and LYVE-1. It may be very likely that certain tissues of the eye utilise these cells to maintain a lymphatic free, immune privileged, environment in the steady state, whilst maintaining the capacity to rapidly induce lymphatics through transdifferentiation when necessary.

Interestingly, aqueous humor outflow tissues have similar characteristics to that of lymphatic vessels and may play a role in fulfilling surrogate lymphatic functions. Endothelial cells of Schlemm's canal do not express lymphatic associated biomarkers such as VEGFR-3 or LYVE-1, however, they do show responsiveness to VEGF-C–induced lymphangiogenesis (Aspelund et al. 2014; Truong et al. 2014), and the outer wall endothelium express high levels of PDPN. PDPN is also expressed by trabecular cells throughout all layers of the trabecular meshwork, the trabeculum ciliare, and cells of anterior ciliary muscle tips, despite the lack of other lymphatic markers (Birke et al. 2010). In contrast to immunofluorescence staining results where Prox-1 could not be detected, amplificates of the Prox-1 mRNA were obtained, indicating low-level expression of this factor at least on the transcriptional level (Birke et al. 2010). Extensions of the anterior border layer are continuous with the trabecular beams of the trabecular meshwork and so this tissue can also be described as part of the aqueous outflow pathway. Intense PDPN expression was also observed on all cells at the iris anterior surface (Birke et al. 2010). In addition, PDPN+ dendriform cells were detected throughout the entire stroma, displaying a diffuse but homogeneous distribution. LYVE-1 dendriform cells were observed throughout the entire iris stroma but they appeared to be more concentrated close to vessels or even within the vessels. Double staining for Pdpn and Lyve-1 revealed that only a small number of the dendriform cells within the stroma, but also at the anterior surface, expressed both markers. In contrast, Schrödl et al. (2008) found that LYVE-1 and PDPN were absent in the vessel walls of the human choroid, although the same antibody labelled them in choroidal macrophages.

The presence of T cells within the highly vascular iris and ciliary body, could be explained by the fact that both of these tissues sequester the movement of infiltrating

cells from the posterior chamber due to their inner dual epithelial layers which form the continuous wall known as the blood-aqueous barrier. This barrier regulates exchanges between the blood and the intraocular fluids (Lugossy 1959; Shiose 1970; Smith 1971; Raviola 1974). Because of its location the absence of T cells in the posterior compartment was expected, but the presence of extravascular T cells in the iris and ciliary body was surprising. One explanation for this observation could be that the T cells may have remained there after the resolution of an adaptive immune response initiated by local APCs (McMenamin 1997;1999;2000). Indeed, such resident memory T-cells (TRM) have previously been found at other epithelial barrier sites in grafts from ganglia, skin, and intestine (Gebhardt et al. 2009; Masopust et al. 2010; Jiang et al. 2012; Schenkel et al. 2013), at the initial site of infections, and found to provide very regional immune surveillance and protection against re-infection (Wakim et al. 2008; Masopust et al. 2010; Masopust et al. 2013; Zaid et al. 2014). Indeed, some of the T cells I found in the mouse eye share characteristics with these TEM cells found at other sites, expressing CD44 and low levels of CD62L (as shown in chapter 4).

Furthermore, to explain the presence of these TMR cells in the eye, we must also discuss the deviated mechanisms of regulating immune responses within the eye. The eye has a unique mechanism of suppressing the delayed-type hypersensitivity (DHT) response, mediated by effector T cells responding to the same antigen (Taylor 2016). This is known as anterior chamber associated immune deviation (ACAID). It is mediated by the efferent dissemination (via the blood vessels) of antigen specific tolerogenic CD8 T cells (Willbanks and Streilein 1990; Faunce and Stein-Streilein 2002; Jiang et al. 2009; Paunicka et al. 2012; Hsu et al. 2014). However, little is known of the fate of these CD8 T cells after resolution. In my study using flow cytometry I was able to show for the first time, that the ratio of CD8 to TH cells in digests of the human

anterior uvea is increased compared to peripheral blood. These CD8 T cells could in fact be efferent CD8 T cells left as memory cells after ACAID.

To address the T cells, I found within the trabecular meshwork at the entrance to Schlemm's canal in more detail, we must look at how immune cells are able to exit the eye during an immune response. It is well known that the aqueous outflow channels are the main migration route for ocular antigen-bearing cells wishing to traffic directly to the spleen via the blood vasculature (Wilbanks et al. 1991; Wilbanks and Streilein 1991; Hara et al. 1992; Wilbanks et al. 1992; Wilbanks and Streilein 1992). If T cells are resident or remain in the eye, outside of an immune response, the mechanical contractions of the anterior uvea may push these cells towards the anterior chamber (as entry is denied to the posterior chamber by the blood aqueous barrier) and enter the aqueous of the anterior chamber freely through the anterior border layer and irideocorneal angle (which has no blood aqueous barrier). Caught in the current generated by the pressure of new aqueous produced in the posterior chamber, T cells would be directed towards, and filter through the PDPN + epithelial cells of the trabecular meshwork where they would then exit the eye through Schlemm's canal. It is those PDPN+ epithelial cells that could also generate a chemokine gradient directing T cells towards this area.

The biological roles of PDPN are still poorly understood (reviewed in Ugorski et al. 2016). Of note is the interaction of PDPN with CCL19 and the constitutively expressed chemokine CCL21 (Kerjaschki 2006), which in non-lymphoid organs are expressed on the initial segments of lymphatic vessels and both bind to PDPN with high affinity. This interaction facilitates the recruitment of lymphocytes expressing the chemokine receptor CCR7 (Gunn et al. 1998; Yoshida et al. 1998; Stein et al. 2000) including: naïve B cells (Reif et al. 2002), semi-mature and mature DCs (Ohl et al. 2004), and by

several T-cell sub-populations including regulatory (Szanya et al. 2002), naïve, and central memory T cells (Sallusto et al. 1999).

Even though I did not show that CCL19 and CCL21 expression is colocalised with PDPN expression on cells of the anterior compartment in my study (due to time limitations), a previous study by Kodati et al. (2014) described this colocalisation on epithelial trabecular cells (throughout all layers of the trabecular meshwork), the trabeculum ciliare, cells of anterior ciliary muscle tips, and iris stroma - with the highest concentration found in the anterior border layer.

To show that this chemokine gradient is active within the eye it would also be expected that some cells in the eye would be expressing CCR7. Indeed, CCR7 expression was also demonstrated on single cells within the anterior compartment (Birke et al. 2010). Furthermore, in a study by (Kodati et al. 2014) it was shown that this chemokine gradient is operational during an immune response of the eye, as CCR7 regulated homing by Th17 cells was necessary for the pathogenesis of dry eye disease.

Specifically, I found T cells on the cribriform layer of the trabecular meshwork. This final layer would provide the highest level of resistance for cells within the aqueous fluid, before exiting the anterior chamber via Schlemm’s canal. It is not surprising that I found T cells in this layer by histological examination, as T cells are able to pass through the other two layers of the trabecular meshwork much faster and spend the most time in the cribriform meshwork before exiting. Alternatively, T cells may be intentionally/tactically retained on the trabeculae strands to perform surveillance of elements in the aqueous being filtered through the trabecular meshwork and exiting through Schlemm’s canal.

The T cells I found in the stromal layer of the limbal sclera may be present due to the non-canonical aqueous outflow pathway. The non-canonical flow of aqueous humour involves its diffusion, first through the ciliary body into the supraciliary space (Inomata et al. 1972; Alm et al. 1973; Bill 1975; Tripathy 1977; Lindsey and Weinreb 2002), where it can exit through the vortex veins of the choroid (Bárány 1967; Pederson et al. 1977; Sherman et al. 1978), or alternatively through the stromal sclera, where it can exit through veins in the episclera (Bill 1966a; Bill and Phillips 1971; Bill 1975; Barrie et al. 1985; Suguro et al. 1985; Gabelt and Kaufman 1989). T cells in the aqueous humour of the anterior chamber, or those that I found in the extravascular tissue of the ciliary body, could potentially disseminate in the direction of this flow. The dense composition of collagen fibres in the stromal sclera would offer the highest level of resistance to the flow of T cells travelling along the non-canonical pathway. This would explain why I found an accumulation of T cells in this tissue. This theory is strengthened by the observation I made showing that these T cells are morphologically different to other T cells in the eye with cell membranes of elongated (or “squashed”) appearance. Again, this could represent an immunological mechanism employed in the eye to perform immune surveillance of these tissues in co-ordination with local APCs.

In a future study I would like to assess if blockade of IL-23 signalling can significantly modify human anterior uveitis. To date, drug treatment of SpA has been based on blockade of tumour necrosis factor (TNF) or the use of nonsteroidal anti-inflammatory drugs (NSAIDs), leading to effective reduction in chronic inflammation and pain. Historically, treatment of uveitis has been effectively controlled by glucocorticoids (Leopold et al. 1951). However, the success of the VISUAL-I and VISUAL-II studies and approval of anti-TNFα has provided uveitis specialists with a powerful new tool to

control disease without the use of steroids (Jaffe et al. 2016; Nguyen et al. 2016). However, since some patients do not respond to either TNF blockers or NSAIDs, there is still a need for alternative therapies.

Modern day medicine has seen an explosion in the number of biologic therapies brought to market for the treatment of systemic inflammatory diseases. Only a handful of these new agents have been tested systematically in patients with uveitis (Mesquida et al. 2014; Suhler et al. 2014). The evidence-based medicine approach calls for an ordered process including identification of central mechanisms of disease followed by development and testing of targeted therapies. I believe that evidence shown in this thesis has identified IL-23 as having a critical role in the pathogenesis of anterior uveitis in mice. However, this approach has limitations because rodent eyes and immune systems are not identical to the human systems they model, and there can be layers of complexity in the roles of individual cytokines in immune health and disease.

The critical role for IL-23 that I have demonstrated in the initiation of murine anterior uveitis makes a compelling case for further investigation in the context of human ophthalmological disease and specifically for the utility of IL-23 as a therapeutic target which could potentially be validated in the context of carefully designed clinical trials. In advance of a potential future clinical studies, I have already established a methodology in this study that enables T cell subpopulations to be phenotyped by flow cytometry from small clinical waste samples, from consenting patients, arising during common ophthalmic surgeries including trabeculectomy and strabismus.

Targeting this pathway has already been shown to be effective patients with active psoriasis (Blauvelt et al. 2017; Papp et al. 2017; Reich 2017; and reviewed in Pithadia

et al. 2019), PsA – both synovial and entheseal disease (Mease et al. 2018), and Crohn's disease (Feagan et al. 2017), diseases all associated with SpA. This theory is further reinforced by promising results arising from clinical trials of IL-23p40 inhibition (ustekinumab) in small cohorts of uveitis patients. However, this inhibitor targets the shared subunit (p40) of both IL-23 and IL-12, meaning that IL-12 could be responsible for diving pathology just as much as IL-23 could be.

There is also speculation that specifically targeting IL-23 in established uveitis may not be effective - as, despite all the disease associations and the shared underlying genetics between AS and other diseases associated with SpA (including non-infectious anterior uveitis) (Van Praet et al. 2011; Jacques et al. 2012), the most recent study of an IL-23p19 inhibitior (risankizumab) in patients with active AS failed to meet the primary endpoint (Ankylosing Spondylitis Disease Activity Score with an improvement of 40% (ASDAS40) at week 12), with no improvements in clinical or MRI outcomes compared with placebo (Baeten et al. 2018), whereas secukinumab (the inhibitor targeting the IL-17 cytokine which is downstream of IL-23) was demonstrated to have efficacy in disease modification of AS (Baeten et al. 2015). This raises the question of the importance of IL-23 and the targeting of the IL-23 pathway in established disease. Future work that explores the use of IL-23 pathway inhibitors during established disease initiated by the ShH10 IL-23 AAV mouse model of uveitis will be essential in elucidating the role of IL-23 in established disease.

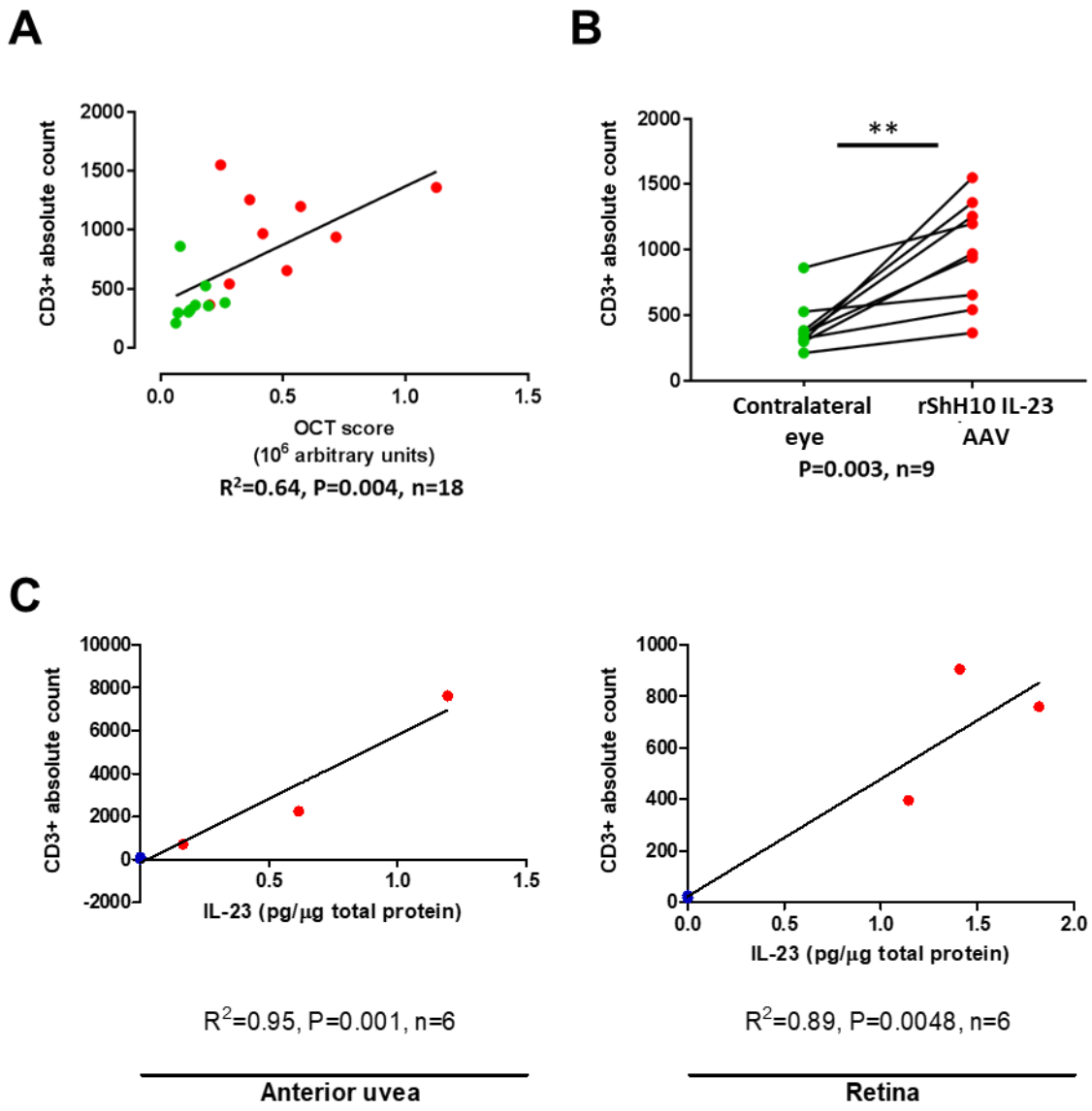
Appendicies

APPENDIX I SUPPLEMENTARY FIGURES

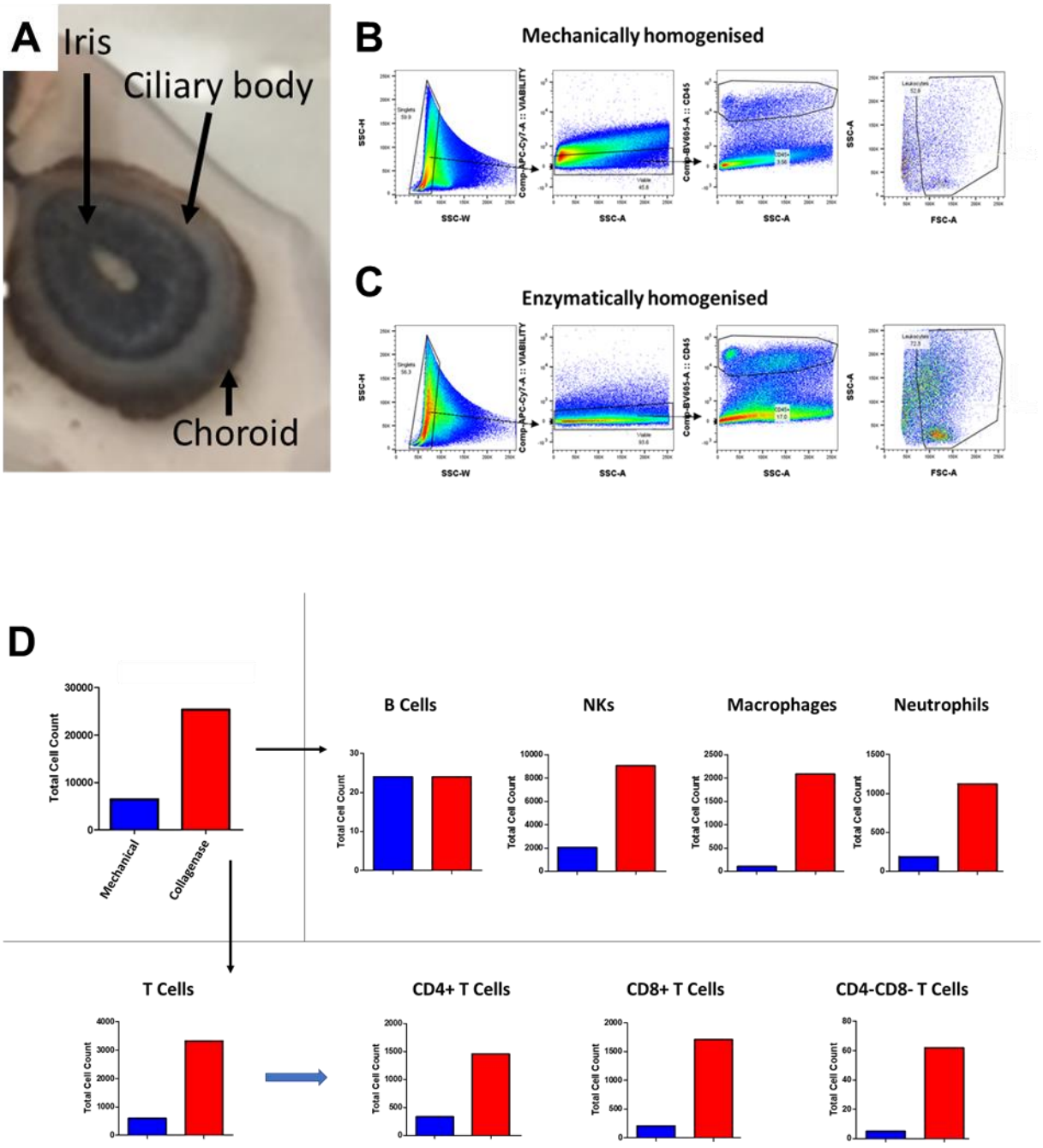
APPENDIX II PUBLICATIONS AND ABSTRACTS

Appendix I

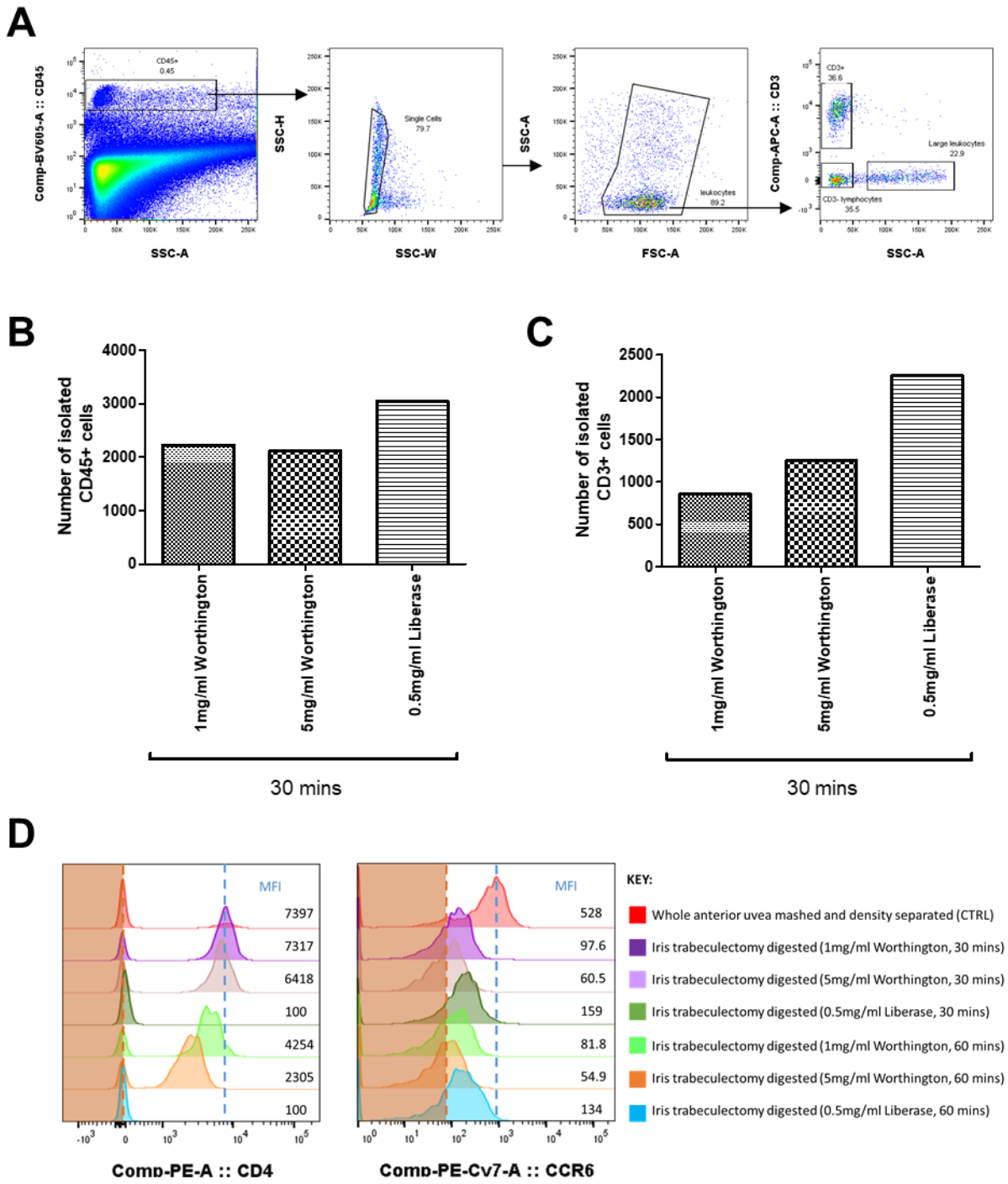
Supplementary Figures.



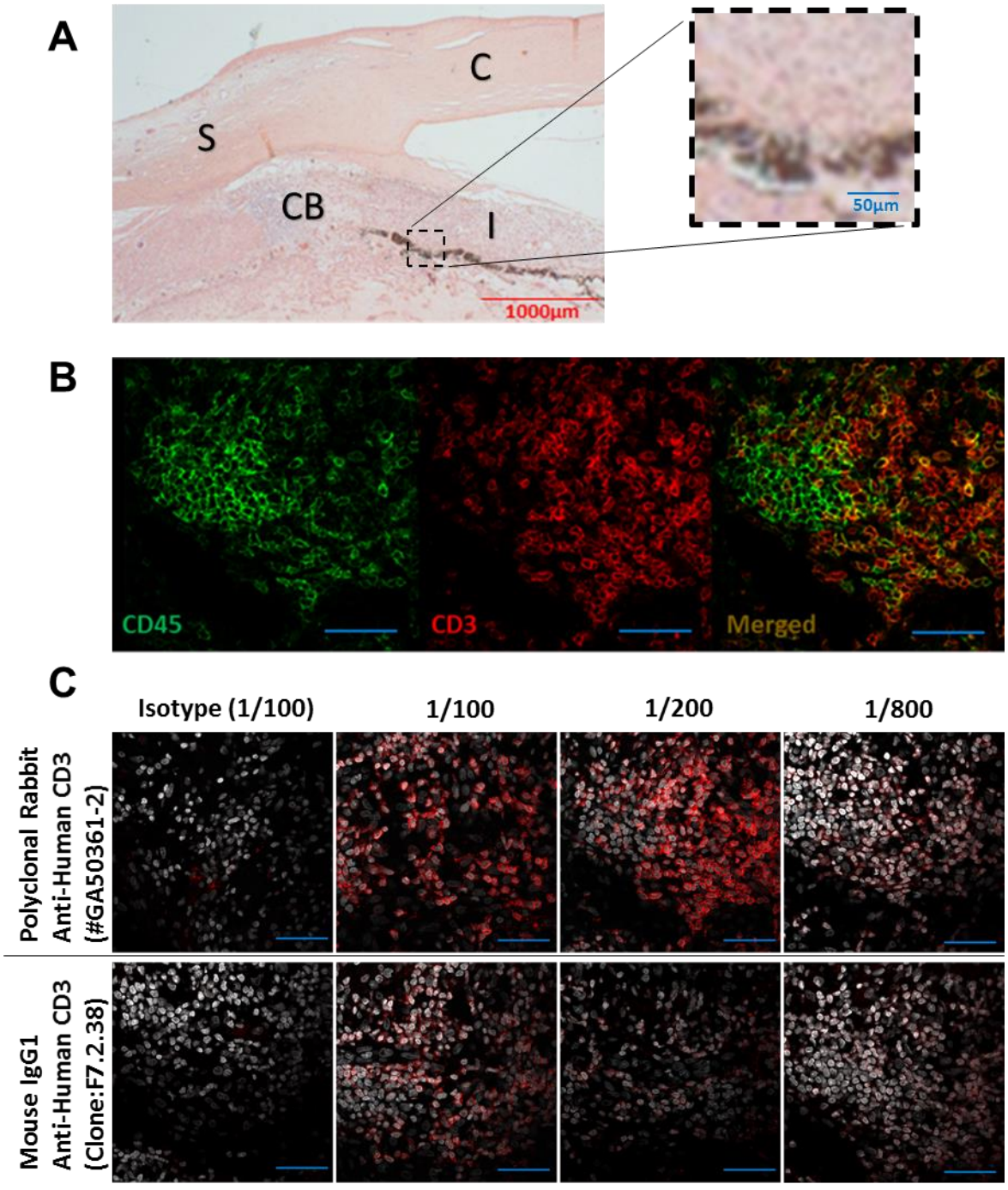
Supplementary figure 2.1: T cell infiltration correlates with clinical disease score and IL-23 titre in the eye injected with ShH10 IL-23 AAV. (A) Linear regression shows that CD3+ T cell infiltration into C57BL/6 after injection with rShH10 IL-23 AAV high titre ($2x10^{10}$ VP) correlates significantly with OCT disease score. (B) CD3+ T cell count is significantly higher in the eye injected with rShH10 IL-23 AAV, indicating that infiltration is restricted to the eye injected with rShH10 IL-23 AAV. (C) CD3+ T cell infiltration into the anterior uvea and retina significantly correlates with IL-23 titre in a dose dependent manner. FACS analysis was used to quantify absolute leukocyte counts and ELISA was used to quantify IL-23 cytokine titres from homogenisation supernatants.



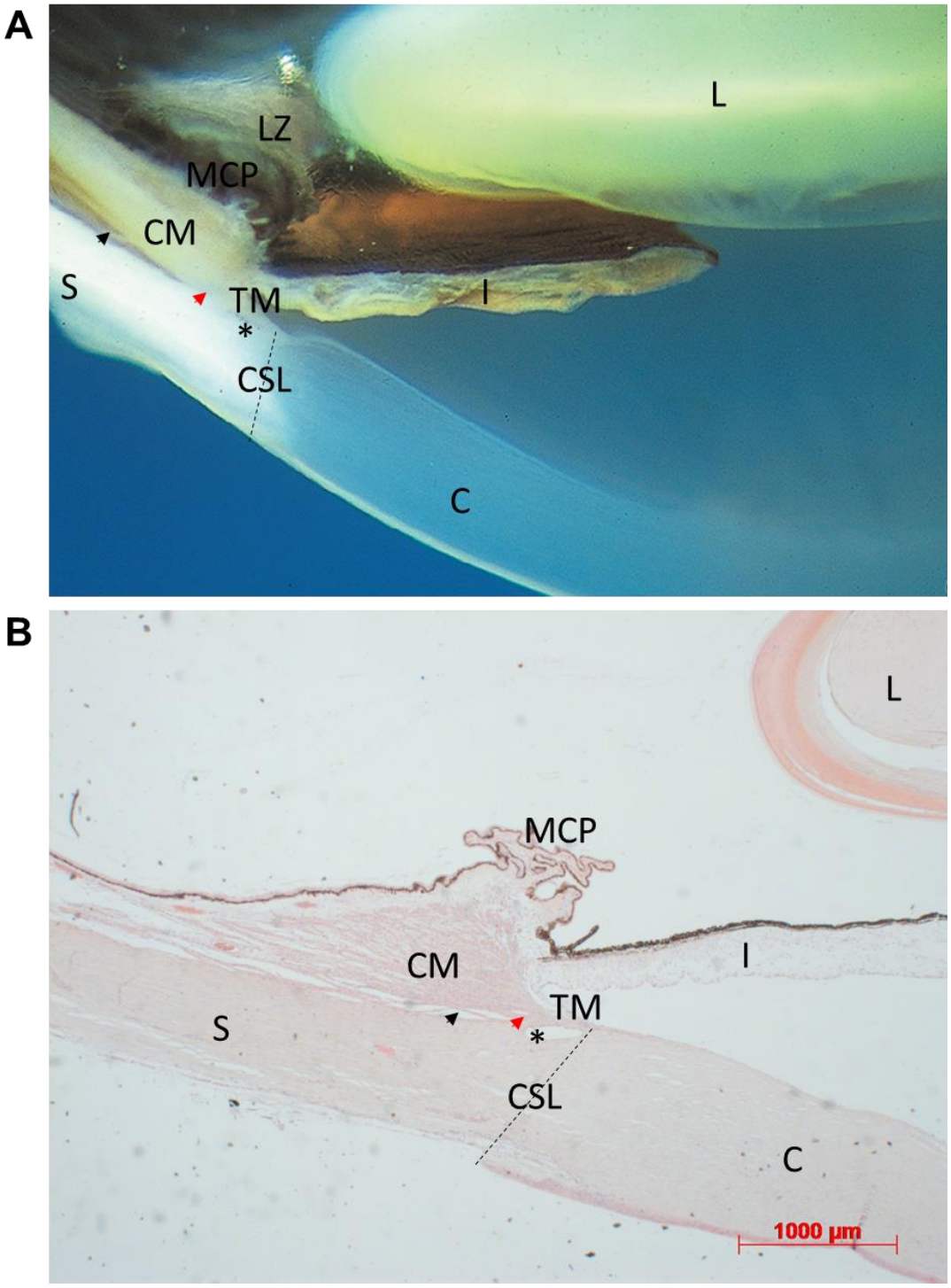
Supplementary Figure 3.1: Comparison of mechanical vs combined mechanical and enzymatic (5mg/mL Worthington Collagenase Type II, 1 hour) homogenisation for the extraction of different leukocyte populations. (A) Photographic image depicting the dissection of the anterior uvea from cadaver globes. Representative gating strategies show flow cytometric analysis for uveal Leukocytes in mechanically homogenised (B) vs combined mechanical and enzymatic homogenised (C) tissue. (D) Bar charts showing the total recovered amount of leukocyte sub populations from uveal tissue after mechanical or combined mechanical and enzymatic homogenisation.



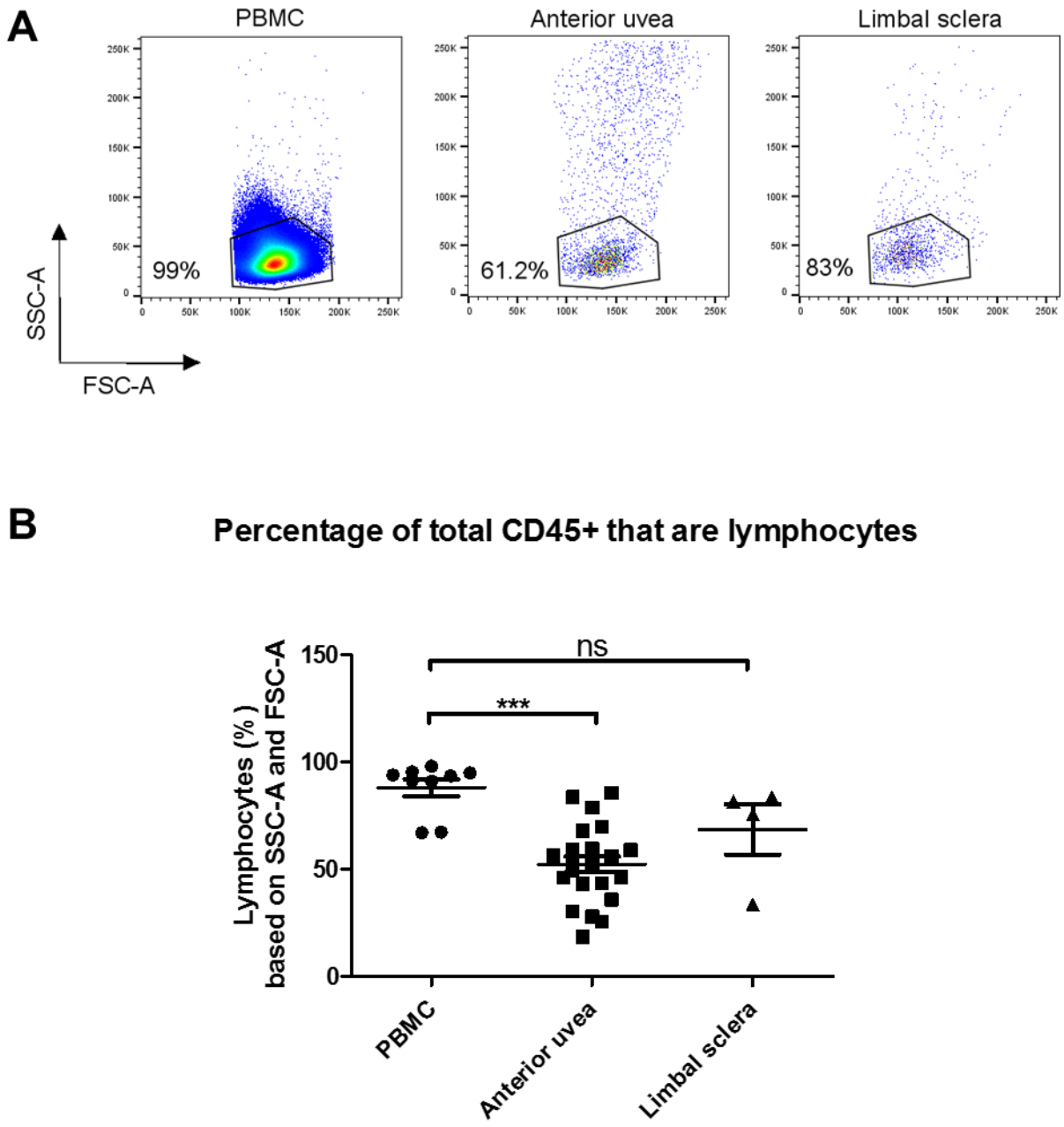
Supplemental Figure 3.2: Comparison of different collagenases, and concentrations of collagenase on cell yield and surface marker cleavage. (A) Representative gating strategy showing flow cytometric analysis for uveal Leukocytes isolated from mechanically homogenised tissue. This strategy was used to determine the number of (B) CD45+ Leukocytes (Based on FSC-A and SSC-A) and (C) CD3+T cells isolated from tissue after 30 minutes enzymatic digestion with either 1mg/mL or 5mg/mL Worthington Type II collagenase, or 0.4mg/mL Liberase. (D) MFI was measured to assess the amount of cleavage of cell surface markers (CD4 and CCR6) caused by different enzymes and concentrations.



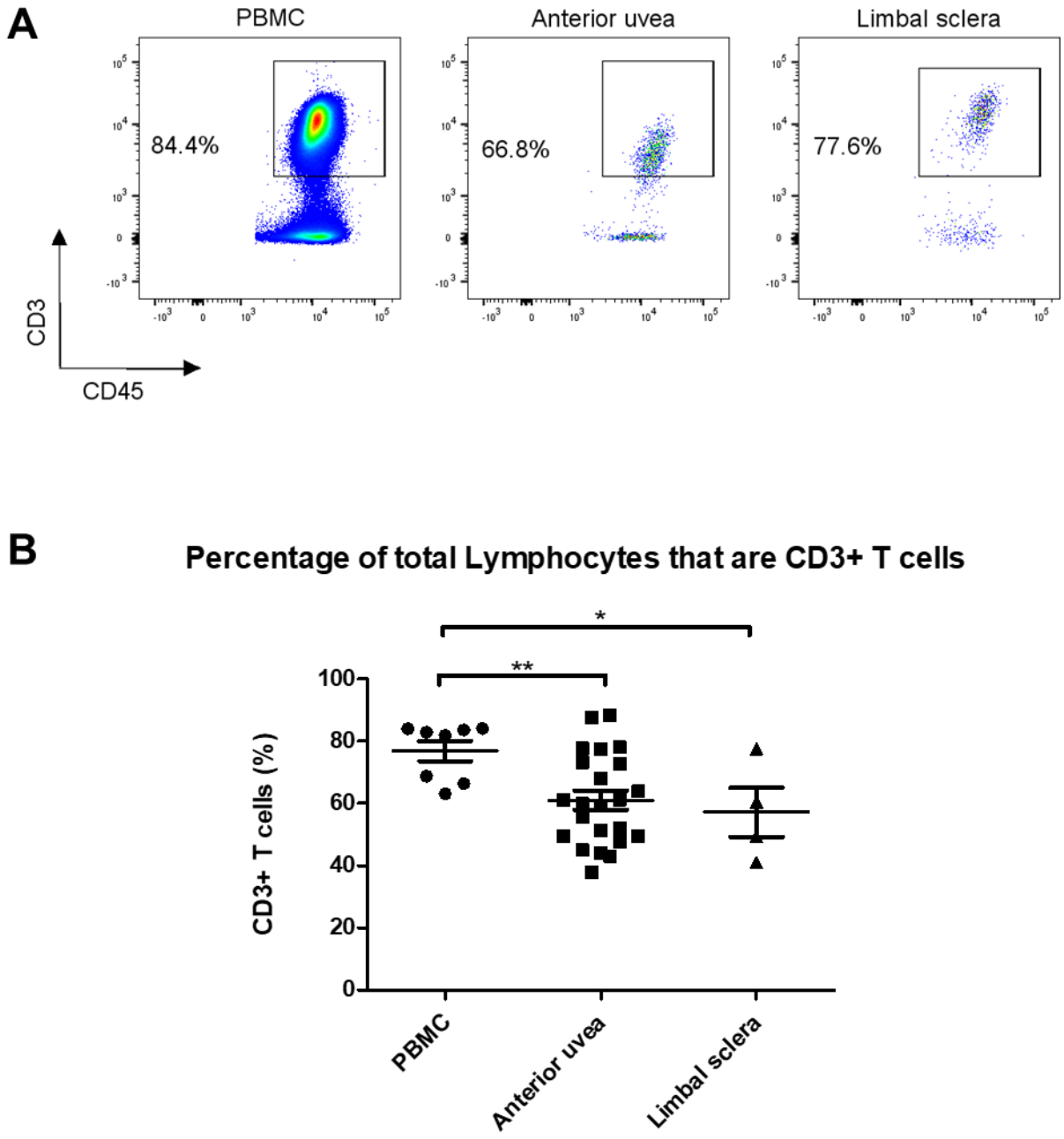
Supplementary Figure 3.3: Validation that the anti-CD3 clones used in this study bind specifically to T cells. (A) Low power light micrograph (2.5x objective) of an enucleated human eye with a history of uveitis – a positive control tissue for CD3+ T cells. Tissue surrounding the anterior cavity is stained with haematoxylin and eosin. The region of iris tissue used in B and C is outlined and magnified. (B) CD3 signal co-localises with CD45 (pan leukocyte antigen) signal. Immunofluorescent staining for CD45 (green) and rabbit poluclonal anti-human CD3 (red; DAKO; #GA50361-2). (C) CD3 clones but not isotype controls bind to the surface of cells with optimum fluorescence above 1/200 dilution. Immunofluorescent staining for nucleus (grey) and titrations of either mouse IgG1 anti-human CD3 (red; DAKO; Clone: F7.2.38), rabbit poluclonal anti-human CD3 (red; DAKO; #GA50361-2), or isotype control (red). C – cornea, S – sclera, CB – ciliary body, and I – iris. Blue scale bar indicates 50µm.



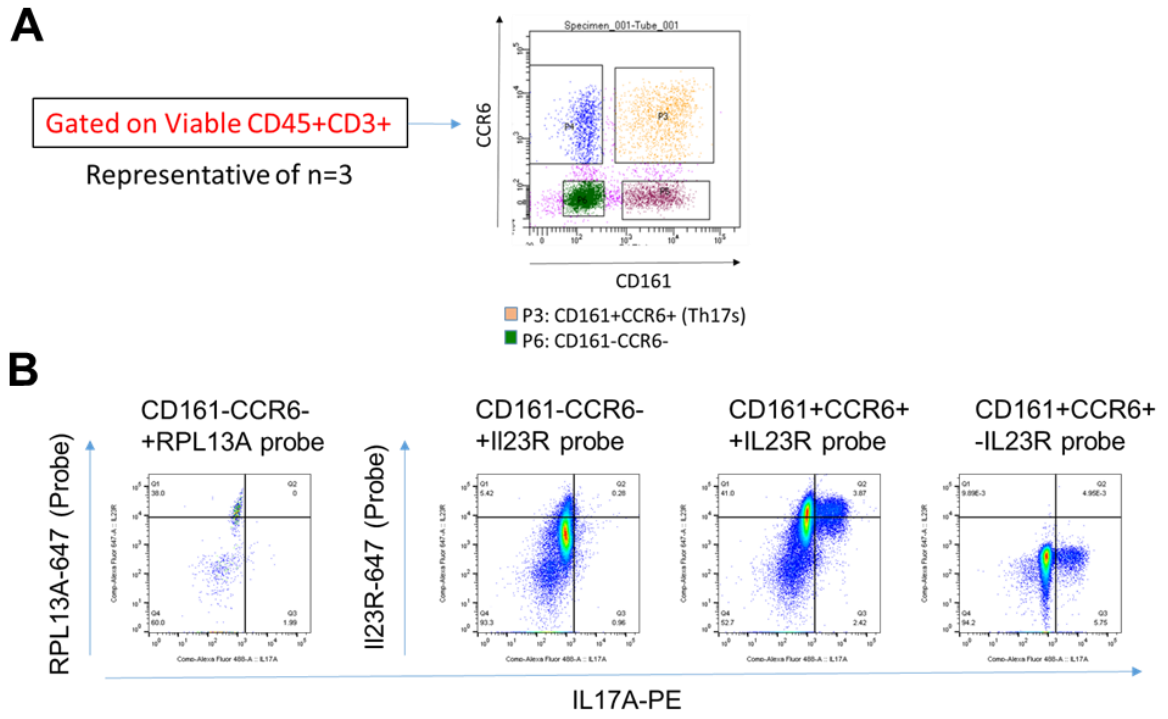
Supplementary Figure 3.4: The anterior segment of the human eye. (A) Macroscopic photograph of the anterior segment of the human eye. (B) Low power light micrograph (10x objective) of a meridional section of the anterior segment of an enucleated healthy human eye stained with haematoxylin and eosin. The corneoscleral coat (cornea and sclera seen as a continuous structure) and uveal tract (iris, ciliary body, and choroid seen as a continuous structure) are the outer and inner layers of the eye, joined anteriorly by the scleral spur (red arrow head) and posteriorly by the suprachoroidal lamina, generating the supraciliary space (black arrowhead). The canal of Schlemm (black asterisk) lies between the outer aspect of the trabecular meshwork and the corneoscleral coat. Note that the lens zonules projecting between the lens capsule and ciliary processes cannot be observed in the low power light micrograph (B). C – cornea, S – sclera, CSL – corneoscleral limbus, CM – ciliary muscle, MCP – major ciliary processes, TM – trabecular meshwork, and I – iris.



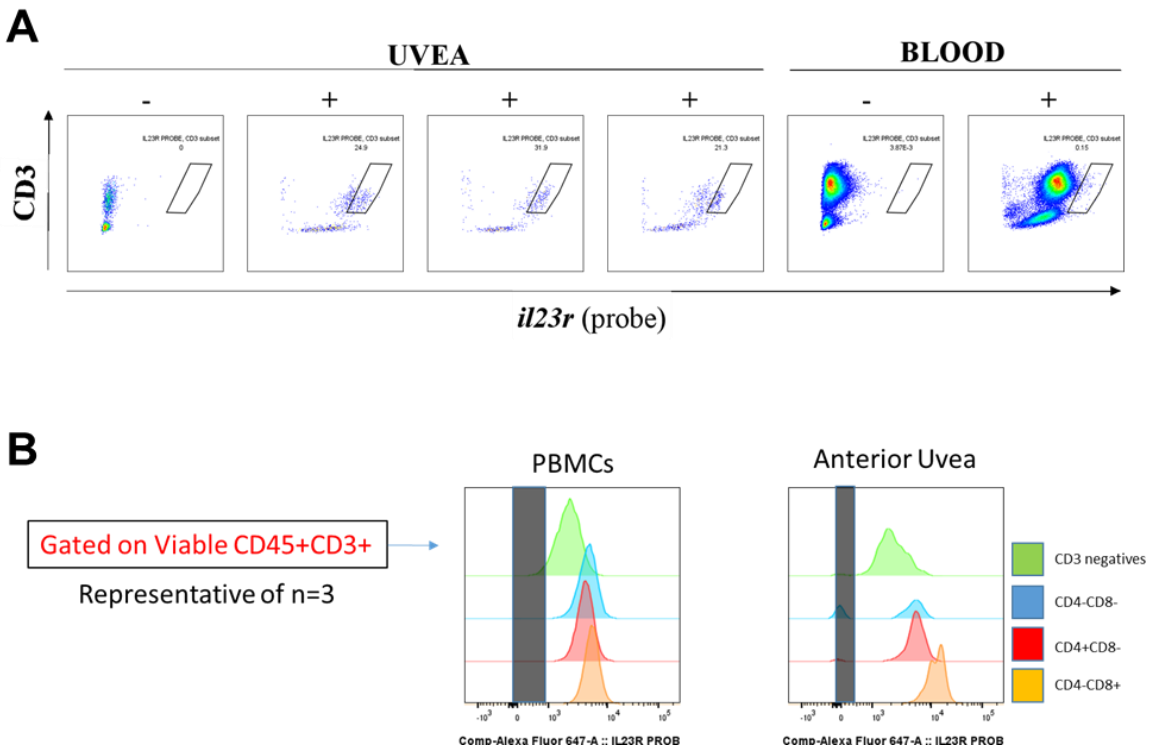
Supplementary Figure 3.5: Fluorescence activated cell sorting (FACS) analysis of healthy anterior uvea and limbal sclera shows a reduction in relative frequency of lymphocytes to that found in Peripheral blood mononuclear cells (PBMCs). (A) Representative plots show flow cytometric analysis for uveal and sclera CD45+ lymphocytes (based on SSC-A and FSC-A light scatter) in contrast to those isolated from peripheral blood mononuclear cells (PBMCs). (B) FACS compiled frequency data for the percentage of live CD45+ lymphocytes in healthy anterior uvea (n = 19; data obtained from 7 independent experiments), limbal sclera (n = 4; data obtained from 2 independent experiments), and control blood (n = 9; data obtained from 4 independent experiments). Mean percentage is represented by the central line with error bars showing SEM; ns = $P<0.05$ and *** = $P<0.001$ (unpaired Student's two-tailed t-test



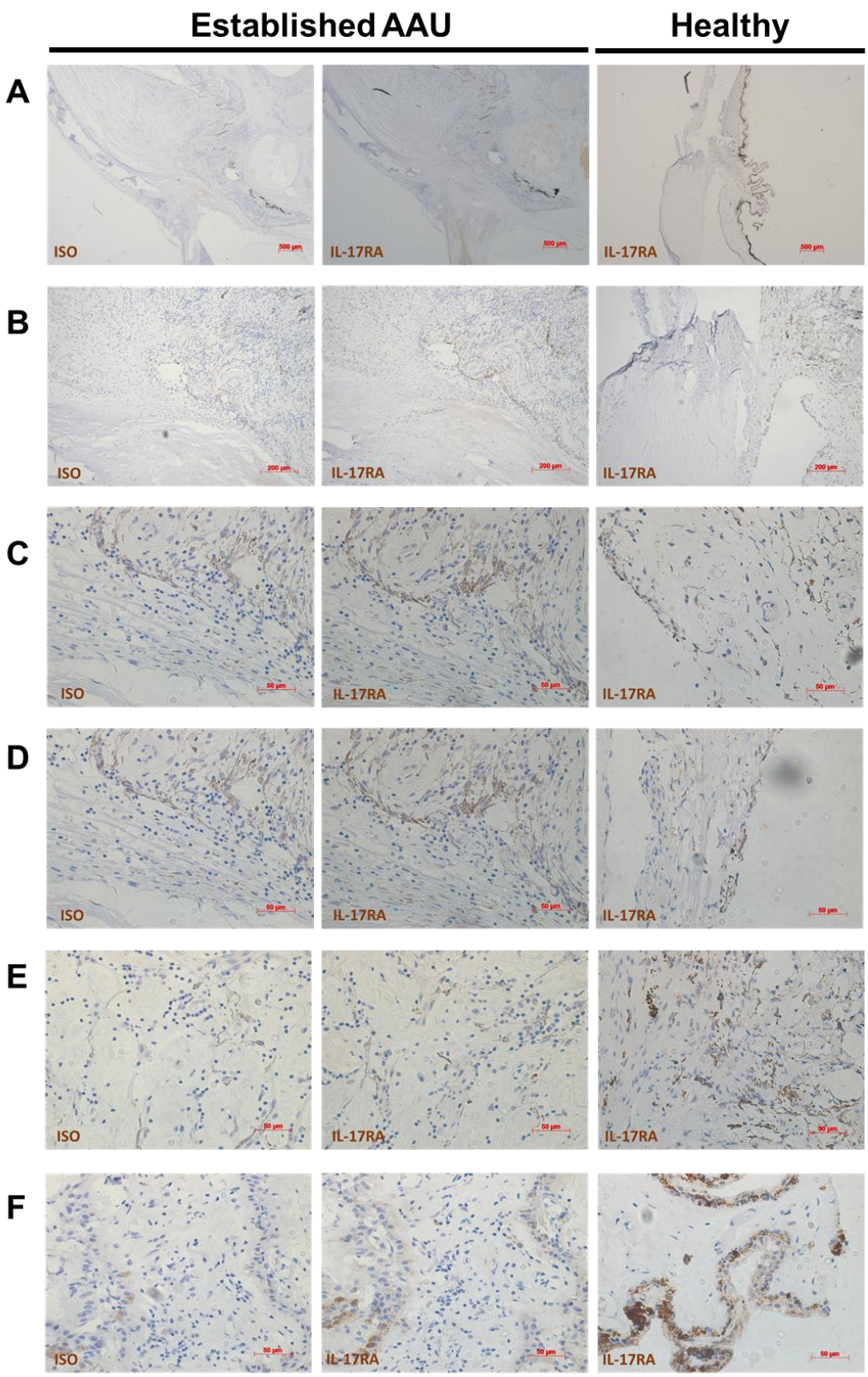
Supplementary Figure 3.6: Fluorescence activated cell sorting (FACS) analysis of healthy anterior uvea and limbal sclera shows a reduction in relative frequency of CD3+ T cells to that found in Peripheral blood mononuclear cells (PBMCs). (A) Representative plots show flow cytometric analysis for uveal and sclera $CD3^+$ T cells in contrast to those isolated from peripheral blood mononuclear cells (PBMCs). (B) FACS compiled frequency data for the percentage of live $CD3^+$ T cells in healthy anterior uvea (n = 19; data obtained from 7 independent experiments), limbal sclera (n = 4; data obtained from 2 independent experiments), and control blood (n = 9; data obtained from 4 independent experiments). Mean percentage is represented by the central line with error bars showing SEM, * = $P<0.05$ and ** = $P<0.01$ (unpaired Student's two-tailed t-test).



Supplementary Figure 4.1 PrimeFlow™ RNA Assay is able to distinguish between IL-23R positive and negative T cells. The PrimeFlow™ RNA Assay is an in situ hybridization assay that combines the power of branched-DNA technology with the single-cell resolution of flow cytometry, enabling the simultaneous detection of RNA targets in combination with immunophenotyping for cell surface and intracellular proteins using fluorochrome-conjugated antibodies. (A) T cells in human blood were sorted for the CD161+CCR6 (Th17) and CD161-CCR6- (non TH17) subpopulations. (B) After stimulation with PMA/ionomycin the control RPL13A mRNA targets could be found in both sub populations but only the IL-17A producing Th17 subpopulation was positive for IL-23R mRNA targets.



Supplementary Figure 4.2. A large population of T cells in the anterior uvea of the human eye are positive for IL-23R mRNA transcripts. (A) The PrimeFlow™ RNA Assay was able to detect IL-23R mRNA transcripts in human cadaver anterior uveal samples and blood samples. (B) All samples, showed increased background staining for IL-23R mRNA transcripts compared to IL-23R FMOs. The CD4-CD8+ subpopulation of T cells in the anterior uvea showed the highest expression of IL-23R mRNA transcripts.



Supplementary Figure 4.3. Validation of IL-17RA staining in human anterior uvea samples from cadavers with a history of uveitis or no history of uveitis. DAB staining was captured on sections of tissue for the expression of IL-17RA in: (A) 2.5X magnification image of the entire anterior uvea; (B) 10X magnification of the anterior uvea; (C) 20X magnification of the iris root; (D) 20X magnification of the trabecular meshwork; (E) 20X magnification of the ciliary body; (F) 20X magnification of the ciliary processes.

Appendix II

Publications

Dakin, S. G., Newton, J., Martinez, F. O., **Hedley, R.**, Gwilym, S., Jones, N., Reid, H. A. B., Wood, S., Wells, G., Appleton, L., Wheway, K., Watkins, B., Carr, A. J. Chronic inflammation is a feature of Achilles tendinopathy and rupture. Br J Sports Med. 2018 Mar;52(6):359-367. doi: 10.1136/bjsports-2017-098161. Epub 2017 Nov 8. PMID: 29118051; PMCID: PMC5867427.

Dakin, S. G., Buckley, C. D., Al-Mossawi, M. H., **Hedley, R.**, Martinez, F. O., Wheway, K., Watkins, B., Carr, A. J. Persistent stromal fibroblast activation is present in chronic tendinopathy. Arthritis Res Ther. 2017 Jan 25;19(1):16. doi: 10.1186/s13075-016-1218-4. PMID: 28122639; PMCID: PMC5264298.

Abstracts

Powell, N. Lo, J.W. Kudo, H. Stolarczyk, E. Garrido-Mesa, N. **Hedley, R.** Jackson, I. Goldin, R. MacDonald, T.T. and Lord, G.M. 2014. "NKp46^{+} innate lymphocytes mediate interferon-γ dependent acute hepatitis following activation of the CD40 pathway" – Poster presented at EMBO ILC conference, Paris, 09/2014; Abstract also accepted at the BSI, Brighton, 12/2014.

Hedley, R. Swingler, T. Kramm, A. Yapp, C. Oppermann, U. Carr, A.J. and Snelling, S.J.B. 2014. "Epigenetic modifying compounds alter activity of primary human articular chondrocytes and mesenchymal stem cells undergoing chondrogenesis" – Poster presented at OARSI, Paris, 04/2014.

References

Abtin, A., R. Jain, A. J. Mitchell, B. Roediger, A. J. Brzoska, S. Tikoo, Q. Cheng, L. G. Ng, L. L. Cavanagh, U. H. von Andrian, M. J. Hickey, N. Firth, and W. Weninger. 2014. 'Perivascular macrophages mediate neutrophil recruitment during bacterial skin infection', *Nat Immunol*, 15: 45-53.

Abu El-Asrar, A. M., N. Berghmans, S. A. Al-Obeidan, P. W. Gikandi, G. Opdenakker, J. Van Damme, and S. Struyf. 2019. 'The CC chemokines CCL8, CCL13 and CCL20 are local inflammatory biomarkers of HLA-B27-associated uveitis', *Acta Ophthalmol*, 97: e122-e28.

Abu El-Asrar, A. M., N. Berghmans, S. A. Al-Obeidan, A. Mousa, G. Opdenakker, J. Van Damme, and S. Struyf. 2016. 'The Cytokine Interleukin-6 and the Chemokines CCL20 and CXCL13 Are Novel Biomarkers of Specific Endogenous Uveitic Entities', *Invest Ophthalmol Vis Sci*, 57: 4606-13.

Acott, T. S., P. D. Kingsley, J. R. Samples, and E. M. Van Buskirk. 1988. 'Human trabecular meshwork organ culture: morphology and glycosaminoglycan synthesis', *Invest Ophthalmol Vis Sci*, 29: 90-100.

Adamopoulos, I. E., E. Suzuki, C. C. Chao, D. Gorman, S. Adda, E. Maverakis, K. Zarbalis, R. Geissler, A. Asio, W. M. Blumenschein, T. McClanahan, R. De Waal Malefyt, M. E. Gershwin, and E. P. Bowman. 2015. 'IL-17A gene transfer induces bone loss and epidermal hyperplasia associated with psoriatic arthritis', *Ann Rheum Dis*, 74: 1284-92.

Adamopoulos, I. E., M. Tessmer, C. C. Chao, S. Adda, D. Gorman, M. Petro, C. C. Chou, R. H. Pierce, W. Yao, N. E. Lane, D. Laface, and E. P. Bowman. 2011. 'IL-23 is critical for induction of arthritis, osteoclast formation, and maintenance of bone mass', *J Immunol*, 187: 951-9.

Aggarwal, S., N. Ghilardi, M. H. Xie, F. J. de Sauvage, and A. L. Gurney. 2003. 'Interleukin-23 promotes a distinct CD4 T cell activation state characterized by the production of interleukin-17', *J Biol Chem*, 278: 1910-4.

Ahern, P. P., C. Schiering, S. Buonocore, M. J. McGeachy, D. J. Cua, K. J. Maloy, and F. Powrie. 2010. 'Interleukin-23 drives intestinal inflammation through direct activity on T cells', *Immunity*, 33: 279-88.

Amadi-Obi, A., C. R. Yu, X. Liu, R. M. Mahdi, G. L. Clarke, R. B. Nussenblatt, I. Gery, Y. S. Lee, and C. E. Egwuagu. 2007. 'TH17 cells contribute to uveitis and scleritis and are expanded by IL-2 and inhibited by IL-27/STAT1', *Nat Med*, 13: 711-8.

Ambarus, C. A., N. Yeremenko, and D. L. Baeten. 2018. 'Altered cytokine expression by macrophages from HLA-B27-positive spondyloarthritis patients without evidence of endoplasmic reticulum stress', *Rheumatol Adv Pract*, 2: rky014.

Antoniou, A. N., S. Ford, J. D. Taurog, G. W. Butcher, and S. J. Powis. 2004. 'Formation of HLA-B27 homodimers and their relationship to assembly kinetics', *J Biol Chem*, 279: 8895-902.

Araujo, E. G., M. Englbrecht, S. Hoepken, S. Finzel, E. Kampylafka, A. Kleyer, S. Bayat, V. Schoenau, A. Hueber, J. Rech, and G. Schett. 2019. 'Effects of ustekinumab versus tumor necrosis factor inhibition on enthesitis: Results from the enthesial clearance in psoriatic arthritis (ECLIPSA) study', *Semin Arthritis Rheum*, 48: 632-37.

Armitage, W. J., A. B. Tullo, and D. F. Larkin. 2006. 'The first successful full-thickness corneal transplant: a commentary on Eduard Zirm's landmark paper of 1906', *Br J Ophthalmol*, 90: 1222-3.

Arnold, I. C., S. Mathisen, J. Schulthess, C. Danne, A. N. Hegazy, and F. Powrie. 2016. 'CD11c(+) monocyte/macrophages promote chronic Helicobacter

hepaticus-induced intestinal inflammation through the production of IL-23', *Mucosal Immunol*, 9: 352-63.
Ashton, N., and R. Smith. 1953. 'Anatomical study of Schlemm's canal and aqueous veins by means of neoprene casts. III. Arterial relations of Schlemm's canal', *Br J Ophthalmol*, 37: 577-86.
Aspelund, A., S. Antila, S. T. Proulx, T. V. Karlsen, S. Karaman, M. Detmar, H. Wiig, and K. Alitalo. 2015. 'A dural lymphatic vascular system that drains brain interstitial fluid and macromolecules', *J Exp Med*, 212: 991-9.
Astarita, J. L., S. E. Acton, and S. J. Turley. 2012. 'Podoplanin: emerging functions in development, the immune system, and cancer', *Front Immunol*, 3: 283.
Awasthi, A., L. Riol-Blanco, A. Jäger, T. Korn, C. Pot, G. Galileos, E. Bettelli, V. K. Kuchroo, and M. Oukka. 2009. 'Cutting edge: IL-23 receptor gfp reporter mice reveal distinct populations of IL-17-producing cells', *J Immunol*, 182: 5904-8.
Babu, K., and P. Mahendradas. 2013. 'Medical management of uveitis - current trends', *Indian J Ophthalmol*, 61: 277-83.
Baerveldt, E. M., J. H. Kappen, H. B. Thio, J. A. van Laar, P. M. van Hagen, and E. P. Prens. 2013. 'Successful long-term triple disease control by ustekinumab in a patient with Behcet's disease, psoriasis and hidradenitis suppurativa', *Ann Rheum Dis*, 72: 626-7.
Baeten, D., M. Østergaard, J. C. Wei, J. Sieper, P. Järvinen, L. S. Tam, C. Salvarani, T. H. Kim, A. Solinger, Y. Datsenko, C. Pamulapati, S. Visvanathan, D. B. Hall, S. Aslanyan, P. Scholl, and S. J. Padula. 2018. 'Risankizumab, an IL-23 inhibitor, for ankylosing spondylitis: results of a randomised, double-blind, placebo-controlled, proof-of-concept, dose-finding phase 2 study', *Ann Rheum Dis*, 77: 1295-302.
Baeten, D., J. Sieper, J. Braun, X. Baraliakos, M. Dougados, P. Emery, A. Deodhar, B. Porter, R. Martin, M. Andersson, S. Mpofu, and H. B. Richards. 2015. 'Secukinumab, an Interleukin-17A Inhibitor, in Ankylosing Spondylitis', *N Engl J Med*, 373: 2534-48.
Bansal, S., V. A. Barathi, D. Iwata, and R. Agrawal. 2015. 'Experimental autoimmune uveitis and other animal models of uveitis: An update', *Indian J Ophthalmol*, 63: 211-8.
Becher, B., B. G. Durell, and R. J. Noelle. 2002. 'Experimental autoimmune encephalitis and inflammation in the absence of interleukin-12', *J Clin Invest*, 110: 493-7.
Bernstein, C. N., J. F. Blanchard, P. Rawsthorne, and N. Yu. 2001. 'The prevalence of extraintestinal diseases in inflammatory bowel disease: a population-based study', *Am J Gastroenterol*, 96: 1116-22.
Bill, A. 1973. 'The role of ciliary blood flow and ultrafiltration in aqueous humor formation', *Exp Eye Res*, 16: 287-98.
———. 1975. 'Blood circulation and fluid dynamics in the eye', *Physiol Rev*, 55: 383-417.
Billiau, A., H. Heremans, F. Vandekerckhove, R. Dijkmans, H. Sobis, E. Meulepas, and H. Carton. 1988. 'Enhancement of experimental allergic encephalomyelitis in mice by antibodies against IFN-gamma', *J Immunol*, 140: 1506-10.
Birke, K., E. Lütjen-Drecoll, D. Kerjaschki, and M. T. Birke. 2010. 'Expression of podoplanin and other lymphatic markers in the human anterior eye segment', *Invest Ophthalmol Vis Sci*, 51: 344-54.

Bito, L. Z. 1970. 'Intraocular fluid dynamics. I. Steady-state concentration gradients of magnesium, potassium and calcium in relation to the sites and mechanisms of ocular cation transport processes', *Exp Eye Res*, 10: 102-16.
———. 1977. 'The physiology and pathophysiology of intraocular fluids', *Exp Eye Res*, 25 Suppl: 273-89.
Blauvelt, A., K. A. Papp, C. E. Griffiths, B. Randazzo, Y. Wasfi, Y. K. Shen, S. Li, and A. B. Kimball. 2017. 'Efficacy and safety of guselkumab, an anti-interleukin-23 monoclonal antibody, compared with adalimumab for the continuous treatment of patients with moderate to severe psoriasis: Results from the phase III, double-blinded, placebo- and active comparator-controlled VOYAGE 1 trial', *J Am Acad Dermatol*, 76: 405-17.
Bose, T., R. Lee, A. Hou, L. Tong, and K. G. Chandy. 2017. 'Tissue resident memory T cells in the human conjunctiva and immune signatures in human dry eye disease', *Sci Rep*, 7: 45312.
Bowness, P., A. Ridley, J. Shaw, A. T. Chan, I. Wong-Baeza, M. Fleming, F. Cummings, A. McMichael, and S. Kollnberger. 2011. 'Th17 cells expressing KIR3DL2+ and responsive to HLA-B27 homodimers are increased in ankylosing spondylitis', *J Immunol*, 186: 2672-80.
Braakman, S. T., J. E. Moore, Jr., C. R. Ethier, and D. R. Overby. 2016. 'Transport across Schlemm's canal endothelium and the blood-aqueous barrier', *Exp Eye Res*, 146: 17-21.
Brewerton, D. A., F. D. Hart, A. Nicholls, M. Caffrey, D. C. James, and R. D. Sturrock. 1973. 'Ankylosing spondylitis and HL-A 27', *Lancet*, 1: 904-7.
Bridgewood, C., K. Sharif, J. Sherlock, A. Watad, and D. McGonagle. 2020. 'Interleukin-23 pathway at the enthesis: The emerging story of enthesitis in spondyloarthropathy', *Immunol Rev*, 294: 27-47.
Bridgewood, C., A. Watad, R. J. Cuthbert, and D. McGonagle. 2018. 'Spondyloarthritis: new insights into clinical aspects, translational immunology and therapeutics', *Curr Opin Rheumatol*, 30: 526-32.
Brophy, S., S. Hickey, A. Menon, G. Taylor, L. Bradbury, J. Hamersma, and A. Calin. 2004. 'Concordance of disease severity among family members with ankylosing spondylitis?', *J Rheumatol*, 31: 1775-8.
Brown, M. A., S. Brophy, L. Bradbury, J. Hamersma, A. Timms, S. Laval, L. Cardon, A. Calin, and B. P. Wordsworth. 2003. 'Identification of major loci controlling clinical manifestations of ankylosing spondylitis', *Arthritis Rheum*, 48: 2234-9.
Brown, M. A., L. G. Kennedy, A. J. MacGregor, C. Darke, E. Duncan, J. L. Shatford, A. Taylor, A. Calin, and P. Wordsworth. 1997. 'Susceptibility to ankylosing spondylitis in twins: the role of genes, HLA, and the environment', *Arthritis Rheum*, 40: 1823-8.
Bullard, D. C., X. Hu, T. R. Schoeb, R. C. Axtell, C. Raman, and S. R. Barnum. 2005. 'Critical requirement of CD11b (Mac-1) on T cells and accessory cells for development of experimental autoimmune encephalomyelitis', *J Immunol*, 175: 6327-33.
Buonocore, S., P. P. Ahern, H. H. Uhlig, Ivanov, II, D. R. Littman, K. J. Maloy, and F. Powrie. 2010. 'Innate lymphoid cells drive interleukin-23-dependent innate intestinal pathology', *Nature*, 464: 1371-5.
Burton, P. R., D. G. Clayton, L. R. Cardon, N. Craddock, P. Deloukas, A. Duncanson, D. P. Kwiatkowski, M. I. McCarthy, W. H. Ouwehand, N. J. Samani, J. A. Todd, P. Donnelly, J. C. Barrett, D. Davison, D. Easton, D. M. Evans, H. T. Leung, J. L. Marchini, A. P. Morris, C. C. Spencer, M. D. Tobin, A. P. Attwood, J. P.

Boorman, B. Cant, U. Everson, J. M. Hussey, J. D. Jolley, A. S. Knight, K. Koch, E. Meech, S. Nutland, C. V. Prowse, H. E. Stevens, N. C. Taylor, G. R. Walters, N. M. Walker, N. A. Watkins, T. Winzer, R. W. Jones, W. L. McArdle, S. M. Ring, D. P. Strachan, M. Pembrey, G. Breen, D. St Clair, S. Caesar, K. Gordon-Smith, L. Jones, C. Fraser, E. K. Green, D. Grozeva, M. L. Hamshere, P. A. Holmans, I. R. Jones, G. Kirov, V. Moskivina, I. Nikolov, M. C. O'Donovan, M. J. Owen, D. A. Collier, A. Elkin, A. Farmer, R. Williamson, P. McGuffin, A. H. Young, I. N. Ferrier, S. G. Ball, A. J. Balmforth, J. H. Barrett, T. D. Bishop, M. M. Iles, A. Maqbool, N. Yuldasheva, A. S. Hall, P. S. Braund, R. J. Dixon, M. Mangino, S. Stevens, J. R. Thompson, F. Bredin, M. Tremelling, M. Parkes, H. Drummond, C. W. Lees, E. R. Nimmo, J. Satsangi, S. A. Fisher, A. Forbes, C. M. Lewis, C. M. Onnie, N. J. Prescott, J. Sanderson, C. G. Matthew, J. Barbour, M. K. Mohiuddin, C. E. Todhunter, J. C. Mansfield, T. Ahmad, F. R. Cummings, D. P. Jewell, J. Webster, M. J. Brown, M. G. Lathrop, J. Connell, A. Dominiczak, C. A. Marcano, B. Burke, R. Dobson, J. Gungadoo, K. L. Lee, P. B. Munroe, S. J. Newhouse, A. Onipinla, C. Wallace, M. Xue, M. Caulfield, M. Farrall, A. Barton, I. N. Bruce, H. Donovan, S. Eyre, P. D. Gilbert, S. L. Hilder, A. M. Hinks, S. L. John, C. Potter, A. J. Silman, D. P. Symmons, W. Thomson, J. Worthington, D. B. Dunger, B. Widmer, T. M. Frayling, R. M. Freathy, H. Lango, J. R. Perry, B. M. Shields, M. N. Weedon, A. T. Hattersley, G. A. Hitman, M. Walker, K. S. Elliott, C. J. Groves, C. M. Lindgren, N. W. Rayner, N. J. Timpson, E. Zeggini, M. Newport, G. Sirugo, E. Lyons, F. Vannberg, A. V. Hill, L. A. Bradbury, C. Farrar, J. J. Pointon, P. Wordsworth, M. A. Brown, J. A. Franklyn, J. M. Heward, M. J. Simmonds, S. C. Gough, S. Seal, M. R. Stratton, N. Rahman, M. Ban, A. Goris, S. J. Sawcer, A. Compston, D. Conway, M. Jallow, M. Newport, G. Sirugo, K. A. Rockett, S. J. Bumpstead, A. Chaney, K. Downes, M. J. Ghori, R. Gwilliam, S. E. Hunt, M. Inouye, A. Keniry, E. King, R. McGinnis, S. Potter, R. Ravindrarajah, P. Whittaker, C. Widden, D. Withers, N. J. Cardin, D. Davison, T. Ferreira, J. Pereira-Gale, I. B. Hallgrimsdo'ttir, B. N. Howie, Z. Su, Y. Y. Teo, D. Vukcevic, D. Bentley, M. A. Brown, A. Compston, M. Farrall, A. S. Hall, A. T. Hattersley, A. V. Hill, M. Parkes, M. Pembrey, M. R. Stratton, S. L. Mitchell, P. R. Newby, O. J. Brand, J. Carr-Smith, S. H. Pearce, R. McGinnis, A. Keniry, P. Deloukas, J. D. Reveille, X. Zhou, A. M. Sims, A. Dowling, J. Taylor, T. Doan, J. C. Davis, L. Savage, M. M. Ward, T. L. Learch, M. H. Weisman, and M. Brown. 2007. 'Association scan of 14,500 nonsynonymous SNPs in four diseases identifies autoimmunity variants', *Nat Genet*, 39: 1329-37.

Butler, T. L., and P. G. McMenamin. 1996. 'Resident and infiltrating immune cells in the uveal tract in the early and late stages of experimental autoimmune uveoretinitis', *Invest Ophthalmol Vis Sci*, 37: 2195-210.

Bylsma, S. S., J. R. Samples, T. S. Acott, and E. M. Van Buskirk. 1988. 'Trabecular cell division after argon laser trabeculoplasty', *Arch Ophthalmol*, 106: 544-7.

Caffrey, M. F., and D. C. James. 1973. 'Human lymphocyte antigen association in ankylosing spondylitis', *Nature*, 242: 121.

Cambré, I., D. Gaublomme, A. Burssens, P. Jacques, N. Schryvers, A. De Muynck, L. Meuris, S. Lambrecht, S. Carter, P. de Bleser, Y. Saeys, L. Van Hoorebeke, G. Kollias, M. Mack, P. Simoens, R. Lories, N. Callewaert, G. Schett, and D. Elewaut. 2018. 'Mechanical strain determines the site-specific localization of inflammation and tissue damage in arthritis', *Nat Commun*, 9: 4613.

Cann, M., A. V. Ramanan, A. Crawford, A. D. Dick, S. L. N. Clarke, F. Rashed, and C. M. Guly. 2018. 'Outcomes of non-infectious Paediatric uveitis in the era of biologic therapy', *Pediatr Rheumatol Online J*, 16: 51.

Canouï-Poitrine, F., F. K. Lekpa, V. Farrenq, V. Boissinot, C. Hacquard-Bouder, D. Comet, S. Bastuji-Garin, E. Thibout, and P. Claudepierre. 2012. 'Prevalence and factors associated with uveitis in spondylarthritis patients in France: results from an observational survey', *Arthritis Care Res (Hoboken)*, 64: 919-24.

Carding, S. R., and P. J. Egan. 2002. 'Gammadelta T cells: functional plasticity and heterogeneity', *Nat Rev Immunol*, 2: 336-45.

Caspi, R. R. 2010. 'A look at autoimmunity and inflammation in the eye', *J Clin Invest*, 120: 3073-83.

Cella, M., A. Fuchs, W. Vermi, F. Facchetti, K. Otero, J. K. Lennerz, J. M. Doherty, J. C. Mills, and M. Colonna. 2009. 'A human natural killer cell subset provides an innate source of IL-22 for mucosal immunity', *Nature*, 457: 722-5.

Chan, A. T., S. D. Kollnberger, L. R. Wedderburn, and P. Bowness. 2005. 'Expansion and enhanced survival of natural killer cells expressing the killer immunoglobulin-like receptor KIR3DL2 in spondylarthritis', *Arthritis Rheum*, 52: 3586-95.

Chan, J. R., W. Blumenschein, E. Murphy, C. Diveu, M. Wiekowski, S. Abbondanzo, L. Lucian, R. Geissler, S. Brodie, A. B. Kimball, D. M. Gorman, K. Smith, R. de Waal Malefyt, R. A. Kastelein, T. K. McClanahan, and E. P. Bowman. 2006. 'IL-23 stimulates epidermal hyperplasia via TNF and IL-20R2-dependent mechanisms with implications for psoriasis pathogenesis', *J Exp Med*, 203: 2577-87.

Chan, N. S., and S. P. Chee. 2019. 'Demystifying viral anterior uveitis: A review', *Clin Exp Ophthalmol*, 47: 320-33.

Chan, Y. K., S. K. Wang, C. J. Chu, D. A. Copland, A. J. Letizia, H. Costa Verdera, J. J. Chiang, M. Sethi, M. K. Wang, W. J. Neidermyer, Jr., Y. Chan, E. T. Lim, A. R. Graveline, M. Sanchez, R. F. Boyd, T. S. Vihtelic, Rgco Inciong, J. M. Slain, P. J. Alphonse, Y. Xue, L. R. Robinson-McCarthy, J. M. Tam, M. H. Jabbar, B. Sahu, J. F. Adeniran, M. Muhuri, P. W. L. Tai, J. Xie, T. B. Krause, A. Vernet, M. Pezone, R. Xiao, T. Liu, W. Wang, H. J. Kaplan, G. Gao, A. D. Dick, F. Mingozzi, M. A. McCall, C. L. Cepko, and G. M. Church. 2021. 'Engineering adeno-associated viral vectors to evade innate immune and inflammatory responses', *Sci Transl Med*, 13.

Chang, J. H., and D. Wakefield. 2002. 'Uveitis: a global perspective', *Ocul Immunol Inflamm*, 10: 263-79.

Chen, F., A. Cao, S. Yao, H. L. Evans-Marin, H. Liu, W. Wu, E. D. Carlsen, S. M. Dann, L. Soong, J. Sun, Q. Zhao, and Y. Cong. 2016. 'mTOR Mediates IL-23 Induction of Neutrophil IL-17 and IL-22 Production', *J Immunol*, 196: 4390-9.

Chen, L. 2009. 'Ocular lymphatics: state-of-the-art review', *Lymphology*, 42: 66-76.

Chen, L., M. Deshpande, M. Grisotto, P. Smaldini, R. Garcia, Z. He, P. S. Gulko, S. A. Lira, and G. C. Furtado. 2020. 'Skin expression of IL-23 drives the development of psoriasis and psoriatic arthritis in mice', *Sci Rep*, 10: 8259.

Chen, L., Z. He, A. C. Iuga, S. N. Martins Filho, J. J. Faith, J. C. Clemente, M. Deshpande, A. Jayaprakash, J. F. Colombel, J. J. Lafaille, R. Sachidanandam, G. C. Furtado, and S. A. Lira. 2018. 'Diet Modifies Colonic Microbiota and CD4(+) T-Cell Repertoire to Induce Flares of Colitis in Mice With Myeloid-Cell Expression of Interleukin 23', *Gastroenterology*, 155: 1177-91.e16.

Chen, L., Z. He, E. Slinger, G. Bongers, T. L. S. Lapenda, M. E. Pacer, J. Jiao, M. F. Beltrao, A. J. Soto, N. Harpaz, R. E. Gordon, J. C. Ochando, M. Oukka, A. C. Iuga, S. W. Chensue, J. M. Blander, G. C. Furtado, and S. A. Lira. 2015. 'IL-23 activates innate lymphoid cells to promote neonatal intestinal pathology', *Mucosal Immunol*, 8: 390-402.

Chen, S. C., and S. J. Sheu. 2017. 'Recent advances in managing and understanding uveitis', *F1000Res*, 6: 280.

Chen, W., W. Jin, N. Hardegen, K. J. Lei, L. Li, N. Marinos, G. McGrady, and S. M. Wahl. 2003. 'Conversion of peripheral CD4+CD25- naive T cells to CD4+CD25+ regulatory T cells by TGF-beta induction of transcription factor Foxp3', *J Exp Med*, 198: 1875-86.

Chen, W. S., Y. S. Chang, K. C. Lin, C. C. Lai, S. H. Wang, K. H. Hsiao, H. T. Lee, M. H. Chen, C. Y. Tsai, and C. T. Chou. 2012. 'Association of serum interleukin-17 and interleukin-23 levels with disease activity in Chinese patients with ankylosing spondylitis', *J Chin Med Assoc*, 75: 303-8.

Cher, I. 2014. 'Ocular surface concepts: development and citation', *Ocul Surf*, 12: 10-3.

Chi, H. H., K. F. Hua, Y. C. Lin, C. L. Chu, C. Y. Hsieh, Y. J. Hsu, S. M. Ka, Y. L. Tsai, F. C. Liu, and A. Chen. 2017. 'IL-36 Signaling Facilitates Activation of the NLRP3 Inflammasome and IL-23/IL-17 Axis in Renal Inflammation and Fibrosis', *J Am Soc Nephrol*, 28: 2022-37.

Chien, Y. H., X. Zeng, and I. Prinz. 2013. 'The natural and the inducible: interleukin (IL)-17-producing γδ T cells', *Trends Immunol*, 34: 151-4.

Chu, C. J., S. E. Barker, A. D. Dick, and R. R. Ali. 2012. 'Gene therapy for noninfectious uveitis', *Ocul Immunol Inflamm*, 20: 394-405.

Ciccia, F., A. Accardo-Palumbo, A. Rizzo, G. Guggino, S. Raimondo, A. Giardina, A. Cannizzaro, R. A. Colbert, R. Alessandro, and G. Triolo. 2014. 'Evidence that autophagy, but not the unfolded protein response, regulates the expression of IL-23 in the gut of patients with ankylosing spondylitis and subclinical gut inflammation', *Ann Rheum Dis*, 73: 1566-74.

Ciccia, F., M. Bombardieri, A. Principato, A. Giardina, C. Tripodo, R. Porcasi, S. Peralta, V. Franco, E. Giardina, A. Craxi, C. Pitzalis, and G. Triolo. 2009. 'Overexpression of interleukin-23, but not interleukin-17, as an immunologic signature of subclinical intestinal inflammation in ankylosing spondylitis', *Arthritis Rheum*, 60: 955-65.

Ciofani, M., and J. C. Zúñiga-Pflücker. 2010. 'Determining γδ versus αß T cell development', *Nat Rev Immunol*, 10: 657-63.

Colbert, R. A., M. L. DeLay, G. Layh-Schmitt, and D. P. Sowders. 2009. 'HLA-B27 misfolding and spondyloarthropathies', *Prion*, 3: 15-26.

Colmegna, I., R. Cuchacovich, and L. R. Espinoza. 2004. 'HLA-B27-associated reactive arthritis: pathogenetic and clinical considerations', *Clin Microbiol Rev*, 17: 348-69.

Conrady, C. D., M. Larochelle, P. Pecen, A. Palestine, A. Shakoor, and A. Singh. 2018. 'Checkpoint inhibitor-induced uveitis: a case series', *Graefes Arch Clin Exp Ophthalmol*, 256: 187-91.

Copland, D. A., J. Liu, L. P. Schewitz-Bowers, V. Brinkmann, K. Anderson, L. B. Nicholson, and A. D. Dick. 2012. 'Therapeutic dosing of fingolimod (FTY720) prevents cell infiltration, rapidly suppresses ocular inflammation, and maintains the blood-ocular barrier', *Am J Pathol*, 180: 672-81.

Cordero-Coma, M., T. Yilmaz, and S. Onal. 2013. 'Systematic review of anti-tumor necrosis factor-alpha therapy for treatment of immune-mediated uveitis', *Ocul Immunol Inflamm*, 21: 19-27.

Cortes, A., and M. A. Brown. 2011. 'Promise and pitfalls of the Immunochip', *Arthritis Res Ther*, 13: 101.

Cortes, A., J. Hadler, J. P. Pointon, P. C. Robinson, T. Karaderi, P. Leo, K. Cremin, K. Pryce, J. Harris, S. Lee, K. B. Joo, S. C. Shim, M. Weisman, M. Ward, X. Zhou, H. J. Garchon, G. Chiocchia, J. Nossent, B. A. Lie, Ø Førre, J. Tuomilehto, K. Laiho, L. Jiang, Y. Liu, X. Wu, L. A. Bradbury, D. Elewaut, R. Burgos-Vargas, S. Stebbings, L. Appleton, C. Farrah, J. Lau, T. J. Kenna, N. Haroon, M. A. Ferreira, J. Yang, J. Mulero, J. L. Fernandez-Sueiro, M. A. Gonzalez-Gay, C. Lopez-Larrea, P. Deloukas, P. Donnelly, P. Bowness, K. Gafney, H. Gaston, D. D. Gladman, P. Rahman, W. P. Maksymowych, H. Xu, J. B. Crusius, I. E. van der Horst-Bruinsma, C. T. Chou, R. Valle-Oñate, C. Romero-Sánchez, I. M. Hansen, F. M. Pimentel-Santos, R. D. Inman, V. Videm, J. Martin, M. Breban, J. D. Reveille, D. M. Evans, T. H. Kim, B. P. Wordsworth, and M. A. Brown. 2013. 'Identification of multiple risk variants for ankylosing spondylitis through high-density genotyping of immune-related loci', *Nat Genet*, 45: 730-8.

Cortes, A., S. L. Pulit, P. J. Leo, J. J. Pointon, P. C. Robinson, M. H. Weisman, M. Ward, L. S. Gensler, X. Zhou, H. J. Garchon, G. Chiocchia, J. Nossent, B. A. Lie, Ø Førre, J. Tuomilehto, K. Laiho, L. A. Bradbury, D. Elewaut, R. Burgos-Vargas, S. Stebbings, L. Appleton, C. Farrah, J. Lau, N. Haroon, J. Mulero, F. J. Blanco, M. A. Gonzalez-Gay, C. Lopez-Larrea, P. Bowness, K. Gaffney, H. Gaston, D. D. Gladman, P. Rahman, W. P. Maksymowych, J. B. Crusius, I. E. van der Horst-Bruinsma, R. Valle-Oñate, C. Romero-Sánchez, I. M. Hansen, F. M. Pimentel-Santos, R. D. Inman, J. Martin, M. Breban, B. P. Wordsworth, J. D. Reveille, D. M. Evans, P. I. de Bakker, and M. A. Brown. 2015. 'Major histocompatibility complex associations of ankylosing spondylitis are complex and involve further epistasis with ERAP1', *Nat Commun*, 6: 7146.

Crellin, N. K., S. Trifari, C. D. Kaplan, N. Satoh-Takayama, J. P. Di Santo, and H. Spits. 2010. 'Regulation of cytokine secretion in human CD127(+) LTi-like innate lymphoid cells by Toll-like receptor 2', *Immunity*, 33: 752-64.

Cua, D. J., J. Sherlock, Y. Chen, C. A. Murphy, B. Joyce, B. Seymour, L. Lucian, W. To, S. Kwan, T. Churakova, S. Zurawski, M. Wiekowski, S. A. Lira, D. Gorman, R. A. Kastelein, and J. D. Sedgwick. 2003. 'Interleukin-23 rather than interleukin-12 is the critical cytokine for autoimmune inflammation of the brain', *Nature*, 421: 744-8.

Cua, D. J., and J. P. Sherlock. 2011. 'Autoimmunity's collateral damage: Gut microbiota strikes 'back'', *Nat Med*, 17: 1055-6.

Cunha-Vaz, J. G., and D. M. Maurice. 1967. 'The active transport of fluorescein by the retinal vessels and the retina', *J Physiol*, 191: 467-86.

Cunningham, E. T., Jr., and J. D. Wender. 2010. 'Practical approach to the use of corticosteroids in patients with uveitis', *Can J Ophthalmol*, 45: 352-8.

Cuthbert, R. J., E. M. Fragkakis, R. Dunsmuir, Z. Li, M. Coles, H. Marzo-Ortega, P. V. Giannoudis, E. Jones, Y. M. El-Sherbiny, and D. McGonagle. 2017. 'Brief Report: Group 3 Innate Lymphoid Cells in Human Enthesis', *Arthritis Rheumatol*, 69: 1816-22.

Cuthbert, R. J., A. Watad, E. M. Fragkakis, R. Dunsmuir, P. Loughenbury, A. Khan, P. A. Millner, A. Davison, H. Marzo-Ortega, D. Newton, C. Bridgewood, and D. G. McGonagle. 2019. 'Evidence that tissue resident human enthesis γδT-cells can

produce IL-17A independently of IL-23R transcript expression', *Ann Rheum Dis*, 78: 1559-65.

Czegley, C., C. Gillmann, C. Schauer, L. Seyler, C. Reinwald, M. Hahn, M. Uder, K. Jochmann, E. Naschberger, M. Stock, G. Schett, T. Bäuerle, and M. H. Hoffmann. 2018. 'A model of chronic enthesitis and new bone formation characterized by multimodal imaging', *Dis Model Mech*, 11.

D'Amato, M., M. T. Fiorillo, C. Carcassi, A. Mathieu, A. Zuccarelli, P. P. Bitti, R. Tosi, and R. Sorrentino. 1995. 'Relevance of residue 116 of HLA-B27 in determining susceptibility to ankylosing spondylitis', *Eur J Immunol*, 25: 3199-201.

Da Cunha, A. P., Q. Zhang, M. Prentiss, X. Q. Wu, V. Kainz, Y. Y. Xu, J. Vrouvlianis, H. Li, N. Rangaswamy, B. Leehy, T. L. McGee, C. L. Bell, C. E. Bigelow, V. Kansara, Q. Medley, Q. Huang, and H. Y. Wu. 2018. 'The Hierarchy of Proinflammatory Cytokines in Ocular Inflammation', *Curr Eye Res*, 43: 553-65.

Dakin, S. G., C. D. Buckley, M. H. Al-Mossawi, R. Hedley, F. O. Martinez, K. Wheway, B. Watkins, and A. J. Carr. 2017. 'Persistent stromal fibroblast activation is present in chronic tendinopathy', *Arthritis Res Ther*, 19: 16.

Davidson, S. I., X. Wu, Y. Liu, M. Wei, P. A. Danoy, G. Thomas, Q. Cai, L. Sun, E. Duncan, N. Wang, Q. Yu, A. Xu, Y. Fu, M. A. Brown, and H. Xu. 2009. 'Association of ERAP1, but not IL23R, with ankylosing spondylitis in a Han Chinese population', *Arthritis Rheum*, 60: 3263-8.

de, Blecourt J., A. Polman, and Blecourt-Meindersma de. 1961. 'Hereditary factors in rheumatoid arthritis and ankylosing spondylitis', *Ann Rheum Dis*, 20: 215-20.

DeLay, M. L., M. J. Turner, E. I. Klenk, J. A. Smith, D. P. Sowders, and R. A. Colbert. 2009. 'HLA-B27 misfolding and the unfolded protein response augment interleukin-23 production and are associated with Th17 activation in transgenic rats', *Arthritis Rheum*, 60: 2633-43.

Deodhar, A., L. S. Gensler, J. Sieper, M. Clark, C. Calderon, Y. Wang, Y. Zhou, J. H. Leu, K. Campbell, K. Sweet, D. D. Harrison, E. C. Hsia, and D. van der Heijde. 2019. 'Three Multicenter, Randomized, Double-Blind, Placebo-Controlled Studies Evaluating the Efficacy and Safety of Ustekinumab in Axial Spondyloarthritis', *Arthritis Rheumatol*, 71: 258-70.

Deodhar, A., A. B. Gottlieb, W. H. Boehncke, B. Dong, Y. Wang, Y. Zhuang, W. Barchuk, X. L. Xu, and E. C. Hsia. 2018. 'Efficacy and safety of guselkumab in patients with active psoriatic arthritis: a randomised, double-blind, placebo-controlled, phase 2 study', *Lancet*, 391: 2213-24.

Derksen, Vfam, T. W. J. Huizinga, and D. van der Woude. 2017. 'The role of autoantibodies in the pathophysiology of rheumatoid arthritis', *Semin Immunopathol*, 39: 437-46.

Dick, A. D., J. T. Rosenbaum, H. A. Al-Dhibi, R. Belfort, Jr., A. P. Brézin, S. P. Chee, J. L. Davis, A. V. Ramanan, K. H. Sonoda, E. Carreño, H. Nascimento, S. Salah, S. Salek, J. Siak, and L. Steeples. 2018. 'Guidance on Noncorticosteroid Systemic Immunomodulatory Therapy in Noninfectious Uveitis: Fundamentals Of Care for UveitiS (FOCUS) Initiative', *Ophthalmology*, 125: 757-73.

Dick, A. D., I. Tugal-Tutkun, S. Foster, M. Zierhut, S. H. Melissa Liew, V. Bezlyak, and S. Androudi. 2013. 'Secukinumab in the treatment of noninfectious uveitis: results of three randomized, controlled clinical trials', *Ophthalmology*, 120: 777-87.

Ding, L., X. Wang, X. Hong, L. Lu, and D. Liu. 2018. 'IL-36 cytokines in autoimmunity and inflammatory disease', *Oncotarget*, 9: 2895-901.

Dong, H., Q. Li, Y. Zhang, W. Tan, and Z. Jiang. 2013. 'IL23R gene confers susceptibility to ankylosing spondylitis concomitant with uveitis in a Han Chinese population', *PLoS One*, 8: e67505.

Duerr, R. H., K. D. Taylor, S. R. Brant, J. D. Rioux, M. S. Silverberg, M. J. Daly, A. H. Steinhart, C. Abraham, M. Regueiro, A. Griffiths, T. Dassopoulos, A. Bitton, H. Yang, S. Targan, L. W. Datta, E. O. Kistner, L. P. Schumm, A. T. Lee, P. K. Gregersen, M. M. Barmada, J. I. Rotter, D. L. Nicolae, and J. H. Cho. 2006. 'A genome-wide association study identifies IL23R as an inflammatory bowel disease gene', *Science*, 314: 1461-3.

Eadie, B., M. Etminan, and F. S. Mikelberg. 2015. 'Risk for uveitis with oral moxifloxacin: a comparative safety study', *JAMA Ophthalmol*, 133: 81-4.

Eder, L., T. Law, V. Chandran, S. Shanmugarajah, H. Shen, C. F. Rosen, R. J. Cook, and D. D. Gladman. 2011. 'Association between environmental factors and onset of psoriatic arthritis in patients with psoriasis', *Arthritis Care Res (Hoboken)*, 63: 1091-7.

Egeberg, A., U. Khalid, G. H. Gislason, L. Mallbris, L. Skov, and P. R. Hansen. 2015. 'Association of Psoriatic Disease With Uveitis: A Danish Nationwide Cohort Study', *JAMA Dermatol*, 151: 1200-5.

Eichhorn, M., K. Inada, and E. Lütjen-Drecoll. 1991. 'Human ciliary body in organ culture', *Curr Eye Res*, 10: 277-86.

El-Behi, M., B. Ciric, H. Dai, Y. Yan, M. Cullimore, F. Safavi, G. X. Zhang, B. N. Dittel, and A. Rostami. 2011. 'The encephalitogenicity of T(H)17 cells is dependent on IL-1- and IL-23-induced production of the cytokine GM-CSF', *Nat Immunol*, 12: 568-75.

El-Zayadi, A. A., E. A. Jones, S. M. Churchman, T. G. Baboolal, R. J. Cuthbert, J. J. El-Jawhari, A. M. Badawy, A. A. Alase, Y. M. El-Sherbiny, and D. McGonagle. 2017. 'Interleukin-22 drives the proliferation, migration and osteogenic differentiation of mesenchymal stem cells: a novel cytokine that could contribute to new bone formation in spondyloarthropathies', *Rheumatology (Oxford)*, 56: 488-93.

Ellinghaus, D., L. Jostins, S. L. Spain, A. Cortes, J. Bethune, B. Han, Y. R. Park, S. Raychaudhuri, J. G. Pouget, M. Hübenthal, T. Folseraas, Y. Wang, T. Esko, A. Metspalu, H. J. Westra, L. Franke, T. H. Pers, R. K. Weersma, V. Collij, M. D'Amato, J. Halfvarson, A. B. Jensen, W. Lieb, F. Degenhardt, A. J. Forstner, A. Hofmann, S. Schreiber, U. Mrowietz, B. D. Juran, K. N. Lazaridis, S. Brunak, A. M. Dale, R. C. Trembath, S. Weidinger, M. Weichenthal, E. Ellinghaus, J. T. Elder, J. N. Barker, O. A. Andreassen, D. P. McGovern, T. H. Karlsen, J. C. Barrett, M. Parkes, M. A. Brown, and A. Franke. 2016. 'Analysis of five chronic inflammatory diseases identifies 27 new associations and highlights disease-specific patterns at shared loci', *Nat Genet*, 48: 510-8.

Ethier, C. R. 2002. 'The inner wall of Schlemm's canal', *Exp Eye Res*, 74: 161-72.

Evans, D. M., C. C. Spencer, J. J. Pointon, Z. Su, D. Harvey, G. Kochan, U. Oppermann, A. Dilthey, M. Pirinen, M. A. Stone, L. Appleton, L. Moutsianas, S. Leslie, T. Wordsworth, T. J. Kenna, T. Karaderi, G. P. Thomas, M. M. Ward, M. H. Weisman, C. Farrar, L. A. Bradbury, P. Danoy, R. D. Inman, W. Maksymowych, D. Gladman, P. Rahman, A. Morgan, H. Marzo-Ortega, P. Bowness, K. Gaffney, J. S. Gaston, M. Smith, J. Bruges-Armas, A. R. Couto, R. Sorrentino, F. Paladini, M. A. Ferreira, H. Xu, Y. Liu, L. Jiang, C. Lopez-Larrea, R. Díaz-Peña, A. López-Vázquez, T. Zayats, G. Band, C. Bellenguez, H. Blackburn, J. M. Blackwell, E. Bramon, S. J. Bumpstead, J. P. Casas, A.

Corvin, N. Craddock, P. Deloukas, S. Dronov, A. Duncanson, S. Edkins, C. Freeman, M. Gillman, E. Gray, R. Gwilliam, N. Hammond, S. E. Hunt, J. Jankowski, A. Jayakumar, C. Langford, J. Liddle, H. S. Markus, C. G. Mathew, O. T. McCann, M. I. McCarthy, C. N. Palmer, L. Peltonen, R. Plomin, S. C. Potter, A. Rautanen, R. Ravindrarajah, M. Ricketts, N. Samani, S. J. Sawcer, A. Strange, R. C. Trembath, A. C. Viswanathan, M. Waller, P. Weston, P. Whittaker, S. Widaa, N. W. Wood, G. McVean, J. D. Reveille, B. P. Wordsworth, M. A. Brown, and P. Donnelly. 2011. 'Interaction between ERAP1 and HLA-B27 in ankylosing spondylitis implicates peptide handling in the mechanism for HLA-B27 in disease susceptibility', *Nat Genet*, 43: 761-7.

Fabiani, C., A. Vitale, D. Rigante, G. Emmi, G. Lopalco, J. Sota, L. Vannozzi, S. Guerriero, A. Bitossi, I. Orlando, R. Franceschini, B. Frediani, M. Galeazzi, F. Iannone, G. M. Tosi, and L. Cantarini. 2019. 'Efficacy of anti-tumour necrosis factor-α monoclonal antibodies in patients with non-infectious anterior uveitis', *Clin Exp Rheumatol*, 37: 301-05.

Fan, X., and A. Y. Rudensky. 2016. 'Hallmarks of Tissue-Resident Lymphocytes', *Cell*, 164: 1198-211.

Farquhar, D. R., M. J. Chamberlain, G. A. McCain, and W. K. Morgan. 1989. 'Clearance of inhaled particles in ankylosing spondylitis', *Ann Rheum Dis*, 48: 974-7.

Faunce, D. E., and J. Stein-Streilein. 2002. 'NKT cell-derived RANTES recruits APCs and CD8+ T cells to the spleen during the generation of regulatory T cells in tolerance', *J Immunol*, 169: 31-8.

Feagan, B. G., J. Panés, M. Ferrante, A. Kaser, G. R. D'Haens, W. J. Sandborn, E. Louis, M. F. Neurath, D. Franchimont, O. Dewit, U. Seidler, K. J. Kim, C. Selinger, S. J. Padula, I. Herichova, A. M. Robinson, K. Wallace, J. Zhao, M. Minocha, A. A. Othman, A. Soaita, S. Visvanathan, D. B. Hall, and W. O. Böcher. 2018. 'Risankizumab in patients with moderate to severe Crohn's disease: an open-label extension study', *Lancet Gastroenterol Hepatol*, 3: 671-80.

Feagan, B. G., W. J. Sandborn, G. D'Haens, J. Panés, A. Kaser, M. Ferrante, E. Louis, D. Franchimont, O. Dewit, U. Seidler, K. J. Kim, M. F. Neurath, S. Schreiber, P. Scholl, C. Pamulapati, B. Lalovic, S. Visvanathan, S. J. Padula, I. Herichova, A. Soaita, D. B. Hall, and W. O. Böcher. 2017. 'Induction therapy with the selective interleukin-23 inhibitor risankizumab in patients with moderate-to-severe Crohn's disease: a randomised, double-blind, placebo-controlled phase 2 study', *Lancet*, 389: 1699-709.

Feagan, B. G., W. J. Sandborn, C. Gasink, D. Jacobstein, Y. Lang, J. R. Friedman, M. A. Blank, J. Johanns, L. L. Gao, Y. Miao, O. J. Adedokun, B. E. Sands, S. B. Hanauer, S. Vermeire, S. Targan, S. Ghosh, W. J. de Villiers, J. F. Colombel, Z. Tulassay, U. Seidler, B. A. Salzberg, P. Desreumaux, S. D. Lee, E. V. Loftus, Jr., L. A. Dieleman, S. Katz, and P. Rutgeerts. 2016. 'Ustekinumab as Induction and Maintenance Therapy for Crohn's Disease', *N Engl J Med*, 375: 1946-60.

Fehling, H. J., A. Krotkova, C. Saint-Ruf, and H. von Boehmer. 1995. 'Crucial role of the pre-T-cell receptor alpha gene in development of alpha beta but not gamma delta T cells', *Nature*, 375: 795-8.

Feldtkeller, E., M. A. Khan, D. van der Heijde, S. van der Linden, and J. Braun. 2003. 'Age at disease onset and diagnosis delay in HLA-B27 negative vs. positive patients with ankylosing spondylitis', *Rheumatol Int*, 23: 61-6.

Ferber, I. A., S. Brocke, C. Taylor-Edwards, W. Ridgway, C. Dinisco, L. Steinman, D. Dalton, and C. G. Fathman. 1996. 'Mice with a disrupted IFN-gamma gene are susceptible to the induction of experimental autoimmune encephalomyelitis (EAE)', *J Immunol*, 156: 5-7.

Fernández-Melón, J., S. Muñoz-Fernández, V. Hidalgo, G. Bonilla-Hernán, A. Schlincker, A. Fonseca, J. Vieitez, and E. Martín-Mola. 2004. 'Uveitis as the initial clinical manifestation in patients with spondyloarthropathies', *J Rheumatol*, 31: 524-7.

Fletcher, E. L., A. I. Jobling, U. Greferath, S. A. Mills, M. Waugh, T. Ho, R. U. de Iongh, J. A. Phipps, and K. A. Vessey. 2014. 'Studying age-related macular degeneration using animal models', *Optom Vis Sci*, 91: 878-86.

Forrester, J. V., A. D. Dick, P. G. McMenamin, F Roberts, and E Pearlman. 2021. *The Eye* (Elsevier: London, England).

Forrester, J. V., H. Xu, L. Kuffová, A. D. Dick, and P. G. McMenamin. 2010. 'Dendritic cell physiology and function in the eye', *Immunol Rev*, 234: 282-304.

Gabelt, B. T., J. Gottanka, E. Lütjen-Drecoll, and P. L. Kaufman. 2003. 'Aqueous humor dynamics and trabecular meshwork and anterior ciliary muscle morphologic changes with age in rhesus monkeys', *Invest Ophthalmol Vis Sci*, 44: 2118-25.

Gabelt, B. T., and P. L. Kaufman. 2005. 'Changes in aqueous humor dynamics with age and glaucoma', *Prog Retin Eye Res*, 24: 612-37.

Gaffen, S. L., R. Jain, A. V. Garg, and D. J. Cua. 2014. 'The IL-23-IL-17 immune axis: from mechanisms to therapeutic testing', *Nat Rev Immunol*, 14: 585-600.

Gagliani, N., M. C. Amezcua Vesely, A. Iseppon, L. Brockmann, H. Xu, N. W. Palm, M. R. de Zoete, P. Licona-Limón, R. S. Paiva, T. Ching, C. Weaver, X. Zi, X. Pan, R. Fan, L. X. Garmire, M. J. Cotton, Y. Drier, B. Bernstein, J. Geginat, B. Stockinger, E. Esplugues, S. Huber, and R. A. Flavell. 2015. 'Th17 cells transdifferentiate into regulatory T cells during resolution of inflammation', *Nature*, 523: 221-5.

Gaida, J. E., J. Bagge, C. Purdam, J. Cook, H. Alfredson, and S. Forsgren. 2012. 'Evidence of the TNF-α system in the human Achilles tendon: expression of TNF-α and TNF receptor at both protein and mRNA levels in the tenocytes', *Cells Tissues Organs*, 196: 339-52.

Ghoreschi, K., A. Laurence, X. P. Yang, C. M. Tato, M. J. McGeachy, J. E. Konkel, H. L. Ramos, L. Wei, T. S. Davidson, N. Bouladoux, J. R. Grainger, Q. Chen, Y. Kanno, W. T. Watford, H. W. Sun, G. Eberl, E. M. Shevach, Y. Belkaid, D. J. Cua, W. Chen, and J. J. O'Shea. 2010. 'Generation of pathogenic T(H)17 cells in the absence of TGF-β signalling', *Nature*, 467: 967-71.

Goel, M., R. G. Picciani, R. K. Lee, and S. K. Bhattacharya. 2010. 'Aqueous humor dynamics: a review', *Open Ophthalmol J*, 4: 52-9.

Goepfert, A., S. Lehmann, E. Wirth, and J. M. Rondeau. 2017. 'The human IL-17A/F heterodimer: a two-faced cytokine with unique receptor recognition properties', *Sci Rep*, 7: 8906.

Gordon, K. B., K. C. Duffin, R. Bissonnette, J. C. Prinz, Y. Wasfi, S. Li, Y. K. Shen, P. Szapary, B. Randazzo, and K. Reich. 2015. 'A Phase 2 Trial of Guselkumab versus Adalimumab for Plaque Psoriasis', *N Engl J Med*, 373: 136-44.

Gracey, E., L. Vereecke, D. McGovern, M. Fröhling, G. Schett, S. Danese, M. De Vos, F. Van den Bosch, and D. Elewaut. 2020. 'Revisiting the gut-joint axis: links between gut inflammation and spondyloarthritis', *Nat Rev Rheumatol*, 16: 415-33.

Greenstein, A. J., H. D. Janowitz, and D. B. Sachar. 1976. 'The extra-intestinal complications of Crohn's disease and ulcerative colitis: a study of 700 patients', *Medicine (Baltimore)*, 55: 401-12.

Gueudry, J., F. Majo, A. Delcampe, and M. Muraine. 2019. 'Panorama of limbal changes', *J Fr Ophtalmol*, 42: e83-e94.

Haas, J. D., F. H. González, S. Schmitz, V. Chennupati, L. Föhse, E. Kremmer, R. Förster, and I. Prinz. 2009. 'CCR6 and NK1.1 distinguish between IL-17A and IFN-gamma-producing gammadelta effector T cells', *Eur J Immunol*, 39: 3488-97.

Haas, J. D., S. Ravens, S. Düber, I. Sandrock, L. Oberdörfer, E. Kashani, V. Chennupati, L. Föhse, R. Naumann, S. Weiss, A. Krueger, R. Förster, and I. Prinz. 2012. 'Development of interleukin-17-producing γδ T cells is restricted to a functional embryonic wave', *Immunity*, 37: 48-59.

Haines, C. J., Y. Chen, W. M. Blumenschein, R. Jain, C. Chang, B. Joyce-Shaikh, K. Porth, K. Boniface, J. Mattson, B. Basham, S. M. Anderton, T. K. McClanahan, S. Sadekova, D. J. Cua, and M. J. McGeachy. 2013. 'Autoimmune memory T helper 17 cell function and expansion are dependent on interleukin-23', *Cell Rep*, 3: 1378-88.

Hamanaka, T. 1989. 'Scleral spur and ciliary muscle in man and monkey', *Jpn J Ophthalmol*, 33: 221-36.

Hamersma, J., L. R. Cardon, L. Bradbury, S. Brophy, I. van der Horst-Bruinsma, A. Calin, and M. A. Brown. 2001. 'Is disease severity in ankylosing spondylitis genetically determined?', *Arthritis Rheum*, 44: 1396-400.

Haroon, M., M. O'Rourke, P. Ramasamy, C. C. Murphy, and O. FitzGerald. 2015. 'A novel evidence-based detection of undiagnosed spondyloarthritis in patients presenting with acute anterior uveitis: the DUET (Dublin Uveitis Evaluation Tool)', *Ann Rheum Dis*, 74: 1990-5.

Hassan, M., S. Karkhur, J. H. Bae, M. S. Halim, M. S. Ormaechea, N. Onghanseng, N. V. Nguyen, R. Afridi, Y. J. Sepah, D. V. Do, and Q. D. Nguyen. 2019. 'New therapies in development for the management of non-infectious uveitis: A review', *Clin Exp Ophthalmol*, 47: 396-417.

Heilig, J. S., and S. Tonegawa. 1986. 'Diversity of murine gamma genes and expression in fetal and adult T lymphocytes', *Nature*, 322: 836-40.

Hirahara, K., K. Ghoreschi, A. Laurence, X. P. Yang, Y. Kanno, and J. J. O'Shea. 2010. 'Signal transduction pathways and transcriptional regulation in Th17 cell differentiation', *Cytokine Growth Factor Rev*, 21: 425-34.

Hirano, M., P. Guo, N. McCurley, M. Schorpp, S. Das, T. Boehm, and M. D. Cooper. 2013. 'Evolutionary implications of a third lymphocyte lineage in lampreys', *Nature*, 501: 435-8.

Hirota, K., H. Yoshitomi, M. Hashimoto, S. Maeda, S. Teradaira, N. Sugimoto, T. Yamaguchi, T. Nomura, H. Ito, T. Nakamura, N. Sakaguchi, and S. Sakaguchi. 2007. 'Preferential recruitment of CCR6-expressing Th17 cells to inflamed joints via CCL20 in rheumatoid arthritis and its animal model', *J Exp Med*, 204: 2803-12.

Hou, S., A. Kijlstra, and P. Yang. 2015. 'Molecular Genetic Advances in Uveitis', *Prog Mol Biol Transl Sci*, 134: 283-98.

Hou, S., D. Liao, J. Zhang, J. Fang, L. Chen, J. Qi, Q. Zhang, Y. Liu, L. Bai, Y. Zhou, A. Kijlstra, and P. Yang. 2015. 'Genetic variations of IL17F and IL23A show associations with Behçet's disease and Vogt-Koyanagi-Harada syndrome', *Ophthalmology*, 122: 518-23.

Hsu, S. M., R. Mathew, A. W. Taylor, and J. Stein-Streilein. 2014. 'Ex-vivo tolerogenic F4/80^{+} antigen-presenting cells (APC) induce efferent CD8^{+} regulatory T cell-dependent suppression of experimental autoimmune uveitis', *Clin Exp Immunol*, 176: 37-48.

Hueber, W., B. E. Sands, S. Lewitzky, M. Vandemeulebroecke, W. Reinisch, P. D. Higgins, J. Wehkamp, B. G. Feagan, M. D. Yao, M. Karczewski, J. Karczewski, N. Pezous, S. Bek, G. Bruin, B. Mellgard, C. Berger, M. Londei, A. P. Bertolino, G. Tougas, and S. P. Travis. 2012. 'Secukinumab, a human anti-IL-17A monoclonal antibody, for moderate to severe Crohn's disease: unexpected results of a randomised, double-blind placebo-controlled trial', *Gut*, 61: 1693-700.

Ichiyama, K., H. Yoshida, Y. Wakabayashi, T. Chinen, K. Saeki, M. Nakaya, G. Takaesu, S. Hori, A. Yoshimura, and T. Kobayashi. 2008. 'Foxp3 inhibits RORgammat-mediated IL-17A mRNA transcription through direct interaction with RORgammat', *J Biol Chem*, 283: 17003-8.

Imrie, F. R., and A. D. Dick. 2007. 'Biologics in the treatment of uveitis', *Curr Opin Ophthalmol*, 18: 481-6.

In, T. S. H., A. Trotman-Grant, S. Fahl, E. L. Y. Chen, P. Zarin, A. J. Moore, D. L. Wiest, J. C. Zúñiga-Pflücker, and M. K. Anderson. 2017. 'HEB is required for the specification of fetal IL-17-producing γδ T cells', *Nat Commun*, 8: 2004.

Jaakkola, E., I. Herzberg, K. Laiho, M. C. Barnardo, J. J. Pointon, M. Kauppi, K. Kaarela, E. Tuomilehto-Wolf, J. Tuomilehto, B. P. Wordsworth, and M. A. Brown. 2006. 'Finnish HLA studies confirm the increased risk conferred by HLA-B27 homozygosity in ankylosing spondylitis', *Ann Rheum Dis*, 65: 775-80.

Jabs, D. A., R. B. Nussenblatt, and J. T. Rosenbaum. 2005. 'Standardization of uveitis nomenclature for reporting clinical data. Results of the First International Workshop', *Am J Ophthalmol*, 140: 509-16.

Jacques, P., S. Lambrecht, E. Verheugen, E. Pauwels, G. Kollias, M. Armaka, M. Verhoye, A. Van der Linden, R. Achten, R. J. Lories, and D. Elewaut. 2014. 'Proof of concept: enthesitis and new bone formation in spondyloarthritis are driven by mechanical strain and stromal cells', *Ann Rheum Dis*, 73: 437-45.

Jiang, L., H. He, P. Yang, X. Lin, H. Zhou, X. Huang, and A. Kijlstra. 2009. 'Splenic CD8+ T cells secrete TGF-beta1 to exert suppression in mice with anterior chamber-associated immune deviation', *Graefes Arch Clin Exp Ophthalmol*, 247: 87-92.

Juanola, X., E. Loza Santamaría, and M. Cordero-Coma. 2016. 'Description and Prevalence of Spondyloarthritis in Patients with Anterior Uveitis: The SENTINEL Interdisciplinary Collaborative Project', *Ophthalmology*, 123: 1632-36.

Jung, J. H., G. G. Song, J. H. Kim, Y. H. Seo, and S. J. Choi. 2017. 'The association between genetic polymorphisms of the interleukin-23 receptor gene and susceptibility to uveitis: a meta-analysis', *BMC Ophthalmol*, 17: 81.

Kaji, E. H., and J. M. Leiden. 2001. 'Gene and stem cell therapies', *Jama*, 285: 545-50.

Kanski, J. J, and B Bowling. 2011. *Clinical Ophthalmology: A Systematic Approach* (Elsevier).

Kenna, T. J., S. I. Davidson, R. Duan, L. A. Bradbury, J. McFarlane, M. Smith, H. Weedon, S. Street, R. Thomas, G. P. Thomas, and M. A. Brown. 2012. 'Enrichment of circulating interleukin-17-secreting interleukin-23 receptor-

positive γ/δ T cells in patients with active ankylosing spondylitis', *Arthritis Rheum*, 64: 1420-9.
Kerr, E. C., B. J. Raveney, D. A. Copland, A. D. Dick, and L. B. Nicholson. 2008. 'Analysis of retinal cellular infiltrate in experimental autoimmune uveoretinitis reveals multiple regulatory cell populations', *J Autoimmun*, 31: 354-61.
Khan, D., and S. Ansar Ahmed. 2015. 'Regulation of IL-17 in autoimmune diseases by transcriptional factors and microRNAs', *Front Genet*, 6: 236.
Kim, K., S. Y. Bang, S. Lee, H. S. Lee, S. C. Shim, Y. M. Kang, C. H. Suh, C. Sun, S. K. Nath, S. C. Bae, and T. H. Kim. 2015. 'An HLA-C amino-acid variant in addition to HLA-B*27 confers risk for ankylosing spondylitis in the Korean population', *Arthritis Res Ther*, 17: 342.
Kitani, A., I. Fuss, K. Nakamura, F. Kumaki, T. Usui, and W. Strober. 2003. 'Transforming growth factor (TGF)-beta1-producing regulatory T cells induce Smad-mediated interleukin 10 secretion that facilitates coordinated immunoregulatory activity and amelioration of TGF-beta1-mediated fibrosis', *J Exp Med*, 198: 1179-88.
Knickelbein, J. E., K. R. Armbrust, M. Kim, H. N. Sen, and R. B. Nussenblatt. 2017. 'Pharmacologic Treatment of Noninfectious Uveitis', *Handb Exp Pharmacol*, 242: 231-68.
Kodati, S., S. K. Chauhan, Y. Chen, T. H. Dohlman, P. Karimian, D. Saban, and R. Dana. 2014. 'CCR7 is critical for the induction and maintenance of Th17 immunity in dry eye disease', *Invest Ophthalmol Vis Sci*, 55: 5871-7.
Kolls, J. K., and A. Lindén. 2004. 'Interleukin-17 family members and inflammation', *Immunity*, 21: 467-76.
Korn, T., E. Bettelli, M. Oukka, and V. K. Kuchroo. 2009. 'IL-17 and Th17 Cells', *Annu Rev Immunol*, 27: 485-517.
Krause, U., and V. Raunio. 1969. 'Proteins of the normal human aqueous humour', *Ophthalmologica*, 159: 178-85.
Kruh, J. N., P. Yang, A. M. Suelves, and C. S. Foster. 2014. 'Infliximab for the treatment of refractory noninfectious Uveitis: a study of 88 patients with long-term follow-up', *Ophthalmology*, 121: 358-64.
Lai, T. Y. Y. 2021. 'Ocular imaging at the cutting-edge', *Eye (Lond)*, 35: 1-3.
Lambert, J. R., and V. Wright. 1976. 'Eye inflammation in psoriatic arthritis', *Ann Rheum Dis*, 35: 354-6.
Langrish, C. L., Y. Chen, W. M. Blumenschein, J. Mattson, B. Basham, J. D. Sedgwick, T. McClanahan, R. A. Kastelein, and D. J. Cua. 2005. 'IL-23 drives a pathogenic T cell population that induces autoimmune inflammation', *J Exp Med*, 201: 233-40.
Leal, I., F. B. Rodrigues, D. C. Sousa, G. S. Duarte, V. C. Romão, C. Marques-Neves, J. Costa, and J. E. Fonseca. 2019. 'Anti-TNF Drugs for Chronic Uveitis in Adults-A Systematic Review and Meta-Analysis of Randomized Controlled Trials', *Front Med (Lausanne)*, 6: 104.
Lee, E., W. L. Trepicchio, J. L. Oestreicher, D. Pittman, F. Wang, F. Chamian, M. Dhodapkar, and J. G. Krueger. 2004. 'Increased expression of interleukin 23 p19 and p40 in lesional skin of patients with psoriasis vulgaris', *J Exp Med*, 199: 125-30.
Lee, J. S., C. M. Tato, B. Joyce-Shaikh, M. F. Gulen, C. Cayatte, Y. Chen, W. M. Blumenschein, M. Judo, G. Ayanoglu, T. K. McClanahan, X. Li, and D. J. Cua. 2015. 'Interleukin-23-Independent IL-17 Production Regulates Intestinal Epithelial Permeability', *Immunity*, 43: 727-38.

Letko, E., S. Yeh, C. S. Foster, U. Pleyer, M. Brigell, and C. L. Grosskreutz. 2015. 'Efficacy and safety of intravenous secukinumab in noninfectious uveitis requiring steroid-sparing immunosuppressive therapy', *Ophthalmology*, 122: 939-48.

Levin, A. A., and A. B. Gottlieb. 2014. 'Specific targeting of interleukin-23p19 as effective treatment for psoriasis', *J Am Acad Dermatol*, 70: 555-61.

Li, Y., L. Zhu, Z. Chu, T. Yang, H. X. Sun, F. Yang, W. Wang, Y. Hou, P. Wang, Q. Zhao, Y. Tao, L. Zhang, X. Zhang, and Y. Zhao. 2018. 'Characterization and biological significance of IL-23-induced neutrophil polarization', *Cell Mol Immunol*, 15: 518-30.

Li, Z., and M. A. Brown. 2017. 'Progress of genome-wide association studies of ankylosing spondylitis', *Clin Transl Immunology*, 6: e163.

Lim, L. L., F. W. Fraunfelder, and J. T. Rosenbaum. 2007. 'Do tumor necrosis factor inhibitors cause uveitis? A registry-based study', *Arthritis Rheum*, 56: 3248-52.

Lin, P. 2015. 'Infectious Uveitis', *Curr Ophthalmol Rep*, 3: 170-83.

Littman, D. R., and A. Y. Rudensky. 2010. 'Th17 and regulatory T cells in mediating and restraining inflammation', *Cell*, 140: 845-58.

Liu, M. M., J. Tuo, and C. C. Chan. 2011. 'Gene therapy for ocular diseases', *Br J Ophthalmol*, 95: 604-12.

Lochner, M., L. Peduto, M. Cherrier, S. Sawa, F. Langa, R. Varona, D. Riethmacher, M. Si-Tahar, J. P. Di Santo, and G. Eberl. 2008. 'In vivo equilibrium of proinflammatory IL-17+ and regulatory IL-10+ Foxp3+ RORgamma t+ T cells', *J Exp Med*, 205: 1381-93.

Louveau, A., I. Smirnov, T. J. Keyes, J. D. Eccles, S. J. Rouhani, J. D. Peske, N. C. Derecki, D. Castle, J. W. Mandell, K. S. Lee, T. H. Harris, and J. Kipnis. 2015. 'Structural and functional features of central nervous system lymphatic vessels', *Nature*, 523: 337-41.

———. 2016. 'Corrigendum: Structural and functional features of central nervous system lymphatic vessels', *Nature*, 533: 278.

Lowder, C., R. Belfort, Jr., S. Lightman, C. S. Foster, M. R. Robinson, R. M. Schiffman, X. Y. Li, H. Cui, and S. M. Whitcup. 2011. 'Dexamethasone intravitreal implant for noninfectious intermediate or posterior uveitis', *Arch Ophthalmol*, 129: 545-53.

Lublin, F. D., R. L. Knobler, B. Kalman, M. Goldhaber, J. Marini, M. Perrault, C. D'Imperio, J. Joseph, S. S. Alkan, and R. Korngold. 1993. 'Monoclonal anti-gamma interferon antibodies enhance experimental allergic encephalomyelitis', *Autoimmunity*, 16: 267-74.

Luci, C., A. Reynders, Ivanov, II, C. Cognet, L. Chiche, L. Chasson, J. Hardwigsen, E. Anguiano, J. Banchereau, D. Chaussabel, M. Dalod, D. R. Littman, E. Vivier, and E. Tomasello. 2009. 'Influence of the transcription factor RORgammat on the development of NKp46+ cell populations in gut and skin', *Nat Immunol*, 10: 75-82.

Luger, D., P. B. Silver, J. Tang, D. Cua, Z. Chen, Y. Iwakura, E. P. Bowman, N. M. Sgambellone, C. C. Chan, and R. R. Caspi. 2008. 'Either a Th17 or a Th1 effector response can drive autoimmunity: conditions of disease induction affect dominant effector category', *J Exp Med*, 205: 799-810.

Lugossy, G. 1957. '[Effect of antigens on the fluorescein permeability of blood-aqueous humor barrier]', *Orv Hetil*, 98: 1380-2.

Lyons, J. L., and J. T. Rosenbaum. 1997. 'Uveitis associated with inflammatory bowel disease compared with uveitis associated with spondyloarthropathy', *Arch Ophthalmol*, 115: 61-4.

Maini, R., E. W. St Clair, F. Breedveld, D. Furst, J. Kalden, M. Weisman, J. Smolen, P. Emery, G. Harriman, M. Feldmann, and P. Lipsky. 1999. 'Infliximab (chimeric anti-tumour necrosis factor alpha monoclonal antibody) versus placebo in rheumatoid arthritis patients receiving concomitant methotrexate: a randomised phase III trial. ATTRACT Study Group', *Lancet*, 354: 1932-9.

Mangan, P. R., L. E. Harrington, D. B. O'Quinn, W. S. Helms, D. C. Bullard, C. O. Elson, R. D. Hatton, S. M. Wahl, T. R. Schoeb, and C. T. Weaver. 2006. 'Transforming growth factor-beta induces development of the T(H)17 lineage', *Nature*, 441: 231-4.

Mantegazza, R., P. Bernasconi, and P. Cavalcante. 2018. 'Myasthenia gravis: from autoantibodies to therapy', *Curr Opin Neurol*, 31: 517-25.

Marshall, G. E., A. G. Konstas, and W. R. Lee. 1993. 'Collagens in ocular tissues', *Br J Ophthalmol*, 77: 515-24.

Martin, B., K. Hirota, D. J. Cua, B. Stockinger, and M. Veldhoen. 2009. 'Interleukin-17-producing gammadelta T cells selectively expand in response to pathogen products and environmental signals', *Immunity*, 31: 321-30.

Martin, T. M., J. R. Smith, and J. T. Rosenbaum. 2002. 'Anterior uveitis: current concepts of pathogenesis and interactions with the spondyloarthropathies', *Curr Opin Rheumatol*, 14: 337-41.

Mathur, A. N., H. C. Chang, D. G. Zisoulis, G. L. Stritesky, Q. Yu, J. T. O'Malley, R. Kapur, D. E. Levy, G. S. Kansas, and M. H. Kaplan. 2007. 'Stat3 and Stat4 direct development of IL-17-secreting Th cells', *J Immunol*, 178: 4901-7.

Mattapallil, M. J., E. F. Wawrousek, C. C. Chan, H. Zhao, J. Roychoudhury, T. A. Ferguson, and R. R. Caspi. 2012. 'The Rd8 mutation of the Crb1 gene is present in vendor lines of C57BL/6N mice and embryonic stem cells, and confounds ocular induced mutant phenotypes', *Invest Ophthalmol Vis Sci*, 53: 2921-7.

Maxwell, J. R., Y. Zhang, W. A. Brown, C. L. Smith, F. R. Byrne, M. Fiorino, E. Stevens, J. Bigler, J. A. Davis, J. B. Rottman, A. L. Budelsky, A. Symons, and J. E. Towne. 2015. 'Differential Roles for Interleukin-23 and Interleukin-17 in Intestinal Immunoregulation', *Immunity*, 43: 739-50.

McDonald, D. R. 2012. 'TH17 deficiency in human disease', *J Allergy Clin Immunol*, 129: 1429-35; quiz 36-7.

McGeachy, M. J., Y. Chen, C. M. Tato, A. Laurence, B. Joyce-Shaikh, W. M. Blumenschein, T. K. McClanahan, J. J. O'Shea, and D. J. Cua. 2009. 'The interleukin 23 receptor is essential for the terminal differentiation of interleukin 17-producing effector T helper cells in vivo', *Nat Immunol*, 10: 314-24.

McGeachy, M. J., D. J. Cua, and S. L. Gaffen. 2019. 'The IL-17 Family of Cytokines in Health and Disease', *Immunity*, 50: 892-906.

McGhee, C. N. 1992. 'Pharmacokinetics of ophthalmic corticosteroids', *Br J Ophthalmol*, 76: 681-4.

McGonagle, D., and T. Georgouli. 2008. 'The importance of 'Mechnikov's thorn' for an improved understanding of 21st century medicine and immunology: a view from the eye', *Scand J Immunol*, 68: 129-39.

McGonagle, D., L. Stockwin, J. Isaacs, and P. Emery. 2001. 'An enthesitis based model for the pathogenesis of spondyloarthropathy. additive effects of microbial adjuvant and biomechanical factors at disease sites', *J Rheumatol*, 28: 2155-9.

McGonagle, D., R. C. Thomas, and G. Schett. 2014. 'Spondyloarthritis: may the force be with you?', *Ann Rheum Dis*, 73: 321-3.
McInnes, I. B., A. Kavanaugh, A. B. Gottlieb, L. Puig, P. Rahman, C. Ritchlin, C. Brodmerkel, S. Li, Y. Wang, A. M. Mendelsohn, and M. K. Doyle. 2013. 'Efficacy and safety of ustekinumab in patients with active psoriatic arthritis: 1 year results of the phase 3, multicentre, double-blind, placebo-controlled PSUMMIT 1 trial', *Lancet*, 382: 780-9.
McKenzie, B. S., R. A. Kastelein, and D. J. Cua. 2006. 'Understanding the IL-23-IL-17 immune pathway', *Trends Immunol*, 27: 17-23.
McKenzie, D. R., E. E. Kara, C. R. Bastow, T. S. Tyllis, K. A. Fenix, C. E. Gregor, J. J. Wilson, R. Babb, J. C. Paton, A. Kallies, S. L. Nutt, A. Brüstle, M. Mack, I. Comerford, and S. R. McColl. 2017. 'IL-17-producing γδ T cells switch migratory patterns between resting and activated states', *Nat Commun*, 8: 15632.
McMenamin, P. G. 1997. 'The distribution of immune cells in the uveal tract of the normal eye', *Eye (Lond)*, 11 (Pt 2): 183-93.
———. 1999. 'Dendritic cells and macrophages in the uveal tract of the normal mouse eye', *Br J Ophthalmol*, 83: 598-604.
McMenamin, P. G., D. R. Saban, and S. J. Dando. 2019. 'Immune cells in the retina and choroid: Two different tissue environments that require different defenses and surveillance', *Prog Retin Eye Res*, 70: 85-98.
Mease, P. J., I. B. McInnes, B. Kirkham, A. Kavanaugh, P. Rahman, D. van der Heijde, R. Landewé, P. Nash, L. Pricop, J. Yuan, H. B. Richards, and S. Mpofu. 2015. 'Secukinumab Inhibition of Interleukin-17A in Patients with Psoriatic Arthritis', *N Engl J Med*, 373: 1329-39.
Mease, P. J., P. Rahman, A. B. Gottlieb, A. P. Kollmeier, E. C. Hsia, X. L. Xu, S. Sheng, P. Agarwal, B. Zhou, Y. Zhuang, D. van der Heijde, and I. B. McInnes. 2020. 'Guselkumab in biologic-naive patients with active psoriatic arthritis (DISCOVER-2): a double-blind, randomised, placebo-controlled phase 3 trial', *Lancet*, 395: 1126-36.
Mease, P. J., D. van der Heijde, C. T. Ritchlin, M. Okada, R. S. Cuchacovich, C. L. Shuler, C. Y. Lin, D. K. Braun, C. H. Lee, and D. D. Gladman. 2017. 'Ixekizumab, an interleukin-17A specific monoclonal antibody, for the treatment of biologic-naive patients with active psoriatic arthritis: results from the 24-week randomised, double-blind, placebo-controlled and active (adalimumab)-controlled period of the phase III trial SPIRIT-P1', *Ann Rheum Dis*, 76: 79-87.
Medawar, P. B. 1948. 'Immunity to homologous grafted skin; the fate of skin homografts transplanted to the brain, to subcutaneous tissue, and to the anterior chamber of the eye', *Br J Exp Pathol*, 29: 58-69.
Mei, Y., F. Pan, J. Gao, R. Ge, Z. Duan, Z. Zeng, F. Liao, G. Xia, S. Wang, S. Xu, J. Xu, L. Zhang, and D. Ye. 2011. 'Increased serum IL-17 and IL-23 in the patient with ankylosing spondylitis', *Clin Rheumatol*, 30: 269-73.
Mercier, A. E., E. Ribeiro, J. F. Korobelnik, M. N. Delyfer, and M. B. Rougier. 2018. 'Efficacy of Anti-TNF-α Therapy for the Treatment of Non-infectious Uveitis: A Retrospective Study of 21 Patients', *Ocul Immunol Inflamm*, 26: 477-84.
Milz, S., M. Benjamin, and R. Putz. 2005. 'Molecular parameters indicating adaptation to mechanical stress in fibrous connective tissue', *Adv Anat Embryol Cell Biol*, 178: 1-71.
Milz, S., A. Rufai, A. Buettner, R. Putz, J. R. Ralphs, and M. Benjamin. 2002. 'Three-dimensional reconstructions of the Achilles tendon insertion in man', *J Anat*, 200: 145-52.

Milz, S., T. Tischer, A. Buettner, M. Schieker, M. Maier, S. Redman, P. Emery, D. McGonagle, and M. Benjamin. 2004. 'Molecular composition and pathology of entheses on the medial and lateral epicondyles of the humerus: a structural basis for epicondylitis', *Ann Rheum Dis*, 63: 1015-21.

Miserocchi, E., G. Fogliato, G. Modorati, and F. Bandello. 2013. 'Review on the worldwide epidemiology of uveitis', *Eur J Ophthalmol*, 23: 705-17.

Mitulescu, T. C., M. Trandafir, M. G. Dimăncescu, R. C. Ciuluvică, V. Popescu, D. Predeșteanu, S. Istrate, and L. M. Voinea. 2018. 'Advances in the treatment of uveitis in patients with spondyloarthritis - is it the time for biologic therapy?', *Rom J Ophthalmol*, 62: 114-22.

Moll, J. M., G. Johnson, and V. Wright. 1974. 'Psoriatic arthritis: a unique family', *Rheumatol Rehabil*, 13: 154-7.

Mombaerts, P., J. Iacomini, R. S. Johnson, K. Herrup, S. Tonegawa, and V. E. Papaioannou. 1992. 'RAG-1-deficient mice have no mature B and T lymphocytes', *Cell*, 68: 869-77.

Monnet, D., M. Breban, C. Hudry, M. Dougados, and A. P. Brézin. 2004. 'Ophthalmic findings and frequency of extraocular manifestations in patients with HLA-B27 uveitis: a study of 175 cases', *Ophthalmology*, 111: 802-9.

Morrison, J. C., and E. M. Van Buskirk. 1983. 'Anterior collateral circulation in the primate eye', *Ophthalmology*, 90: 707-15.

Mosmann, T. R., H. Cherwinski, M. W. Bond, M. A. Giedlin, and R. L. Coffman. 1986. 'Two types of murine helper T cell clone. I. Definition according to profiles of lymphokine activities and secreted proteins', *J Immunol*, 136: 2348-57.

Mugheddu, C., L. Atzori, M. Del Piano, A. Lappi, M. Pau, S. Murgia, I. Zucca, and F. Rongioletti. 2017. 'Successful ustekinumab treatment of noninfectious uveitis and concomitant severe psoriatic arthritis and plaque psoriasis', *Dermatol Ther*, 30.

Muñoz-Fernández, S., and E. Martín-Mola. 2006. 'Uveitis', *Best Pract Res Clin Rheumatol*, 20: 487-505.

Muñoz-Ruiz, M., N. Sumaria, D. J. Pennington, and B. Silva-Santos. 2017. 'Thymic Determinants of γδ T Cell Differentiation', *Trends Immunol*, 38: 336-44.

Murphy, C. A., C. L. Langrish, Y. Chen, W. Blumenschein, T. McClanahan, R. A. Kastelein, J. D. Sedgwick, and D. J. Cua. 2003. 'Divergent pro- and antiinflammatory roles for IL-23 and IL-12 in joint autoimmune inflammation', *J Exp Med*, 198: 1951-7.

Murphy, C. C., K. Greiner, J. Plskova, N. A. Frost, J. V. Forrester, and A. D. Dick. 2007. 'Validity of using vision-related quality of life as a treatment end point in intermediate and posterior uveitis', *Br J Ophthalmol*, 91: 154-6.

Narayan, K., K. E. Sylvia, N. Malhotra, C. C. Yin, G. Martens, T. Vallerskog, H. Kornfeld, N. Xiong, N. R. Cohen, M. B. Brenner, L. J. Berg, and J. Kang. 2012. 'Intrathymic programming of effector fates in three molecularly distinct γδ T cell subtypes', *Nat Immunol*, 13: 511-8.

Nasution, A. R., A. Mardjuadi, S. Kunmartini, N. G. Suryadhana, B. Setyohadi, D. Sudarsono, N. M. Lardy, and T. E. Feltkamp. 1997. 'HLA-B27 subtypes positively and negatively associated with spondyloarthropathy', *J Rheumatol*, 24: 1111-4.

Nayak, S., and R. W. Herzog. 2010. 'Progress and prospects: immune responses to viral vectors', *Gene Ther*, 17: 295-304.

Neerinckx, B., S. Carter, and R. J. Lories. 2014. 'No evidence for a critical role of the unfolded protein response in synovium and blood of patients with ankylosing spondylitis', *Ann Rheum Dis*, 73: 629-30.

Németh, T., A. Mócsai, and C. A. Lowell. 2016. 'Neutrophils in animal models of autoimmune disease', *Semin Immunol*, 28: 174-86.

Neumann, A., J. Haschka, A. Kleyer, L. Schuster, M. Englbrecht, A. Berlin, C. P. Figueiredo, D. Simon, C. Muschitz, R. Kocijan, H. Resch, J. Rech, and G. Schett. 2018. 'Cortical bone loss is an early feature of nonradiographic axial spondyloarthritis', *Arthritis Res Ther*, 20: 202.

Newton, R. H., and K. M. Meek. 1998. 'Circumcorneal annulus of collagen fibrils in the human limbus', *Invest Ophthalmol Vis Sci*, 39: 1125-34.

Nian, H., D. Liang, A. Zuo, R. Wei, H. Shao, W. K. Born, H. J. Kaplan, and D. Sun. 2012. 'Characterization of autoreactive and bystander IL-17+ T cells induced in immunized C57BL/6 mice', *Invest Ophthalmol Vis Sci*, 53: 897-905.

Noack, M., N. Ndongo-Thiam, and P. Miossec. 2016. 'Interaction among activated lymphocytes and mesenchymal cells through podoplanin is critical for a high IL-17 secretion', *Arthritis Res Ther*, 18: 148.

Noske, W., B. Levarlet, K. M. Kreusel, M. Fromm, and M. Hirsch. 1994. 'Tight junctions and paracellular permeability in cultured bovine corneal endothelial cells', *Graefes Arch Clin Exp Ophthalmol*, 232: 608-13.

Oppmann, B., R. Lesley, B. Blom, J. C. Timans, Y. Xu, B. Hunte, F. Vega, N. Yu, J. Wang, K. Singh, F. Zonin, E. Vaisberg, T. Churakova, M. Liu, D. Gorman, J. Wagner, S. Zurawski, Y. Liu, J. S. Abrams, K. W. Moore, D. Rennick, R. de Waal-Malefyt, C. Hannum, J. F. Bazan, and R. A. Kastelein. 2000. 'Novel p19 protein engages IL-12p40 to form a cytokine, IL-23, with biological activities similar as well as distinct from IL-12', *Immunity*, 13: 715-25.

Paiva, E. S., D. C. Macaluso, A. Edwards, and J. T. Rosenbaum. 2000. 'Characterisation of uveitis in patients with psoriatic arthritis', *Ann Rheum Dis*, 59: 67-70.

Pang, J., M. Cheng, S. E. Haire, E. Barker, V. Planelles, and J. C. Blanks. 2006. 'Efficiency of lentiviral transduction during development in normal and rd mice', *Mol Vis*, 12: 756-67.

Papp, K. A., A. Blauvelt, M. Bukhalo, M. Gooderham, J. G. Krueger, J. P. Lacour, A. Menter, S. Philipp, H. Sofen, S. Tyring, B. R. Berner, S. Visvanathan, C. Pamulapati, N. Bennett, M. Flack, P. Scholl, and S. J. Padula. 2017. 'Risankizumab versus Ustekinumab for Moderate-to-Severe Plaque Psoriasis', *N Engl J Med*, 376: 1551-60.

Parham, C., M. Chirica, J. Timans, E. Vaisberg, M. Travis, J. Cheung, S. Pflanz, R. Zhang, K. P. Singh, F. Vega, W. To, J. Wagner, A. M. O'Farrell, T. McClanahan, S. Zurawski, C. Hannum, D. Gorman, D. M. Rennick, R. A. Kastelein, R. de Waal Malefyt, and K. W. Moore. 2002. 'A receptor for the heterodimeric cytokine IL-23 is composed of IL-12Rbeta1 and a novel cytokine receptor subunit, IL-23R', *J Immunol*, 168: 5699-708.

Parsanejad, R., W. R. Fields, T. J. Steichen, B. R. Bombick, and D. J. Doolittle. 2008. 'Distinct regulatory profiles of interleukins and chemokines in response to cigarette smoke condensate in normal human bronchial epithelial (NHBE) cells', *J Interferon Cytokine Res*, 28: 703-12.

Patel, D. V., A. Horne, M. House, I. R. Reid, and C. N. McGhee. 2013. 'The incidence of acute anterior uveitis after intravenous zoledronate', *Ophthalmology*, 120: 773-6.

Paunicka, K., P. W. Chen, and J. Y. Niederkorn. 2012. 'Role of IFN-γ in the establishment of anterior chamber-associated immune deviation (ACAID)-induced CD8+ T regulatory cells', *J Leukoc Biol*, 91: 475-83.

Peluso, R., S. Iervolino, M. Vitiello, V. Bruner, G. Lupoli, and M. N. Di Minno. 2015. 'Extra-articular manifestations in psoriatic arthritis patients', *Clin Rheumatol*, 34: 745-53.

Poetker, D. M., and D. D. Reh. 2010. 'A comprehensive review of the adverse effects of systemic corticosteroids', *Otolaryngol Clin North Am*, 43: 753-68.

Polansky, J. R., I. S. Wood, M. T. Maglio, and J. A. Alvarado. 1984. 'Trabecular meshwork cell culture in glaucoma research: evaluation of biological activity and structural properties of human trabecular cells in vitro', *Ophthalmology*, 91: 580-95.

Prinz, I., B. Silva-Santos, and D. J. Pennington. 2013. 'Functional development of γδ T cells', *Eur J Immunol*, 43: 1988-94.

Przepiera-Będzak, H., K. Fischer, and M. Brzosko. 2016. 'Extra-Articular Symptoms in Constellation with Selected Serum Cytokines and Disease Activity in Spondyloarthritis', *Mediators Inflamm*, 2016: 7617954.

Raveney, B. J., D. A. Copland, L. B. Nicholson, and A. D. Dick. 2008. 'Fingolimod (FTY720) as an acute rescue therapy for intraocular inflammatory disease', *Arch Ophthalmol*, 126: 1390-5.

Raviola, G. 1971. 'The fine structure of the ciliary zonule and ciliary epithelium. With special regard to the organization and insertion of the zonular fibrils', *Invest Ophthalmol*, 10: 851-69.

———. 1974. 'Effects of paracentesis on the blood-aqueous barrier: an electron microscope study on Macaca mulatta using horseradish peroxidase as a tracer', *Invest Ophthalmol*, 13: 828-58.

———. 1977. 'The structural basis of the blood-ocular barriers', *Exp Eye Res*, 25 Suppl: 27-63.

———. 1982. 'Schwalbe line's cells: a new cell type in the trabecular meshwork of Macaca mulatta', *Invest Ophthalmol Vis Sci*, 22: 45-56.

Raviola, G., and E. Raviola. 1978. 'Intercellular junctions in the ciliary epithelium', *Invest Ophthalmol Vis Sci*, 17: 958-81.

Reich, K., A. W. Armstrong, P. Foley, M. Song, Y. Wasfi, B. Randazzo, S. Li, Y. K. Shen, and K. B. Gordon. 2017. 'Efficacy and safety of guselkumab, an anti-interleukin-23 monoclonal antibody, compared with adalimumab for the treatment of patients with moderate to severe psoriasis with randomized withdrawal and retreatment: Results from the phase III, double-blind, placebo- and active comparator-controlled VOYAGE 2 trial', *J Am Acad Dermatol*, 76: 418-31.

Reinhardt, A., T. Yevsa, T. Worbs, S. Lienenklaus, I. Sandrock, L. Oberdörfer, T. Korn, S. Weiss, R. Förster, and I. Prinz. 2016. 'Interleukin-23-Dependent γ/δ T Cells Produce Interleukin-17 and Accumulate in the Enthesis, Aortic Valve, and Ciliary Body in Mice', *Arthritis Rheumatol*, 68: 2476-86.

Reveille, J. D., A. M. Sims, P. Danoy, D. M. Evans, P. Leo, J. J. Pointon, R. Jin, X. Zhou, L. A. Bradbury, L. H. Appleton, J. C. Davis, L. Diekman, T. Doan, A. Dowling, R. Duan, E. L. Duncan, C. Farrar, J. Hadler, D. Harvey, T. Karaderi, R. Mogg, E. Pomeroy, K. Pryce, J. Taylor, L. Savage, P. Deloukas, V. Kumanduri, L. Peltonen, S. M. Ring, P. Whittaker, E. Glazov, G. P. Thomas, W. P. Maksymowych, R. D. Inman, M. M. Ward, M. A. Stone, M. H. Weisman, B. P. Wordsworth, and M. A. Brown. 2010. 'Genome-wide association study of

ankylosing spondylitis identifies non-MHC susceptibility loci', *Nat Genet*, 42: 123-7.

Rezaiemanesh, A., M. Mahmoudi, A. A. Amirzargar, M. Vojdanian, A. R. Jamshidi, and M. H. Nicknam. 2017. 'Ankylosing spondylitis M-CSF-derived macrophages are undergoing unfolded protein response (UPR) and express higher levels of interleukin-23', *Mod Rheumatol*, 27: 862-67.

Ribot, J. C., A. deBarros, D. J. Pang, J. F. Neves, V. Peperzak, S. J. Roberts, M. Girardi, J. Borst, A. C. Hayday, D. J. Pennington, and B. Silva-Santos. 2009. 'CD27 is a thymic determinant of the balance between interferon-gamma- and interleukin 17-producing gammadelta T cell subsets', *Nat Immunol*, 10: 427-36.

Robinson, P. C., T. A. Claushuis, A. Cortes, T. M. Martin, D. M. Evans, P. Leo, P. Mukhopadhyay, L. A. Bradbury, K. Cremin, J. Harris, W. P. Maksymowych, R. D. Inman, P. Rahman, N. Haroon, L. Gensler, J. E. Powell, I. E. van der Horst-Bruinsma, A. W. Hewitt, J. E. Craig, L. L. Lim, D. Wakefield, P. McCluskey, V. Voigt, P. Fleming, M. Degli-Esposti, J. J. Pointon, M. H. Weisman, B. P. Wordsworth, J. D. Reveille, J. T. Rosenbaum, and M. A. Brown. 2015. 'Genetic dissection of acute anterior uveitis reveals similarities and differences in associations observed with ankylosing spondylitis', *Arthritis Rheumatol*, 67: 140-51.

Robinson, P. C., P. J. Leo, J. J. Pointon, J. Harris, K. Cremin, L. A. Bradbury, S. Stebbings, A. A. Harrison, E. L. Duncan, D. M. Evans, P. B. Wordsworth, and M. A. Brown. 2016. 'Exome-wide study of ankylosing spondylitis demonstrates additional shared genetic background with inflammatory bowel disease', *NPJ Genom Med*, 1: 16008.

Rohen, J. W., R. Futa, and E. Lütjen-Drecoll. 1981. 'The fine structure of the cribriform meshwork in normal and glaucomatous eyes as seen in tangential sections', *Invest Ophthalmol Vis Sci*, 21: 574-85.

Rohen, J. W., and E. van der Zypen. 1968. 'The phagocytic activity of the trabecularmeshwork endothelium. An electron-microscopic study of the vervet (Cercopithecus aethiops)', *Albrecht Von Graefes Arch Klin Exp Ophthalmol*, 175: 143-60.

Roldan, C. A., J. Chavez, P. W. Wiest, C. R. Qualls, and M. H. Crawford. 1998. 'Aortic root disease and valve disease associated with ankylosing spondylitis', *J Am Coll Cardiol*, 32: 1397-404.

Rosenbaum, J. T. 1989. 'Characterization of uveitis associated with spondyloarthritis', *J Rheumatol*, 16: 792-6.

———. 2015. 'Nibbling away at the diagnosis of idiopathic uveitis', *JAMA Ophthalmol*, 133: 146-7.

———. 2019. 'The eye in spondyloarthritis(☆)', *Semin Arthritis Rheum*, 49: S29-s31.

Rosenbaum, J. T., and A. D. Dick. 2018. 'The Eyes Have it: A Rheumatologist's View of Uveitis', *Arthritis Rheumatol*, 70: 1533-43.

Rossi, D. C., C. Ribi, and Y. Guex-Crosier. 2019. 'Treatment of chronic non-infectious uveitis and scleritis', *Swiss Med Wkly*, 149: w20025.

Rothova, A., T. T. Berendschot, K. Probst, B. van Kooij, and G. S. Baarsma. 2004. 'Birdshot chorioretinopathy: long-term manifestations and visual prognosis', *Ophthalmology*, 111: 954-9.

Rothova, A., M. S. Suttorp-van Schulten, W. Frits Treffers, and A. Kijlstra. 1996. 'Causes and frequency of blindness in patients with intraocular inflammatory disease', *Br J Ophthalmol*, 80: 332-6.

Rothschild, B. 2013. 'Mechanical solution for a mechanical problem: Tennis elbow', *World J Orthop*, 4: 103-6.

Rua, R., and D. B. McGavern. 2018. 'Advances in Meningeal Immunity', *Trends Mol Med*, 24: 542-59.

Rudwaleit, M., and D. Baeten. 2006. 'Ankylosing spondylitis and bowel disease', *Best Pract Res Clin Rheumatol*, 20: 451-71.

Sakaguchi, N., T. Takahashi, H. Hata, T. Nomura, T. Tagami, S. Yamazaki, T. Sakihama, T. Matsutani, I. Negishi, S. Nakatsuru, and S. Sakaguchi. 2003. 'Altered thymic T-cell selection due to a mutation of the ZAP-70 gene causes autoimmune arthritis in mice', *Nature*, 426: 454-60.

Sakaguchi, S., N. Sakaguchi, H. Yoshitomi, H. Hata, T. Takahashi, and T. Nomura. 2006. 'Spontaneous development of autoimmune arthritis due to genetic anomaly of T cell signal transduction: Part 1', *Semin Immunol*, 18: 199-206.

Sanos, S. L., V. L. Bui, A. Mortha, K. Oberle, C. Heners, C. Johner, and A. Diefenbach. 2009. 'RORgammat and commensal microflora are required for the differentiation of mucosal interleukin 22-producing NKp46+ cells', *Nat Immunol*, 10: 83-91.

Satoh-Takayama, N., C. A. Vosshenrich, S. Lesjean-Pottier, S. Sawa, M. Lochner, F. Rattis, J. J. Mention, K. Thiam, N. Cerf-Bensussan, O. Mandelboim, G. Eberl, and J. P. Di Santo. 2008. 'Microbial flora drives interleukin 22 production in intestinal NKp46+ cells that provide innate mucosal immune defense', *Immunity*, 29: 958-70.

Savage, L., M. Goodfield, L. Horton, A. Watad, E. Hensor, P. Emery, R. Wakefield, M. Wittmann, and D. McGonagle. 2019. 'Regression of Peripheral Subclinical Enthesopathy in Therapy-Naive Patients Treated With Ustekinumab for Moderate-to-Severe Chronic Plaque Psoriasis: A Fifty-Two-Week, Prospective, Open-Label Feasibility Study', *Arthritis Rheumatol*, 71: 626-31.

Schlosstein, L., P. I. Terasaki, R. Bluestone, and C. M. Pearson. 1973. 'High association of an HL-A antigen, W27, with ankylosing spondylitis', *N Engl J Med*, 288: 704-6.

Sharif, K., C. Bridgewood, S. Dubash, and D. McGonagle. 2020. 'Intestinal and enthesis innate immunity in early axial spondyloarthropathy', *Rheumatology (Oxford)*, 59: iv67-iv78.

Sharma, S. M., E. Damato, A. E. Hinchcliffe, C. D. Andrews, K. Myint, R. Lee, and A. D. Dick. 2019. 'Long-term efficacy and tolerability of TNFα inhibitors in the treatment of non-infectious ocular inflammation: an 8-year prospective surveillance study', *Br J Ophthalmol*.

Sharma, S. M., A. D. Dick, and A. V. Ramanan. 2009. 'Non-infectious pediatric uveitis: an update on immunomodulatory management', *Paediatr Drugs*, 11: 229-41.

Sharma, S. M., and D. Jackson. 2017. 'Uveitis and spondyloarthropathies', *Best Pract Res Clin Rheumatol*, 31: 846-62.

Shen, H., J. C. Goodall, and J. S. Hill Gaston. 2009. 'Frequency and phenotype of peripheral blood Th17 cells in ankylosing spondylitis and rheumatoid arthritis', *Arthritis Rheum*, 60: 1647-56.

Sherlock, J. P., B. Joyce-Shaikh, S. P. Turner, C. C. Chao, M. Sathe, J. Grein, D. M. Gorman, E. P. Bowman, T. K. McClanahan, J. H. Yearley, G. Eberl, C. D. Buckley, R. A. Kastelein, R. H. Pierce, D. M. Laface, and D. J. Cua. 2012. 'IL-23 induces spondyloarthropathy by acting on ROR-γt+ CD3+CD4-CD8- entheseal resident T cells', *Nat Med*, 18: 1069-76.

Shi, Q., Z. Yin, B. Zhao, F. Sun, H. Yu, X. Yin, L. Zhang, and S. Wang. 2015. 'PGE2 Elevates IL-23 Production in Human Dendritic Cells via a cAMP Dependent Pathway', *Mediators Inflamm*, 2015: 984690.

Shiose, Y. 1970. '[Morphological study on the permeability of the blood aqueous barrier]', *Nippon Ganka Gakkai Zasshi*, 74: 1248-55.

Shiose, Y., and M. Oguri. 1969. '[Electron microscopic studies on the blood-retinal barrier and the blood-aqueous barrier]', *Nippon Ganka Gakkai Zasshi*, 73: 1606-22.

Sieper, J., J. Braun, M. Dougados, and D. Baeten. 2015. 'Axial spondyloarthritis', *Nat Rev Dis Primers*, 1: 15013.

Simon, D., A. Kleyer, S. Bayat, K. Tascilar, E. Kampylafka, T. Meinderink, L. Schuster, R. Petrov, A. M. Liphardt, J. Rech, G. Schett, and A. J. Hueber. 2019. 'Effect of disease-modifying anti-rheumatic drugs on bone structure and strength in psoriatic arthritis patients', *Arthritis Res Ther*, 21: 162.

Smith, J. R., R. M. Braziel, S. Paoletti, M. Lipp, M. Uguccioni, and J. T. Rosenbaum. 2003. 'Expression of B-cell-attracting chemokine 1 (CXCL13) by malignant lymphocytes and vascular endothelium in primary central nervous system lymphoma', *Blood*, 101: 815-21.

Smith, J. R., J. T. Rosenbaum, D. J. Wilson, N. D. Doolittle, T. Siegal, E. A. Neuwelt, and J. Pe'er. 2002. 'Role of intravitreal methotrexate in the management of primary central nervous system lymphoma with ocular involvement', *Ophthalmology*, 109: 1709-16.

Smith, R. S. 1971. 'Ultrastructural studies of the blood-aqueous barrier. I. Transport of an electron-dense tracer in the iris and ciliary body of the mouse', *Am J Ophthalmol*, 71: 1066-77.

Sonsino, J., H. Gong, P. Wu, and T. F. Freddo. 2002. 'Co-localization of junction-associated proteins of the human blood--aqueous barrier: occludin, ZO-1 and F-actin', *Exp Eye Res*, 74: 123-9.

Sood, A. B., and S. T. Angeles-Han. 2017. 'An Update on Treatment of Pediatric Chronic Non-Infectious Uveitis', *Curr Treatm Opt Rheumatol*, 3: 1-16.

Spaide, R. F., J. G. Fujimoto, N. K. Waheed, S. R. Sadda, and G. Staurenghi. 2018. 'Optical coherence tomography angiography', *Prog Retin Eye Res*, 64: 1-55.

Stamer, W. D. 2012. 'The cell and molecular biology of glaucoma: mechanisms in the conventional outflow pathway', *Invest Ophthalmol Vis Sci*, 53: 2470-2.

Stamer, W. D., and T. S. Acott. 2012. 'Current understanding of conventional outflow dysfunction in glaucoma', *Curr Opin Ophthalmol*, 23: 135-43.

Sumaria, N., C. L. Grandjean, B. Silva-Santos, and D. J. Pennington. 2017. 'Strong TCRγδ Signaling Prohibits Thymic Development of IL-17A-Secreting γδ T Cells', *Cell Rep*, 19: 2469-76.

Sun, D., D. Liang, H. J. Kaplan, and H. Shao. 2015. 'The role of Th17-associated cytokines in the pathogenesis of experimental autoimmune uveitis (EAU)', *Cytokine*, 74: 76-80.

Sutton, C. E., S. J. Lalor, C. M. Sweeney, C. F. Brereton, E. C. Lavelle, and K. H. Mills. 2009. 'Interleukin-1 and IL-23 induce innate IL-17 production from gammadelta T cells, amplifying Th17 responses and autoimmunity', *Immunity*, 31: 331-41.

Suttorp-Schulten, M. S., and A. Rothova. 1996. 'The possible impact of uveitis in blindness: a literature survey', *Br J Ophthalmol*, 80: 844-8.

Takatori, H., Y. Kanno, W. T. Watford, C. M. Tato, G. Weiss, Ivanov, II, D. R. Littman, and J. J. O'Shea. 2009. 'Lymphoid tissue inducer-like cells are an innate source of IL-17 and IL-22', *J Exp Med*, 206: 35-41.

Tam, A. L., N. Gupta, Z. Zhang, and Y. H. Yücel. 2011. 'Quantum dots trace lymphatic drainage from the mouse eye', *Nanotechnology*, 22: 425101.
———. 2013. 'Latanoprost Stimulates Ocular Lymphatic Drainage: An In Vivo Nanotracer Study', *Transl Vis Sci Technol*, 2: 3.
Taurog, J. D. 2007. 'The mystery of HLA-B27: if it isn't one thing, it's another', *Arthritis Rheum*, 56: 2478-81.
Taurog, J. D., A. Chhabra, and R. A. Colbert. 2016. 'Ankylosing Spondylitis and Axial Spondyloarthritis', *N Engl J Med*, 374: 2563-74.
Tesmer, L. A., S. K. Lundy, S. Sarkar, and D. A. Fox. 2008. 'Th17 cells in human disease', *Immunol Rev*, 223: 87-113.
Thaçi, D., A. Blauvelt, K. Reich, T. F. Tsai, F. Vanaclocha, K. Kingo, M. Ziv, A. Pinter, S. Hugot, R. You, and M. Milutinovic. 2015. 'Secukinumab is superior to ustekinumab in clearing skin of subjects with moderate to severe plaque psoriasis: CLEAR, a randomized controlled trial', *J Am Acad Dermatol*, 73: 400-9.
Trivedi, A., and C. Katelaris. 2019. 'The use of biologic agents in the management of uveitis', *Intern Med J*, 49: 1352-63.
Tsirouki, T., A. Dastiridou, C. Symeonidis, O. Tounakaki, I. Brazitikou, C. Kalogeropoulos, and S. Androudi. 2018. 'A Focus on the Epidemiology of Uveitis', *Ocul Immunol Inflamm*, 26: 2-16.
Tugal-Tutkun, I., S. Onal, R. Altan-Yaycioglu, H. Huseyin Altunbas, and M. Urgancioglu. 2004. 'Uveitis in Behçet disease: an analysis of 880 patients', *Am J Ophthalmol*, 138: 373-80.
Turchinovich, G., and A. C. Hayday. 2011. 'Skint-1 identifies a common molecular mechanism for the development of interferon-γ-secreting versus interleukin-17-secreting γδ T cells', *Immunity*, 35: 59-68.
Turner, M. J., D. P. Sowders, M. L. DeLay, R. Mohapatra, S. Bai, J. A. Smith, J. R. Brandewie, J. D. Taurog, and R. A. Colbert. 2005. 'HLA-B27 misfolding in transgenic rats is associated with activation of the unfolded protein response', *J Immunol*, 175: 2438-48.
Ugorski, M., P. Dziegiel, and J. Suchanski. 2016. 'Podoplanin - a small glycoprotein with many faces', *Am J Cancer Res*, 6: 370-86.
Ugur, M., N. K. Baygutalp, M. A. Melikoglu, F. Baygutalp, E. U. Altas, and B. Seferoglu. 2015. 'Elevated serum interleukin-23 levels in ankylosing spondylitis patients and the relationship with disease activity', *Nagoya J Med Sci*, 77: 621-7.
Valenzuela, R. A., I. Flores, B. Urrutia, F. Fuentes, P. E. Sabat, C. Llanos, L. Cuitino, and C. A. Urzua. 2020. 'New Pharmacological Strategies for the Treatment of Non-Infectious Uveitis. A Minireview', *Front Pharmacol*, 11: 655.
Vallet, H., P. Seve, L. Biard, J. Baptiste Fraison, P. Bielefeld, L. Perard, B. Bienvenu, S. Abad, A. Rigolet, A. Deroux, D. Sene, A. Perlat, I. Marie, E. Feurer, E. Hachulla, O. Fain, G. Clavel, S. Riviere, P. A. Bouche, J. Gueudry, G. Pugnet, P. Le Hoang, M. Resche Rigon, P. Cacoub, B. Bodaghi, and D. Saadoun. 2016. 'Infliximab Versus Adalimumab in the Treatment of Refractory Inflammatory Uveitis: A Multicenter Study From the French Uveitis Network', *Arthritis Rheumatol*, 68: 1522-30.
Van Buskirk, E. M. 1989. 'The anatomy of the limbus', *Eye (Lond)*, 3 (Pt 2): 101-8.
van der Heijde, D., J. Cheng-Chung Wei, M. Dougados, P. Mease, A. Deodhar, W. P. Maksymowych, F. Van den Bosch, J. Sieper, T. Tomita, R. Landewé, F. Zhao, E. Krishnan, D. H. Adams, B. Pangallo, and H. Carlier. 2018. 'Ixekizumab, an interleukin-17A antagonist in the treatment of ankylosing spondylitis or

radiographic axial spondyloarthritis in patients previously untreated with biological disease-modifying anti-rheumatic drugs (COAST-V): 16 week results of a phase 3 randomised, double-blind, active-controlled and placebo-controlled trial', *Lancet*, 392: 2441-51.

van Hamburg, J. P., P. S. Asmawidjaja, N. Davelaar, A. M. Mus, E. M. Colin, J. M. Hazes, R. J. Dolhain, and E. Lubberts. 2011. 'Th17 cells, but not Th1 cells, from patients with early rheumatoid arthritis are potent inducers of matrix metalloproteinases and proinflammatory cytokines upon synovial fibroblast interaction, including autocrine interleukin-17A production', *Arthritis Rheum*, 63: 73-83.

Velez, G., C. N. Roybal, D. Colgan, S. H. Tsang, A. G. Bassuk, and V. B. Mahajan. 2016. 'Precision Medicine: Personalized Proteomics for the Diagnosis and Treatment of Idiopathic Inflammatory Disease', *JAMA Ophthalmol*, 134: 444-8.

Wakefield, D., and J. H. Chang. 2005. 'Epidemiology of uveitis', *Int Ophthalmol Clin*, 45: 1-13.

Wakefield, D., P. McCluskey, and P. Palladinetti. 1992. 'Distribution of lymphocytes and cell adhesion molecules in iris biopsy specimens from patients with uveitis', *Arch Ophthalmol*, 110: 121-5.

Wang, S., P. Xia, Y. Chen, Y. Qu, Z. Xiong, B. Ye, Y. Du, Y. Tian, Z. Yin, Z. Xu, and Z. Fan. 2017. 'Regulatory Innate Lymphoid Cells Control Innate Intestinal Inflammation', *Cell*, 171: 201-16.e18.

Ward, N. L., and D. T. Umetsu. 2014. 'A new player on the psoriasis block: IL-17A- and IL-22-producing innate lymphoid cells', *J Invest Dermatol*, 134: 2305-07.

Watad, A., C. Bridgewood, T. Russell, H. Marzo-Ortega, R. Cuthbert, and D. McGonagle. 2018. 'The Early Phases of Ankylosing Spondylitis: Emerging Insights From Clinical and Basic Science', *Front Immunol*, 9: 2668.

Weaver, C. T., L. E. Harrington, P. R. Mangan, M. Gavrieli, and K. M. Murphy. 2006. 'Th17: an effector CD4 T cell lineage with regulatory T cell ties', *Immunity*, 24: 677-88.

Wei, Y. L., A. Han, J. Glanville, F. Fang, L. A. Zuniga, J. S. Lee, D. J. Cua, and Y. H. Chien. 2015. 'A Highly Focused Antigen Receptor Repertoire Characterizes γδ T Cells That are Poised to Make IL-17 Rapidly in Naive Animals', *Front Immunol*, 6: 118.

Weiss, P. F. 2012. 'Diagnosis and treatment of enthesitis-related arthritis', *Adolesc Health Med Ther*, 2012: 67-74.

Wilbanks, G. A., and J. W. Streilein. 1990. 'Characterization of suppressor cells in anterior chamber-associated immune deviation (ACAID) induced by soluble antigen. Evidence of two functionally and phenotypically distinct T-suppressor cell populations', *Immunology*, 71: 383-9.

Willenborg, D. O., S. Fordham, C. C. Bernard, W. B. Cowden, and I. A. Ramshaw. 1996. 'IFN-gamma plays a critical down-regulatory role in the induction and effector phase of myelin oligodendrocyte glycoprotein-induced autoimmune encephalomyelitis', *J Immunol*, 157: 3223-7.

Williamson, J. S., D. Bradley, and J. W. Streilein. 1989. 'Immunoregulatory properties of bone marrow-derived cells in the iris and ciliary body', *Immunology*, 67: 96-102.

Wohn, C., J. L. Ober-Blöbaum, S. Haak, S. Pantelyushin, C. Cheong, S. P. Zahner, S. Onderwater, M. Kant, H. Weighardt, B. Holzmann, B. Reizis, B. Becher, E. P. Prens, and B. E. Clausen. 2013. 'Langerin(neg) conventional dendritic cells

produce IL-23 to drive psoriatic plaque formation in mice', *Proc Natl Acad Sci U S A*, 110: 10723-8.

Wylęgała, A., B. Bolek, and E. Wylęgała. 2020. 'Trends in optical coherence tomography angiography use in university clinic and private practice setting between 2014-2018', *Expert Rev Med Devices*, 17: 1109-13.

Xu, J., Y. Qin, R. Chang, H. Tan, Q. Wang, G. Su, Q. Cao, A. Kijlstra, and P. Yang. 2020. 'Aqueous cytokine levels in four common uveitis entities', *Int Immunopharmacol*, 78: 106021.

Yago, T., Y. Nanke, M. Kawamoto, T. Furuya, T. Kobashigawa, N. Kamatani, and S. Kotake. 2007. 'IL-23 induces human osteoclastogenesis via IL-17 in vitro, and anti-IL-23 antibody attenuates collagen-induced arthritis in rats', *Arthritis Res Ther*, 9: R96.

Yanoff, M, and J Sassani. 2015. *Ocular Pathology* (Elsevier: London, England).

Yazid, S., P. J. Gardner, L. Carvalho, C. J. Chu, R. J. Flower, E. Solito, R. W. Lee, R. R. Ali, and A. D. Dick. 2015. 'Annexin-A1 restricts Th17 cells and attenuates the severity of autoimmune disease', *J Autoimmun*, 58: 1-11.

Ye, P., F. H. Rodriguez, S. Kanaly, K. L. Stocking, J. Schurr, P. Schwarzenberger, P. Oliver, W. Huang, P. Zhang, J. Zhang, J. E. Shellito, G. J. Bagby, S. Nelson, K. Charrier, J. J. Peschon, and J. K. Kolls. 2001. 'Requirement of interleukin 17 receptor signaling for lung CXC chemokine and granulocyte colony-stimulating factor expression, neutrophil recruitment, and host defense', *J Exp Med*, 194: 519-27.

Yen, D., J. Cheung, H. Scheerens, F. Poulet, T. McClanahan, B. McKenzie, M. A. Kleinschek, A. Owyang, J. Mattson, W. Blumenschein, E. Murphy, M. Sathe, D. J. Cua, R. A. Kastelein, and D. Rennick. 2006. 'IL-23 is essential for T cell-mediated colitis and promotes inflammation via IL-17 and IL-6', *J Clin Invest*, 116: 1310-6.

Yilmaz, S., E. Aydemir, A. Maden, and B. Unsal. 2007. 'The prevalence of ocular involvement in patients with inflammatory bowel disease', *Int J Colorectal Dis*, 22: 1027-30.

Yoshiki, R., K. Kabashima, T. Honda, S. Nakamizo, Y. Sawada, K. Sugita, H. Yoshioka, S. Ohmori, B. Malissen, Y. Tokura, and M. Nakamura. 2014. 'IL-23 from Langerhans cells is required for the development of imiquimod-induced psoriasis-like dermatitis by induction of IL-17A-producing γδ T cells', *J Invest Dermatol*, 134: 1912-21.

Yu, J. J., M. J. Ruddy, G. C. Wong, C. Sfintescu, P. J. Baker, J. B. Smith, R. T. Evans, and S. L. Gaffen. 2007. 'An essential role for IL-17 in preventing pathogen-initiated bone destruction: recruitment of neutrophils to inflamed bone requires IL-17 receptor-dependent signals', *Blood*, 109: 3794-802.

Yücel, Y. H., M. G. Johnston, T. Ly, M. Patel, B. Drake, E. Gümüş, S. A. Fraenkl, S. Moore, D. Tobbia, D. Armstrong, E. Horvath, and N. Gupta. 2009. 'Identification of lymphatics in the ciliary body of the human eye: a novel "uveolymphatic" outflow pathway', *Exp Eye Res*, 89: 810-9.

Zeboulon, N., M. Dougados, and L. Gossec. 2008. 'Prevalence and characteristics of uveitis in the spondyloarthropathies: a systematic literature review', *Ann Rheum Dis*, 67: 955-9.

Zeng, L., M. J. Lindstrom, and J. A. Smith. 2011. 'Ankylosing spondylitis macrophage production of higher levels of interleukin-23 in response to lipopolysaccharide without induction of a significant unfolded protein response', *Arthritis Rheum*, 63: 3807-17.

Zeng, X., Y. L. Wei, J. Huang, E. W. Newell, H. Yu, B. A. Kidd, M. S. Kuhns, R. W. Waters, M. M. Davis, C. T. Weaver, and Y. H. Chien. 2012. 'γδ T cells recognize a microbial encoded B cell antigen to initiate a rapid antigen-specific interleukin-17 response', *Immunity*, 37: 524-34.

Zhang, G. X., B. Gran, S. Yu, J. Li, I. Siglienti, X. Chen, M. Kamoun, and A. Rostami. 2003. 'Induction of experimental autoimmune encephalomyelitis in IL-12 receptor-beta 2-deficient mice: IL-12 responsiveness is not required in the pathogenesis of inflammatory demyelination in the central nervous system', *J Immunol*, 170: 2153-60.

Zhao, Z., Y. Liang, Y. Liu, P. Xu, M. J. Flamme-Wiese, D. Sun, J. Sun, R. F. Mullins, Y. Chen, and J. Cai. 2017. 'Choroidal γδ T cells in protection against retinal pigment epithelium and retinal injury', *Faseb j*, 31: 4903-16.

Zhou, L., Ivanov, II, R. Spolski, R. Min, K. Shenderov, T. Egawa, D. E. Levy, W. J. Leonard, and D. R. Littman. 2007. 'IL-6 programs T(H)-17 cell differentiation by promoting sequential engagement of the IL-21 and IL-23 pathways', *Nat Immunol*, 8: 967-74.

Zhou, L., J. E. Lopes, M. M. Chong, Ivanov, II, R. Min, G. D. Victora, Y. Shen, J. Du, Y. P. Rubtsov, A. Y. Rudensky, S. F. Ziegler, and D. R. Littman. 2008. 'TGF-beta-induced Foxp3 inhibits T(H)17 cell differentiation by antagonizing RORgammat function', *Nature*, 453: 236-40.

Zhuang, Z., Y. Wang, G. Zhu, Y. Gu, L. Mao, M. Hong, Y. Li, and M. Zheng. 2017. 'Imbalance of Th17/Treg cells in pathogenesis of patients with human leukocyte antigen B27 associated acute anterior uveitis', *Sci Rep*, 7: 40414.

Zuberbuehler, M. K., M. E. Parker, J. D. Wheaton, J. R. Espinosa, H. R. Salzler, E. Park, and M. Ciofani. 2019. 'The transcription factor c-Maf is essential for the commitment of IL-17-producing γδ T cells', *Nat Immunol*, 20: 73-85.

Zúñiga, L. A., R. Jain, C. Haines, and D. J. Cua. 2013. 'Th17 cell development: from the cradle to the grave', *Immunol Rev*, 252: 78-88.